INFORMATION TO USERS

This manuscript has been reproduced from the microfilm master. UMI films the text directly from the original or copy submitted. Thus, some thesis and dissertation copies are in typewriter face, while others may be from any type of computer printer.

The quality of this reproduction is dependent upon the quality of the copy submitted. Broken or indistinct print, colored or poor quality illustrations and photographs, print bleedthrough, substandard margins, and improper alignment can adversely affect reproduction.

In the unlikely event that the author did not send UMI a complete manuscript and there are missing pages, these will be noted. Also, if unauthorized copyright material had to be removed, a note will indicate the deletion.

Oversize materials (e.g., maps, drawings, charts) are reproduced by sectioning the original, beginning at the upper left-hand corner and continuing from left to right in equal sections with small overlaps.

Photographs included in the original manuscript have been reproduced xerographically in this copy. Higher quality 6" x 9" black and white photographic prints are available for any photographs or illustrations appearing in this copy for an additional charge. Contact UMI directly to order.

ProQuest Information and Learning
300 North Zeeb Road, Ann Arbor, MI 48106-1346 USA
800-521-0600

Université d'Ottawa · University of Ottawa

PUNCHING SHEAR IN EDGE AND CORNER COLUMN SLAB CONNECTIONS OF FLAT PLATE STRUCTURES

by
I Ketut Sudarsana

A thesis
presented to the University of Ottawa in partial fulfillment of the requirements for
Doctor of Philosophy in Civil Engineering

Department of Civil Engineering
University of Ottawa
Ottawa, Canada
K1N 6N5

December 2001

The Doctor of Philosophy in Civil Engineering is a joint program
with Carleton University administered by the
Ottawa-Carleton Institute for Civil Engineering

To my Parents,

my wife, Putu Sari,

and my lovely son, Putu Brahmanda

ACKNOWLEDGEMENTS

Praise and glory due to God to whom the author attributes all his knowledge and success in his life.

The author would like to express his deepest gratitude to his supervisor, Prof. Dr. N.J. Gardner, for his continuous guidance, untiring advise, encouragement and support throughout this research project.

The author thanks the technical staffs of the Civil Engineering Department of the University of Ottawa, especially Mr. Derek Mes, Mr. Robert Moore and Mr. Madan Makasare, for their help during the experimental work. The author also would like to thank his friends and the structural graduate students for their help during casting of the slabs.

The financial support received from the Indonesian Government, Engineering Education Development Project (EEDP), under the term of scholarship to study at the University of Ottawa in Civil Engineering is deeply appreciated.

The author would like to express his deep appreciation to his wife for her understanding, patient and continuous encouragement during his study in the University of Ottawa. The author would like to say to his lovely son, Putu Brahmanda, that hopefully one day you would understand why we missed many weekends together in Ottawa.

Last, but certainly not least, the author is grateful to his parents, sisters and brother for their unlimited love and support on his whole life.

ABSTRACT

The behavior and strength of edge and corner column slab connections of flat plate structures subjected to shear force only, moment only as well as combined shear force and moment were investigated. A two bay by two bay flat plate structure (nine columns) and eight isolated edge column slab connections were constructed and tested to failure. After the tests of the four edge column connections of the continuous slab were completed, the edge connections were repaired using two types of concretes (normal concrete and CAH expansive concrete) and tested to failure.

Interaction diagrams between shear force and unbalanced moment at edge column slab connections based on building code provisions (ACI 318-99, CSA A23.3-94 and CEB-FIP MC90) and three alternative approaches (Regan's approach, the Truss Model and the Strip Model) proposed in the literature are examined using the results of the present experimental work. Interaction diagrams for corner connections calculated using Regan's approach and the building code provisions are compared with the experimental results.

The shear strength of edge and corner connections is calculated according to ACI 318-99, CSA A23.3-85, BS8110-85, CEB-FIP MC90 and the alternative approaches of Regan, Sherif, Gardner, Elgabry, the Truss Model and the Strip Model. All alternative approach predictions of shear strength of edge connections, except Sherif's, are conservative. The average ratio of measured shear strength to calculated shear strength ranges from 0.90 to 1.30 with coefficients of variation (*COV*) ranging from 0.18 to 0.40. Gardner's approach, that considered a linear shear stress distribution as in ACI 318-99, with a critical shear section taken at the column perimeter or perimeter of loaded area gives the most conservative and the least scatter of the test results compared with the other proposed approaches. The measured shear strengths of the corner connections are compared to the calculated shear strengths based on the building code provisions and five

alternative approaches available in the literature (i.e. Ingvarsson's, Regan's, Zaghlool's, Gardner's and Desayi's approach).

On the basis of the present test results, the effects of load eccentricity (M/V) and reinforcement ratio (ρ_{avg}) on shear strength of edge column slab connections are investigated. The reduction in shear capacity of edge connections due to the increase in M/V ratios approximates a logarithmic function. The effect of the reinforcement ratio on the shear strength of the present tests on the edge and corner connections calculated using the North American codes is not obvious. However, tests by Zaghlool (1973) and Regan (1981) show that the shear strength increased with an increase in reinforcement ratio.

The strength and stiffness of repaired edge connections were investigated using the four, previously failed, edge connections of the continuous slab specimen. Connections repaired using normal concrete can have similar strength and stiffness as the original connections. However, the connections repaired using the CAH expansive concrete exhibited less strength and stiffness compared to the original edge connections.

TABLE OF CONTENTS

DEDICATION i
ACKNOWLEDGEMENT ii
ABSTRACT iii
TABLE OF CONTENTS v
LIST OF TABLES xi
LIST OF FIGURES xiii
NOTATION xxiii

CHAPTER 1: INTRODUCTION 1
1.1 GENERAL 1
1.2 HISTORY OF TWO-WAY SLABS 1
1.3 PUNCHING SHEAR PHENOMENON 3
1.4 PREVIOUS RESEARCH AT THE UNIVERSITY OF OTTAWA 5
1.5 RESEARCH OBJECTIVES 5
1.6 SCOPE 6

CHAPTER 2: LITERATURE REVIEW 8
2.1 EDGE COLUMN WITH UNBALANCED MOMENTS 8
2.1.1 General 8
2.1.2 Unbalanced moment acts in one direction 8
2.1.2.1 Andersson's approach 8
2.1.2.2 Kinnunen's Approach 9
2.1.2.3 The Approach by Regan 11
2.1.2.4 Beam Analogy Approach 14
2.1.2.4.1 Hawkins and Corley (1971) 14
2.1.2.4.2 Stamenkovic and Chapman (1969) 15
2.1.2.5 Pöllet's approach (1983) 19
2.1.2.6 Moehle's approach (1988) 21
2.1.2.7 Truss Model approach 24
2.1.2.8 Gardner and Shao's approach 25
2.1.2.9 Elgabry and Ghali's approach (1996) 26

2.1.2.10 Sherif and Dilger's approach (1995) 28
2.1.2.11 Strip Model Approach (1998) 31
2.2 CORNER COLUMN SLAB CONNECTION 35
2.2.1 General 35
2.2.2 Ingvarsson's approach (1977) 35
2.2.3 Regan, P.E. (1981) 36
2.2.4 Zaghlool et.al. (1970, 1973a,b) 38
2.2.5 Desayi and Seshadri's approach (1997) 39
2.3 CODE PROVISIONS FOR MOMENT TRANSFER 41
2.3.1 American Code (ACI 318–99) 41
2.3.2 Canadian Code (CSA A23.3-94) 46
2.3.3 British Code (BS 8110-85) 47
2.3.4 CEB Model Code (CEB-FIP MC 1990) 48
2.4 INFORMATION FROM TESTS ON EDGE CONNECTIONS 52
2.4.1 Shear-moment interaction 52
2.4.2 Effect of ρ_{c2+3h} on shear stress 54
2.4.3 Load eccentricity effects on the shear strength 56
2.5 INFORMATION FROM TESTS OF CORNER CONNECTIONS 57
2.5.1 Interaction between shear and moment 57
2.5.2 Effect of steel ratio on the shear strength 59
2.5.3 Effect of load eccentricity ($e_s = M_{code}/V_u$) on shear strength 60
2.6 BIAXIAL UNBALANCED MOMENT 61
2.7 REPAIRED CONCRETE CONNECTIONS 62

CHAPTER 3: EXPERIMENTAL PROGRAM 64
3.1 GENERAL 64
3.2 CONTINUOUS SLAB SPECIMEN 65
3.2.1 General 65
3.2.2 Continuous slab dimension 65
3.2.3 Slab flexural reinforcement 66
3.2.4 Column reinforcement 67
3.2.5 Construction of the specimen 67
3.2.6 Concrete properties 68
3.2.7 Test set-up 70
3.2.8 Isolated support 70

3.2.9 Steel strain measurement 71
3.2.10 Deflection measurement 71
3.2.11 Testing of the specimen 71
3.2.11.1 Connection under vertical loading only (Connection E_2) ... 72
3.2.11.2 Connection subjected to bending moment only (Connection E_3) 72
3.2.11.3 Connections subjected to combined vertical and bending moment (Connections E_1 and E_4) 73
3.3 REPAIR OF THE EDGE COLUMN SLAB CONNECTIONS 73
3.3.1 Properties of repaired materials 73
3.3.1.1 Concrete properties 73
3.3.1.2 Bonding agent 74
3.3.2 Repair procedures 75
3.3.3 Testing of repair connections 75
3.4 TESTING OF CORNER COLUMN SLAB CONNECTIONS 76
3.4.1 Connection subjected to vertical load only (Connection C_5) 76
3.4.2 Connection subjected to combined vertical load and diagonal moments (connection C_6) 77
3.4.3 Connections subjected to combined vertical load and diagonal moments (connections C_7 and C_8) 77
3.5 ISOLATED SLAB SPECIMENS 77
3.5.1 Slab dimension and reinforcement 78
3.5.2 Column dimension and reinforcement 79
3.5.3 Construction of the specimens 79
3.5.4 Material properties 80
3.5.4.1 Concretes 80
3.5.4.2 Flexural reinforcement 81
3.5.5 Instrumentation 81
3.5.6 Test set-up of the isolated specimens 82
3.5.7 Testing of the isolated specimens 82
3.5.7.1 Specimen E_{1-1} 82
3.5.7.2 Specimens E_{1-2}, E_{1-3}, E_{1-4} 83
3.5.7.3 Specimens E_{2-1}, E_{2-2}, E_{2-3} and E_{2-4} 85

CHAPTER 4: TEST RESULTS 112
4.1 GENERAL 112
4.2 TEST RESULTS OF EDGE COLUMN SLAB CONNECTIONS 113

4.2.1 Failure load and mode of failure 113
4.2.2 Crack patterns 113
4.2.2.1 Edge connection subjected to vertical load only (E_2) 113
4.2.2.2 Edge connection subjected to bending moment only (E_3) 116
4.2.2.3 Connections subjected to combined vertical load and bending moment (E_1, E_4) 117
4.2.2.4 Isolated column slab specimens in Series I (connections E_{1-1}, E_{1-2}, E_{1-3} and E_{1-4}) 118
4.2.2.5 Isolated column slab specimen Series II (E_{2-1}, E_{2-2}, E_{2-3} and E_{2-4}) 121
4.2.3 Flexural steel strains 123
4.2.4 Out-of-plane slab deflection 131
4.2.5 Column rotations 134
4.3 REPAIRED EDGE CONNECTIONS 135
4.3.1 General 135
4.3.2 Ultimate load capacity and failure mechanisms 135
4.3.3 Crack patterns of the repaired connections 136
4.3.3.1 Connections repaired using normal concrete 136
4.3.3.2 Connections repaired using non-shrinkable CAH concrete 138
4.3.4 Flexural steel strains 140
4.3.5 Out-of-plane deflection of the slab 144
4.3.6 Column rotations 147
4.4 CORNER COLUMN SLAB CONNECTIONS 148
4.4.1 General 148
4.4.2 Ultimate load capacity and failure mechanisms 148
4.4.3 Crack patterns 149
4.4.3.1 Corner connection C_5 149
4.4.3.2 Corner connection C_6 150
4.4.3.3 Corner connections C_7 and C_8 151
4.4.4 Flexural steel strains 152
4.4.5 Out-of-plane slab deflections 156
4.4.6 Column rotations 158

CHAPTER 5: DISCUSSION ON EDGE CONNECTIONS 159
5.1 GENERAL 159
5.2 INTERACTION BETWEEN SHEAR FORCE AND MOMENT 159
5.2.1 ACI 318-99 and CSA A23.3-94 Codes 160

5.2.2 CEB-FIP MC 1990 164
5.2.3 No interaction between shear force and moment 167
5.2.4 Alternative approaches 169
5.3 COMPARISON OF LOAD CAPACITY 173
5.3.1 Using building code provisions 173
5.3.2 Using proposed approaches 176
5.4 EFFECTIVE WIDTH FOR FLEXURAL RESISTANCE 180
5.5 EFFECT OF ECCENTRICITY (M_{co}/V_u) ON SHEAR CAPACITY 181
5.6 EFFECT OF STEEL RATIO ON SHEAR STRENGTH 182
5.7 REPAIRED EDGE CONNECTIONS 182
5.7.1 Effect of repair technique 182
5.7.2 Repair using normal concrete 183
5.7.3 Repair using CAH expansive concrete 184
5.7.4 Stiffness of repaired connections 184

CHAPTER 6: DISCUSSION ON CORNER CONNECTIONS 195
6.1 GENERAL 195
6.2 INTERACTION BETWEEN SHEAR FORCE AND MOMENT 195
6.2.1 Building code provisions 195
6.2.1.1 The American ACI 318-99 code 195
6.2.1.2 The Canadian CSA A23.3-94 code 197
6.2.1.3 The European CEB-FIP MC90 198
6.2.2 Alternative approaches 199
6.3 COMPARISON OF LOAD CAPACITY 200
6.3.1 Building code provisions 200
6.3.2 Alternative approaches 203
6.3.2.1 Ingvarsson's approach (1977) 205
6.3.2.2 Zaghlool's approach (1973) 205
6.3.2.3 Regan's approach (1981) 205
6.3.2.4 Gardner's approach (1995) 206
6.3.2.5 Desayi and Sheshadri's approach (1997) 206
6.4 EFFECT OF STEEL RATIO ON SHEAR STRENGTH 207

CHAPTER 7: SUMMARY AND CONCLUSIONS **208**
7.1 GENERAL 208
7.2 SUMMARY 208
7.3 CONCLUSIONS 209
7.3.1 Conclusions related to experimental work 210
7.3.2 Conclusions related to analysis data 211
7.4 RECOMMENDATION FOR FUTURE RESEARCH 213

REFERENCES **215**

APPENDIX A **222**

LIST OF TABLES

Table 2.1 The effect of the steel ratio c_2+3h on the shear strength of edge connections according to ACI or CSA codes 54

Table 2.2 The effect of steel ratio on the shear stress of corner connections calculating based ACI or CSA Codes 59

Table 3.1 Summary of flexural reinforcement of the continuous flat plate specimen... 66

Table 3.2 Properties of concretes used in the continuous flat plate specimen..... 69

Table 3.3 Properties of the concretes used to repair the edge column slab connection of the continuous flat plate specimen..... 74

Table 3.4 Concrete properties used in the isolated edge column slab specimens of Series I and Series II. 80

Table 3.5 Properties of flexural reinforcement used in the isolated edge column slab specimens of Series I and II..... 81

Table 4.1 Ultimate load capacity of edge column slab connections and mode of the failures. 114

Table 4.2 Ultimate load capacity of the repaired edge column slab connections..... 136

Table 4.3 Ultimate load capacity and failure modes of the corner connections..... 148

Table 5.1 Summary of statistical results of code predictions on the strength of edge column slab connections..... 173

Table 5.2 Summary of statistical results of the proposed approaches on the strength of edge column slab connections 177

Table 5.3 Comparison of flexural capacity of edge column slab connections using two effective widths..... 180

Table 5.4 Comparison between failure and predicted shear stress according to the American ACI 318-99 and the Canadian CSA A23.3-94 Codes..... 186

Table 5.5 Comparison between failure and predicted shear stress according to the British BS 8110-85 Code..... 187

Table 5.6 Comparison between failure and predicted shear stress according to the European CEB-FIP MC90 Method-1 and Method-2 188

Table 5.7 Comparison between failure and predicted shear force and moment according to Regan's approach (1981) 189

Table 5.8 Comparison between failure and predicted shear forces and moments according to the Truss Model (1987) 190

Table 5.9 Comparison between failure and predicted shear force and moment according to the Strip Model (1998) 191

Table 5.10 Comparison between failure and predicted shear stress according to the Sherif's approach (1995) 192

Table 5.11 Comparison between failure and predicted shear stress according to the Gardner's approach (1996) 193

Table 5.12 Comparison between failure and predicted shear stress according to the Elgabry and Ghali's approach 194

Table 6.1 Comparison between failure and predicted shear stress of corner connections according to the code provisions 201

Table 6.2 Comparison between failure and predicted shear capacity of corner connections according to the proposed approach in the literature 204

LIST OF FIGURES

Figure 2.1 Local yield line at an edge column 10

Figure 2.2 Column connected to slab at one face as starting point of Regan's approach 11

Figure 2.3 Areas resisting shear and active width in flexure 12

Figure 2.4 Shear moment interaction diagram based on Regan's approach 13

Figure 2.5 Beam analogy critical section for edge column-slab connection 15

Figure 2.6 Interaction curve-edge 127mm(5 in) square column with normal moment. 17

Figure 2.7 Interaction curve-edge 127 mm (5 in) square column with tangential moment 18

Figure 2.8 Pöllet Approach (1983) for edge column connections 19

Figure 2.9 Pöllet's typical moment-shear interaction at an edge column 20

Figure 2.10 Interaction between shear and moment after Moehle (1988). 21

Figure 2.11 Effective width of flexure resistance at edge connection [Moehle, 1988] ... 23

Figure 2.12 Moment-shear force interaction at the centroid of the ACI Code critical shear section. 23

Figure 2.13 Shear-moment interaction diagram for edge column connections according to truss model by Simmonds and Alexander (1987) 24

Figure 2.14 Gardner and Shao's interaction diagram using a simple multiplier 26

Figure 2.15 Direction of coordinate axes and forces on slab critical section of edge column slab connection (Elgabry and Ghali, 1996) 27

Figure 2.16 Sherif and Dilger's proposed strut and tie model for edge column-slab connection 28

Figure 2.17 Interaction diagram between shear and moment for edge column slab connection according to Sherif's proposed model. 30

Figure 2.18 Shear moment diagram for edge column slab connections based on the Strip Model 32

Figure 2.19 Ingvarsson-definitions of symbols (a) and distribution of shear stress (b) at corner column connections. 36

Figure 2.20 Regan's limiting condition for shear force-moment interaction at corner column slab connections 37

Figure 2.21 Critical shear section and distribution of slab shear stress for edge column connections transferring shear and unbalanced moment of the ACI Code. . 42

Figure 2.22 Shear moment interaction relationship for edge column connection based on linear shear stress distributions of ACI Code. 44

Figure 2.23 Assumed critical section and distribution of slab shear stress for corner column connections transferring shear and unbalanced moment of the ACI Code. 45

Figure 2.24 CEB-FIP 1990 control perimeters at edge columns: (a) perimeter u_1; (b) perimeter u_1* 49

Figure 2.25 CEB-FIP-1990 Control perimeter at corner column: (a) perimeter u_1; (b) perimeter u_1* 51

Figure 2.26 Interaction between shear and moment of ACI 318-99 provisions on the edge column slab connections 52

Figure 2.27 Interaction between shear and moment of the CEB-FIP MC90 provisions on the edge column slab connections 53

Figure 2.28 Effect of steel ratio on shear strength of edge connections calculated according to ACI and CSA code 55

Figure 2.29 Effect of load eccentricity $e_s=M_s/V_u$ on the failure shear strength calculated using ACI or CSA Code 56

Figure 2.30 Interaction between shear and moment of ACI 318-99 provisions on the corner column slab connections 57

Figure 2.31 Interaction between shear and moment of CEB-FIP MC90 on the corner column slab connections 58

Figure 2.32 Effect of the steel ratio on shear strength of corner connections calculated according to ACI and CSA codes 60

Figure 2.33 Effect of load eccentricity ($e_s = M_{code}/V_u$) on the shear strength of the corner connections predicted by ACI and CSA Codes 61

Figure 3.1 Dimensions of continuous flat plate specimen 87

Figure 3.2 Negative (top) and Bottom reinforcement of continuous slab specimen; All bars #10M (Φ = 11.3 mm, A_s = 100 mm^2) 88

Figure 3.3 Field lay out of slab reinforcement; (a) overall specimen, (b) edge connections, (c) corner connections 89

Figure 3.4 Stress - strain relationship of steel #10M for continuous flat plate specimen 89

Figure 3.5 Column cages of continuous slab specimen; (a) for three edge columns, (b) for the fourth edge column, (c) for corner columns and (d) for interior column 90

Figure 3.6 Polyetheline covers on slab formwork before casting 91

Figure 3.7 Casting concrete of the continuous flat plate specimen 91

Figure 3.8 Compressive strength of concrete cylinders of the continuous slab specimen at 28 days 92

Figure 3.9 Compressive strength over time of concrete cylinders of continuous slab specimen 92

Figure 3.10 Test setup for edge column slab connection of the continuous slab specimen subjected to vertical load only 93

Figure 3.11 Test setup for edge column slab connection of the continuous slab specimen subjected to bending moment only 93

Figure 3.12 Test setup for edge column slab connection of the continuous slab specimen subjected to combined vertical load and bending moment 94

Figure 3.13 Strain gauges position on the negative reinforcement of connections E_1 and E_2 of the continuous slab specimen; all the gauges are at 25 mm from the column faces 95

Figure 3.14 Strain gauges position on the negative reinforcement of connections E_3 and E_4 of the continuous slab specimen; all the gauges are at 25 mm from the column faces 96

Figure 3.15 Strain gauges position on the negative reinforcement of the corner column slab connection of the continuous slab specimen; all the gauges are at 25 mm from the column faces 97

Figure 3.16 Strain gauges position on the bottom reinforcement of the continuous slab specimen; all the gauges are at 25 mm from the column faces 98

Figure 3.17 Typical position of LVDT's and dial gauges to measure out-of-plane deflection on the test of the edge column slab connections 99

Figure 3.18 Typical position of LVDT's and dial gauges to measure out-of-plane deflection on the test of the corner column slab connections..... 99

Figure 3.19 Repair edge column slab connections; (a) Damaged concrete to be remove; (b) & (d) Edge reinforcement after removing concrete; (c) Formwork and application of bonding agent before concrete casting 100

Figure 3.20 Stress strain relationship of the non-shrinkable concrete cylinder at 28 days for repairing edge connections; (a) E_{2R} Connection; (b) E_{1R} Connection.. 100

Figure 3.21 Bond strength (14 days) versus open time of SikaTop Armatec 110 EpoCem bonding agent. 101

Figure 3.22 Typical test setup of corner column slab connections..... 101

Figure 3.23 Reinforcement of the isolated slab specimen of Series I (all bars are #10M. unless indicated in the drawing) 102

Figure 3.24 Reinforcement of the isolated slab specimen Series II (all bar are #10M. unless indicated in the drawing) 103

Figure 3.25 Arrangement of rebars in the isolated slab specimens; (a) slab reinforcement. (b) column reinforcement, and (c) the specimens before casting..... 104

Figure 3.26 Typical stress-strain relationship of concrete cylinder of the isolated slab specimen 104

Figure 3.27 Compressive strength development over time of concrete cylinder of the isolated slab specimen 105

Figure 3.28 Typical stress-strain relationship of bar #10M and #15M used in the isolated slab specimen..... 105

Figure 3.29 Typical position of strain gauges on the negative reinforcement of the isolated slab Series I; all of the strain gauges are at 25 mm from the column faces 106

Figure 3.30 Typical position of strain gauges on the negative reinforcement of the isolated slab Series II; all of the strain gauges are at 25 mm from the column faces 107

Figure 3.31 Position of applied vertical loads and gauges for specimen in Series I; (a) specimen $E_{1\text{-}2}$, (b) specimen $E_{1\text{-}3}$, (c) specimen $E_{1\text{-}4}$, and (d) Test of specimen $E_{1\text{-}2}$ 108

Figure 3.32 Position of applied vertical loads and gauges of isolated edge connection $E_{2\text{-}1}$ of Series II 109

Figure 3.33 Position of applied vertical loads and gauges of isolated edge connection $E_{2\text{-}2}$ of Series II 109

Figure 3.34 Position of applied vertical loads and gauges of isolated edge connection $E_{2\text{-}3}$ of Series II 110

Figure 3.35 Position of applied vertical loads and gauges of isolated edge connection $E_{2\text{-}4}$ of Series II 110

Figure 3.36 Test setup of isolated column slab connections in Series II 111

Figure 4.1 Crack patterns of connection E_2 on the first test; (a) cracks on the slab tension side, (b) cracks on the slab free edge 115

Figure 4.2 Crack patterns at the failure of second test of connection E_2; (a) cracks on the slab tension side, (b) cracks on the slab free edge 115

Figure 4.3 Crack patterns at failure of connection E_3; (a) cracks on the slab tension surface, (b) cracks on the slab free edge 116

Figure 4.4 Crack patterns of connection E_1; (a) cracks on the slab tension surface, (b) cracks on the slab free edge 117

Figure 4.5 Crack patterns of connection E_4; (a) cracks on the slab tension surface, (b) cracks on the slab free edge 118

Figure 4.6 Crack pattern at the failure of connection $E_{1\text{-}1}$; (a) cracks at the slab tension side, (b) cracks at the slab free edge 119

Figure 4.7 Crack patterns at the failure of connection $E_{1\text{-}2}$; (a) cracks on the slab tension surface, (b) cracks on the slab free edge 120

Figure 4.8 Crack patterns at the failure of connection $E_{1\text{-}4}$; (a) cracks on the slab tension surface, (b) cracks on the slab free edge 120

Figure 4.9 Crack patterns at the failure of connection $E_{1\text{-}3}$; (a) cracks on the slab tension surface, (b) cracks on the slab free edge 121

Figure 4.10 Crack patterns at the failure of connection $E_{2\text{-}1}$; (a) cracks on the slab tension surface, (b) cracks on the slab free edge 122

Figure 4.11 Crack patterns at the failure of connection $E_{2\text{-}2}$; (a) cracks on the slab tension surface, (b) cracks on the slab free edge 122

Figure 4.12 Crack patterns at the failure of connection E_{2-3}; (a) cracks on the slab tension surface, (b) cracks on the slab free edge 123

Figure 4.13 Crack patterns at the failure of connection E_{2-4}; (a) cracks on the slab tension surface, (b) cracks on the slab free edge 123

Figure 4.14 Steel strains on negative reinforcement of connection E_1 of the continuous slab specimen 125

Figure 4.15 Steel strains on negative reinforcement of connection E_2 of the continuous slab specimen 125

Figure 4.16 Steel strains on negative reinforcement of connection E_3 of the continuous slab specimen 126

Figure 4.17 Steel strains on negative reinforcement of connection E_4 of the continuous slab specimen 126

Figure 4.18 Steel strains on negative reinforcement of isolated slab connection E_{1-1} of the Series I 127

Figure 4.19 Steel strains on negative reinforcement of isolated slab connection E_{1-2} of the Series I 127

Figure 4.20 Steel strains on negative reinforcement of isolated slab connection E_{1-3} of the Series I 128

Figure 4.21 Steel strains on negative reinforcement of isolated slab connection E_{1-4} of the Series I 128

Figure 4.22 Steel strains on negative reinforcement of isolated slab connection E_{2-1} of the Series II 129

Figure 4.23 Steel strains on negative reinforcement of isolated slab connection E_{2-2} of the Series II 129

Figure 4.24 Steel strains on negative reinforcement of isolated slab connection E_{2-3} of the Series II 130

Figure 4.25 Steel strains on negative reinforcement of isolated slab connection E_{2-4} of the Series II 130

Figure 4.26 Slab deflections on the first test of connection E_2 of the continuous slab specimen 131

Figure 4.27 Slab deflection on the second test of connection E_2 of the continuous slab specimen 132

Figure 4.28 Slab deflection on the test of connection E_1 of the continuous slab specimen 132

Figure 4.29 Slab deflection on the test of connection E_4 of the continuous slab specimen 133

Figure 4.30 Column rotation of connections E_2, E_3 and E_4 of the continuous slab specimen 135

Figure 4.31 Crack patterns of connection E_{3R} at the end of the first test; (a)&(b) cracks on the slab tension surface 137

Figure 4.32 Crack patterns of the second test of connection E_{3R} at the failure ; (a) cracks on the slab tension surface, (b) cracks on the slab free edge 137

Figure 4.33 Crack patterns of connection E_{4R} at the failure; (a) cracks on the slab tension surface, (b) cracks on the slab free edge 138

Figure 4.34 Crack patterns of connection E_{1R} at the failure; (a) cracks on the slab tension surface, (b) cracks on the slab free edge 139

Figure 4.35 Crack patterns of connection E_{2R} at the failure; (a) cracks on the slab tension surface, (b) cracks on the slab free edge 139

Figure 4.36 Steel strains on the negative reinforcement on the first test of connection E_{3R}* of the continuous slab specimen 141

Figure 4.37 Steel strains on the negative reinforcement on the second test of connection E_{3R} of the continuous slab specimen 141

Figure 4.38 Steel strains on the negative reinforcement of connection E_{4R} of the continuous slab specimen 142

Figure 4.39 Steel strains on the negative reinforcement of connection E_{2R} of the continuous slab specimen 142

Figure 4.40 Steel strains on the negative reinforcement of connection E_{1R} of the continuous slab specimen 143

Figure 4.41 Slab deflection on the first test of repaired connection E_{3R} of the continuous slab specimen 144

Figure 4.42 Slab deflection on the second test of repaired connection E_{3R} of the continuous slab specimen 145

Figure 4.43 Slab deflection on the test of repaired connection E_{4R} of the continuous slab specimen 145

Figure 4.44 Slab deflection on the test of repaired connection E_{1R} of the continuous slab specimen 146

Figure 4.45 Slab deflection on the test of repaired connection E_{2R} of the continuous slab specimen 146

Figure 4.46 Column rotations on the tests of connections E_{1R}, E_{2R}, E_{3R} and E_{4R} of the continuous slab specimen 147

Figure 4.47 Crack patterns at the end of the first test of connection C_5; (a) cracks on the tension surface of the slab, (b) Cracks on the bottom slab surface 149

Figure 4.48 Crack patterns at the failure of connection C_5; (a) cracks on the tension surface of the slab, (b) Cracks on the slab free edge 150

Figure 4.49 Crack patterns at the failure of connection C_6; (a) cracks on the tension surface of the slab, (b) cracks on the slab free edge 151

Figure 4.50 Crack patterns at the failure of connection C_7; (a) cracks on the tension surface of the slab, (b) cracks on the slab free edge 151

Figure 4.51 Crack patterns at the failure of connection C_8; (a) cracks on the tension surface of the slab, (b) cracks on the slab free edge 152

Figure 4.52 Steel strain on the test of corner connection C_5 of the continuous slab specimen 154

Figure 4.53 Steel strain on the test of corner connection C_6 of the continuous slab specimen 154

Figure 4.54 Steel strain on the test of corner connection C_7 of the continuous slab specimen 155

Figure 4.55 Steel strain on the test of corner connection C_8 of the continuous slab specimen 155

Figure 4.56 Slab out-of-plane deflections on the test of connection C_6 of the continuous slab specimen 156

Figure 4.57 Slab out-of-plane deflections on the test of connection C_7 of the continuous slab specimen 157

Figure 4.58 Slab out-of-plane deflections on the test of connection C_8 of the continuous slab specimen 157

Figure 4.59 Diagonal column rotation on the tests of connections C_6, C_7 and C_8 of the continuous slab specimen 158

Figure 5.1 Interaction between shear force and moment at edge connections according to ACI 318-99; (a) test of continuous slab and repaired slab; (b) test of isolated slab series I and II 162

Figure 5.2 Interaction between shear force and moment at edge connection according to CSA A23.3-94; (a) test of continuous slab and repaired slab; (b) test of isolated slabs series I and II 163

Figure 5.3 Interaction between shear force and moment at edge connection according to CEB-FIP Model Code 1990; (a) test of continuous slab and repaired slab; (b) test of isolated slab series I and II 166

Figure 5.4 Interaction between shear force and moment based on Moehle's approach (1988) considering the moment at centroid of critical shear section 168

Figure 5.5 Interaction between shear force and moment based on Moehle's approach (1988) considering the moment at column centroid 168

Figure 5.6 Shear-moment interaction of edge column slab connections of the continuous slab for f_{cm} = 42.4 MPa using Regan's approach, the Truss Model and the Strip Model 171

Figure 5.7 Shear-moment interaction of isolated edge column slab connections of series I for f_{cm}=52.8 MPa using Regan's approach, the Truss Model and the Strip Model 172

Figure 5.8 Shear-moment interaction of isolated edge column slab connections of series II for f_{cm}=52.8 MPa using Regan's approach, the Truss Model and the Strip Model 172

Figure 5.9 Effect of load eccentricity (M_{col}/V_u) on shear capacity of edge column slab connections 181

Figure 5.10 Effect of average reinforcement ratio on shear strength according to ACI 318-99 and CSA A23.3-94 codes 182

Figure 5.11 Comparison of out-of-plane deflection between original (E_4) and repaired (E_{4R}) test of connection repairing using normal concrete 185

Figure 5.12 Comparison of out-of-plane deflection between original (E_1) and repaired (E_{1R}) test of connection repairing using expansive (CAH) concrete 185

Figure 6.1 Shear moment interaction of corner column connections according to ACI 318-99 Code 197

Figure 6.2 Shear moment interaction of corner column connections according to CSA A23.3-94 Code 198

Figure 6.3 Shear moment interaction of corner column connections according to CEB-FIP 1990 Model Code 199

Figure 6.4 Shear-moment interaction of corner column slab connections according to Regan's approach (1981) 200

Figure 6.5 Definition of one-way shear perimeters for corner column slab connections 202

Figure 6.6 Effect of steel ratio on strength of corner column slab connections according to the ACI 318-99 and the CSA A23.3-94 207

NOTATION

a_i = cross sectional area of bar i

a_{ri} = a constant for bar i

A_c = area of slab critical section located at $d/2$ from column faces

A_b = area of a single bar

A_s = area of total bar within the slab strip

A_s^+ = area of positive reinforcement within the slab strip

$A^+_{s,total}$ = area of total positive reinforcement

A_{sf} = area of tensile reinforcement passing through the column face perpendicular to slab edge

A_{st} = area of steel parallel to the slab free edge passing through the column faces

α_m = negative moment resistance per unit width provided by the top reinforcement parallel to the slab edge passing through the column

α = angle between the slab free edge and the yield line

b_x = width of slab strip of Desayi and Sheshadri's method

b_w = length of diagonal critical section at corner connections

β_c = the ratio of long side to short side of the column, concentrated load or reaction area ($\beta_c \leq 2$)

β_m = positive moment resistance per unit width provided by the bottom reinforcement parallel to the slab edge passing through the column

c_1 = the length of the column face perpendicular to the bending axis

c_2 = the length of column face parallel to the bending axis

c_{AB} = distance from the centroid of critical shear section to the inner side of critical section

c_{AC} = distance from the centroid of critical shear section to the side AC

c_{BD} = distance from the centroid of critical shear section to the side BD

c_{CD} = distance from the centroid of critical shear section to the side CD

c_t = length of torsion yiels line intersects the slab free edge

c_x = column side face in radial strip

c_y = column side face in spandrel strip

d = effective slab depth

d' = concrete cover

dl = an elementary length of the perimeter (CEB-FIP MC90)

Δ_{bottom} = horizontal deflection of bottom column stub

Δ_{top} = horizontal deflection of top column stub

e = load eccentricity

e_s = eccentricity of the loads acting at the centroid of critical shear section

e_1 = diagonal distance from the centroid of the critical shear section of corner connections to point *B*

e_2 = diagonal distance from the centroid of the critical shear section of corner connections to point *A or D*

$|e|$ = the distance of dl from the moment (M_{sd}) axis (CEB-FIP MC90)

E_s = Modulus elasticity of steel

E_{cm} = average measured modulus elasticity of concrete

ε_{om} = measured average concrete strain at maximum stress

ε_y = yield strain of steel

f'_c = specified compressive strength of concrete cylinders

f_{ck} = characteristic compressive strength of concrete cylinders

f_{cm} = measured average compressive strength of concrete cylinders

$f_{cm.28}$ = measured average compressive strength of concrete cylinders at 28 days

f_{ct} = calculated compressive strength of concrete cylinders at time *t*

f_{cu} = compressive strength of concrete cube (= $1.25 f_{ck}$)

f_y = nominal yield strength of steel

F_{sd} = factored applied shear force at centroid of the shear perimeter (CEB-FIP MC90)

$F_{sd.ef}$ = the enhanced punching load to allow the effect of an eventual moment transfer (CEB-FIP MC90)

g_x = distance from the column centroid to the centroid of critical section in *X* direction

g_y = distance from the column centroid to the centroid of critical section in *Y* direction

γ_{cm} = a partial safety factor in CEB-FIP MC90 (= *1.5*)

γ_f = a fraction of unbalanced moment transferred by flexure

γ_m = a partial safety factor in BS 8110-85 (= *1.25*)

γ_v = a fraction of unbalanced moment transferred by shear

γ_{vx} = a fraction of unbalanced moment about principal axis X transferred by shear

γ_{vy} = a fraction of unbalanced moment about principal axis Y transferred by shear

h = slab thickness

I_x = moment area of the assumed critical section about principal axis X

I_y = moment area of the assumed critical section about principal axis Y

J_c = property of assumed critical section analogous to the polar inertia

J_x = polar moment inertia about X axis

J_y = polar moment inertia about Y axis

K = coefficient determining a fraction of M_{sd} resisted by shear stresses (CEB-FIP MC90)

K_c = a constant in the expression for bending resistance, relating to compressive stress in concrete

K_s = a constant in the expression for bending resistance, relating to vertical shear stress

ξ = size effect

l = the subscript refers to perimeter u_l (CEB-FIP MC90)

l_x = length of projection of critical section onto the principal axis X

l_y = length of projection of critical section onto the principal axis Y

λ = concrete density factor (*1* for normal weight, *0.85* for semi light weight)

m = negative moment resistance per unit width provided by the top reinforcement perpendicular to the free edge on either side of the column

ml = moment resistance per unit width provided by the reinforcement perpendicular to the slab edge

mll = moment resistance per unit width provided by the reinforcement parallel to the slab edge

M_{ACI} = unbalanced moment at centroid of *ACI 318-99* critical shear section

M_{BS} = unbalanced moment at centroid of *BS 8110-85* critical shear section

M_{CEB} = unbalanced moment at centroid of *CEB-FIP MC90* critical shear section

M_{CSA} = unbalanced moment at centroid of *CSA A23.3-94* critical shear section

M_{col} = moment capacity of connections at column centroid

M_f = flexural moment provide by the top reinforcement perpendicular to slab edge passing through the column

M_{flex} = flexural capacity of connections

M_{neg} = moment capacity near the support

M_o = bending moment capacity in the absence of shear force

M_p = predicted moment capacity of the connection

M_{pos} = moment capacity near the line of zero shear

M_s = applied moment at the centroid of critical shear section

M_{strip} = total moment of the slab strips

M_{sd} = factored applied unbalanced moment at the centroid shear perimeter (CEB-FIP MC90)

M_{sx}^- = negative moment provided by top reinforcement within radial strip

M_{sx}^+ = positive moment at the remote end of radial strip

M_{sy}^- = negative moment provided by top reinforcement within spandrel strips

M_{sy}^+ = positive moment at the remote end of spandrel strips

M_{tr} = torsion resistance provided by column slab interfaces perpendicular to the slab edge

M_t = design factored moment transferred to the column (BS 8110-85)

M_{tc} = torsion along side face of the column

M_{tx} = torsion along side face of radial strip

M_{ty} = torsion along side face of spandrel strips

M^*_{test} = normalized moment capacity

M_u = ultimate failure moment

M_{ux} = unbalanced moment about a principal axis X

M_{uy} = unbalanced moment about a principal axis Y

n = number of slab column interfaces where torsion resistance is developed

P_x = load transferred through interior radial strip

P_y = load transferred through spandrel strips

P_{strip} = punching shear strength of the slab strips

ρ = reinforcement ratio associated to A_{sf} within the column width

ρ_{avg} = average reinforcement ratio of steel parallel and perpendicular to the slab edge

ρ_l = ratio of reinforcement perpendicular to the free edge

ρ_{neg} = reinforcement ratio in the slab strip near the supports

ρ_{pos} = reinforcement ratio in the slab strip near the line of zero shear

ρ_t = ratio of reinforcement parallel to the free edge

ϕ = a safety factor of ACI 318-99 (= *0.85* for shear)

ϕ_c = concrete partial safety factor of CSA A23.3-94 (= *0.6*)

Φ = diameter of steel

s_i = tributary spacing of bar *i*

Σ_o = sum of perimeters of top or bottom bars, whichever is the smaller (slab reinforcement passing through column side normal to the moment plane)

T = torque

Ti = tensile force in bar *i*

θ_c = rotation between two sections of slab computed from concrete strain, in plane perpendicular to neutral axis of failure surface

θ_{col} = column rotation (radian)

θ_i = angle between bar *i* and concrete compressive strut *i*

θ_s = rotation of section of slab computed from steel strain, in plane perpendicular to neutral axis of failure surface

τ_{sd} = factored applied shear stress according to CEB-FIP MC90

u = length of the critical section taken at *1.5d* from the column faces (BS 8110-85)

u_o = perimeter of square column section or the same cross sectional area

u_1 = length of critical shear section taken at *2d* from column faces (CEB-FIP MC90)

u_1^* = length of reduced critical shear section (CEB-FIP MC90)

v = nominal shear stress

v_A = shear stress at critical shear section at point *A*

v_{aci} = shear stress resistance according to ACI Code

v_B = shear stress at critical shear section at point *B*

v_{bs} = shear stress resistance according to BS 8110-85

v_c = shear stress provided by concrete

v_{ceb} = shear stress resistance according to CEB-FIP MC90

v_{csa} = shear stress resistance according to CSA Code

v_D = shear stress at critical shear section at point *D*

v_{gdr} = shear stress resistance according to Gardner's approach

v_{max} = maximum shear stress allowed by the codes (ACI 318-99 or CSA A 23.3-94)

v_{shf} = shear stress resistance according to Sherif's approach

v_u = shear stress at failure

v_{u1} = shear stress at failure according to CEB-FIP Method-1 and Gardner's Method-1

v_{u2} = shear stress at failure according to CEB-FIP Method-2 and Gardner's Method-2

v_{test} = shear stress calculated from test result

v_{pred} = predicted shear stress according to alternative approaches or the codes

V_c = shear stress at critical shear section

V_{col} = shear capacity of connection measured at column centroid

V_{eff} = design effective shear force

V_{flex} = shear capacity of connections fail in bending

V_o = shear capacity in the absence of moments

V_p = predicted shear force

V_t = design shear force (BS 8110-85)

V^*_{test} = normalized shear capacity

w_x = bond model loading term from one adjacent quadrant of plate in X direction

w_y = bond model loading term from one adjacent quadrant of plate in Y direction

w = equivalent load on the strip per unit length

x = length of the side of perimeter parallel to the axis of bending (BS 8110-85)

X_{eg} = distance from column centroid to the centroid of critical shear section (Sherif's approach)

z = moment arm of concrete section taken as $0.9d$

Z = lever arm of two equal horizontal applied loads

CHAPTER 1
INTRODUCTION

1.1 GENERAL

Flat-plate structures are structural systems consisting of plates with uniform thickness supported directly on columns without spandrel beams or column capitals in the column regions. Flat-plate structures are used widely in many countries for medium height, multistory, commercial and residential buildings. The structural system is preferred because no spandrel beams or column capitals are required ensuring a minimum storey height and the structure becomes more economical. Construction is greatly simplified by using flying forms that are easily moved as a unit from one floor to other floors reducing construction time and labor costs. In addition, the plain bottom slab surface facilitates installing electrical and mechanical devices. The simplifications associated with both the structural form, and the technology required in their construction, is unfortunately accompanied by some difficulties in analysis and design in ensuring safety and serviceability when compared to the traditional beam-column skeletal structures.

1.2 HISTORY OF TWO-WAY SLABS

Sozen and Seiss (1963) claimed in their review of the history of slabs that the first flat slab structures in the USA were built at the beginning of the 19th century by C.A.P. Turner who constructed the five-story C.A. Bovey building in Minneapolis in 1906. Turner's two-way slabs were called 'mushroom slabs' where a reinforced concrete slab is supported on columns with flared column capitals (Simmonds, 1999). Design of this structure was based on incomplete plate analysis theory so load tests were used to validate the design (MacGregor, 1998; Simmonds, 1999). In the same year, a flat slab structure was built in Switzerland by Maillart.

In 1914, J.R. Nichols computed the total moments in a square slab panel without beams using statics theory. Nichols' analysis invited pro and con discussions. The engineers who opposed Nichols' analysis used slab test results to calculate the moments based on measured steel strains. The measured moments did not satisfy the equilibrium requirement so that they questioned on the validity of Nichols' analysis. However, in 1921, Westergaard and Slater, using laboratory experimental results reported in [66], showed the sum of the actual moments corresponding to measured steel strains were in close agreement to the moments predicted by Nichols' analysis. They also found that the straight-line method to calculate moments from the measured steel strains underestimates the moment due to ignoring the effect of concrete tensile stiffening.

Since that time, a number of semi-empirical design methods have been developed to design flat slab structures and these types of structures have become an interesting topic for study. Many researches have been conducted to investigate the behavior of flat slab structures in both flexure and shear. One of the major problems of the flat-plate structures is their susceptibility to punching shear failures that are characterized as very brittle failures. The first mechanical model of punching shear failure was proposed by Kinnunen and Nylander in 1959. The model predicted the failure mechanism of interior column slab connections subjected to symmetric vertical load.

All building codes, in every country, have provisions to deal with the punching shear problems in flat plate structures. The code provisions have been developed based on empirical approaches on data available in the literature and are only valid for slabs within the limits of the data used. Although researches have been carried out for several decades, there are still areas in which our knowledge is limited. Punching shear failure becomes more complex when unbalanced moments have to be transferred from the slabs to the columns, which cannot be avoided at edge column slab connections and corner column slab connections.

Much research has been carried out to investigate the punching strength of column slab connections subjected to vertical load only and some on combined vertical load and unbalanced moment. Most of the information available in the literature was

developed from tests on isolated slab-column connections. According to Regan et.al. (1979), the boundary conditions of isolated slab-column specimens may not represent the behavior of a similar region in a complete structure in which the lines of contra-flexure vary as the loading changes. In addition, when the specimens transmit unbalanced moments from a slab to a column, there is the more serious problem that an isolated specimen fails if the moment resistance is fully utilized while in a real structure the moment might remain constant while the shear increases with further loading due to the ability of the real structure to distribute internal forces before the ultimate capacity is reached in such a location.

The purposes of the current study are to investigate the punching strength of edge and corner column slab connections of flat plate structures subjected to combined shear force and unbalanced moment perpendicular to the slab free edge and biaxial moment, respectively. Using the test results, the interaction between punching shear and unbalanced moment for edge and corner column connections are investigated and the code provisions are examined.

1.3 PUNCHING SHEAR PHENOMENON

Punching shear under a single concentrated load is similar to punching shear around a column but the consequences of punching shear at a column can be a brittle mode of failure. It happens suddenly without any warning signs. Punching shear failures are usually progressive involving several bays of many stories. The failure usually happens at the slab column connections or under a heavy concentrated load. The form of local shear failure in the vicinity of the columns, or the loaded area, is a truncated cone or pyramid where a portion of the concrete slab around the column is left after failure along the diagonal tension cracks.

There are many cases reported where structures failed due to punching shear. Feld (1964) reported the collapse, due to punching shear during construction, of the east wing of a 4-story concrete office building, Jackson, in Michigan. The failures started from an area about 22 m x 44 m on the second floor, which collapsed onto the first floor which

then collapsed into the cellar. All of the columns remained standing full height after the failure.

Engineering News Record, July 15, 1971, reported the January 1971 collapse of a 16-story reinforced concrete flat slab structure in Boston due to punching shear failure around an interior column (E_5) at the roof slab. Two thirds of the structure starting from the roof to the first floor collapsed completely to the basement. Investigators identified that construction and materials failures at the roof slab as main causes of the structural collapse. Design slab thickness of 222 mm (8.75 in) with concrete compressive strength of 20.7 MPa at 28 days at the slab roof could not be satisfied. Investigators found actual slab thickness was 191 mm (7.5 in) with compressive strength far below 20.7 MPa at the time of collapse (at least 47 days). Detailing errors in column rebars was also found where only six rebars were used instead of eight rebars as required. Furthermore, lack of reshores under the roof slab where the mechanical room floor was located, contributed to the construction failure.

Engineering News Record, March 1973, carried extensive reports on the collapse, during construction, of a 26-story cast-in-place flat plate reinforced concrete apartment building, Bailey's Crossroad, Fairfax, Virginia. Premature reshoring removal between the 22nd and 23rd floors, during the placement of fresh concrete on 24th floor, was blamed for the collapse of the structure. The collapse of the structure split the building into two parts and caused collapse of neighboring 104 x 120 m (340 x 395 ft) post-tensioned parking garage. No information on structural deficiencies was reported except the construction mistake on reshore removal. The temperature was cool which would have delayed concrete strength development.

The most recent disaster due to punching shear failure happened on June 29, 1995 in Seoul, South Korea. An entire wing of a 5-story flat plate structure of the Sampoong Department Store collapsed catastrophically killing over 500 people. There was no extreme weather or seismic activity during the collapse of the structure. The investigative committee concluded that collapse was initiated at the fifth floor around column *5E* due to construction and material deficiencies. Slab effective depth of 360 mm and

compressive concrete strength of 18 MPa were used instead of 410 mm and 21 MPa, respectively, as required in the design. Deficiency on the column dimension was also observed where column diameter was only 600 mm instead of 800 mm used in calculations.

This research project also proposes investigating the strength of repaired edge column slab connections after experiencing punching shear failure.

1.4 PREVIOUS RESEARCH AT THE UNIVERSITY OF OTTAWA

A two bay by two bay flat plate floor was constructed and tested to failure in the University of Ottawa in 1993 by Shao and Gardner, under uniform surface load which was simulated by means of 40 concentrated loads over the slab surface. The interior column (#1) failed at a uniform load w_u = 34.4 kN/m^2 including slab self-weight. The slab was unloaded and eight reshores were provided around the interior column at 127mm from column faces. The slab was reloaded and edge column slab connection (#5) failed at the same uniformly distributed surface load w_u = 34.4 kN/m^2. From this research, it was concluded that, depending on the column or capital size, edge column slab connections subjected to combined shear and moment can fail at a similar surface load to an interior column under shear only.

1.5 RESEARCH OBJECTIVES

The objectives of the research project presented in this thesis can be divided into the following categories:

1. Investigate the punching shear strength of edge and corner column slab connections of reinforced concrete flat plate structures subjected to combined vertical load and unbalanced moments perpendicular to the free edge of the plate.

2. Examine code provisions and alternative approaches for edge and corner column slab connections and compare with the present test results.

3. Examine punching shear–moment transfer interaction under vertical load and unbalanced moment based on code provisions and selected alternative approaches available in the literatures.

4. Investigate the strength of repaired edge column-slab connections and compare the results to the strength of the original column-slab connections.

1.6 SCOPE

In this thesis, the punching shear behavior of the edge and corner column connections of flat plate structures is presented. The information is presented in seven chapters:

Chapter 1 presents general information of flat plate structures including examples of structural collapse due to punching shear failure. Brief description of a previous test of a flat plate structure in the University of Ottawa, objective of the project and scope of thesis are presented.

Chapter 2 presents a literature review of the research related to punching shear with moment transfer (without shear reinforcement) on the edge and corner column connections including the provisions of the American ACI 318-99, Canadian CSA A23.3-94, British BS8110-85 and the CEB-FIP MC90 Codes. A summary of the code predictions of the shear strength of edge and corner column slab connections using the information available from the literature is also presented.

Chapter 3 outlines the experimental program completed by the author. Details of the specimens (a two bay by two bay continuous slab and eight isolated column slab, two sets of four specimens and four repaired edge connections), test setup, instrumentation and test procedures are described.

Chapter 4 presents the test results of edge and corner column slab connections, describes the formation of crack patterns, failure loads, behavior of the slab reinforcement, slab deflections and column rotations during the tests of the connections.

Chapter 5 discusses the results of the edge column slab connection tests. Interaction diagrams between shear and unbalanced moment of the building code provisions and alternative approaches are developed and discussed. Code predicted shear strengths are compared to the strength of the 13-edge connections of the present study. The effect of load eccentricity (M/V) and material properties on the strength of the connections are also discussed.

Chapter 6 contains a discussion on the test results of corner column slab connections. Interaction diagrams and load capacities of the connections calculated using the building code provisions are examined. Alternative approaches proposed in literature are also examined using the test results. The effect of reinforcement ratio on shear strength is presented

Chapter 7 contains summaries and conclusions of the thesis. Recommendations for the future research are suggested.

Appendix A

CHAPTER 2
LITERATURE REVIEW

2.1 EDGE COLUMN WITH UNBALANCED MOMENTS

2.1.1 General

The problems of punching shear strength of reinforced concrete flat-plates at the column slab connections have been investigated extensively during the last three decades due to the increase in development and use of flat plate structures. Most test results available in the literature can be divided into two major groups. Punching shear under symmetric load in which the shear stress can be assumed to be uniformly distributed around a control perimeter and non-symmetric punching shear in which the shear stress on the critical section is not uniform due to the contribution of the unbalanced moment. Unbalanced moment can occur at the interior column slab connections.

Unlike interior columns, the design of edge and corner column slab connections always have to consider the effects of unbalanced moments. Such moments are unavoidable on edge and corner column slab connections. Unbalanced moments are due to span discontinuity at the slab free edge, different span lengths in the adjacent spans for edge column connections, or unbalanced moment due to lateral loads caused by earthquake and wind. In this section, the different approaches from previous research to deal with edge column connections resisting lateral loads are presented briefly, including the interaction diagrams where available. Some selected data from the tests are also discussed by considering their relevancy to the present research.

2.1.2 Unbalanced moment acts in one direction

2.1.2.1 Andersson's approach

Andersson (1966) proposed a theoretical approach to punching at edge column slab connections after having tested three specimens. Andersson observed that the failure

criterion appeared to be similar to that of an interior column. Failure occurred when a limiting tangential compressive stress on the bottom surface of the concrete was reached. In the case of edge column connections, this condition was reached near the inner face of the columns. Andersson determined the nominal shear stress at a distance *d/2* from the inner face of the column. Part of the moment transmitted to the column was assumed to be provided by torsion at the side faces. This portion was taken as $0.4M = 0.4Ve$, where e is the eccentricity of the load from the center of the column. The torsion was assumed to create downward forces near the inner corners of the column and added to the forces created by the direct shear force (V). The resultant forces were assumed to act only on the compression area. Andersson's expression for nominal shear strength was given by:

$$v = \frac{V}{d^2}\left[1 + \frac{0.4e}{2(c_1 - d/3)}\right] \Big/ \left[\frac{c_2}{d} + \frac{c_1}{d}\left(1 + \frac{c_1}{6e}\right) + \frac{\pi}{2}\right] \qquad (2.1)$$

Where:

v = the nominal shear stress

e = the eccentricity of the load from the center of the column

c_1 = the length of the column face perpendicular to the bending axis

c_2 = the length of the column face parallel to the bending axis

d = the effective slab depth

Anderson proposed that the limiting value for shear strength of edge connections should be taken to be the same as for interior connections, however, he suggested that for design purposes, the basic (v) value from equation 2.1 should be used in connection with an eccentricity increased by 20%.

2.1.2.2 Kinnunen's Approach

Kinnunen (1971) extended the application of the Kinnunen and Nylander theory to edge column slab connections. Much of the theoretical work in this report was related to flexure. The treatment of punching shear is similar to Andersson's but the total torque T was calculated from a yield line analysis of the slab.

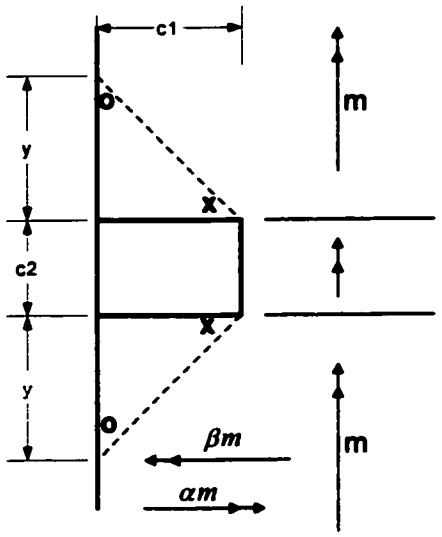

x & o are nodal forces

Figure 2.1 Local yield line at an edge column

With this method of determining the torsion, punching load becomes a function of the arrangement of the reinforcement in the slab. The larger the proportion of the unbalanced moment accommodated by reinforcement passing through the inner face of the column, the higher the punching resistance.

Both Andersson and Kinnunen determined the moment capacities of edge column connections from the yield line theory. The local yield lines correspond to the formation of a hinge between the slab and the column, with its axis at the inner face of the column are shown in Figure 2.1.

The distance from the column faces to the point of intersection of the yield lines and the slab edges, y, is:

$$y = c_1 \sqrt{\alpha_m + \beta_m} \tag{2.2}$$

Where:

α_m = negative moment resistance per unit width provided by the top reinforcement parallel to the edge and passing through the column.

β_m = positive moment resistance per unit width provided by the bottom reinforcement parallel to the free edge and passing through the column.

m = negative moment resistance per unit width provided by the top reinforcement perpendicular to the free edge and on either side of the column.

The sum of the two negative moments to the sides of the column is:

$$2T = 4c_1 m\sqrt{\alpha_m + \beta_m} \tag{2.3}$$

Each torque, T, is twice the moment provided by the steel perpendicular to the edge crossing the relevant yield line. The additional moment is provided by a pair of nodal forces as indicated on Figure 2.1. Each force is equal to $T/2c_1$.

2.1.2.3 The Approach by Regan

Regan (1981) discussed the local strength of edge column slab connections in different terms. The initial point of his approach is the behavior of a slab connected only at the inner face of the edge column as shown in Figure 2.2.

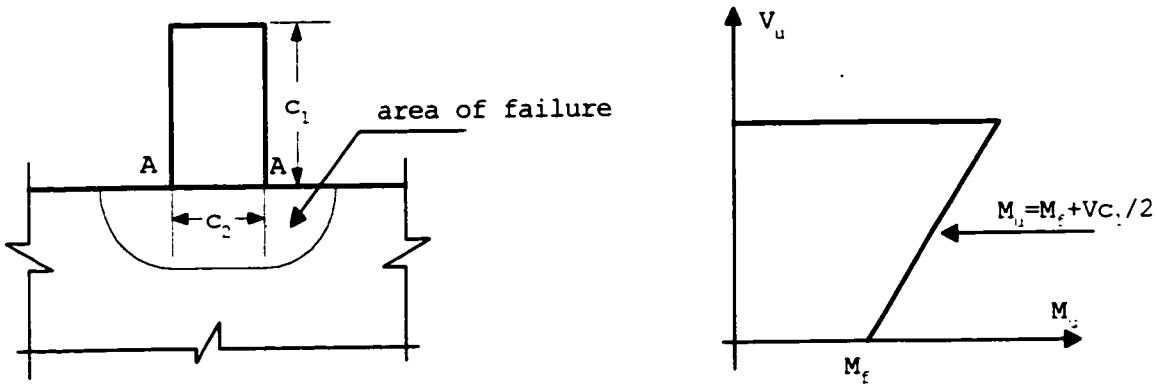

Figure 2.2 Column connected to slab at one face as starting point of Regan's approach.

The pure bending resistance is the ultimate moment at the line AA (M_f). When the shear force is added, provided the failure is still flexural, the ultimate moment about the column center becomes:

$$M_u = M_f + \frac{Vc_1}{2} \tag{2.4}$$

For the common form of edge column slab connections shown in Figure 2.3, the least possible strength (V_1) corresponding to a shear failure is defined by the limiting nominal stress and the area of the surface shaded in Figure 2.3a. The greatest possible shear resistance ($V_2 + V_3$) is given by the same limiting nominal stress acting on the areas shown in Figure 2.3b.

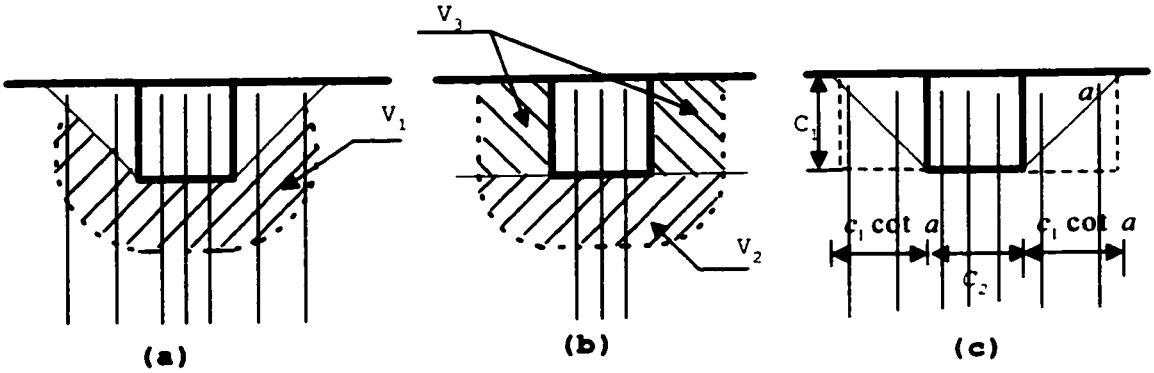

Figure 2.3 Areas resisting shear and active width in flexure

Regan assumed that the pure bending resistance is limited to the ultimate moment provided by the reinforcement perpendicular to the edge crossing the inner face of the column and the two local "yield lines" running from the inner corners to the slab edge as shown in Figure 2.3a. For uniform steel distribution, the angle α is calculated from:

$$\cot\alpha = \sqrt{\frac{m_{11}}{m_1}} \tag{2.5}$$

Where:

m_{11} = moment resistance per unit width provided by the reinforcement parallel to the slab edge.

m_1 = moment resistance per unit width provided by the reinforcement perpendicular to the slab edge.

The interaction diagram between moment and shear is shown in Figure 2.4. It is based on the value of shear to be resisted by the connection in accordance with the three different shear fracture surfaces as shown in Figure 2.3.

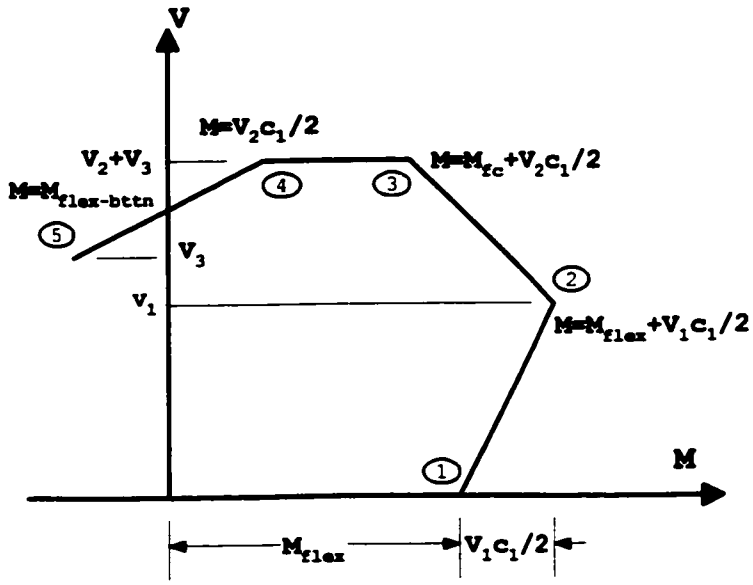

Figure 2.4 Shear moment interaction diagram based on Regan's approach

Each point on the interaction diagram represents a set of internal force combinations due to the applied load. This is represented by the areas shaded in Figure 2.3 and developed as follows:

The pure flexural capacity is calculated from:

$$M_{flex} = M_f + 2c_1\sqrt{m_{11}m_1} \tag{2.6}$$

The maximum moment resistance of the connection is the sum of this flexural strength and $V_1c_1/2$ and occurs simultaneously with shear V_1. For higher shears to be resisted, the moment must be reduced and it is assumed that $(V_2 + V_3)$ is attainable only in the absence of torsion so that:

$$M_u \le M_f + \frac{V_2c_1}{2} \tag{2.7}$$

The shear resistance ($V_2 + V_3$) remains available for flexural moments $0<M<M_f$ or total moments:

$$\frac{V_2c_1}{2} \le M_u \le M_f + \frac{V_2c_1}{2} \tag{2.8}$$

The shear resistance declines as the load develops an outward eccentricity and reaches the value for two "edge beams" (V_3) for a reversed moment corresponding to the capacity of the positive (bottom) reinforcement.

2.1.2.4 Beam Analogy Approach

2.1.2.4.1 Hawkins and Corley (1971)

Beam analogies have been proposed by a number of researchers. In principal, the resistance of each beam to the combined effects of bending, shear and torsion can be estimated by standard methods, although the applicability of code approaches to the side face beams with high torsion loads is still debatable.

Application of the beam analogy for dealing with punching shear–moment transfer on edge column slab connections was described by Hawkins and Corley (1971). The control perimeter adopted was *d/2* from the column faces as in the ACI Code and the CSA Code. For edge column slab connections, the number of limiting strength combinations is only two. These limitations are much less than those for interior column connections, therefore, the application of this method becomes simple.

The two possible modes of failure terms are moment-torsion failure and shear-torsion failure as shown in Figure 2.5. In moment – torsion failure, full flexural capacity is developed at face *BC* and the sides *AB* and *CD* develop ultimate torque. In shear-torsion failure, the critical actions are shear on *BC* and torsion on *AB* and *CD*. The equations to determine shears, moments, and torsion for each case were given by Hawkins and Corley. The basic differences between the two possible mode failures lie in the conditions at the inner face (*BC*), where the situation is critical either for bending or shear. The side faces are always predicted to reach a critical condition under combined actions with shear force (V) and torsion (T).

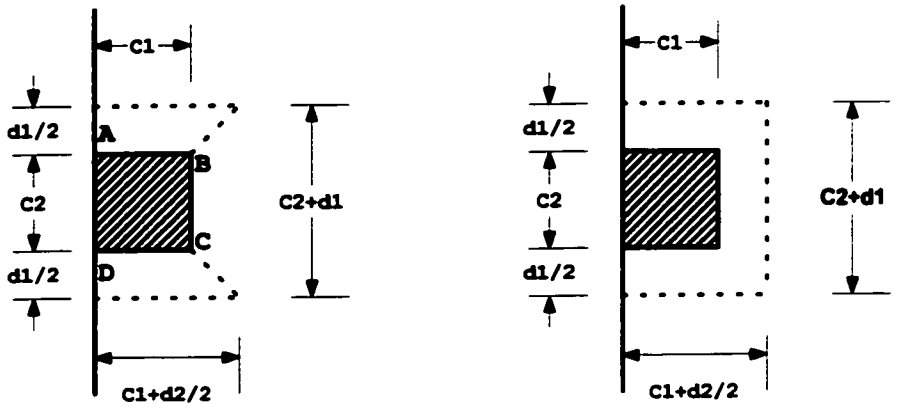

Figure 2.5 Beam analogy critical section for edge column-slab connection

2.1.2.4.2 Stamenkovic and Chapman (1969)

Stamenkovic and Chapman (1969) used beam analogy to develop interaction's expressions for edge column connections. They assumed a width for each beam equal to the width of the column face. Twelve isolated slabs supported by square edge columns were tested. Unbalanced moments perpendicular to the free edge and parallel to the free edge were considered. Bending resistance of the connections was provided by the number of faces parallel to the axis of unbalanced moment. For the case where the bending resistance was provided by one column face only, they limited the capacity of that face to M_{flex} as given by ACI 318-63.

$$M_{flex} = 0.9 A_{sf} f_y d\left(1 - \frac{0.59 \rho f_y}{f'_c}\right) \tag{2.9}$$

Where A_{sf} is the area of the tensile reinforcement passing through the column face perpendicular to moment plane, ρ is the reinforcement ratio associated to A_{sf} within the column width, d is slab effective depth, f_y and f'_c are the steel yield stress and concrete cylinder compressive stress, respectively.

For the case where the bending resistance was provided by two column faces i.e. internal column connection and edge column connection subjected to unbalanced

moment parallel to free edge, they derived the following expression for the combined capacity of the two faces.

$$M_{flex} = K_c 0.85 f_c' c_2 \left(\frac{h}{2}\right)^2 + 0.1 f_c' \Sigma_o c_1 (d - d') + K_s 0.85 f_c' c_2 d c_1 \qquad (2.10)$$

Where K_c and K_s are constants determined from experiment. Based on their test results they concluded that for an edge connection transferring unbalanced moment parallel to the free edge K_c is *0.8* and K_s is *0.07*. Σ_o is the sum of the perimeters of the top or bottom bars passing through the column, whichever is the smaller.

For the beam section in torsion, they used the shear-friction concept to develop the expression for torsional resistance. They assumed that at failure, the shear stress is uniform and friction develops at the face of a crack, the friction force depending on the contact pressure developed by the tensile force in the reinforcement. Assuming the reinforcement yields, the torsional resistance at the column head was expressed as:

$$M_t = 0.5 n k_t' \frac{A_{st} f_y}{bd} d^2 \left(c_1 - \frac{d}{3}\right) \leq 0.4 f'c \qquad (2.11)$$

Where n is the number of interfaces at which torsional resistance is developed, k_t' is a friction coefficient which was determined from the experiments. A_{st} is the area of steel passing through the column-slab interface for this beam; f_y is the steel yield stress.

The interaction diagram of the edge-column slab connection transferring an unbalanced moment vector parallel to the free edge was represented as a quarter circle with the center at the origin and a radius equal to unity as shown in Figure 2.6 and best agreement was obtained with the interaction formula as follows:

$$\left(\frac{V}{V_o}\right)^2 + \left(\frac{M}{M_{flex} + M_{tr}}\right)^2 = 1 \qquad (2.12)$$

Where M_{tr} is calculated from Equation (2.11) for $n = 2$ and V_o is calculated from Equation (2.13), which is originally for interior column, multiplied by the ratio of the edge column critical section to the interior column critical section taken at d from the column faces.

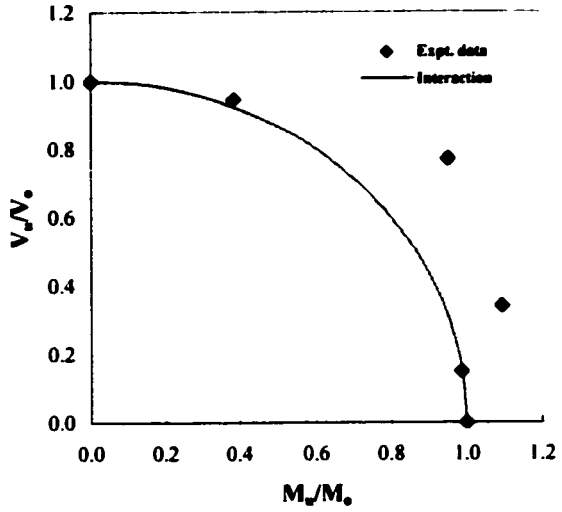

Figure 2.6 Interaction curve-edge 127mm(5 in) square column with normal moment

For square column, V_o is given by:

$$V_o = \left(\frac{3c+4d}{4c+8d}\right)(0.9)\left(\frac{15-0.075\frac{c}{d}}{1+5.25\frac{4cd\sqrt{f'_c}}{V_{flex}}}\right) \tag{2.13}$$

Where V_{flex} is shear capacity of edge connections calculated using yield line method.

For edge columns transferring unbalanced moment vector perpendicular to the free edge, the bending resistance is provided by two faces and the torsional resistance is provided by one face only. The interaction diagram obtained based on test results was represented by a straight line as shown in Figure 2.7. This interaction is similar to the interaction obtained for interior column-slab connections.

The interaction diagram for this connection is represented by the linear equation shown below:

$$\frac{V}{V_o} + \frac{M}{M_{flex} + M_{tr}} = 1 \tag{2.14}$$

Where V_o is determined from Eq.(2.13), M_{flex} from Eq.(2.9) and M_{tr} from Eq.(2.11) with n equal to unity.

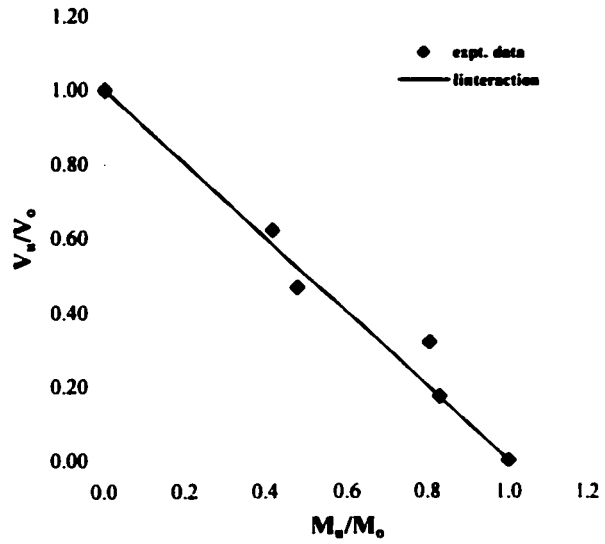

Figure 2.7 Interaction curve-edge 127 mm (5 in) square column with tangential moment

The differences in the interaction diagram between connections transferring unbalanced moments perpendicular and parallel to the free edge is due to the number of slab column interfaces that contribute bending resistance and torsional resistance. For unbalanced moment parallel to free edge, two concrete stress blocks are present while for unbalanced moment perpendicular to free edge, bending resistance is only provided by a single stress block. When vertical and horizontal loads act simultaneously, less interaction is obtained, as the horizontal loads do not produce vertical shear on the bending faces.

For design, the shear and moments are usually expressed in terms of the values on the centroidal axis of the column, V_{col} and M_{col}. However, the moment M, in the beam analogies of Stamenkovic, is the resultant of the moments on the ends of the integral beams framing into the connections. Therefore, for design it is necessary to reduce M_{col} by the amount equal to the moment transferred between the column faces and the column axis by shear and to have that moment less than the moment M predicted by the beam analogy. The reduction of the moment was calculated as follows:

$$M = M^{\bullet}_{test} - \frac{c+2d}{3c+4d} V^{\bullet}_{test} . e \qquad (2.15)$$

Where e is the distance of column-slab interface from column centroid to the critical section, which was taken at a distance d from the column perimeter. $M^{\bullet}_{test}$ and $V^{\bullet}_{test}$ are normalized moments and shear forces for the concrete strength at the column centroid.

2.1.2.5 Pöllet's approach (1983)

Pöllet (1983) proposed an approach to determine the strength resistance of edge column connections by distinguishing between two modes of failure; shear failure and moment-torsion failure.

- **Shear Failure**

The shear mode failure for an edge connection subjected to a load with an eccentricity perpendicular to the slab edge is assumed to be as shown in Figure 2.8a and for calculation purposes it is represented by the control perimeter indicated. The loading is expressed in terms of the vertical load V and the moment $M = V.e$ about the centroid of the control perimeter. The moments on the part b_1 and b_2 of the perimeter are assumed proportional to the length of their projections onto the slab edge. Pöllet derived equations for part 1 of the moment shear interaction diagram shown in Figure 2.9 based on the shear failure mode by assuming a plastic distribution of torsional shear stresses over the area $b_2 d$.

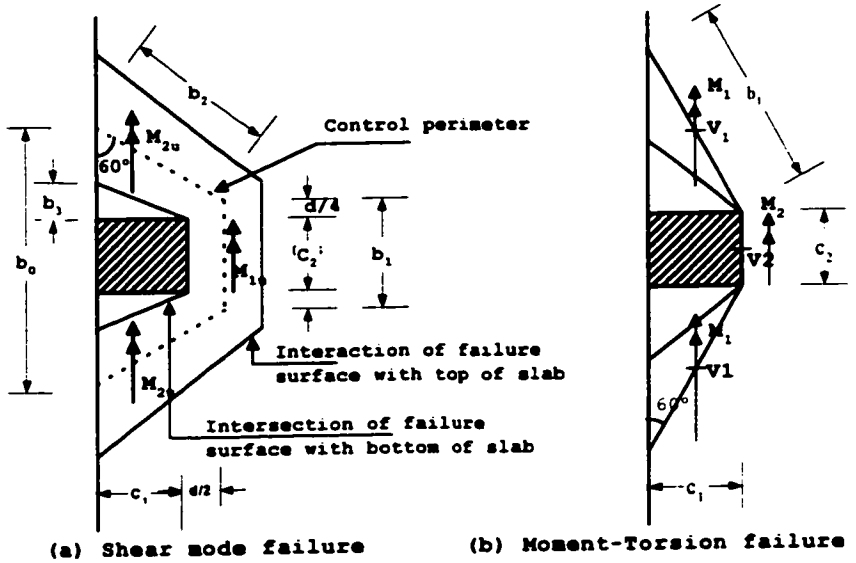

Figure 2.8 Pöllet Approach (1983) for edge column connections

- **Moment-Torsion Failure**

For moment-torsion failure, the failure surface is assumed to be as in Figure 2.8b. The overall equilibrium with a load V_u at an eccentricity $e = M_u/V_u$ is taken with respect to the column center. A finite element analysis was used to derive a coefficient assuming the concrete carries stresses only in compression. The shear stresses are calculated as average values while normal stresses are determined from a rectangular stress block. Pöllet suggested an iterative solution to be applied on the failure criterion to calculate the value of V_u. Part 2 of his interaction diagram, shown in Figure 2.9, reflects moment torsion failure.

The interaction diagram between shear and moment at edge column connection with eccentricity perpendicular to the free edge is given in Figure 2.9. Pollet's approach has some similarities with Regan's approach in the division of failure modes and the prediction of moment failures at resistance below yield line values.

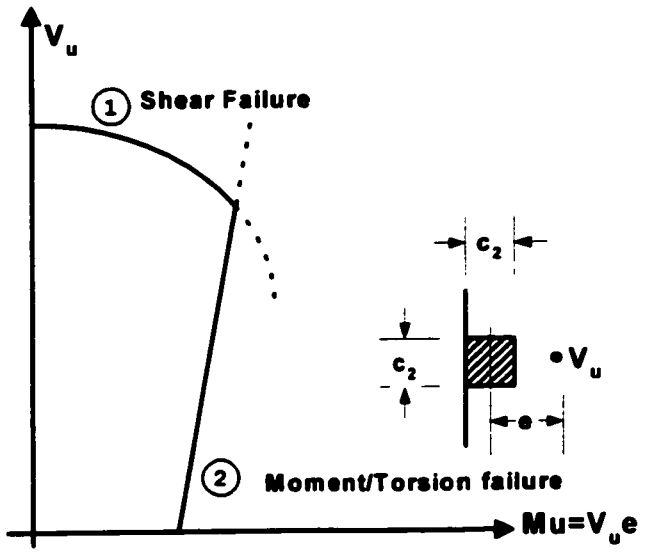

Figure 2.9 Pöllet's typical moment-shear interaction at an edge column

2.1.2.6 Moehle's approach (1988)

Moehle (1988) reviewed selected experimental data on the strength of column slab connections transferring moment perpendicular to the free edge of the slab. Moehle concluded that shear and moment resistance of edge connections are influenced by the slab thickness, column dimensions, material and slab steel ratio in much the same manner as these variables influence the strength of interior connections. However, unlike interior connections, there appears to be less pronounced interaction between shear and moment at the edge connections. Moehle plotted the test data from Stamenkovic and Chapman and a subset of the test series done by Zaghlool in terms of M_u/M_o and V_u/V_o to show the degree of interaction between shear and moment at failure. M_u and V_u are the moment and shear force at failure, respectively. M_o is the failure moment applied to the column in the absence of the applied shear force and V_o is the failure shear force when no moment is applied. Moehle concluded that there is no significant interaction between shear and moment strength. Either the connections fail at its pure shear strength or at its pure flexural strength, whichever is reached first. Thus, the simple square interaction diagram shown in Figure 2.10 was proposed.

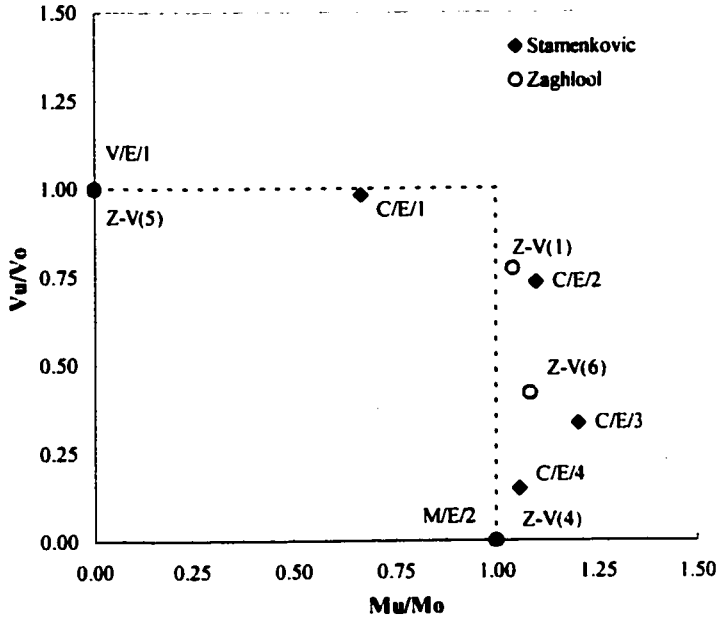

Figure 2.10 Interaction between shear and moment after Moehle (1988).

Moehle also observed that the analysis model incorporated in the ACI 318-99 Code (eccentric shear stress) is excessively conservative and does not correlate well with test results. By reducing the value of γ_v below the specified value in the code, better correlation was found.

It is interesting to note that the loads applied for the test results plotted in the interaction diagram were at the centroid of the column. However, the ACI 318-99 Code approach is based on the forces at the centroid of the critical section.

For design purposes, Moehle suggested that shear and moment act at the centroid of the slab critical section rather than at the centroid of the column cross-section. If the applied shear force (V_u) does not exceed the value $0.75\phi V_o$, where V_o is the shear force resistance calculated using Equation 2.16 as in the ACI Code, then no unbalanced moment is considered to be transferred by shear to the connections.

$$V_o = v_c A_c \tag{2.16}$$

Where:

v_c = the limiting shear stress at the critical section.

$$v_c = 0.17\left(1+\frac{2}{\beta_c}\right)\sqrt{f_c'} \le 0.33\sqrt{f_c'} \text{ (MPa)}$$

A_c = area of the slab critical section located at $d/2$ from the column faces.

The unbalanced moment can be resisted entirely by flexure within the effective width c_2+2c_t as shown in Figure 2.11. Where $c_t = c_1\sqrt{(\rho_t/\rho_l)}$ and ρ_t, ρ_l are the reinforcement ratios for the transverse and longitudinal top reinforcement, respectively.

Moehle's approach was strongly criticized by Dilger and Sherif (1995) as being unsafe to assume that the total unbalanced moment, irrespective of its magnitude, can be resisted by flexural reinforcement provided the direct shear does not exceed $0.75\phi V_o$. It is due to the fact that the flexural moment capacity does not increase linearly with the increase in ρ_{c2+3h} and the yielding of the reinforcement outside the column is independent on the level of the direct shear in the connections.

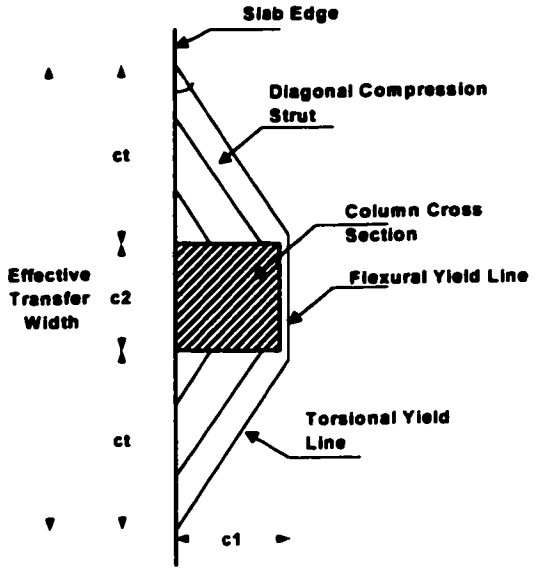

Figure 2.11 Effective width of flexure resistance at edge connection [Moehle, 1988]

In Moehle's interaction, if the moment at the centroid of the critical section (M_s) is used instead of the moment at centroid of the column section (M_u) as shown in Figure 2.12, the degree of interaction between the shear force and the unbalanced moment is much larger. V_o used in the interaction should be the shear force when the moment (M_s) at the centroid of critical section is zero, however, this value is not available from the tests. In this case, V_o is shear force when $M_{applied}$ at the centroid of the column is zero.

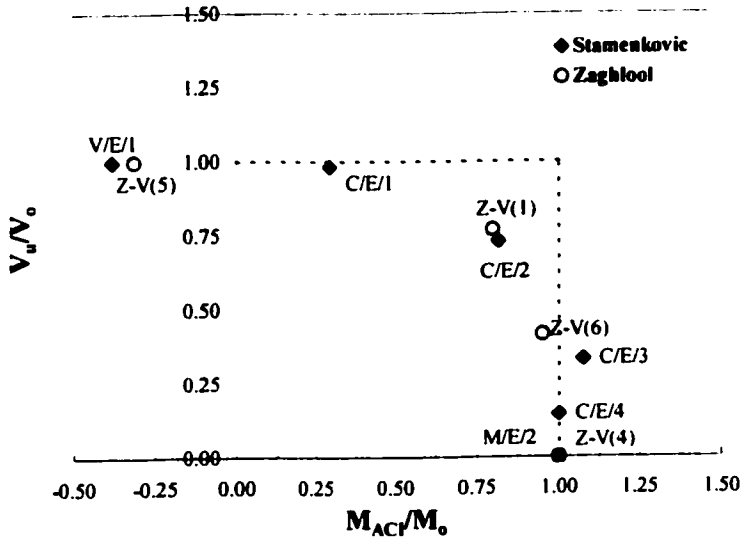

Figure 2.12 Moment-shear force interaction at the centroid of the ACI Code critical shear section.

Ghali and Megally (1995) also criticized Moehle's approach. The focus of their criticisms was based mainly on the fact that assuming no interaction between shear and moment can lead an unsafe design as shown in Figure 2.12.

2.1.2.7 Truss Model Approach

Simmonds and Alexander (1987) extended their truss model, originally developed for interior column slab connections, to deal with edge column connections. The forces involved in failure mechanisms were treated as compression struts and steel tension ties. Two types of compression struts were considered; in-plane, or anchorage struts, which are parallel to the plane of the slab and out-of-plane struts, or shear struts, at an angle to the plane. The primary assumption in this model is that all the reinforcement within the width c_2+2d will always reach yield, and compression failure of the concrete struts does not govern.

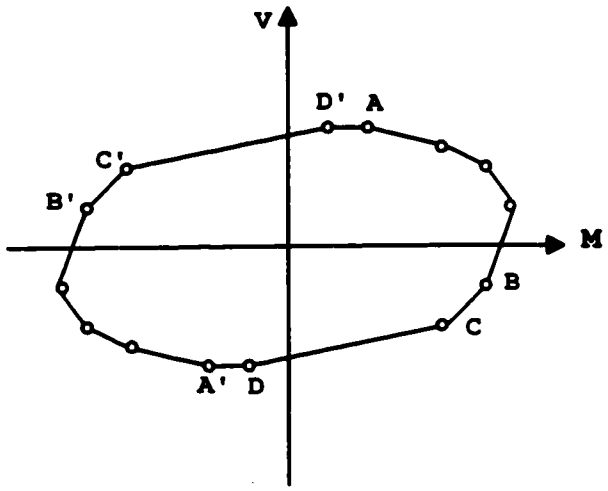

Figure 2.13 Shear-moment interaction diagram for edge column connections according to truss model by Simmonds and Alexander (1987)

They predicted a moment shear interaction for a particular edge column slab connections based on truss model as shown in Figure 2.13. This was achieved by different combinations of the truss model components. By comparing the predicted strength using the truss model with test results available in the literature, Simmonds and Alexander concluded that the model showed excellent agreement with the test results for reinforcement ratios between *0.75%* and *2.5%* within the width c_2+2d, while for ratios

(ρ) greater than *2.5%*, the model tends to overestimate the capacity of the connection. However, reinforcement ratios greater than *2.5%* are unrealistic in practice.

2.1.2.8 Gardner and Shao's Approach

Gardner and Shao (1996) proposed a design expression for calculating the punching shear strength of interior column slab connections of reinforced concrete flat plate structures, by extending the strength enhancement logic of Shehata and Regan (1989) and Shehata (1990). The control perimeter was taken at the periphery of the columns or loaded area. The depth of the compression zone was assumed a function of the tension tie strength ρf_y. To account for the effect of slab thickness, the CEB size effect expression was used. The following equation was derived for non-prestressed slab column connections:

$$V_r = 0.79 u_o d \left(1 + \left(\frac{200}{d}\right)^{0.5}\right)(\rho f_y f_{cm})^{1/3}\left(\frac{d}{4c}\right)^{0.5} \qquad (2.17)$$

Where:

d = effective slab depth

u_o = shear perimeter taken as the perimeter of slab-column interfaces of the equivalent square column

$(d/4c)^{0.5}$ = strength enhancement factor

f_y = yield strength of flexural steel, MPa

f_{cm} = measured average cylinder compressive strength, MPa

ρ = ratio of flexural tensile reinforcement calculated over a width $c+6d$ where c is the column width

Columns with circular and rectangular cross sections were analyzed as a square column with the same cross section area have the side dimension of "c". The coefficients used in the expression were calibrated using a data bank of test results available in the literature.

For combined shear forces and moment transfers, they suggested two alternative methods: using the ACI linear interaction formula with a control perimeter around the loaded area or a simple multiplier. For edge column connections subjected to moment perpendicular to the slab edge, they suggested a single expression independent of the eccentricity of the load: $v_{max} = 1.5\ v_{avg} = 1.5\ V/u_o d$. Using a single multiplier factor implies that the design shear resistance given by equation 2.17 without unbalanced moment ($M_u = 0$) is reduced by a factor *0.67* when unbalanced moment equal to M_{flex} exist at the connections. For corner column connections, however, a multiplier of 2.0 was suggested. The interaction diagram for edge column connection can be drawn as follows:

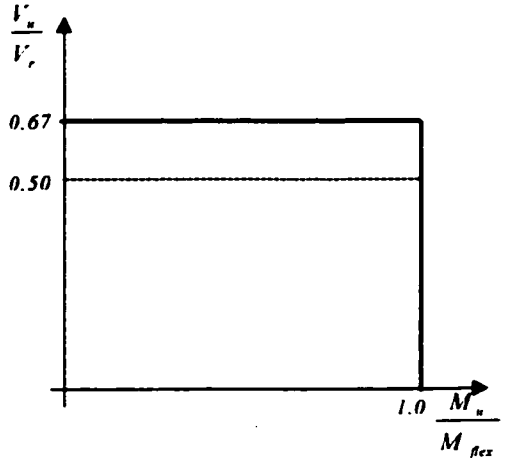

Figure 2.14 Gardner and Shao's interaction diagram using a simple multiplier

2.1.2.9 Elgabry and Ghali (1996)

In the presence of unbalanced moment at the connection, Elgabry and Ghali proposed equation 2.18 to calculate shear stress, which is similar to ACI Code and CSA Code. As in ACI Code, when there is no shear reinforcement, a linear shear stress distribution is taken along the critical section at *½d* from the column faces or loaded area.

$$v = \frac{V}{A_c} \pm \gamma_{vx} \frac{M_{ux} e_y}{I_x} \pm \gamma_{vy} \frac{M_{uy} e_x}{I_y} \qquad (2.18)$$

Instead of using J_x and J_y as in ACI code, Elgabry and Ghali used I_x and I_y which are the second moments of area of the assumed critical section about the centroidal principal axes X and Y; and e_x and e_y are the eccentricities about the principle axis. It is found that using I_x and I_y, the stress distribution has resultants exactly equal to V_u, $(\gamma_v M_u)_x$ and $(\gamma_v M_u)_y$. However, J_x and J_y result in the stress distribution whose resultant components are V_u and moments slightly smaller than $(\gamma_v M_u)_x$ and $(\gamma_v M_u)_y$. Comparing I_x and I_y with J_x and J_y for a rectangle critical section, the difference is of the order of 3%.

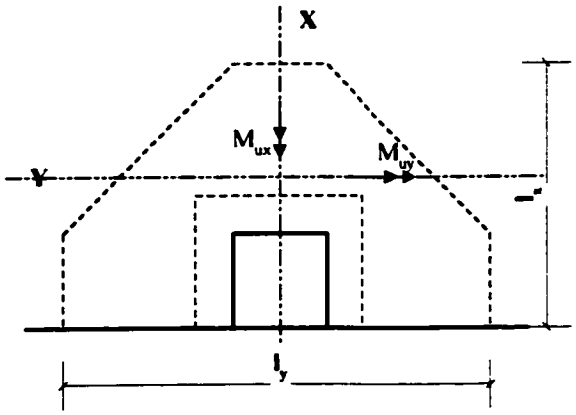

Figure 2.15 Direction of coordinate axes and forces on slab critical section of edge column slab connection (Elgabry and Ghali, 1996)

The fractions of unbalanced moment to be transferred by shear (γ_{vx} and γ_{vy}) are calculated as a function of the ratio l_x/l_y, where l_x and l_y are projections of the critical section onto the principal axes x and y, respectively. When there is no shear reinforcement at the connections, the sides of critical section at ½ d represent l_x and l_y. The value of γ_{vx} and γ_{vy} for edge column slab are given as:

$$\gamma_{vx} = 1 - \frac{1}{1 + \frac{2}{3}\sqrt{\frac{l_y}{l_x}}} \tag{2.19}$$

$$\gamma_{vy} = 1 - \frac{1}{1 + \frac{2}{3}\sqrt{\frac{l_x}{l_y} - 0.2}} \quad \text{when } \frac{l_x}{l_y} \geq 0.2 \tag{2.20}$$

$$\gamma_{vy} = 0 \quad \text{when } \frac{l_x}{l_y} < 0.2 \tag{2.21}$$

The above equations were developed from elastic analysis. The reduction factor of 0.2 from l_x/l_y for γ_{vy} was introduced to account for nonlinear behavior based on experimental data (Ghali and Megally, 1996)

2.1.2.10 Sherif and Dilger's approach (1995)

Sherif and Dilger proposed a modified linear shear stress distribution model. The model is similar to the ACI Code and the CSA Code, however, the value of the portion,γ_v, of the unbalanced moment, which has to be resisted by shear, is changed slightly and calculated as:

$$\gamma_v = 1 - \frac{M_{flex}}{M_s} \tag{2.22}$$

Where: M_{flex} is the moment resisted by flexure at the shear critical section.

M_s is the applied moment at the centroid of the shear critical section and its magnitude can be calculated as:

$$M_s = M_{c.g\ column} - V.X_{eg} \tag{2.23}$$

X_{eg} is the distance from the centroid of the column to the centroid of the shear critical section. Ms_{flex} is calculated based on the truss model as shown in Figure 2.16, using the same

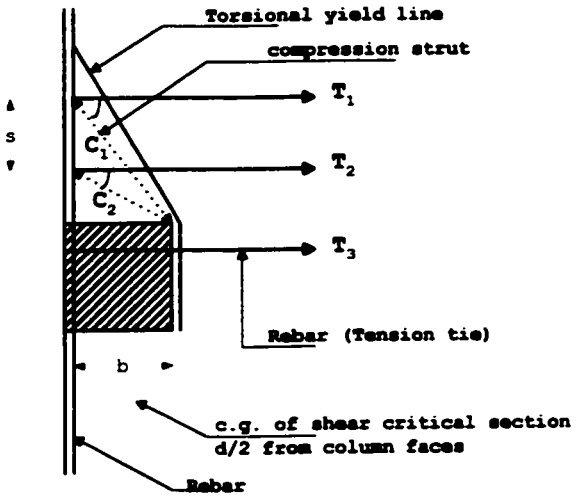

Figure 2.16 Sherif and Dilger's proposed strut and tie model for edge column-slab connection

assumptions as Alexander and Simmonds (1987) and supported by Moe's test results. M_{sflex} is provided by all the bars crossing the yield line that forms an angle α to the free edge. Adopting Regan's approach and the ACI effective width (c_2+$3h$) for resisting the flexural moment, the angle α is calculated as:

$$\tan\alpha = \sqrt{\frac{\rho_t}{\rho_l}} \tag{2.24}$$

Where : ρ_t = the ratio of reinforcement parallel to the free edge

ρ_l = the ratio of reinforcement perpendicular to the free edge

Therefore, the moment M_{sflex} can be calculated as:

$$M_{sflex} = \sum_{i=1}^{n} (T_i a_{ri} z_i) \tag{2.25}$$

Where: T_i = tensile force in bar i

a_{ri} = a constant for bar i

$= 1 - e^{-0.9K}$

n = number of bars within the torsional yield line

z = moment arm of concrete section taken as $0.9d$

The value of K for each bar crossing the assumed yield line was calculated based on Figure 2.16 and given by:

$$K_i = \frac{f_c' s_i (\cos\theta_i)^2 d'}{A_i f_{yt}} \sqrt{\frac{b^2 + s_t^2}{d^2 + s_t^2}} \tag{2.26}$$

Where:

θ_i = angle between bar i and concrete compressive strut i, for bar going through the column, θ_i is Zero

s_i = tributary spacing of bar i

a_i = cross sectional area of bar i

d' = distance from centroid of top reinforcement to the top of slab

The interaction between shear and moment for a particular edge-column slab connection based on modified linear stress distribution is shown in Figure 2.17. They used test results by Stamenkovic (1972) and Zaghlool (1971) to validate the interaction diagram.

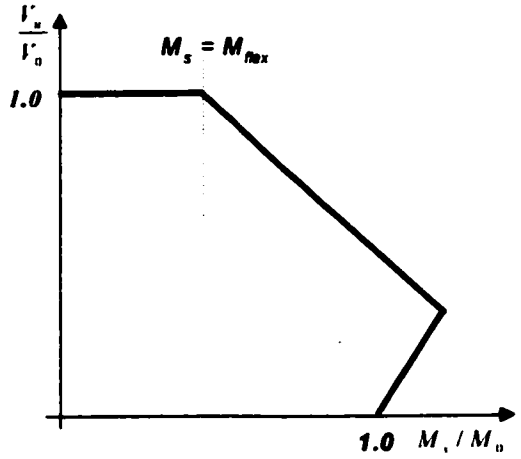

Figure 2.17 Interaction diagram between shear and moment for edge column slab connection according to Sherif proposed model.

The ratio V_u/V_o was plotted against the ratio of M_s/M_o in vertical axis and horizontal axis, respectively. V_u and M_s are the failure shear force and failure moment at the centroid of the assumed critical section, respectively. V_o is the failure shear force when no moment is applied and M_o is the failure moment if no shear force is present. In this case, V_o should be the force where M_s at the centroid of critical section is zero. however, this value was not available from the tests. Therefore, V_o was taken as the shear force with zero moment ($M=0$) applied at the centroid of the column.

If M_s is used instead of M_u in the interaction diagram, the degree of interaction between shear and moment is much higher. They also found that the capacity of an edge column slab connection does not increase proportionally with an increase in the reinforcement ratio within the moment transfer width c_2+3h. Therefore, the proposed model using a linear shear stress distribution, as shown in Figure 2.17, was concluded to be the closest interaction to the experimental results.

It is important to note that Alexander and Simmonds (1991) reexamined their own truss model approach and found that the geometry of the compression strut was a curved

arch rather than a straight line. Based on this, they proposed a new model called the bond model to predict the punching shear strength of interior columns.

2.1.2.11 Strip Model Approach (1998)

The Strip Model was proposed by Afhami, Alexander and Simmonds (1998). The method is a generalization of the bond model proposed by Alexander and Simmonds (1991) for interior connections under concentric load in which only vertical shear is transferred to the columns. As in the bond model, the slab is divided into strips and quadrants. The Strip Model describes the transfer of loads between slab and columns in term of beam action and arching action. Non-proportional behavior of the strips, where not all of the strips are loaded to their nominal capacity, was also recognized in the model. In such behavior, the failure of the connection occurs when the load in any one strip exceeds its ultimate capacity. The share of the load being applied to each strip is determined by considering both equilibrium and compatibility of deformations.

The effective width of the strip in which the non-proportional behavior occurs is greater than the column width. Consequently, the flexural capacity of the strip increases due to the contribution of the bars close to the column and parallel to this strip. In this case, the shear capacity of the strip is also expected to be higher than that of the strip where proportional behavior takes place.

For edge column slab connections, the strips are divided into two spandrel strips and one radial strip that are parallel and perpendicular to the free edge, respectively. Total load to be transferred through the connection, P, and the moment at the centerline of the column, M, consist of three components: (1) negative moment at the column end of the strips, (2) positive moment at the remote end of the strips, (3) torsion along the side faces of the radial strip.

$$P = P_x + 2P_y \tag{2.27}$$

$$M = M_{xx}^{-} + 2M_{tc} + P_x \frac{c_y}{2} \tag{2.28}$$

Where:

P_x, P_y = shear capacity of interior radial strip and spandrel strips, respectively.

M_{tc} = the lesser of two values: torsional moment capacity of the side faces of the column or the flexural capacity associated with the top reinforcement placed perpendicular to the free edge outside the column.

M_{sx}^- = negative moment of the column strips in radial strip.

c_y = column side face in spandrel strip direction

Moment-shear interaction for the capacity of a particular connection subjected to unbalanced moment perpendicular to the free edge was developed by straight lines connecting five distinct points as shown in Figure 2.18. Each point indicates a different degree of interaction between shear and moment.

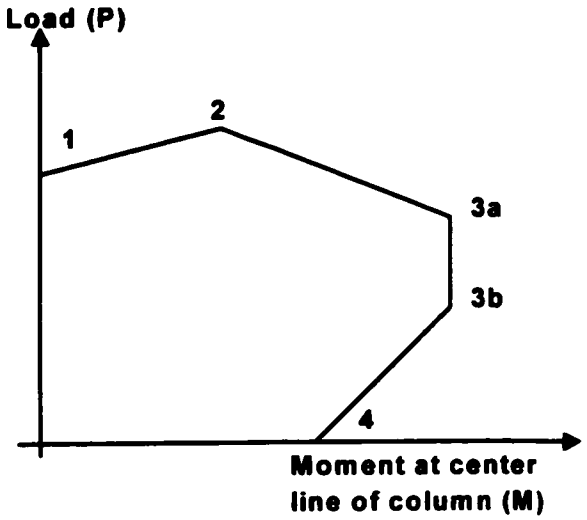

Figure 2.18 Shear moment diagram for edge column slab connections based on Strip Model

Point *4* indicates that the connection resisting pure moment in which $P_4 = 0$. The total moment in the connection is the sum of negative bending moment in radial strip (M_{sx}^-) and torsional moment (M_{tc}).

$$M_4 = M_{sx}^- + 2M_{tc} \tag{2.29}$$

The maximum moment that can be transferred through the edge connections, is indicated as point *3a* and *3b*. In this case, the torsions become significant. The effective width of the spandrel strips is larger than the column width.

The shear is transferred by beam action parallel to the free edge and by arching action normal to the free edge. The only difference between these points is whether the spandrel strips resist the shear or not. At point *3b*, spandrel strips does not carry any shear, while at point *3a*, some shears are transferred through spandrel strips by beam action. The shear force and moment at these points are calculated as follows:

$$P_{3b} = P_x = 2\sqrt{\left(M_{xx}^- + M_{xx}^+ + 2M_{tx}\right)w_x} \tag{2.30}$$

$$M_{3a} = M_{3b} = M_4 + P_{3b}\frac{c_y}{2} \tag{2.31}$$

$$P_{3a} = P_{3b} + 2\beta c_y w \tag{2.32}$$

Where β ranges from 0 to 1

The maximum shear that can be transferred through the connection takes place when all strips reach their nominal capacity. This condition is indicated by point 2 in the interaction diagram. The magnitude of shear force and moment on this point is calculated as:

$$P_2 = 2\sqrt{2\left(M_{sy}^- + M_{sy}^+\right)w_y} + 2\sqrt{\left(M_{xx}^- + M_{xx}^+\right)w_x} \tag{2.33}$$

$$M_2 = M_{xx}^- + c_y\sqrt{\left(M_{xx}^- + M_{xx}^+\right)w_x} \tag{2.34}$$

When unbalanced moment does not exist, the connection only resists shear force as indicated by point 1 in the interaction diagram. In this case, the non-proportional behavior occurs on the radial strip in which the shears are transferred by beam action normal to the free edge and by arching action in the direction parallel to the free edge. The shear capacity of the connection with zero eccentricity of the load is determined as:

$$P_1 = c_x w_y + 2\sqrt{2\left(M_{sy}^- + M_{sy}^+ + M_{ty}\right)w_y} \tag{2.35}$$

To take into account of non-uniform distribution of the reinforcement around the column, the average spacing of the bars was considered within the width c+3h. The

compression block was assumed to have uniform depth within $c+3h$ and the following equations were developed:

$$s_{avg} = \frac{A_b}{A_{s,c+3h}}(c+3h) \tag{2.36}$$

$$A_s = \frac{c}{c+h} A_{s,c+3h} \tag{2.37}$$

Where:

A_b = area of a single bar

$A_{s,c+3h}$ = total area of bar within $c+3h$

The method also considered the case where bottom reinforcement may not yield. In this condition, M_s^+ was taken as the actual moment, M^+ rather than the yield moment, M_y^+.

$$M_s^+ = M^+ \left(\frac{A_s^+}{A_{s,total}^+} \right) \tag{2.38}$$

Where: A_s^+ = area of top reinforcement within the radial strip.

$A_{s,total}^+$ = total area of the positive reinforcement.

2.2 CORNER COLUMN SLAB CONNECTION

2.2.1 General

Many researchers have conducted experiments and analytical work to investigate the behavior of the corner column slab connections, however, it is still unclear how the axial forces interact with the unbalanced moment causing punching failure of corner column slab connections. The following literature review discusses only corner column slab connections subjected to combined vertical force and diagonal bending moments.

2.2.2 Ingvarsson's approach (1977)

Ingvarsson (1977) analyzed shear failure at the corner slab column connection based on the slab action being similar to a diagonal beam. The critical section was taken at *h/2* from the inner corner of the column. The length of the diagonal beam is $b_w = h + \sqrt{2}(c_1 + c_2)$ and a nominal shear stress can be calculated as:

$$v = \frac{V}{h\left(h + \sqrt{2}(c_1 + c_2)\right)} \tag{2.39}$$

Where:

V= applied shear force

h = total slab depth

c_1 and c_2 = column dimensions

Ingvarsson defined the critical shear section and elastic distribution of shear stress on the diagonal perimeter of square corner column slab connections are shown in Figure 2.19a and b, respectively.

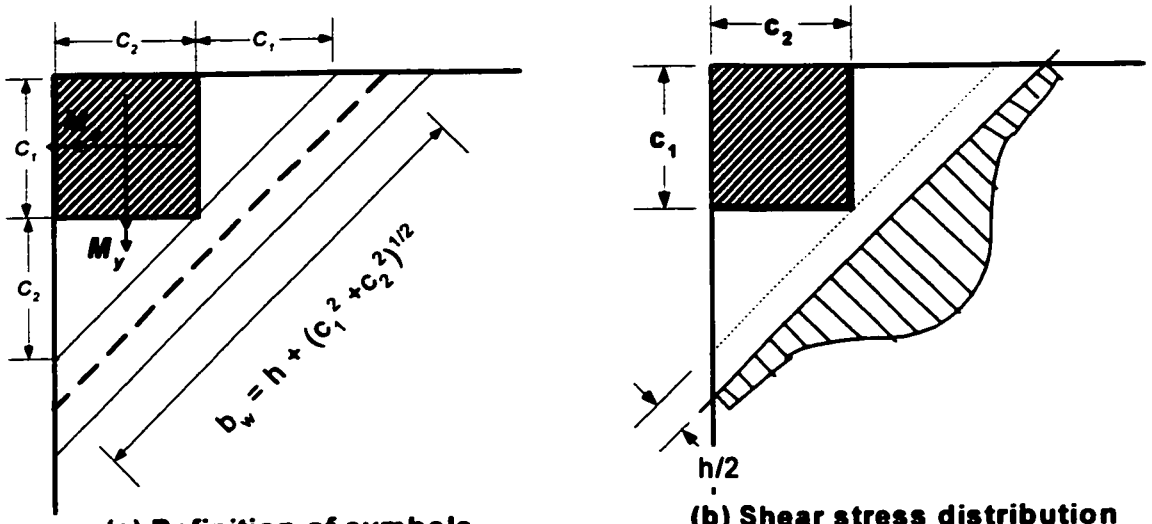

(a) Definition of symbols (b) Shear stress distribution

Figure 2.19 Ingvarsson-definitions of symbols (a) and distribution of shear stress (b) at corner column connections.

On the basis of work on a beam, the ultimate shear stress calculated based on Ingvarsson's approach is:

$$v_u = \eta\xi(0.126 + 2.24\rho)\sqrt{f_c'} \tag{2.40}$$

Where:

ξ = size effect = $1.75\text{-}1.25h \geq 1.0$, with h in meter

η = reduction coefficient = $b_w / \left(b_w + (e_x - e_y) + 0.5(c_1 - c_2)\right)$, with $e_x \geq e_y$ and $c_1 \geq c_2$

ρ = reinforcement ratio = $(A_{sx}+A_{sy})/(b_w h)$

A_{sx}, A_{sy} = the area of reinforcement in X and Y direction, respectively.

f_c' = measured cylinder compressive strength

h = total slab depth

2.2.3 Regan, P.E. (1981)

Regan (1981) treats corner connections similarly to the method for the edge column slab situations described previously. Corner column slab connections subjected to shear forces and biaxial bending develop shear fracture surfaces shown in Figure 2.20.

These shear fracture surfaces are the limiting conditions to develop an interaction diagram.

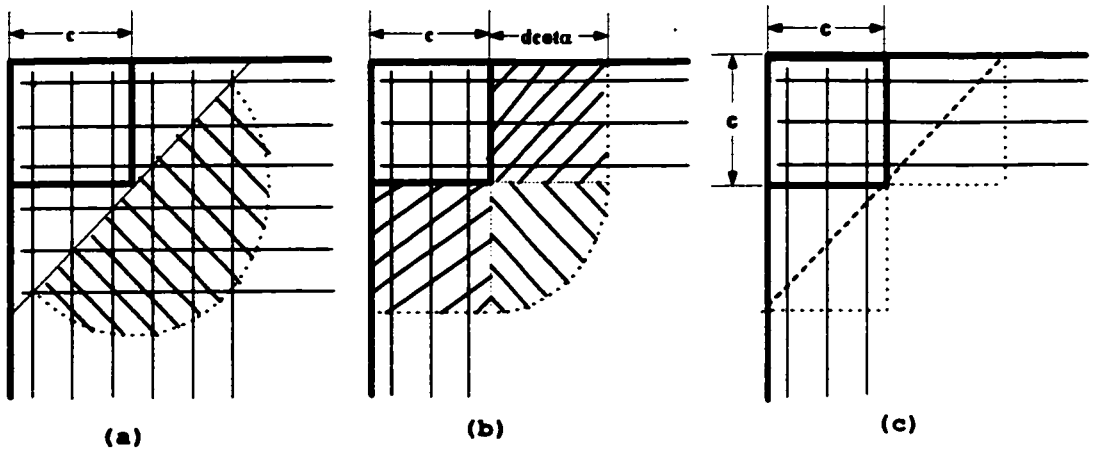

Figure 2.20 Regan's limiting condition for shear force-moment interaction at corner column slab connections

The interaction diagram for corner column slab connections is similar to the interaction diagram in Figure 2.4 for edge column slab connections. The values of V and M for each point in the interaction diagram are calculated based on the limiting conditions shown in Figure 2.20.

If full flexure is developed at the connection, the shear force resistance is provided only by the area bounded by the diagonal line and half circle in front of inner corner of the column (shaded area) as shown in Figure 2.20a. There is no shear developed in the triangles in front of the column faces.

Full shear strength is expected when the shear stress distributes uniformly around the column that may occur only if there is no torsion as shown in Figure 2.20b. The flexure capacity is provided by the negative reinforcement passing through the column faces parallel to the free edges.

The maximum shear stress at the outer corner of the column occurs when the load eccentricity is towards the exterior of the slab. This limiting condition is shown in Figure 2.20c. The shear capacity is provided by the capacity of two imaginary beams and the flexure capacity is provided by the bottom reinforcement crossing the local yield lines connecting the two free edges with the inner corner column.

2.2.4 Zaghlool et.al. (1970, 1973a,b)

Zaghlool (1970, 1973a, 1973b) investigated the behavior of corner column slab connections subjected to axial force and symmetrical biaxial bending moments. The effects of parameters such as *c/d* ratio, slab reinforcement ratio ρ, and *M/V* ratio on the shear strength of the corner slab connection were investigated. Based on observed failures of corner connections during the experiment, an idealized failure mode shape was proposed to develop a theoretical method for the analysis of a corner connection subjected to biaxial bending moment only or combined axial and bending moments.

The theoretical prediction for ultimate shears and moments of a corner connection were based on known material properties, equilibrium and compatibility. Two limiting conditions were assumed to control connection failures.

First, rotational stability is satisfied i.e. $\theta_c=\theta_s$, at an assumed steel stress level below the nominal yield point. The rotations, θ_c and θ_s, between two sections of slab are computed from the concrete strain and the steel strain, respectively, in the plane perpendicular to neutral axis of the failure surface.

Second, stress of tension steel (f_s) and stress of tension steel crossing failure cracks of connection (f_{sp}) reach their yield stress while θ_c is greater that θ_s. When the eccentricity of loading (*M/V*) is small, the failure of connections will be governed by the first case where a sudden shear failure will take place. However, when *M/V* is large, or the connection is subjected to bending only, the second limiting condition will govern and the full yield strength of the connection will be obtained, although the failure may still be accompanied by punching. The application of this theory requires an iterative process to calculate the depth of the concrete compressive zone.

Interaction between biaxial bending moments (*M*) and shear forces (*V*) at the corner column-slab connections was not found to be a straight line as for interior column slab connections. Zaghlool observed that the presence of the shear force does not decrease the ultimate moment capacity of the connections. Zaghlool also concluded that

punching failure of the column through the slab was a secondary phenomenon following the destruction of compressive zone due to the combined action of flexure and shear.

2.2.5 Desayi and Seshadri's approach (1997)

Desayi and Seshadri (1997) proposed a method for computing punching shear strength of corner column slab connection by extending the bond model for interior column connections under concentric load proposed by Alexander and Simmond. The width of the slab strip was taken as the face of the column plus *0.875d* on each side. The shear force transferred to the slab strips is resisted by beam action and arch action along the tangential and radial directions, respectively. The punching shear strength of each slab strip was derived from the equilibrium of the vertical forces and moments. To consider the effect of moment transfer to the connection, in which the punching shear strength decreases with an increase in the moment transfer, a reduction term of ($1 + k_2\, e/b_x$) is included in the expression.

Two different expressions for calculating the strength of the slab strip based on the existence of the torsion are considered. For the strips in which torsion does not exist, the strength of the strip (P_s) is given by:

$$P_s = 1.414\sqrt{M_s(0.166)d\sqrt{f'c}} \tag{2.41}$$

For the strips in which torsion exists, the strength of the strip (P_s) is given by:

$$P_s = \frac{1.414\sqrt{M_s(0.166+0.257)d\sqrt{f'c}}}{1+k_2\frac{e}{b_x}} \tag{2.42}$$

Where:

$M_s = M_{neg} + k_2 M_{pos}$

M_{neg} = moment capacity near the support

$$= \rho_{neg} fyd^2\left(1-\frac{0.59\rho_{neg} fy}{f'c}\right)b_x$$

M_{pos} = moment capacity near the line of zero shear

$$= \rho_{pos} fyd^2 \left(1 - \frac{0.59\rho_{pos} fy}{f'c}\right) b_x$$

ρ_{neg} = reinforcement ratio in the slab strip near the supports

$$= \frac{A_{st}}{b_x d}$$

ρ_{pos} = reinforcement ratio in the slab strips near the line zero shear

$$= \frac{Asb}{b_x d}$$

A_{st} , A_{sb} = total areas of steel within the slab strip near the support and near the line of zero shear, respectively

fy = yield strength of the reinforcement (MPa)

$f'c$ = compressive strength of concrete cylinder (MPa)

b_x = width of the slab strip is equal to the width of column face plus $0.875d$ on each side (mm)

d = effective depth of the slab (mm)

e = load eccentricity (M/V)

$k2$ = a constant determined from the experimental results (= 1)

The punching strength of the slab column connection is the sum of the shear strength of the slab strips that frame into the column.

2.3 CODE PROVISIONS FOR MOMENT TRANSFER

When unbalanced moments exist at slab-column connections, the connection must be designed to transfer moment as well as shear. Moment transfer can occur due to pattern loads, when span lengths of adjacent bays differ, or when the slab column frame has to resist lateral loads. Every code treats this problem in different ways. The following section presents the North American Codes (ACI 318-99 and CSA A23.3-94), the British Code (BS 8110-85) and the CEB Model Code (CEB-FIP MC90) provisions relating to punching shear with moment transfer of the edge and corner column slab connections.

2.3.1 American Code (ACI 318–99)

The ACI 318-99 code considers a critical section to be located at *d/2* from the loaded area or column faces. It is stated in the commentary of the code that the shear stress obtained at location *d/2* is almost independent on the *c/d* (column dimension to effective depth) ratio. The design is based on the inequality equation:

$$v_u < \phi v_c \tag{2.43}$$

Where ϕ is a safety factor and the applied shear stress v_u for connection transferring unbalanced moments is calculated according to equations 2.48 and 2.49 for edge connections. For corner connections, the value of v_u is calculated based on equations 2.50 to 2.52.

The shear resistance of concrete v_c is the smallest of the following three values in S.I. units.

(a) $$v_c = \left(2 + \frac{4}{\beta_c}\right)\frac{\sqrt{f_{ck}}}{12} \qquad \text{(MPa)} \tag{2.44}$$

Where β_c is the ratio of long side to short side of the column, concentrated load or reaction area and should be taken not greater than 2. When β_c is greater than 2, the limiting shear stress $0.333\sqrt{f_{ck}}$ is unconservative. According to ACI-ASCE Committee 426 (1974), when β_c is greater than 2, the actual shear stress on the critical section varies

from a maximum of about $0.333\sqrt{f_{ck}}$ around the corner of the column, down to $0.167\sqrt{f_{ck}}$ or less along the long sides between the two end sections.

(b) $$v_c = \left(\frac{\alpha_s d}{b_o} + 2\right)\frac{\sqrt{f_{ck}}}{12} \quad \text{(MPa)} \tag{2.45}$$

Where α_s is 40 for interior columns, 30 for edge columns, 20 for corner column. The equation takes into account the effect of b_o/d ratio. Tests by Vanderbilt (1972) showed that v_c decreases as the ratio of b_o/d increases.

(c) $$v_c = \frac{1}{3}\sqrt{f_{ck}} \quad \text{(MPa)} \tag{2.46}$$

When gravity load, wind, earthquake or other lateral forces exist in the structure and cause transfer of unbalanced moment M_u to a slab and a column, a portion of this moment $\gamma_v M_u$ is transferred by non uniformed shear stress as shown Figure 2.21 and Figure 2.23.

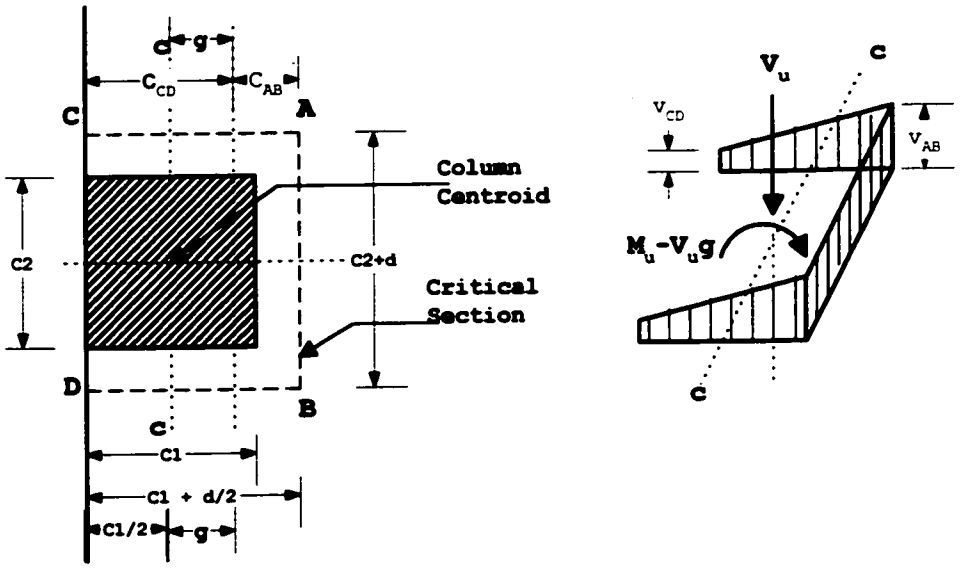

Figure 2.21 Critical shear section and distribution of slab shear stress for edge column connections transferring shear and unbalanced moment of the ACI Code.

The rest of the moment $\gamma_f M_u$ is transferred by flexure (clause 11.12.6.1).

$$\gamma_v = (1 - \gamma_f) \tag{2.47}$$

The factored shear stress is the maximum of the following two equations:

$$v_{AB} = \frac{V_u}{A_c} + \frac{\gamma_v M_s c_{AB}}{J_c} \tag{2.48}$$

$$v_{CD} = \frac{V_u}{A_c} - \frac{\gamma_v M_s c_{CD}}{J_c} \tag{2.49}$$

Where:

c_{AB}, c_{CD} = distance from the centroid of the critical section to the face of the critical section

γ_v = a fraction of unbalanced moment resisted by shear

J = property of assumed critical section analogous to the polar of inertia

A_c = area of critical section.

These parameters are properties of the control perimeter that are different for interior column, edge column and corner column connections. For edge slab column connections, the geometric expressions for critical shear section illustrated Figure 2.21 are given in Appendix A.

Reference 11.49 of the ACI 318–99 states that 60% of unbalanced moment is transferred by flexure and 40% by eccentricity of shear across the perimeter of the critical section. Elgabry (1991) used finite element analysis to investigate the shear distribution. The result of his analysis gave 38% of an unbalanced moment is resisted by flexure, 12% by torsion and 50% by shear.

The non-dimensional interaction between shear force and unbalanced moments at edge column slab connections based on ACI Code 1999 is shown in Figure 2.22. The maximum shear stress on each condition is limited by the least value of the concrete shear resistance as given in equations 2.44 to 2.46.

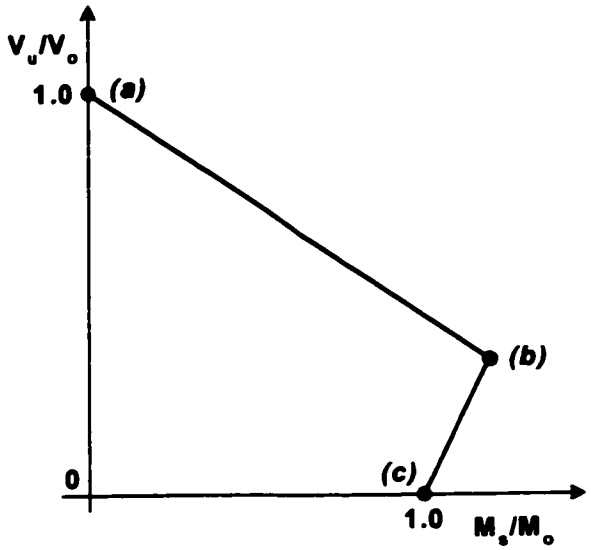

Figure 2.22 Shear moment interaction relationship for edge column connection based on linear shear stress distributions of ACI Code.

The line *a-b* in the diagram represents failure governed by the maximum shear stress (v_{max}) at side AB (v_{AB}) of the critical shear section. The line *b-c* represent the shear stresses v_C and v_D are critical and the failure is governed by the shear stress at *C* and *D* on the slab free edge. The location of point *(b)*, the intersection of Line *a-b* and Line *b-c*, depends on the magnitude of eccentricity, c_{AB} and c_{CD}.

The ACI Code also permits the value of γ_f to be increased to *1.0* provided that V_u at an edge support does not exceed $0.75\phi V_c$. In other word, all of the unbalanced moment shall be resisted by flexure. However, the code limits the reinforcement ratio, ρ, within the effective slab width c_2+3h, to not exceed $0.375\rho_b$.

For corner column connections, the shear stress distribution in the slab when biaxial bending moment is transferred (bending in the *x* and *y* directions) shown in Figure 2.23. If M_{ux} and M_{uy} are the unbalanced bending moments acting at the centroid of the column section in the *x* and *y* directions, the unbalanced bending moments acting at the centroid of the critical section are M_{ux}-$V_u g_x$ and M_{uy}-$V_u g_y$, respectively.

The shear stresses in the slab at point *A*, *B*, and *D* of the critical section are calculated as:

$$v_A = \frac{V_u}{A_c} + \frac{\gamma_{vx}(M_{ux} - V_u g_x)c_{AB}}{J_{cx}} - \frac{\gamma_{vy}(M_{uy} - V_u g_y)c_{AC}}{J_{cy}} \tag{2.50}$$

$$v_B = \frac{V_u}{A_c} + \frac{\gamma_{vx}(M_{ux} - V_u g_x)c_{AB}}{J_{cx}} + \frac{\gamma_{vy}(M_{uy} - V_u g_y)c_{BD}}{J_{cy}} \tag{2.51}$$

$$v_D = \frac{V_u}{A_c} - \frac{\gamma_{vx}(M_{ux} - V_u g_x)c_{CD}}{J_{cx}} + \frac{\gamma_{vy}(M_{uy} - V_u g_y)c_{BD}}{J_{cy}} \tag{2.52}$$

The geometric expression of the critical shear section for corner column slab connections shown in Figure 2.23 are given in Appendix A.

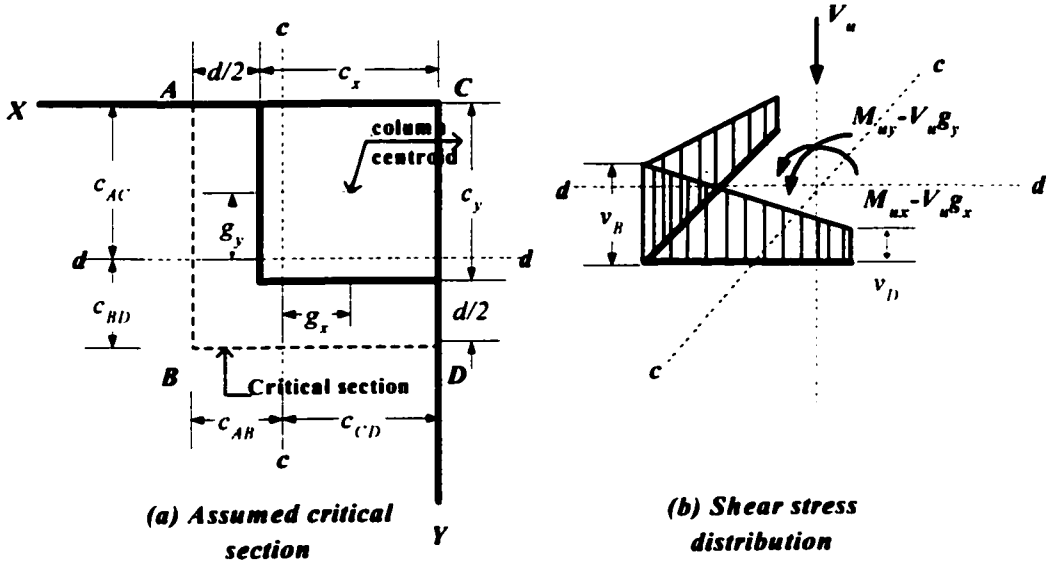

Figure 2.23 Assumed critical section and distribution of slab shear stress for corner column connections transferring shear and unbalanced moment of the ACI Code.

2.3.2 Canadian Code (CSA A23.3-94)

The CSA A23.3-94 code provisions are similar to those of ACI 318-99. The critical section is taken at *d/2* from the faces of the column or loaded area. The maximum shear stress that concrete can resist for two-way shear is limited by the least value of the following equations (*S.I.* units):

(a) $$v_c = \left(1 + \frac{2}{\beta_c}\right) 0.2 \lambda \phi_c \sqrt{f_{ck}} \quad \text{(MPa)} \tag{2.53}$$

Where:

β_c = the ratio of long side to short side of the column, concentrated load, or reaction area.

λ = concrete density factor (1 for normal weight, 0.85 for semi light weight)

ϕ_c = concrete partial safety factor (= 0.6)

(b) $$v_c = \left(\frac{\alpha_s d}{b_o} + 0.2\right) \lambda \phi_c \sqrt{f_{ck}} \quad \text{(MPa)} \tag{2.54}$$

Where:

α_s = 4 for interior columns

α_s = 3 for edge columns

(c) $$v_c = 0.4 \lambda \phi_c \sqrt{f_{ck}} \quad \text{(MPa)} \tag{2.55}$$

The coefficients in Equations 2.53, 2.54 and 2.55 are 21% larger than those in Equations 2.44, 2.45 and 2.46 of the ACI code. The CSA coefficients were increased to offset the decrease in v_c which resulted from using a material partial safety factor (ϕ_c) equal to 0.60.

When unbalanced moment exists at the connection, the equations given in the Canadian code are similar to the ACI code; however, the Canadian code does not allow the reduction in the value of γ_v.

2.3.3 British Code (BS 8110-85)

The British code uses a rectangular critical section at *1.5d* from the loaded area for both circular and rectangular loaded areas. The design shear stress due to a shear force V is calculated as:

$$v = \frac{V}{u.d} \leq v_c \tag{2.56}$$

Where u is the perimeter of the critical section, v_c is the shear capacity of the concrete and given as:

$$v_c = \frac{0.79}{\gamma_m}(100\rho)^{\frac{1}{3}}\left(\frac{400}{d}\right)^{\frac{1}{4}}\left(\frac{f_{cu}}{25}\right)^{\frac{1}{3}} \tag{2.57}$$

Where: γ_m = a partial safety factor (=1.25)

ρ = $(\rho_x+\rho_y)/2$ and calculated for a width equal to (c_2+3d) or $(c_1+1.5d)$

(100ρ) should not be taken greater than 3.

$(400/d)$ should not be taken less than 1.

f_{cu} = characteristic cube concrete strength ($f_{cu} \approx 1.25\, f_{ck}$) and should not be taken less than 25 MPa and not greater than 40 MPa.

To accomodate unbalanced moments at an interior column connection, which have to be transferred between the slab and the column, the design effective shear force V_{eff} should be taken as:

$$V_{eff} = V_t\left(1 + \frac{1.5M_t}{V_t x}\right) \tag{2.58}$$

Where x is the length of the side of the perimeter parallel to the axis of bending. V_t and M_t are the design factored shear force and moment transferred to the column, respectively.

In absence of calculations, the code requires the calculated shear force to be increased to $1.15\ V_t$ for internal columns in braced structures with approximately equal spans; where V_t is calculated by assuming the maximum design load applied to all panels adjacent to the column considered.

For corner and edge column connections where bending moment about an axis parallel to the free edge is being considered, the design effective shear force can be taken as:

$$V_{eff} = 1.25\ V_t \tag{2.59}$$

For edge columns in which bending about an axis perpendicular to the free edge is being considered, the design effective shear force should be calculated as:

$$V_{eff} = V_t(1.25 + \frac{1.5M_t}{V_t x}) \tag{2.60}$$

Alternatively, V_{eff} may be taken as 1.4 V_t for approximately equal spans.

2.3.4 CEB Model Code (CEB-FIP MC 1990)

CEB Model Code considers the critical section at *2d* from the periphery of the loaded areas. The applied shear stress at the critical section due to a factor concentrated force, F_{sd}, is calculated as:

$$\tau_{sd} = \frac{F_{sd}}{u_1 d} \tag{2.61}$$

The shear stress resistance of the concrete is given by:

$$\tau_{sd} = 0.12\xi(100\rho f_{ck})^{\frac{1}{3}} \tag{2.62}$$

Where:

τ_{sd} = shear resistance of concrete, MPa

ξ = size effect = $(1+(200/d)^{0.5}$ with d in mm

ρ = flexural reinforcement ratio = $(\rho_x\rho_y)^{1/2}$

γ_{cm} = a partial safety factor (= 1.5)

If the connection transfers an unbalanced moment (M_{sd}) from the slab to a column, the shear stress distribution at a control perimeter *2d* from the column faces is combined with the effect of the shear stress produced by concentrated shear force (F_{sd}) to find the total shear stress distribution.

For an edge column connection, two different approaches can be used to calculate the shear stress (τ_{sd}), using either the full perimeter (Method-1) or uniform shear on the reduced perimeter (Method-2) shown in Figure 2.24.

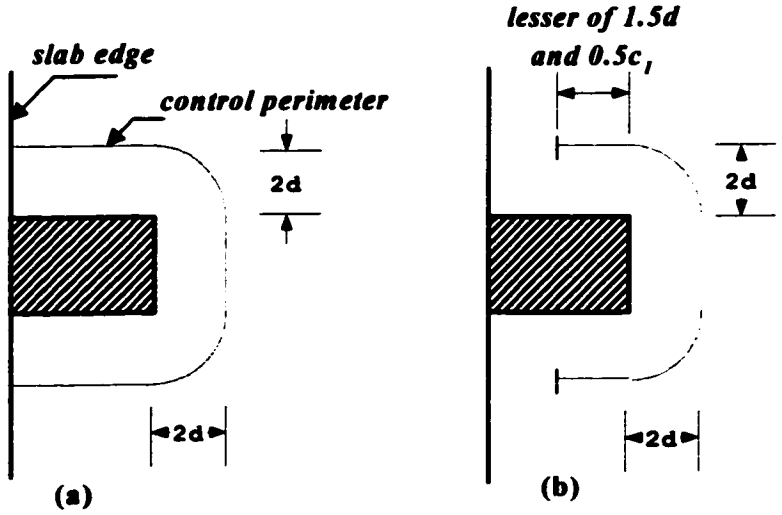

Figure 2.24 CEB-FIP 1990 control perimeters at edge columns: (a) perimeter u_1; (b) perimeter u_1*

When the full control perimeter is considered as shown in Figure 2.24(a), τ_{sd} can be calculated as follows:

$$\tau_{sd} = \frac{F_{sd}}{u_1 d} + \frac{KM_{sd}}{w_1 d} \tag{2.63}$$

Where:

K = coefficient determining a fraction of M_{sd} resisted by shear stresses and is a function of c_1/c_2 and its value is a function of the proportions of the unbalanced moment transmitted by uneven shear on the one hand and by bending and torsion on the other hand. The value of K may be obtained from:

c_1/c_2	0.5	1.0	2.0	3.0
K	0.45	0.6	0.7	0.8

w_1 = a property of the critical section shown in Figure 2.24(a) and given as:

$$w_1 = \int_0^{u1} |e| \, dl \tag{2.64}$$

F_{sd} = applied shear force due to factored loads

M_{sd} = applied unbalanced moment at the critical section due to factored loads

c_1 = columns dimension parallel to the eccentricity of load

c_2 = columns dimension perpendicular to the eccentricity of load

dl = an elementary length of the perimeter

e = the distance of dl from the moment M_{sd} axis

l = the subscript refers to perimeter u_l

d = effective thickness of the slab

Alternatively, when an edge column slab connection is subjected to the load with eccentricity in the direction perpendicular to the free edge, τ_{sd} may be calculated on the assumption of uniform shear on the reduced perimeter u_1* shown on Figure 2.24(b) and calculated as follows:

$$\tau_{sd} = \frac{F_{sd}}{u_1^{\bullet} d} \tag{2.65}$$

For both cases, the maximum shear is calculated as:

$$\tau_{sd} = \frac{F_{sd}}{u_1^{\bullet} d} + \frac{KM_{sd}}{w_1 d} \tag{2.66}$$

Where K may be calculated from the table above with the value of c_1/c_2 replaced by $c_1/2c_2$ and w_1 is calculated for the full perimeter u_1 as in Figure 2.24(a).

CEB-FIP MC90 limited the maximum load for which any connections (including connections with shear reinforcement) may be designed with respect to the column perimeter u_o as:

$$\frac{F_{sd,ef}}{u_o d} \le 0.5 f_{cd2} \tag{2.67}$$

Where:

f_{cd2} $= 0.6(1-f_{ck}/250)f_{cd}$

f_{cd} $= f_{ck}/\gamma_m$

f_{ck} = characteristic concrete cylinder strength

γ_m = a partial reduction factor (=1.5 for concrete)

u_o = length of the periphery of the column or load

$= c_2 + 3d \leq c_x + 2c_y$

$F_{sd.ef}$ = the enhanced punching load to allow the effect of an eventual moment transfer to the column and is determined as:

$$F_{sd.ef} = F_{sd}(1 + K\frac{M_{sd}u_1}{F_{sd}w_1}) \tag{2.68}$$

For corner column connections, the same approach as for edge column connections is used. The control perimeters are shown in Figure 2.25.

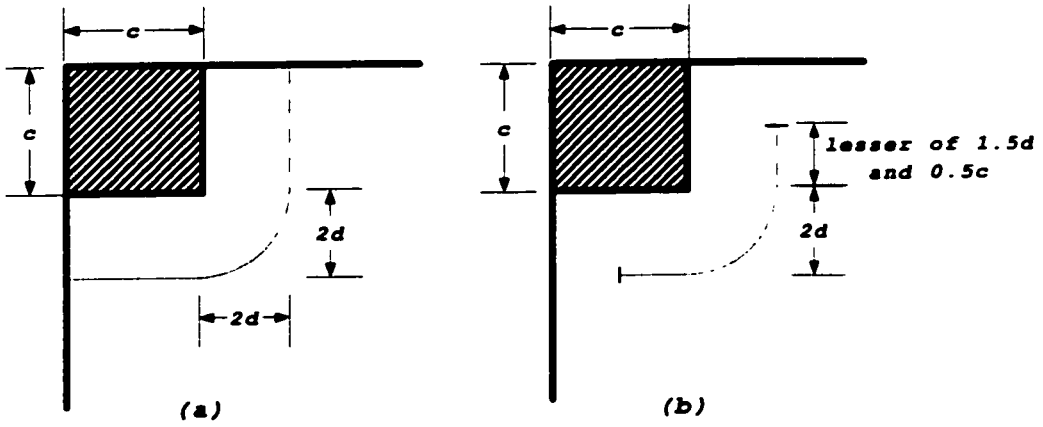

Figure 2.25 CEB-FIP-1990 Control perimeter at corner column: (a) perimeter u_1; (b) perimeter u_1*

The enhanced punching load is to allow for the effects of moment transferred to the corner column. ($F_{sd.ef}$) is equals to the applied factor load and given as:

$$F_{sd.ef} = F_{sd} \tag{2.69}$$

2.4 INFORMATION FROM TESTS ON EDGE CONNECTIONS

Information on the tests of the edge column slab connection available in the literature are used to study the following items:

- Interaction between shear and moment
- Effect of reinforcement ratio ρ on the shear strength
- Effect of load eccentricity on the shear strength

2.4.1 Shear-moment interaction

Test results from Stamenkovic (1972) and Zaghlool (1973) are used to study the degree of interaction between shear and moment on the edge column slab connections of the ACI 318-99, CSA A23.3-94 and CEB-FIP Model Code. The ratio of V_u/V_o is plotted against the M_{code}/M_o ratio as shown in Figure 2.26.

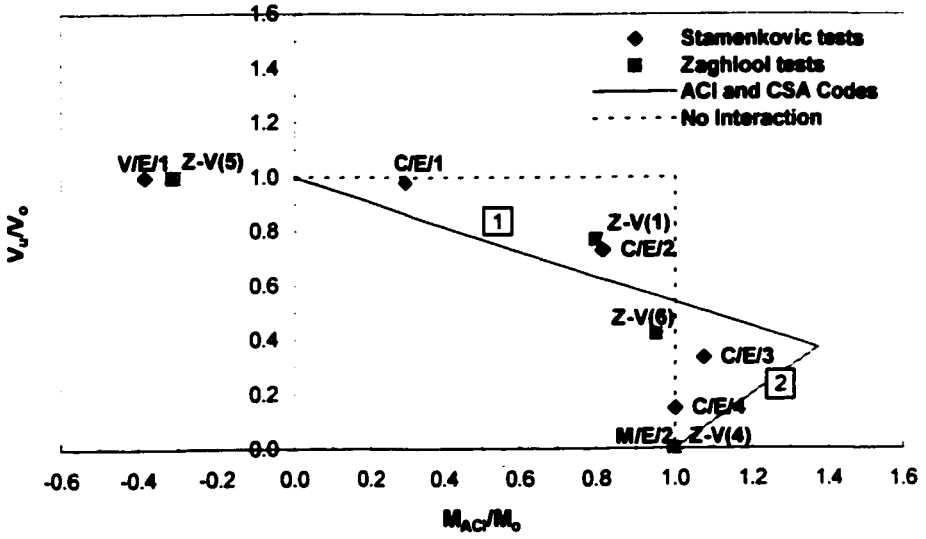

Figure 2.26 Interaction between shear and moment of ACI 318-99 provisions on the edge column slab connections

V_o and M_o should be the forces acting at the centroid of the critical section when the absence of the applied moment and applied shear force at the centroid of the critical section, respectively. However, these data are not available in the literature, therefore, V_o

and M_o are taken as the failure applied shear force and applied moment at the column centroid in the absence of the applied moment and shear force, respectively.

Assuming no interaction as suggested by Moehle (1988) overestimates some of the test results from Stamencovic (1972) and Zaghlool (1973) i.e *C/E/2* and *Z-V(1)*. The trend of the test results indicated a reduction in shear capacity with an increase in applied moment.

ACI and CSA codes assume the interaction between shear and moment consists of two straight lines that are based on the two limiting maximum shear stresses considered. The Line-1 is obtained when the maximum shear stress occurred at the inner side of the critical section and Line-2 represents the maximum shear stress at the two points on the slab free edge. This interaction is derived from the linear stress distribution along the critical section. Line-1 and line-2 meet at one point, which is determined from the magnitudes of c_{AB} and c_{CD}. The ACI and CSA codes underestimate the experimental data having high eccentricity, which cause the maximum stress at the two points along the slab free edge.

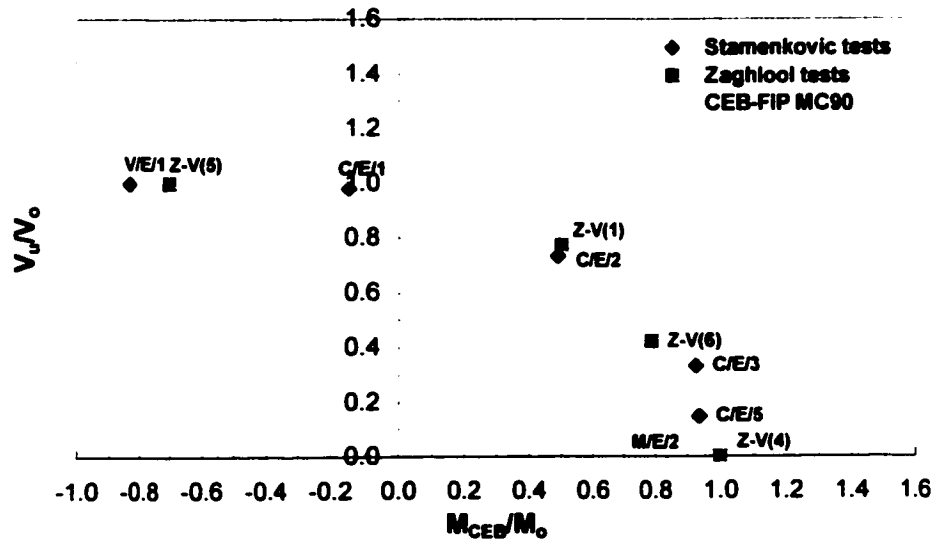

Figure 2.27 Interaction between shear and moment of the CEB-FIP MC90 provisions on the edge column slab connections

The CEB-FIP MC90 interaction between shear force and moment is calculated based on equation 2.63. A linear interaction is obtained as shown in Figure 2.27. The CEB-FIP model code overestimates all of the tests.

2.4.2 Effect of ρ_{c2+3h} on shear stress

Two series of test results from Regan et. al. (1981) and test results from Zaghlool (1973) are used to study the effect of reinforcement ratio within the width c_2+3h parallel to the slab free edge on the shear strength of the connections. The shear stress of the test results is calculated using equations 2.48 and 2.49 whichever is larger. The shear stress is normalized with $\sqrt{f_{cm}}$ to account for the variation in concrete strength, where f_{cm} is the experimental compressive strength of the concrete cylinders. Table 2.1 shows the summary of the calculations.

Table 2.1 Effect of the steel ratio c_2+3h on the shear strength according to ACI or CSA codes

Authors	Test	f_{cm} MPa	ρ_{c2+3h} %	$\rho_{c1+1.5h}$ %	d mm	V_u kN	$M_{u,col}$ kNm	M_s kNm	v_{test} MPa	$\frac{v_{test}}{\sqrt{f_{cm}}}$
Regan (1981)	SE1	44.6	1.20	0.95	98	198	39.5	24.3	2.94	0.49
	SE2	54.6	0.27	0.95	101	192	34.0	19.3	2.69	0.41
Regan (1981)	SE4	34.3	1.04	0.89	98	152	30.5	18.4	2.43	0.46
	SE5	55.2	0.86	0.89	98	164	38.5	25.4	2.84	0.43
	SE6	40.0	0.48	0.89	98	149	27.5	15.6	2.29	0.40
	SE7	49.5	0.71	0.89	98	129	31.7	21.4	2.28	0.36
Zaghlool (1973)	ZV(1)	34.34	1.38	1.06	120.6	215.3	84.6	65.0	3.31	0.63
	ZV(2)	40.48	1.65	1.50	120.6	246.9	93.6	71.1	3.72	0.65
	ZV(3)	38.76	2.19	1.65	120.6	268.2	103.6	79.2	4.09	0.73

In Regan tests (*SE1* and *SE2*), increases in ρ_{c2+3h} from *0.27%* to *1.2 %* increases the failure shear stress about *19.5%*. In test series *SE4*, *SE5*, *SE6* and *SE7*, the shear strength of the test increases by *15%* for an increase in reinforcement ratio from *0.48%* to *1.04%* for specimen *SE6* and *SE4* respectively.

The same trend as in the Regan's results can also be found in Zaghlool experimental results. The steel ratio ρ_{c2+3h} increases about *60%* from *1.38%* (*ZV-1*) to *2.19%* (*ZV-3*) results in the failure shear stress increasing about *24%*. The results of Regan's test together with Zaghlool's test are plotted in Figure 2.28.

It is obvious that the steel ratio affects the shear strength of the test specimens. However, ACI 318-99 and CSA A23.3-94 codes do not include the steel ratio in the shear stress expression that leads to an underestimate of the results.

The British standard (BS 8110-85) and CEB-FIP MC90 recognize and include the effect of reinforcement ratio in the order of cube root in calculating the shear resistance of the concrete.

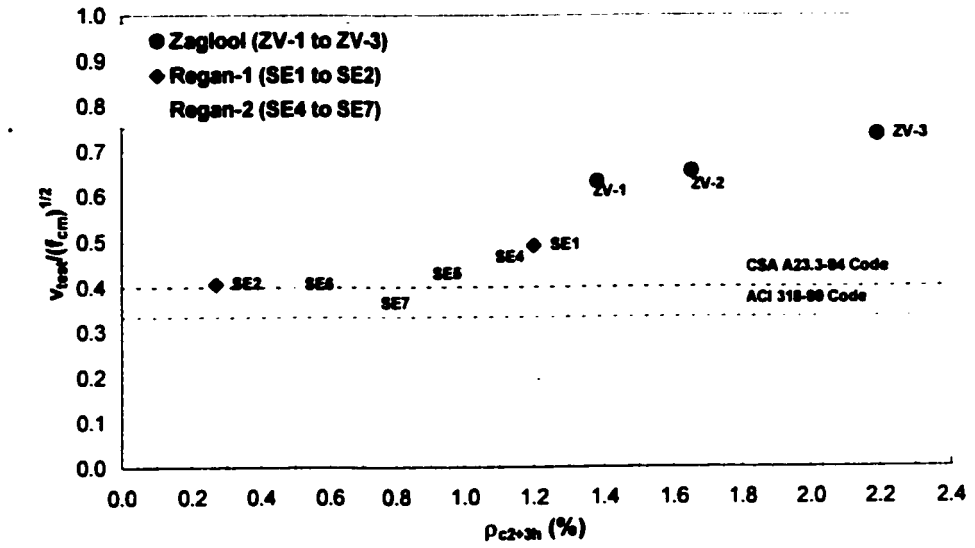

Figure 2.28 Effect of steel ratio on shear strength of edge connections calculated according to ACI and CSA code

A question may arise from here is, does the steel ratio parallel to the slab free edge $\rho_{c1+1.5h}$ have any impacts on the shear strength? Discussion on this issue is described in Chapter 5 of the thesis.

2.4.3 Load eccentricity effects on the shear strength

To study the effect of load eccentricity on the failure shear stress calculated according to ACI and CSA codes, the series of test by Stamenkovic (1972) and the test results by Zaghlool are used. In these two series set of data, the only variable was the ratio M_s/V, where M_s is the moment at the centroid of the critical section.

The failure shear stresses, normalized using $\sqrt{f_{cm}}$, are plotted against the load eccentricity ($e_s = M_s/V_u$) are shown in Figure 2.29, where f_{cm} is experimental compressive strength of concrete cylinders. ACI and CSA shear resistances are also plotted on the same graph with setting any reduction factor equal to unity. It is shown that ACI and CSA codes underestimate the failure shear stress of the tests.

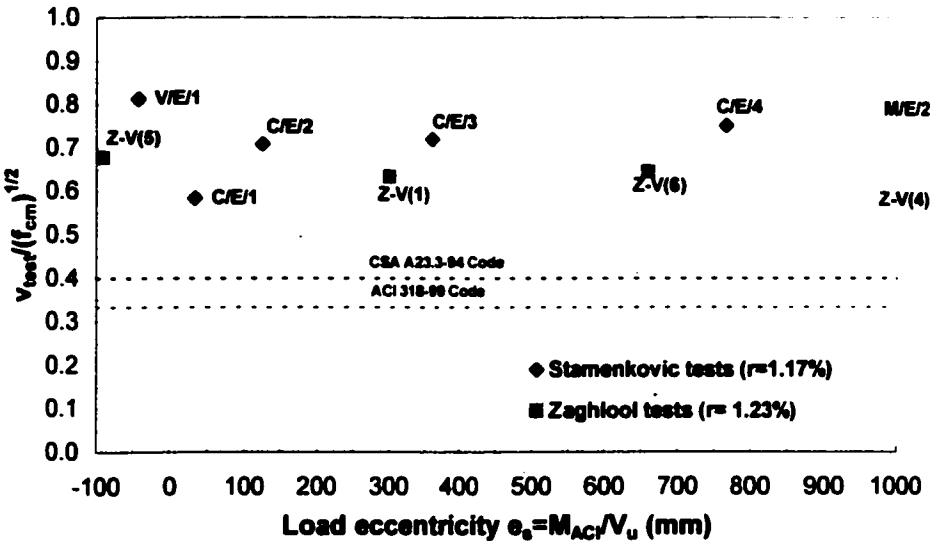

Figure 2.29 Effect of load eccentricity $e_s=M_s/V_u$ on the failure shear strength calculated using ACI or CSA Code

2.5 INFORMATION FROM TESTS OF CORNER CONNECTIONS

The information available in the literature are used to study the code provisions for the corner column slab connections under the same items as for the edge column slab connections:

- Interaction between shear and moment
- Effect of steel ratio on the failure shear stress
- Effect of load eccentricity on the failure shear stress

It should be noted that the data being used to study those items are limited to corner connections subjected to diagonal bending moment.

2.5.1 Interaction between shear and moment

Tests from Zaghlool (1973) on the corner column slab connections with the parameter M_{code}/V ratio are used to study the degree of interaction between shear and moment predicted by the ACI 318-99, CSA A23.3-94 and CEB-FIP MC90. The steel ratio (ρ) on this test series was 1.23% for all specimens. The V_u/V_o ratio is plotted against the M_{code}/M_o ratio as shown in Figure 2.30 and Figure 2.31.

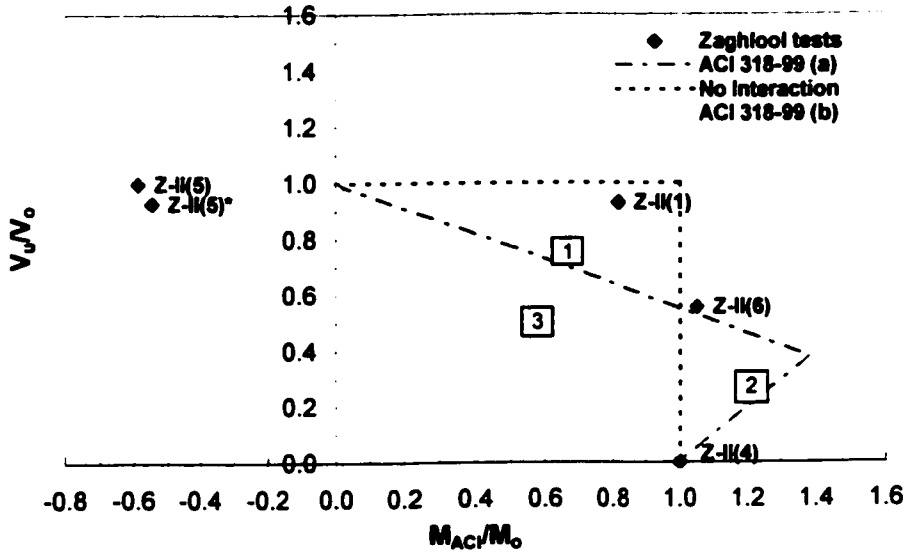

Figure 2.30 Interaction between shear and moment of ACI 318-99 provisions on the corner column slab connections

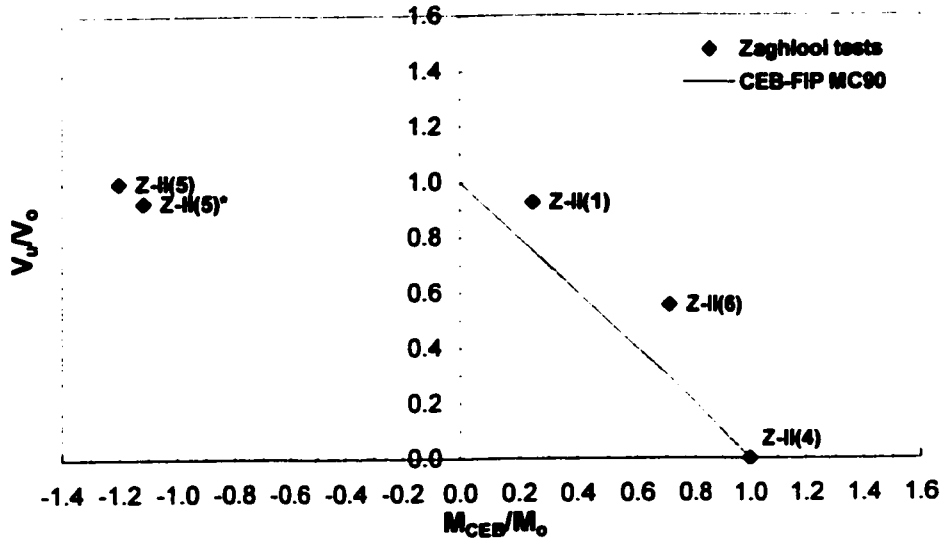

Figure 2.31 Interaction between shear and moment of CEB-FIP MC90 on the corner column slab connections

As for the edge connections, V_o and M_o should be the shear and moment when the absence of the moment and shear at the centroid of the critical section. However, the data of V_o is not available in the literature so that V_o is taken as the shear force in the absence of the applied moment at column centroid.

ACI 318-99 and CSA A23.3-94 codes predict the interaction between shear and moment based on two straight lines that meet at one point. Line-1 is when the maximum shear stress governs at the inner corner of the shear critical section (v_{AB}), while Line-2 is when the maximum shear stress governs at the point on the slab free edges (v_1 or $v_{1'}$). The location of the intersection line-1 and line-2 depends on the magnitude of c_{AB}, c_{AC}, $c_{AB'}$ and c_{CD} as shown in Figure 2.23. For the case of square columns and diagonal applied moment as in Zaglool tests, the interaction can be presented by a straight line (Line-3) as shown in Figure 2.30, since point B and A or D is equal distance to the diagonal moment axis through the centroid of critical shear section as shown in Figure 2.23.

It can be seen that the ACI 318-99 and CSA A23.3-94 codes underestimate the tests for the governing shear stress at the inner corner of the shear critical section. When the moment provided by eccentricity of the shear force to the centroid of critical shear section is larger that the applied moment, the test results were located out range of the

code interaction. It is surprising that assuming no interaction between shear and moment at the corner connections give good agreement with the test results from Zaghlool (1973).

The CEB-FIP MC90 assumes a linear interaction between shear and moment. The CEB-FIP MC90 underestimates all of the tests as shown in Figure 2.31.

2.5.2 Effect of steel ratio on the shear strength

The effect of the steel ratio (ρ) on the shear strength of the corner connections is studied using the tests by Zaghlool (1973) and two groups data from Regan et.al.(1981). Table 2.2 shows the effect of the steel ratio on the shear stress, which is calculated according to North American codes (ACI 318-99 and CSA A23.3-94).

In the tests by Zaghlool (1973), the shear strength increased by 53% when the steel ratio (ρ) increased by 81%, which is from 1.23% (*ZV-1*) to 2.23% (*ZV-3*). The data from Zaghlool are also plotted in Figure 2.32, where the failure shear stress is normalized by $\sqrt{f_{cm}}$, where f_{cm} is the experimental compressive strength of concrete cylinders.

Table 2.2 The effect of steel ratio on the shear stress of corner connections calculating based ACI or CSA Codes

Authors	Test	f_{cm} MPa	ρ_{avg} %	d mm	V_u kN	$M_{u,col}$ kNm	M_s kNm	v_{test} MPa	$\frac{v_{test}}{\sqrt{f_{cm}}}$
Regan (1981)	SC1	55.5	0.66	98	81	36.4	23.6	2.49	0.33
	SC2	61.4	0.42	98	75	35.7	23.9	2.41	0.31
	SC3	48.0	0.88	98	74	45.6	33.9	2.95	0.43
Regan (1981)	SC4	52.3	0.80	98	64	24.0	15.7	2.64	0.37
	SC5	59.6	1.13	98	82	26.9	16.3	3.303	0.39
Zaghlool (1973)	ZII(1)	33.3	1.23	121	137.9	54.5	32.7	3.38	0.59
	ZII(2)	33.5	1.65	121	177.2	75.6	47.5	4.62	0.80
	ZII(3)	27.8	2.23	121	177.9	82.1	53.9	4.94	0.90

In Regan's test, the trend of the shear stress increases due to increase in steel ratio is also found. In the first series (*SC1*, *SC2* and *SC3*), the shear stress increases by 39% when the steel ratio increases by 46% from 0.42% (*SC2*) to 0.88% (*SC3*). In the second data set (*SC4* and *SC5*), the failure shear stress increased only 5% when the steel ratio increases by 41%.

The failure shear stress is not constant on all of the tests as assumed by the ACI and CSA codes; the shear strength increases when the steel ratio increases. This can be seen from Table 2.2 and Figure 2.32.

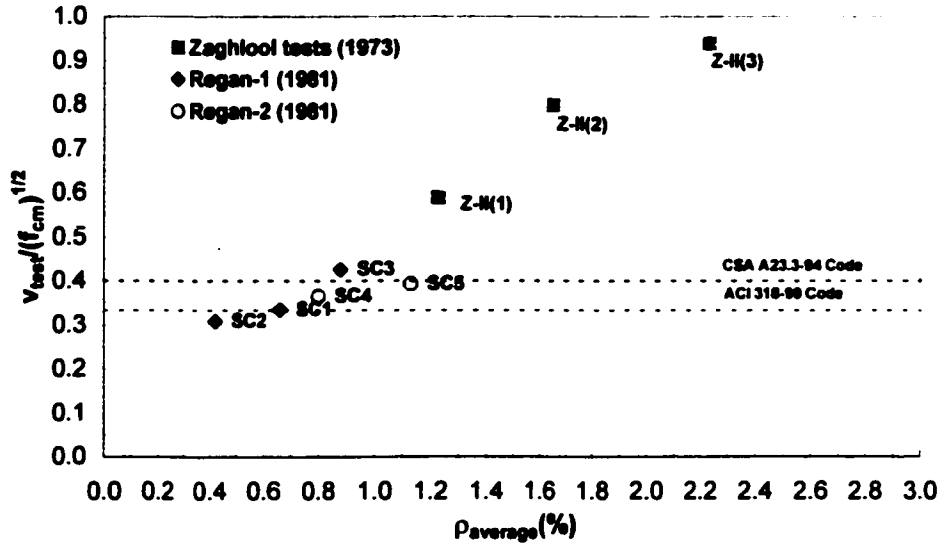

Figure 2.32 Effect of the steel ratio on shear strength of corner connections calculated according to ACI and CSA codes

2.5.3 Effect of load eccentricity ($e_s = M_{code}/V_u$) on shear strength

The tests by Zaghlool (1973), which are used to study the interaction between shear and moment on the corner column slab connections, are again considered here. The only parameter on this test is M_{code}/V ratio. M_{code} is the moment at the centroid of shear critical section. The shear stress is calculated according to ACI 318-99 or CSA A23.3-94 code provisions and the results can be seen in Figure 2.33. The shear resistance of the code provisions is also plotted on the same graph.

The ACI 318-99 and CSA A23.3-94 codes underestimate the shear strength most of the corner column slab connections.

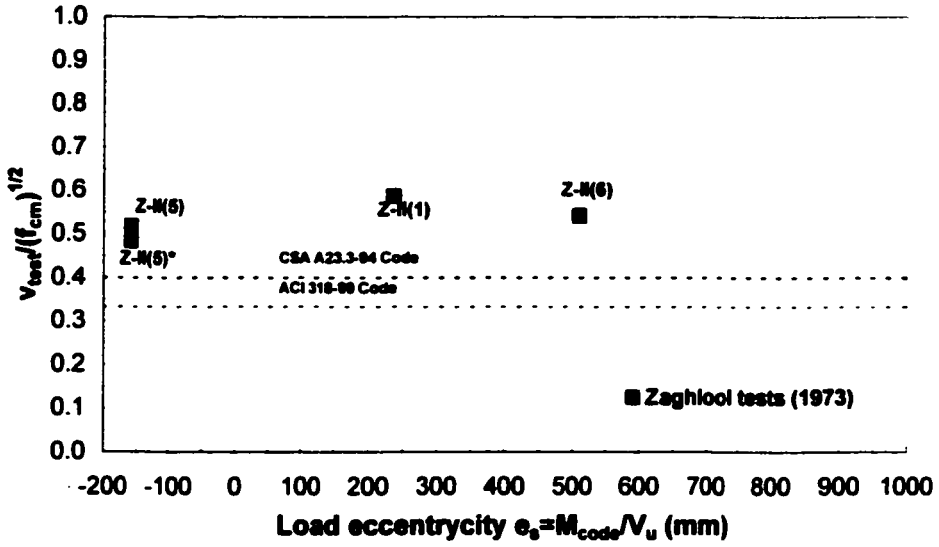

Figure 2.33 Effect of load eccentricity ($e_s = M_{code}/V_u$) on the shear strength of the corner connections predicted by ACI and CSA Codes

2.6 BIAXIAL UNBALANCED MOMENT

Behavior of flat-plate column connections under uniaxial loading has been reported by many researchers. To assess the behavior of slab under realistic lateral loads such as due to wind loading and earthquakes, it is necessary to consider lateral loading from multiple directions. However, experimental data on multiple direction loading. specifically on biaxial lateral behavior of slab-column connections is still limited.

Austin and Moehle (1992) reported their experimental data on the behavior of an interior column-slab connection subjected to gravity load and biaxial lateral load. Five 3962 mm x 3962 mm (13'x13') slabs supported by interior stub columns were tested. Two were subjected to uniaxial lateral loading and the others were subjected to biaxial lateral loading. The results show that biaxial lateral loading had a worse influence on the lateral behavior of slab-column connections. In comparison with the results obtained from equivalent uniaxial tests, the results of biaxial tests resulted in significant reductions

in strength, drift capacity, ductility and stiffness. Austin and Moehle observed that the reduction in strength is 21 percent to 36 percent.

In addition, damage around the slab-column connection of the biaxially loaded specimens was observed to be more extensive. However, it was not stated whether the damage was flexural failure or shear failure.

The present research will investigate the effect of biaxially lateral loading on the corner column-slab connections of a continuous flat-plate structure.

2.7 REPAIRED CONCRETE CONNECTION

Local damage to the connections of real structures may occur during construction or post moderate earthquakes. To avoid demolishing all structures with such damage, connections may be repaired to restore the original strength of the structures. Concrete in the repaired connection behaves as a composite material between old concrete and new concrete. According to Silfwerbrand (1990), the strength of composite old and new concrete depends on the bond strength between the new and old concrete. Factors that affect concrete bond, such as old concrete strength, method of concrete removal, the interface and the strength of new concrete. To assess the strength of the interface concrete, 47 pull-off tests were conducted. The results of the tests showed that the treatment technique on the old concrete surface was very important to improve the bond strength of the interface. Old concrete cleaned of dust and loose particles was observed to have good bond strength with the new concrete. In addition, micro cracks due to surface treatment using a hydraulic jack hammer affected the bond strength of the interface composite concrete. The fewer micro cracks in the old concrete, the stronger the interface composite. However, Silfwerbrand observed that surface roughness did not have a major influence on bond strength and it was believed that there might be a threshold value relating the degree of roughness and tensile stress of interface composite concrete.

The strength of repaired slab-column connections subjected to gravity and biaxial lateral loads was investigated by Austin and Moehle (1992) who repaired the damaged connection using epoxy and grout concrete with a strength of 51 MPa. The behavior of

the repaired connection to resist load was quite good. Even though the connection lost almost one-half of its original lateral strength and stiffness, the repaired connection was still be able to take approximately the same horizontal displacement as the original connection. Shear failure of the repaired connection was observed initially at the interface of the old concrete and grout. This agrees with Silfwerbrand's test results that the strength of the repaired concrete depends on the bond strength at the interface. Austin and Moehle observed that there were significant differences in strength between the two lateral directions of repaired connection. They believed that this might be partly due to uneven damage and yielding of the reinforcement in the original test or inconsistent quality of workmanship during repair.

CHAPTER 3
EXPERIMENTAL PROGRAM

3.1 GENERAL

The following sections describe the experimental program that can be divided into three major parts:

1. A two bay by two bay (9 columns) continuous flat plate with span lengths of 2743 mm center to center of the columns was fabricated. All of the edge and corner column slab connections were tested separately one at a time. The variables were the ratio of column load to column moment and the direction of the unbalanced bending moments.

2. The four edge column slab connections of the continuous flat plate specimen were repaired after experiencing punching failure and re-tested. The variables were the repair concrete properties and the load eccentricity.

3. Eight isolated edge column slab connections were made consisting of two sets of four specimens. Four of the specimens had panel dimension two times that of the continuous flat plate specimen in the direction perpendicular to the free edge and the other four specimens had panel dimension two times that of the continuous flat plate specimen in the direction parallel to the free edge with appropriate flexural reinforcement. Within each series, the variables were the load eccentricity and arrangement of the flexural reinforcement.

3.2 CONTINUOUS SLAB SPECIMEN

3.2.1 General

In North America, flat plate structures are preferred due to the advantages already mentioned. Three continuous flat plate floors have been tested previously in the University of Ottawa, two of them were post-tensioned flat plates and the other was reinforced flat plate. All of them were subjected to uniform distributed load. In this program, a continuous flat plate was constructed and tested separately at each column slab connection with the M/V ratio varied from 0 to ∞ in order to obtain different degrees of interaction between the shear force and the unbalanced moments. The specimens and their material properties will be described in more detail in the following sections.

3.2.2 Continuous slab dimension

A two bay by two bay (nine columns) slab with span lengths of 2744 mm center to center of the columns was chosen. The model was similar to Shao and Gardner's specimen (1990). The size of the slab was chosen as a compromise between the space available in the laboratory and to be as close as possible to full-scale structure to eliminate the effect of scale. The size is about half the slab size in a real structure. The dimensions of the test specimen are shown in Figure 3.1. Two different sizes of columns were chosen. Interior column (#9) and four corner columns (#5~#8) were 305 mm (12 inches) square columns and four edge columns (#1 ~ #4) were 203 mm (8 inches) square columns. The slab thickness was 140 mm (5.5 inches) and the effective slab depth was 105 mm.

The length of the concrete columns above and below the slab was 570 mm. The length chosen was considered long enough to be able to apply the load during the test and to facilitate working and setting the instruments under the slab. The total height from the laboratory floor to the bottom of the slab was 970 mm (38 1/6 inch).

3.2.3 Slab flexural reinforcement

The flexural reinforcement of the slab was designed according to CSA A23.3-94 Code provisions. Ultimate uniformly distributed load (w_u) of 34.4 kN/m^2 was used to design the flexural reinforcement. This load was the ultimate load capacity of the continuous slab tested by Gardner and Shao (1996) when the edge column slab connections failed in punching shear. However, due to test procedure, additional bottom reinforcement at the corner connections was provided to account for load distribution during testing of individual edge and corner columns. To ensure that the connections fail in punching shear, the uniformly distributed load considered in designing the flexural reinforcement was higher than that used in practice.

The slab reinforcement was #10M bars and the distribution of the reinforcement is shown in Table 3.1, and details of the top and bottom reinforcements are shown in Figures 3.2 and 3.3. The clear cover from the bottom of the slab to the bottom of reinforcing mats was 20 mm.

Table 3.1 Summary of flexural reinforcement of the continuous flat plate specimen

Width		Interior Strip			Exterior Strip		
		Edge support	Midspan	Interior Support	Edge support	Midspan	Corner support
Top	Column Strip	8 No.10	-	11 No.10	6 No.10	-	7 No.10
	Half Middle strip	3 No.10	-	-	-	-	3 No.10
Bottom	Column Strip	8 No.10	8 No.10	8 No.10	5 No.10	5 No.10	7 No.10
	Half Middle Strip	3 No.10	8 No.10	3 No.10	2 No.10	2 No.10	2 No.10

The amount of reinforcement was calculated and distributed so that the slab would have sufficient flexural strength and that shear failure would occur at the connections. All top reinforcement passing through the columns were extended to ensure enough anchorage length. Two top and bottom bars perpendicular to the free edge were bent into the column at the edge column-slab connections, and at the corner column-slab connections, three bars were bent into the column. The other top bars perpendicular to the slab edges were hooked into the slab as anchorage. The corner column-slab connections had top and bottom reinforcements to resist the positive moment at the connections during the test on the edge column-slab connection.

All # 10M reinforcing bars had nominal yield strengths (f_y) of 420 MPa. Tension tests were conducted to determine the stress-strain diagram shown in Figure 3.4. The yield strain (ε_y) and modulus of elasticity (E_s) were 2300 micro strain and 18.3 GPa, respectively.

3.2.4 Column reinforcement

The column reinforcement was designed to be able to resist more load than the predicted load capacity of the column slab connections to ensure that the columns did not fail before failure of the connections. This was done because the loads were applied through the column stubs. In case of edge columns, the design load was V= 500 kN and M= 60 kNm and resulted in 4#20M bars. Modification was made for one of the edge columns to enable a diagonally applied moment, resulting in 2#20M and 4#15M bars. For the interior and corner columns, the reinforcement was 8#15M bars and 10#15 M bars, respectively. All the ties of the columns were #10M bars placed with uniform spacing 100 mm center to center. Details of the column reinforcement can be seen in Figure 3.5.

3.2.5 Construction of the specimen

In order to provide the required height of the slab specimen, HSS 153 x 153 x 6.5 mm steel spacers of 400 mm in height were provided at the edge columns and the corner columns. A HSS 203 x 203 x 6.5 mm spacer was used at the interior column. The entire

concrete column base plates were tied down to the laboratory floor, using 25.4 mm Dwidag bars, before casting to prevent any vertical movement during testing of the connections. The bars were attached to a 25.4 mm thick steel plate at the base of the concrete column. The edge columns and corner columns were anchored horizontally to eight steel columns of HSS 203 x 203 x 9.5 mm (8 x 8 x 3/8 inch) using 19 mm diameter threaded rods. These steel columns were fixed by Dwidag bars to the laboratory floor as shown in Figures 3.10 to 3.12.

The column reinforcement cages were placed on the top of the 24.5 mm thick steel plate, which was supported by steel spacer. Steel anchorage 4#10M were provided to anchor the concrete to the steel plate. The column formwork below the slab was 0.75 inches thick plywood sheet that was installed after the column reinforcement cages had been placed. Two bolts were provided on each side of the column faces to hold the column formwork.

The slab formwork was constructed after the bottom column formwork had been installed. The slab formwork was also made of 0.75 inch plywood sheet. The plywood-casting surface of the slab was supported on eighteen aluminum I beams 6.4 m (21 ft.) long. Two different heights of aluminum beams were used; 8 beams 7-1/2 inch high were placed in North-South direction and 10 beams 6-1/2 inch high were placed in East-West direction. The beams in North-South direction were supported directly on concrete blocks and the beams in East-West direction were placed on the top of the beams in the North-South direction. Plywood sheets were nailed to the supporting beams and covered with polyethylene sheeting to avoid bond between the formwork and concrete and to prevent water loss during the hydration process of the cement due to water being absorbing by the wood. Figure 3.6 shows the specimen formwork before placing of the concrete.

3.2.6 Concrete properties

Both slab and columns were cast at the same time using normal density concrete that was ordered from a local ready mix company. Figure 3.7 shows the casting of the specimen. Six cubic meters of ready mix concrete, maximum aggregate size of 10 mm,

specified concrete strength f'_c = 30 MPa and a slump of 65 mm was used. Six-hour retarder was added in the concrete mix. The concrete mix contained slag but no air-entraining agent. The strength of the concrete at the time of the tests was determined from the standard compression test of the concrete cylinders as listed in Table 3.2.

Table 3.2 Properties of concretes used in the continuous flat plate specimen

Column connection	Average compressive strength (f_{cm})	Average modulus elasticity (E_{cm})	f'_c	ε_o
E_1	43.62 MPa	-	34.90 MPa	-
E_2	42.41 MPa	-	33.93 MPa	-
E_3	42.72 MPa	37 GPa	34.18 MPa	0.00203
E_4	43.62 MPa	-	34.90 MPa	-
C_5	44.35 MPa	37 GPa	35.48 MPa	0.00230
C_6	44.35 MPa	-	35.48 MPa	-
C_7	44.35 MPa	-	35.48 MPa	-
C_8	44.35 MPa	-	35.48 MPa	-

The modulus of elasticity E_{cm} of the concrete is calculated according to CSA A23.3-94 Code clause 8.6.2.1 as the secant slope of the origin and $0.4f_{cm}$ of stress-strain curves shown in Figure 3.8. The concrete strength development over time diagram can be seen in Figure 3.9. Gardner's expression (equation 3.1) for concrete strength development over time of cylinder test is fitted to the compressive test results.

$$f_{cm,t} = f_{cm,28}\left(\frac{t^{3/4}}{a + bt^{3/4}}\right) \tag{3.1}$$

Where $f_{cm,28}$ and $f_{cm,t}$ are measured compressive strength at 28 days and at time t (days), constants a and b depend on type of cement used. For cement type I, constants a and b are 2.8 and 0.77, respectively.

3.2.7 Test set-up

Each slab column connection of the continuous slab was tested separately. When testing one connection, the others were fixed to the laboratory floor. Three different load combinations were applied to the edge slab-column connections, namely vertical load only, moment only, combination of vertical and moment perpendicular to free edge. Hydraulic jacks were used to apply the vertical and horizontal forces. The east edge connection (E_2) was subjected to vertical load only, the south edge connection (E_3) was subjected to moment only, north edge connection (E_1) and west edge connection (E_4) were subjected to combined vertical load and bending moment. The corner columns, C_5, C_6, C_7, C_8, were subjected to combined vertical load and biaxial bending moment. The interior slab-column connection was not the concern of the present studies so that this connection was not tested. The moment was provided by applying equal horizontal forces to the column stubs above and below the slab in opposite directions. The lever arm of the horizontal forces was 994 mm.

The moment acting at the edge column connections was about the axis parallel to the free edge i.e. bending of top column outward. At the corner connections, diagonal moment was applied about the axis connecting two corners of the column at the free edge. The loading setups for E_1, E_2, E_3 and E_4 can be seen in Figures 3.10 to 3.12.

3.2.8 Isolated support

A preliminary test of the east edge column slab connection without providing supports along the lines of contra-flexure showed that the slab did not behave according to the loading pattern of the design, which was uniformly distributed load. The behavior was deduced based on the cracks formed during the test. Therefore, a simple support was provided along the lines of contra-flexure, which were calculated at 1/5 of clear span for a uniform load (w_u) of 34.4 kN/m^2. This distance was verified using a commercial finite element program SAP2000™. In order to provide support along the lines of contra flexure, threaded rods 5/8 inches diameter were installed around the edge connection

during the test. The rods were stiffened using ½-inch steel tubes. The rods were fixed to a steel frame that was tied to the laboratory floor.

3.2.9 Steel strain measurement

Ninety one electrical resistance strain gauges (ERSG) type *KFG-10-120-C1-11* were provided on the flexural reinforcement in the continuous slab specimen, namely 12 and 79 strain gauges in the bottom and the top reinforcement, respectively. The strain gauges were located 25 mm from the column faces as shown in Figures 3.13 to 3.16. The strain gauges on the bottom reinforcement were placed at the corner and the interior connections as shown in Figure 3.16.

3.2.10 Deflection measurement

Out-of-plane slab deflections and horizontal column stub deflections were monitored using linear variable differential transformers (LVDT's) and mechanical gauges (dial gauges). Only the spans and the panel associated with a test were instrumented to measure the deflections. Vertical deflection of the slab near the connections and horizontal deflections of the column stubs were measured using LVDT's. The deflections of the slab at mid-span and mid-panel around the tested connection were measured using dial gauges. Five and three dial gauges were placed under the slab near each edge and corner column connection during test, respectively. Typical locations of the instrumentation are shown in Figures 3.17 and 3.18. For the connection subjected to vertical load only, only the vertical displacement was measured while for connections subjected to bending moment and combination of the vertical load and horizontal load, both vertical and horizontal displacements were measured.

3.2.11 Testing of the specimen

The specimen was tested separately at each connection. Three different loading systems when the testing the edge column and corner column slab connections were applied. The following describes the test of each connection.

3.2.11.1 Connection under vertical loading only (Connection E_2)

The east edge connection (E_2) was subjected to vertical load only which was applied through the bottom column. The connection was tested three times. The first test was done without providing support along the lines of contra-flexure. The load was applied in 10 kN increments. When the load reached 82 kN, it was realized, from the crack patterns, that the behavior of the connection did not correspond to the design load pattern, which was uniformly distributed load. Therefore, the connection was unloaded and support was provided along the lines of contra-flexure.

The second test was conducted after the support along the lines of contra-flexure was installed. The load increments were the same as in the first test. When the load reached 220 kN, the applied load was stopped as it reached the capacity of the load cell. The 220 kN load was maintained for one and half-hours and the connection was monitored. No sign of failure was observed so that the connection was unloaded.

The load applied in the third test was monitored using the pressure indicator on the hydraulic pump. The pressure indicator was calibrated with the load cell so the load read by the pressure indicator would not deviate from the reading using the load cell. On the third test, the connection failed due to punching failure at the maximum load of 220 kN; the same as the load reached on the second test.

3.2.11.2 Connection subjected to bending moment only (Connection E_3)

The south column slab connection (E_3) was tested under pure bending moment about the axis parallel to the free edge. The moment was produced by two equal horizontal loads applied on the column above and below the slab, respectively. The lever arm was 994 mm. The horizontal load was increased in 2.5 kN increment up to failure. The connection failed due to the combined effect of flexure and torsion at a moment of 29.2 kNm.

3.2.11.3 Connections subjected to combined vertical and bending moment (Connections E_1 and E_4)

The remaining two edge column slab connections were subjected to combined vertical load and bending moment. These connections were north *(E_1)* and west *(E_4)* edge column slab connections. The loads were applied simultaneously according to the eccentricity *(M/V)* considered for each connection. The average eccentricity of the loads of north edge connection (E_1) was 283 mm and average eccentricity of 112 mm was applied at the west edge column connection (E_4). Load increments of 10 kN were applied for vertical load on both connections. Horizontal load was applied in increments of 2.5 kN and 1.0 kN on the north and the west edge column connections, respectively. The loads were increased until the connections failed in punching failure. Connection E_1 failed at a vertical load of 127.4 kN and a moment of 34.4 kNm. Connection E_4 failed under a vertical load and moment of 116.7 kN and 14.2 kNm, respectively.

3.3 REPAIR OF THE EDGE COLUMN SLAB CONNECTIONS

After the tests of the edge column slab connections were completed, the connections were repaired by removing concrete from the damaged area and casting new concrete in the repair area. Parts of the connection being repaired are shown in Figure 3.19. The objectives of repairing the connection were to investigate the strength that can be developed after punching failure and to compare the strength of the original connection with that of the repaired connection. The following sections present the material properties of the repair concrete, repair procedures and test procedure of the repaired edge column slab connections.

3.3.1 Properties of repaired materials

3.3.1.1 Concrete properties

Two edge column slab connections, north (E_1) and east (E_2) connections were repaired using an expansive concrete produced with Calcium Aluminates Hydrate (CAH) admixture according to mix design developed by the Institute for Research in

Construction of the National Research Council of Canada (CNRC). Mix "A", that contained superplasticizer, was used at the north edge connection (E_{1R}) and Mix "B", without superplasticizer, was used at the east edge connection (E_{2R}). The stress-strain curve for CAH expansive concrete can be seen in Figure 3.20. The reason to use CAH expansive concrete was to avoid the effect of shrinkage cracks on the interface between new concrete and the existing one.

The other two edge column slab connections, south (E_{3R}) and west (E_{4R}) connections, were repaired using Mix "C" that was regular concrete mixed in laboratory. The slump was approximately 75-100 mm. Table 3.3 presents the summary of the repair concretes.

Table 3.3 Properties of the concretes used to repair the edge column slab connection of the continuous flat plate specimen

Type of Concrete Mix	Average compressive strength (f_{cm})	Average modulus of elasticity (E_{cm})	f'_c ($0.8f_{cm}$)	ε_{om}
A (E_{1R})	40.0 MPa	25.9 GPa	32.0 MPa	0.00246
B (E_{2R})	39.8 MPa	28.5 GPa	31.9 MPa	0.00261
C (E_{3R})	40.3 MPa	48.0 GPa	32.2 MPa	0.00181
C (E_{4R})	42.7 MPa	40.6 GPa	34.2 MPa	0.00195

3.3.1.2 Bonding agent

Water based epoxy resin or Portland bonding agent type Sika Top Armatec 110 EpoCem was used at the interface between fresh concrete and the existing concrete. As specified in the manual of the product, bond strength is 2-3 MPa when it is used with concrete.

Figure 3.21 shows the relation between bond strength and open time taken from the product manual. The thickness of the bonding agent applied on the repaired surface was approximately 0.8 mm, which was thicker than the minimum requirement.

3.3.2 Repair procedures

In order to repair the damaged connections, the same procedures were used for all four edge column connections as follows:

- The concrete slab around the edge columns was removed after the first test using an electric hammer. The concrete to be removed from the connection depended on the crack failure of the connection after the first test.
- The loose particles were removed using water pressure.
- The surface was sandblasted and cleaned using air pressure.
- Formwork was constructed around the repaired connection
- The cut surfaces were covered using wet burlap for 24 hours and then dried using air pressure to be saturated surface dry (SSD) before applying the epoxy adhesive agent to bond the existing concrete and the repair material.
- When the contact surfaces were ready, epoxy adhesive agent was applied. The fresh concrete was cast approximately one hour after the application of bonding agent.
- The concrete was moist cured for 14 days.

3.3.3 Testing of repair connections

The test setup for testing of the repaired connections was similar to that of the original edge connections. Two types of loading systems were used to test the repair connections. The south edge connection was tested twice. The first test was subjected to vertical load only (E_{3R}*) and the second test was subjected to combined vertical load and bending moment (E_{3R}). Under vertical load only, the connection was able to resist load of 230 kN, which exceeded the maximum in the previous test, without failure. On the second test, the connection failed due to punching when the combined load reached 129.1 kN and 23.4 kNm for vertical load and moment, respectively.

Connections E_{1R}, E_{2R} and E_{4R} were subjected to combined vertical load and bending moment about the axis parallel to the free edge. The vertical load increment was 10 kN for all connections. The moment was increased by increasing the horizontal load in

increments of 1 kN, 2 kN and 3 kN, respectively for E_{1R}, E_{2R} and E_{4R}. The load was increased until connection failure.

3.4 TESTING OF CORNER COLUMN SLAB CONNECTIONS

The four corner column connections were tested to obtain the interaction between shear and diagonal unbalanced moment. For all tests of corner connections, the vertical load was applied at the centroid of the column section. A simple support was provided along the line of contra flexure obtained for a uniform surface load of 34.4 kN/m^2. Details of the test setup of corner column slab connections are shown in Figure 3.22. The following sections present the testing procedures.

3.4.1 Connection subjected to vertical load only (Connection C_5)

The northwest corner column connection *(C_5)* was subjected to vertical load only. The connection was tested two times. In the first test, the column was allowed to rotate inward freely. Three dial gauges were placed to measure out of plane deflection of the midpanel and the midspan of the slab. Two LVDT's were placed in front of the inner faces of the column. The load was increased by increments of 5 kN and held for 3-5 minutes to read the out-of-plane deflections of midpanel and midspan of the slab around the column. The rotation due to biaxial unbalanced moment caused by the vertical load eccentricity was very high and put the lower surface of the slab into tension. The applied load was stopped at 59.7 kN due to significant tension cracks on the lower surface of the slab and the connection was unloaded.

Observing the behavior of the connection during the first test, it was necessary to apply moments to maintain the column in the original vertical position. To monitor the rotation of the column, two LVDT's were placed horizontally on the top and bottom columns at 343 mm (13.5 inch) from the slab surfaces. The vertical load and moment were applied simultaneously. The same load increment was applied as the first test for the vertical load. On the second test, the connection was able to resist a vertical load of 62.1 kN and a moment of 27.9 kNm before the connection failed in punching. After the

connection failed, the horizontal displacements could not be controlled and changed dramatically due to the change in connection stiffness.

3.4.2 Connection subjected to combined vertical load and diagonal moment (connection C_6)

The northeast column slab connection was subjected to combined loads with no rotation of the column stubs. The load increments, the locations of LVDT's and dial gauges were similar to those in connection C_5. At failure, the connection was able to resist a maximum vertical load of 108.6 kN and a diagonal bending moment of 49.3 kNm which corresponds to an eccentricity of 454 mm.

3.4.3 Connections subjected to combined vertical load and diagonal moments (connections C_7 and C_8)

Two corner column slab connections were tested under combined load with different load eccentricities. The load eccentricity of 498 mm was applied on the southeast connection (C_7) in which the vertical load and moment were increased by increments 10 kN and 4.0 kNm, respectively. Connection C_7 failed in punching shear at a vertical load of 93.7 kN and a moment of 46.6 kNm.

For the southwest column slab connection (C_8), the vertical load was increased by increments of 10 kN. To obtain the required eccentricity of 396 mm, horizontal loads were applied in 3 kN increments simultaneously with the vertical load. Connection C_8 failed in punching shear at a vertical load of 98.1 kN and a diagonal moment of 38.9 kNm.

3.5 ISOLATED SLAB SPECIMENS

The results obtained from the test of continuous slab specimen were not sufficient to define the interaction of shear forces and unbalanced moments at the column slab connections; therefore, eight isolated edge column slab connections were made and tested to get additional information related to the behavior of edge column slab connections.

These specimens were divided into two groups according to the slab dimensions and reinforcement. Each group consisted of four identical specimens. The following sections present the design, material properties, and construction and test setup of the specimens.

3.5.1 Slab dimension and reinforcement

The slab dimensions were chosen to simulate the lines of contra-flexure of a prototype structures with the span length in the direction perpendicular and parallel to the free edge, twice that of the continuous slab for slabs in Series *I* and slabs in Series *II*, respectively. The resulting dimensions of specimens in Series *I* were 1219 mm x 1321 mm (48"x 52") and specimens in Series *II* were 711 mm x 2438 mm (28"x 96") from support to support. To provide anchorage of the reinforcement outside the support, the slab extended 250 mm passed the supports.

Slab reinforcement was #10M bars, except the bars going through to the column in direction parallel to longer span were #15M. The arrangements of the negative (top) and bottom reinforcement are shown in Figures 3.23 and 3.24 for slab series *I* and *II*, respectively. Two bars of the negative reinforcement pass through the column in each direction. All of the negative reinforcements (top bars) perpendicular to the free edge anchored in the column were bent 90° and the other bars were bent 180°. The bottom reinforcement was not provided with hooks. All bottom bars were terminated outside the area of c_2+3h by $c_1+1.5h$, except one bar parallel to the slab edge, was used to provide torsion reinforcement, where c_2 and c_1 are the column dimensions parallel and perpendicular to the free edge, respectively and h is the slab thickness. According to the Canadian Code (CSA A23.3-94), a portion of the unbalanced moment is resisted by flexure provided by the reinforcement within a width c_2+3h. Detailed reinforcements in Figures 3.22 and 3.23 provided $\rho_{(c2+3h)}$, the reinforcement ratio within a width c_2+3h, was 1.38% and 0.7% for Series *I* and *II*, respectively and $\rho_{(c1+1.5h)}$, the reinforcement ratio within a width $c_1+1.5h$, was 0.7% and 1.38% for Series *I* and *II*, respectively.

3.5.2 Column dimension and reinforcement

All isolated slab specimens had column dimensions of 203 mm x 203 mm. The length of the stub columns above and below the slab surface was 570 mm. The column dimensions were the same as that of the continuous slab specimen.

The column reinforcement of the isolated slab specimens was 10#15M bars with 6.3 mm diameter ties at 100 mm center to center as shown in Figure 3.25c. The number of longitudinal bars was increased from the previous test to account for the increase in possible internal forces due to the changes in slab dimension and reinforcement. The steel cages were placed in the column formwork using side spacers to obtain a concrete cover of 20 mm.

3.5.3 Construction of the specimens

The 6.3 mm diameter column ties were fabricated in Laboratory. The other bars were cut and sized in the supplier's company. As for the continuous slab specimen, the eight column cages were assembled in the Laboratory.

The formwork of the isolated slab was similar to that used for the continuous slab. Twenty-three Aluma aluminum "I" beams (6-1/2" high, 21 ft length) were used to build the slab formwork. The columns were not tied either down to the laboratory floor or to the steel column during construction. Steel plates were provided on the bottom of each column. The column formwork rested directly on steel supports to provide working space under the slab. Figure 3.25b shows the slab and column formwork before casting the concrete.

All formwork surfaces that contacted the concrete were covered with polyethylene sheet to reduce water loss. The slab and the columns were cast at the same time.

3.5.4 Material properties

3.5.4.1 Concretes

Four and half cubic meters of ready mix concrete, maximum aggregate size of 10 mm, specified concrete strength f_{ck} = 30 MPa and a slump of 75 mm was used. The strength of the concrete at the time of testing the specimens determined from standard compression test is presented in Table 3.4. Typical stress-strain curve of the concrete cylinders at 28 days is shown in Figure 3.26. The concrete strength at 28 days ($f_{cm.28}$) is 43 MPa with E_{cm} and ε_{om} of 37.5 GPa and 2034 με, respectively. The compressive strength developments of concrete cylinders over time are shown in Figure 3.27. Gardner's expression (equation 3.1) is also plotted together with compressive test results in Figure 3.27.

Table 3.4 Concrete properties used in the isolated edge column slab specimens of Series I and Series II.

Column connection	Average compressive strength (f_{cm})	f'_c ($= 0.8 f_{cm}$)
E_{1-1}	52.8 GPa	42.2 MPa
E_{1-2}	52.8 GPa	42.2 MPa
E_{1-3}	55.0 GPa	44.0 MPa
E_{1-4}	52.8 GPa	42.2 MPa
E_{2-1}	52.8 GPa	42.2 MPa
E_{2-2}	52.8 GPa	42.2 MPa
E_{2-3}	55.0 GPa	44.0 MPa
E_{2-4}	55.0 GPa	44.0 MPa

3.5.4.2 Flexural reinforcement

The nominal yield strength of the #10M and #15M bars were determined from direct tension tests. Stress-strain curves for the #10M and #15M bars can be seen in Figure 3.28. It was found that the nominal yield strength of the #10M and #15M bars were 430 MPa and 403 MPa, respectively. The yield strains were 2.3 x 10^{-3} and 2.35 x 10^{-3} for #10M and #15M bars, respectively.

Table 3.5 Properties of flexural reinforcement used in the isolated edge column slab specimens of Series I and II

SLAB	No. 10M bar (Φ=11.3 mm, As = 100 mm^2)			No. 15M bar (Φ=16 mm, As = 200 mm^2)		
	f_y MPa	ε_y (10^{-6})	E_s (GPa)	f_y MPa	ε_y (10^{-6})	E_s (GPa)
Series I	430	2300	18.7	403	2350	17.3
Series II	430	2300	18.7	403	2350	17.3

3.5.5 Instrumentation

Seventy-six strain gauges, ten for each slab in Series *I* and nine for each slab in Series *II*, were provided to monitor the behavior of the steel bars during the test. The strain gauges were placed on the sides of the rebar 25 mm from the column faces. The location of the strain gauges on the sides of the bars is expected to eliminate the difference of the strain between compressive and tensile sides of the bar. The difference may not that significant because the bar diameter is small (#10M). The locations of the strain gauges in the slab series *I* and *II* are shown in Figures 3.29 and 3.30, respectively.

LVDT's and dial gauges were used to measure the out-of-plane deflections of the slab and the horizontal column deflections during the test. All data from the LVDT's and strain gauges were recorded using a computer based data acquisition system. However, the deflections measured using the dial gauges (D.G.) were recorded manually.

3.5.6 Test set-up of the isolated specimens

Test setup of the isolated slab specimens was similar to that of the edge column-slab connection of the continuous specimen. The only difference from the previous test is the size of the steel frame and the diameter of the threaded rods to support the slab specimens. Due to the increase in size of the nominal slabs, the magnitude of the restraining force was expected to be larger.

Three sides of the slab specimens were simply supported. The supports were made of 18 threaded rods, ¾ inches (19 mm) diameter, placed along the three edges of the slab. To increase the stiffness of the threaded rods against buckling failure, the rods were stiffened using 7/8 inches outside diameter steel tube. The rods were tied to a steel frame bolted to the structural floor. The following sections present testing of the specimens in further details.

3.5.7 Testing of the isolated specimens

3.5.7.1 Specimen E_{1-1}

This specimen was subjected to vertical load only which was applied through the column stubs below the slab. The load was applied at the centroid of the column perimeter. The horizontal displacement of the column was monitored by two LVDT's on the column studs above and below the slab at 343 mm (13.5 in.) from the slab surfaces. Vertical deflections of slab edge along the support were restrained so that compatibility of the deflection along this line was ignored. The vertical load was increased in increments of 5 kN and held 3-5 minutes to check the cracks of the slab. When the load reached 75 kN, there was slight rotation of the column. The test was stopped when a problem occurred in the Data Acquisition System and the specimen was unloaded. It was observed that none of the rebars had reached their nominal yield strength. The residual strains and deflections could not be recorded due to the problem with the Data Acquisition System.

The specimen was reloaded with increments of 10 kN up to 75 kN, and horizontal loads were applied to keep the column in its original vertical position. The specimen failed in punching shear when the vertical load reached 97.83 kN and the moment was 7.3 kNm.

The shorter span from the column faces to the support failed first. It was believed that ignoring the compatibility of the deflection along the slab support caused the shorter span to experience higher load, which produced high curvature. To account for these effects, the rest of the isolated slab specimens were not restrained along the line of contra flexure. The applied load arrangements to produce expected *M/V* ratio are given in details for each specimens.

3.5.7.2 Specimens E_{1-2}, E_{1-3}, E_{1-4}

Vertical loads were applied to the slab using two sets of hydraulic jack with a capacity of 100 kN each. One set of loads was applied in front of the inner column face and a second set was applied in front of the side column faces at distances calculated depending on expected *M/V* ratio on each specimen. Figure 3.31 shows the loading systems of specimens E_{1-2}, E_{1-3} and E_{1-4}. The applied load increments were controlled by the pressure gauges of the hydraulic pumps. The vertical column reaction was measured at the centroid of the column perimeter (68 mm from inner column face) using a load cell of 222 kN capacities. Bending moment was obtained by measuring the two horizontal reactions at the column stubs above and below the slab, respectively, using two of 111 kN capacity hollow load cells. The distance between the two horizontal reactions was 994 mm. Before the loads were applied, the initial vertical and two horizontal reactions of 10.2 kN and 6.12 kN were recorded, respectively, due to specimen self weight.

Vertical applied loads on specimen E_{1-2} were applied using seven hydraulic jacks. Three of them were connected to a pump to apply loads in front of the column face (P_f) and the other four jacks were connected to another pump to applied vertical loads on the side faces of the column, two hydraulic jacks on each side. The front loads (P_f) and the side loads (P_s) were applied simultaneously to reach required load increments for both

load sets. The loads were held 2-3 minutes for each increment to read the slab deflections and to mark slab cracks. Vertical deflections of the slab were measured at six locations. Three locations were measured on the span perpendicular to the slab free edge at 60 mm, 620 mm and 1430 mm from the column face. The other three locations to measure slab deflections were on the span parallel to the slab free edge at 60 mm, 314 mm and 818 mm from the column faces. Considering symmetry in geometry, only one side of the span parallel to the slab edge was instrumented. Locations of the applied loads and measured deflections in specimen E_{I-2} are shown in Figure 3.31a,d. Specimen E_{I-2} failed under combined loads of 88.14 kN and 49.8 kNm, including specimen self weight for shear force and bending moment, respectively.

In specimen E_{I-3}, the vertical applied loads were 191 mm from the column faces for both front loads (P_f) and side loads (P_s). Six hydraulic jacks, two jacks on each side, were used. The applied load procedures were the same as those of specimen E_{I-2}. However, the load increments were different. Slab deflections were measured at the same locations as specimen E_{I-2}. The test set-up of specimen E_{I-3} can be seen in Figure 3.31b. Due to the capacity of the load cell to measure vertical reaction being exceeded, specimen E_{I-3} was tested twice. After the load reached 220 kN, including specimen self weight, on the first test, the specimen was unloaded to remove the vertical load cell. The specimen was retested without using the vertical load cell but measuring the loads from the pressure gauges. Other set-up details were the same as the first test. The vertical reaction on the second test was obtained based on load calibration between the pressure gauge and the load cell reading on the first test. The specimen failed at loads of 307 kN and 32.2 kNm.

The front loads (P_f) and side loads (P_s) in specimen E_{I-4} were applied using three and two jacks, respectively. The locations of the front loads and side loads were 387 mm and 508 mm, respectively, from the column faces. The applied load procedures were similar to tests of E_{I-2} and E_{I-3}. Slab deflections were measured at the same locations as the other specimens in Series I. The positions of the vertical loads and measured slab

deflections in specimen E_{1-4} are shown in Figure 3.31c. Specimen E_{1-4} failed at loads of 118.22 kN and 41.10 kNm for shear force and bending moment, respectively.

3.5.7.3 Specimens E_{2-1}, E_{2-2}, E_{2-3} and E_{2-4}

The loading system for specimens in Series *II* (E_{2-1}, E_{2-2}, E_{2-3}, E_{2-4}) was similar to that of specimens in Series *I* described above. Seven hydraulic jacks were used in specimens E_{2-1} and E_{2-2} to apply vertical loads on the slab. Three jacks were used to apply front loads (P_f) and the other four jacks, two on each side, were used to apply side loads (P_s). The front loads (P_f) for both specimens were located at 508 mm from the column face. However, the side loads of specimens E_{2-1} and E_{2-2} were applied at 1016 mm and 508 mm, respectively, from the column face. In specimens E_{2-3} and E_{2-4}, six hydraulic jacks of 100 kN capacities were used to apply front loads and side loads. Two jacks were placed on each column side. The side loads (P_s) in specimens E_{2-3} and E_{2-4} were located 191 mm from the column face. The front loads were located at 191 mm and 194 mm from the column faces in specimens E_{2-3} and E_{2-4}, respectively. The locations of the vertical loads and measured slab deflections of the specimens in Series *II* can be seen in Figures 3.32 to 3.36. The vertical reaction and the bending moment due to self-weight for the entire specimen were 10.65 KN and 3.25 kNm, respectively.

Slab deflections in Series *II* were measured at six locations. Slab deflection were measured on the span perpendicular to the slab free edge at 60 mm, 254 mm and 758 mm from the column face. The other locations were along one side of the span parallel to the slab free edge at 60 mm, 508 mm and 1266 mm from the column face.

Failure loads of specimen E_{2-1}, including the self-weight, were 130.5 kN and 34.7 kNm. Specimen E_{2-2} failed at combined loads of 178.9 kN and 25.3 kNm including the self-weight of the specimen. Specimen E_{2-3} was loaded twice as the capacity of the vertical load cell was exceeded.

The same procedure as specimen $E_{1\text{-}3}$ was used to obtain the failure loads at the second test that was 328 kN and 9.6 kNm for shear force and bending moments. The last specimen tested in all experimental program was specimen $E_{2\text{-}4}$. The failure loads of specimen $E_{2\text{-}4}$ were 199.4 kN and 16.4 kNm for shear force and bending moment, respectively.

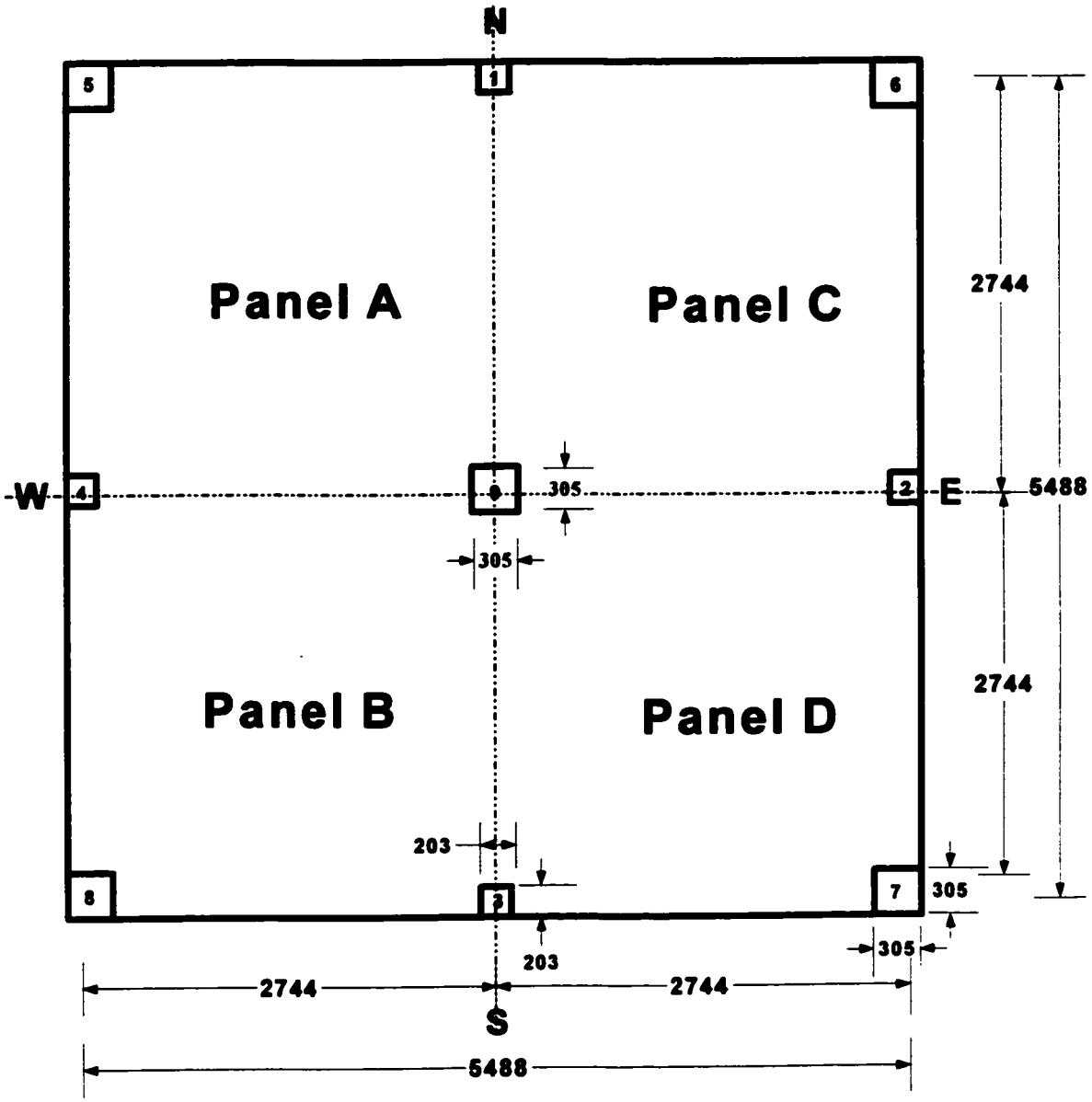

Figure 3.1 Dimensions of continuous flat plate specimen

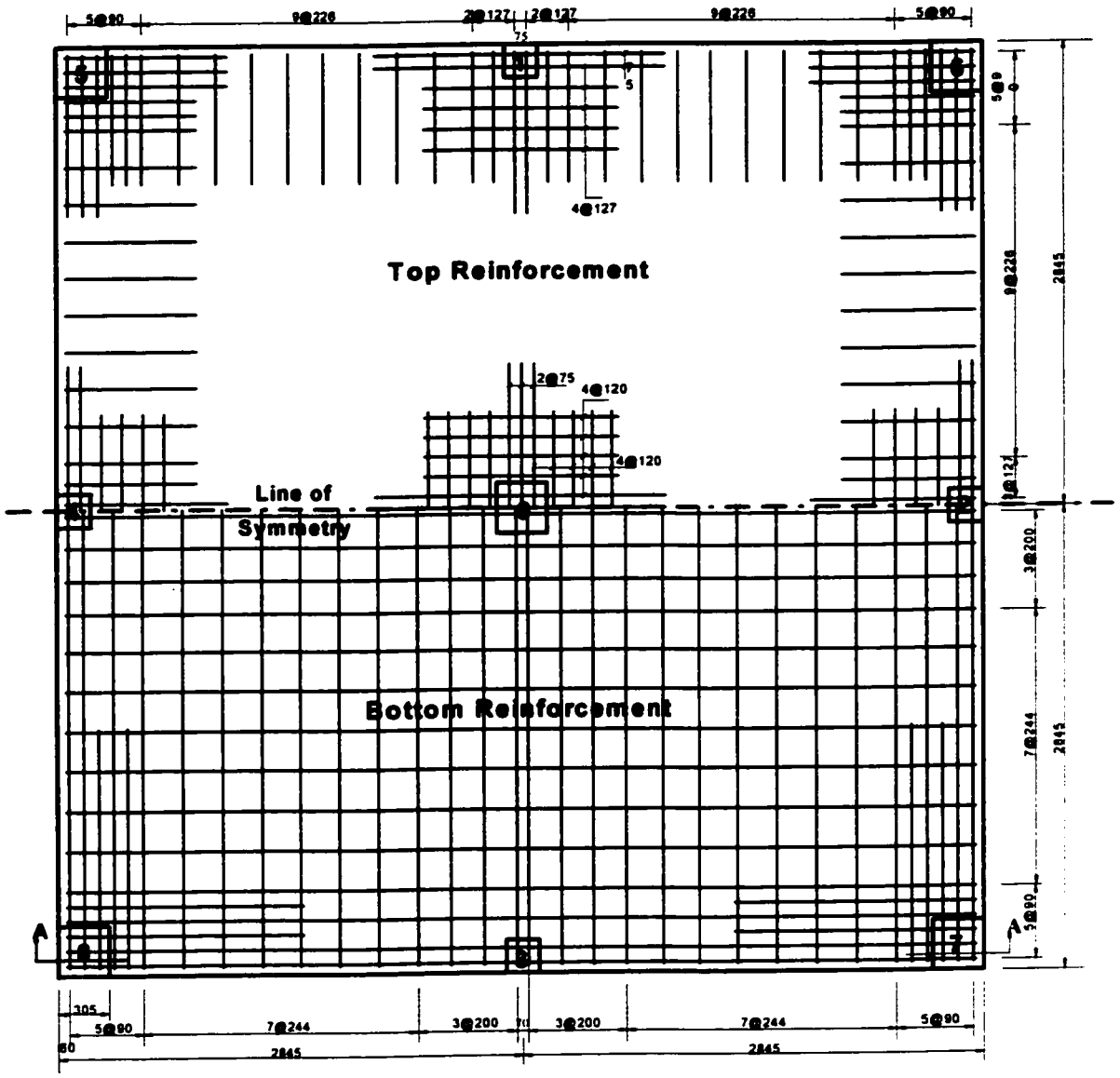

Figure 3.2 Negative (top) and Bottom reinforcement of continuous slab specimen; All bars #10M (Φ = 11.3 mm, As = 100 mm^2)

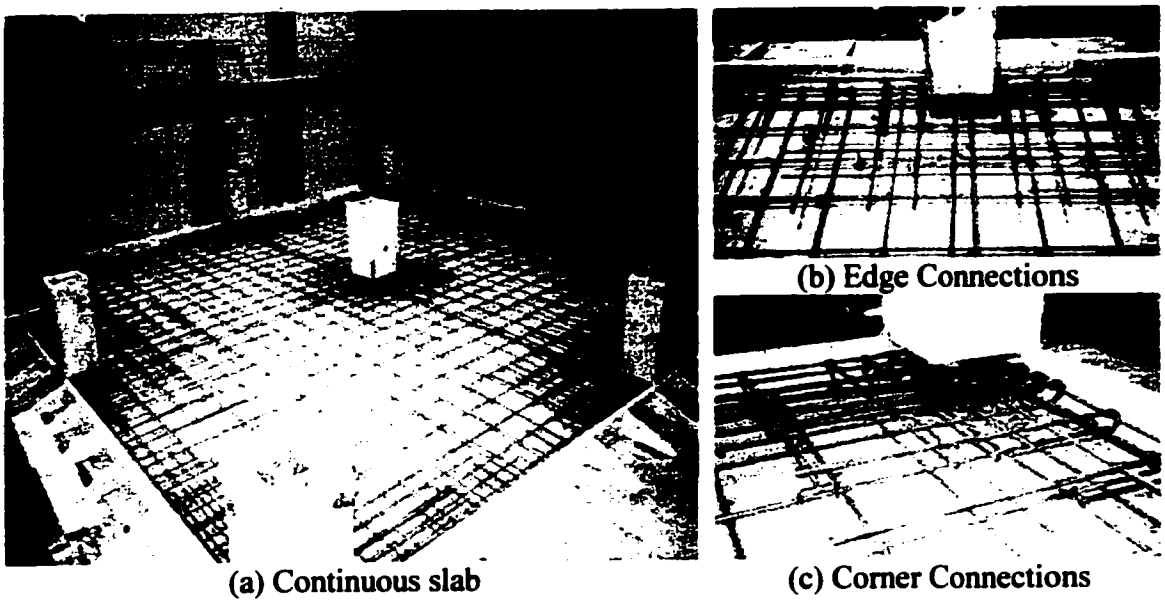

Figure 3.3 Field lay out of slab reinforcement; (a) overall specimen, (b) edge connections, (c) corner connections

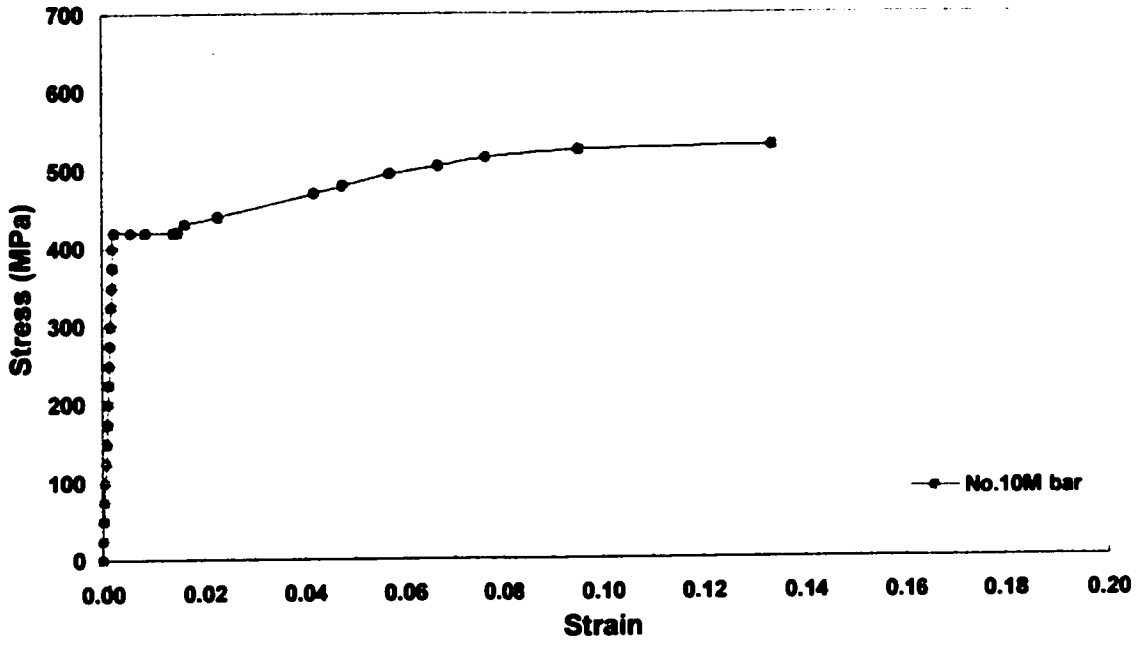

Figure 3.4 Stress - strain relationship of steel #10M for continuous flat plate specimen

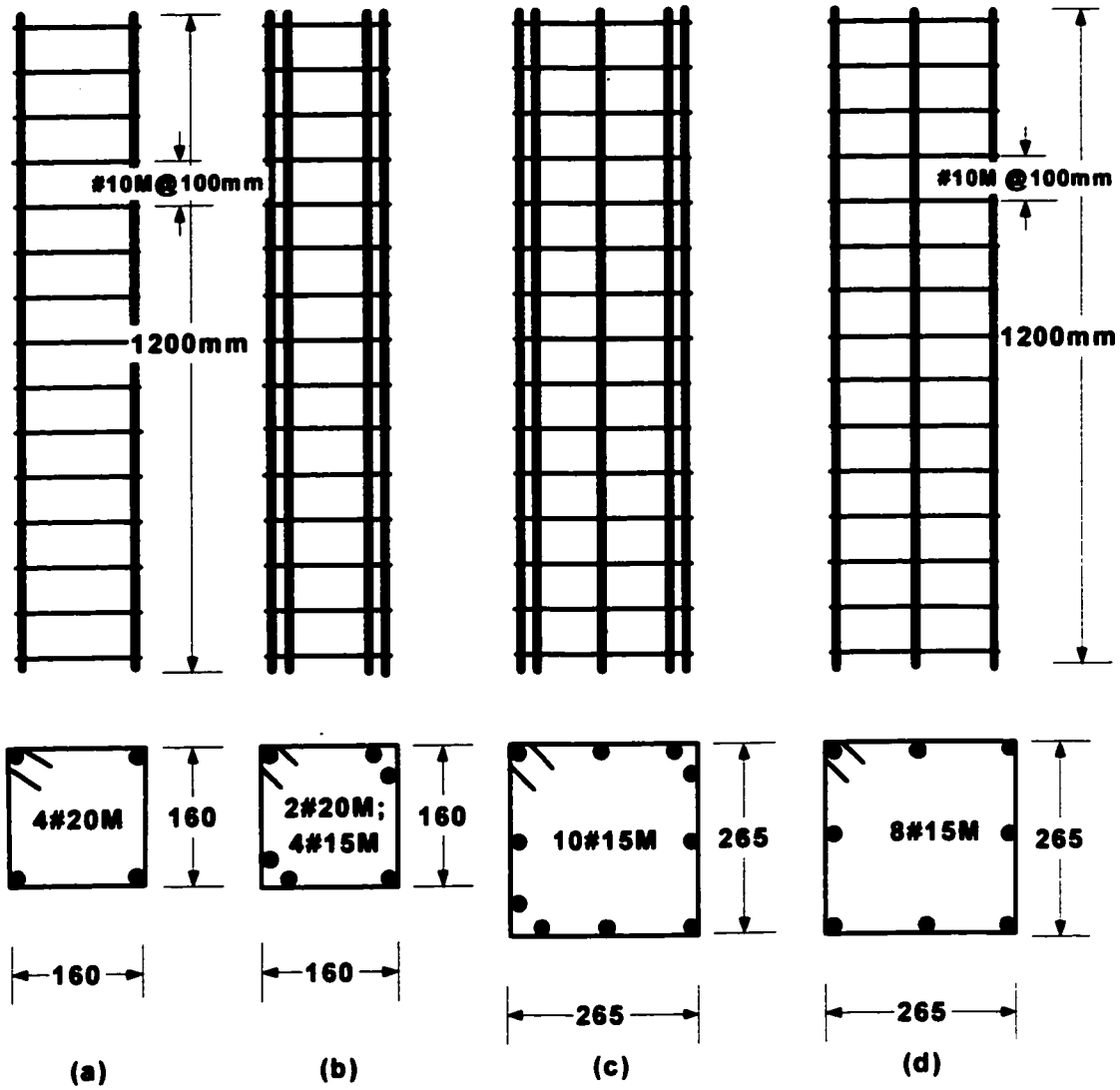

Figure 3.5 Column cages of continuous slab specimen; (a) for three edge columns, (b) for the fourth edge column, (c) for corner columns and (d) for interior column

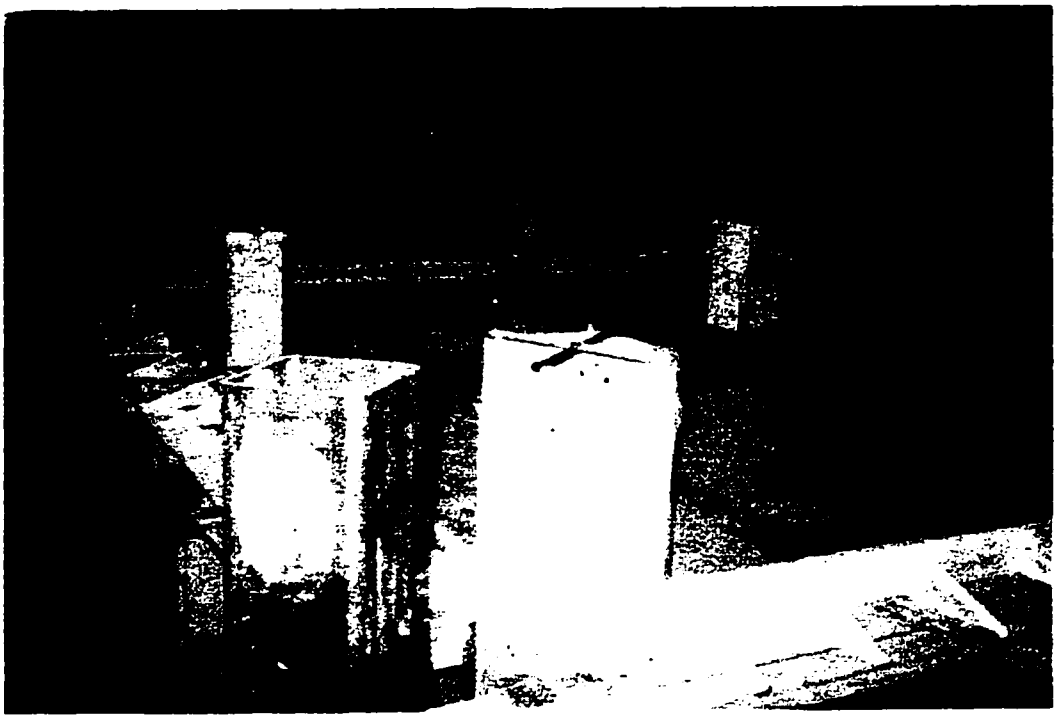

Figure 3.6 Polyetheline covers on slab formwork before casting

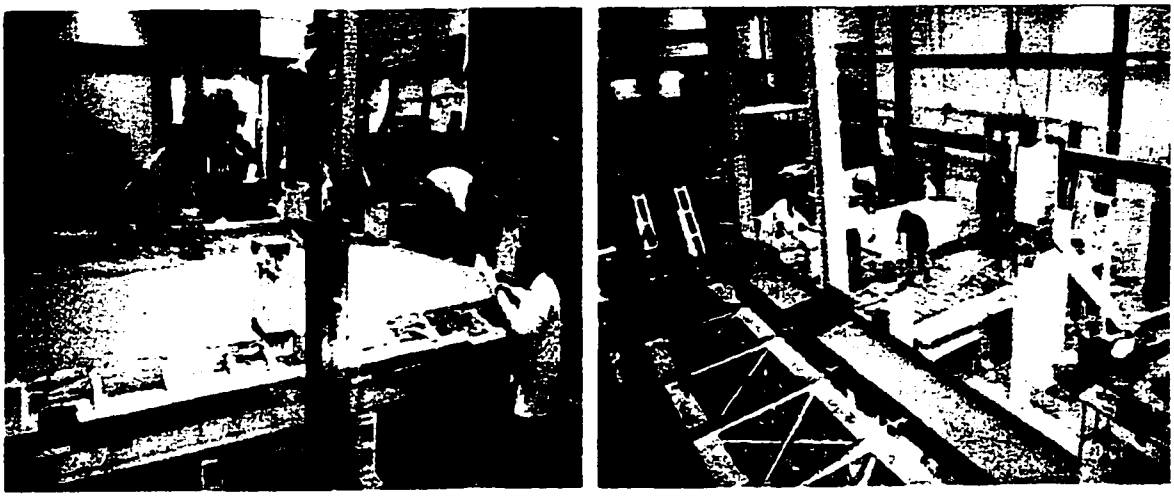

Figure 3.7 Casting concrete of the continuous flat plate specimen

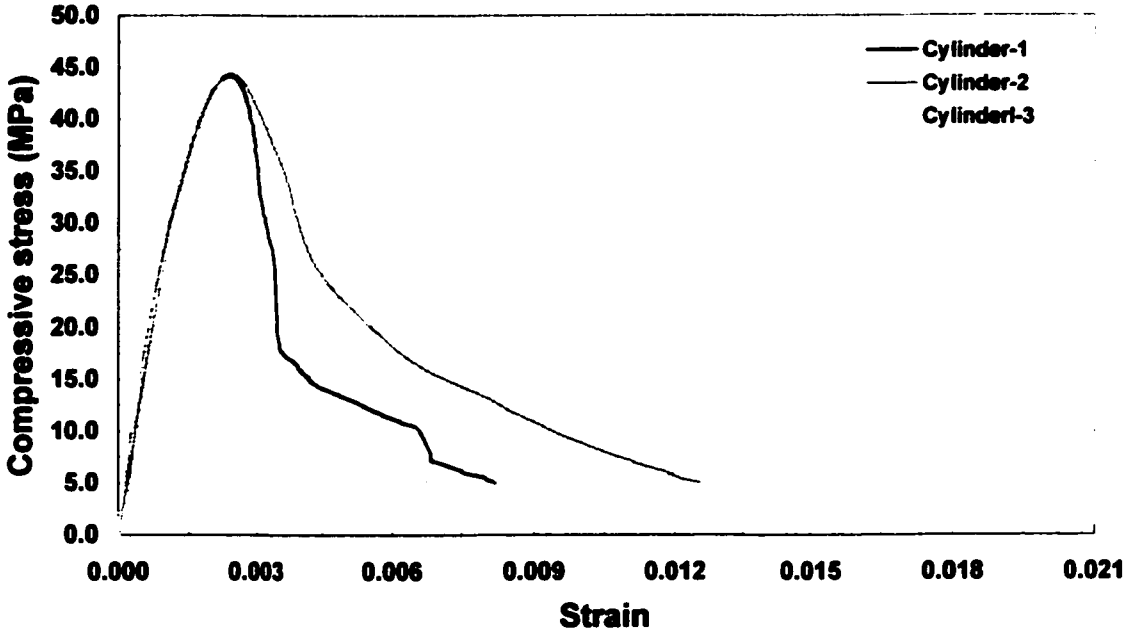

Figure 3.8 Compressive strength of concrete cylinders of the continuous slab specimen at 28 days

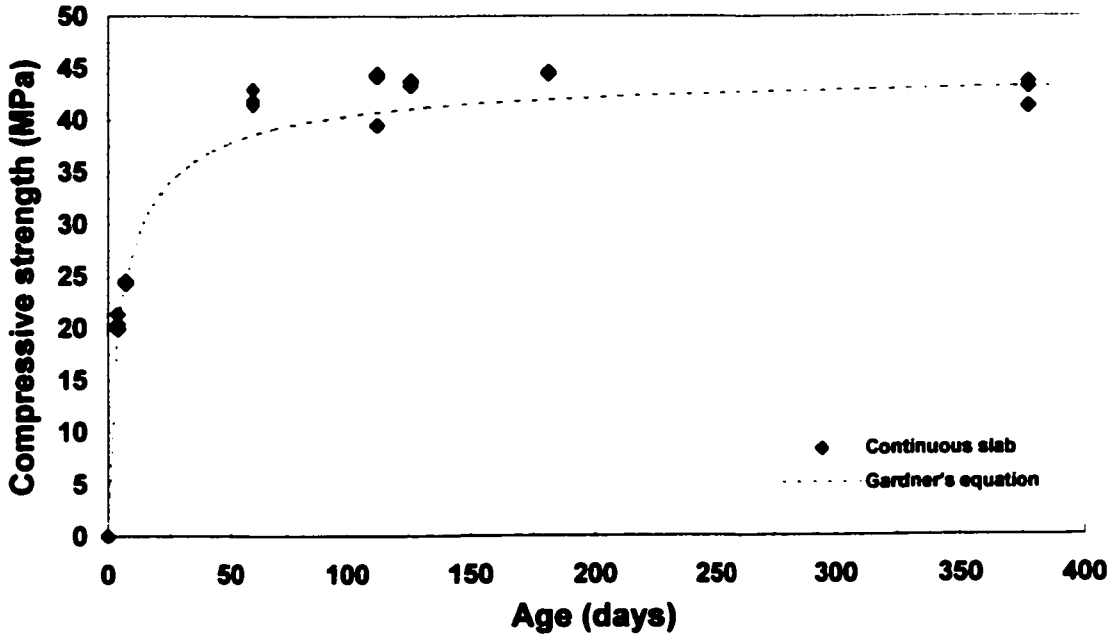

Figure 3.9 Compressive strength over time of concrete cylinders of continuous slab specimen

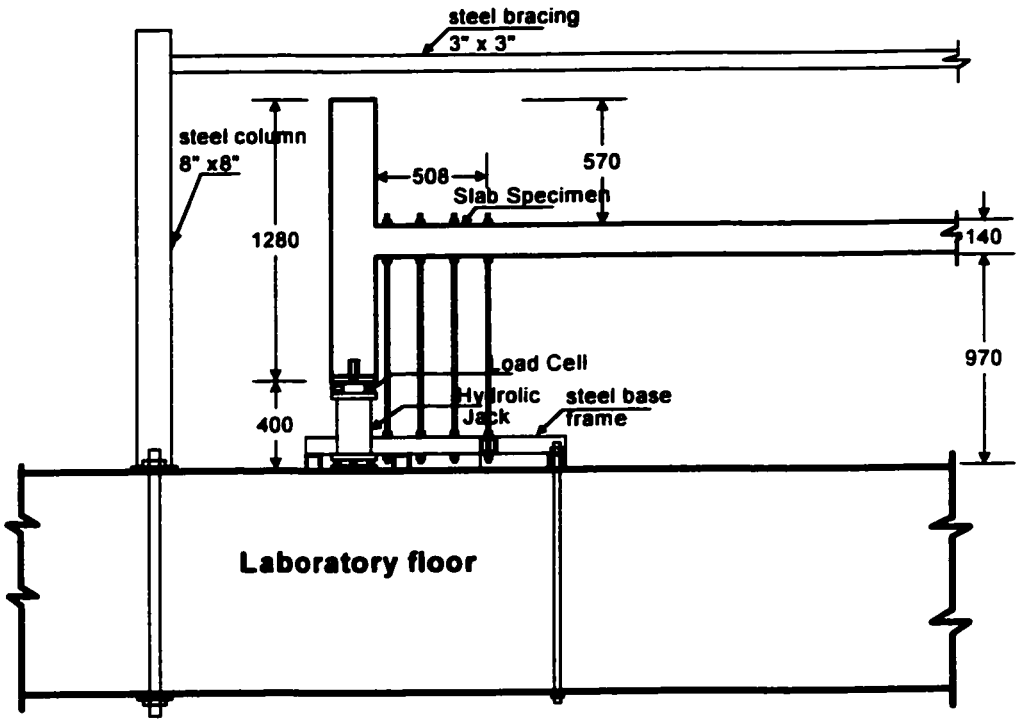

Figure 3.10 Test setup for edge column slab connection of the continuous slab specimen subjected to vertical load only

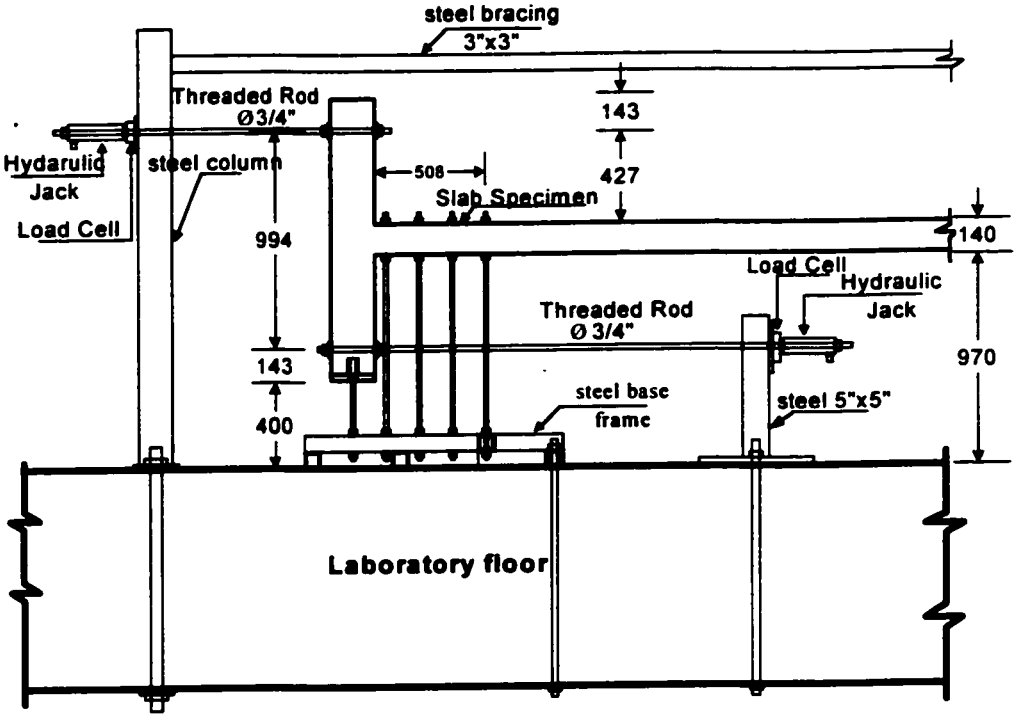

Figure 3.11 Test setup for edge column slab connection of the continuous slab specimen subjected to bending moment only

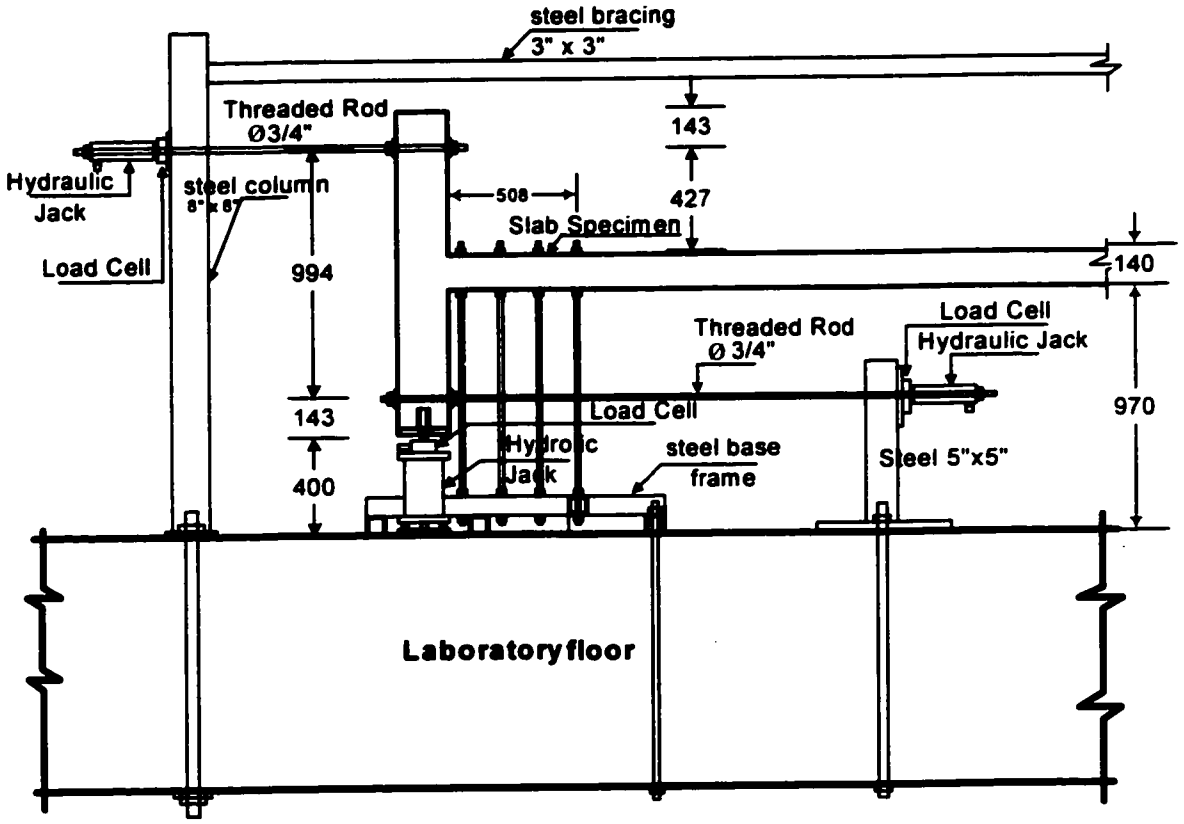

Figure 3.12 Test setup for edge column slab connection of the continuous slab specimen subjected to combined vertical load and bending moment

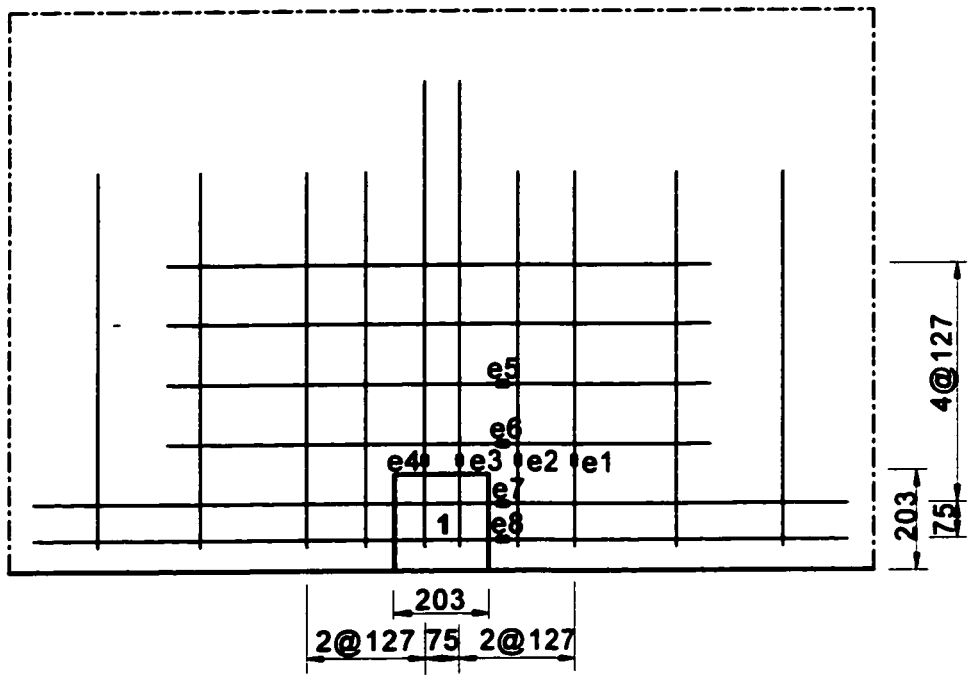

(a) North edge connection (E_1)

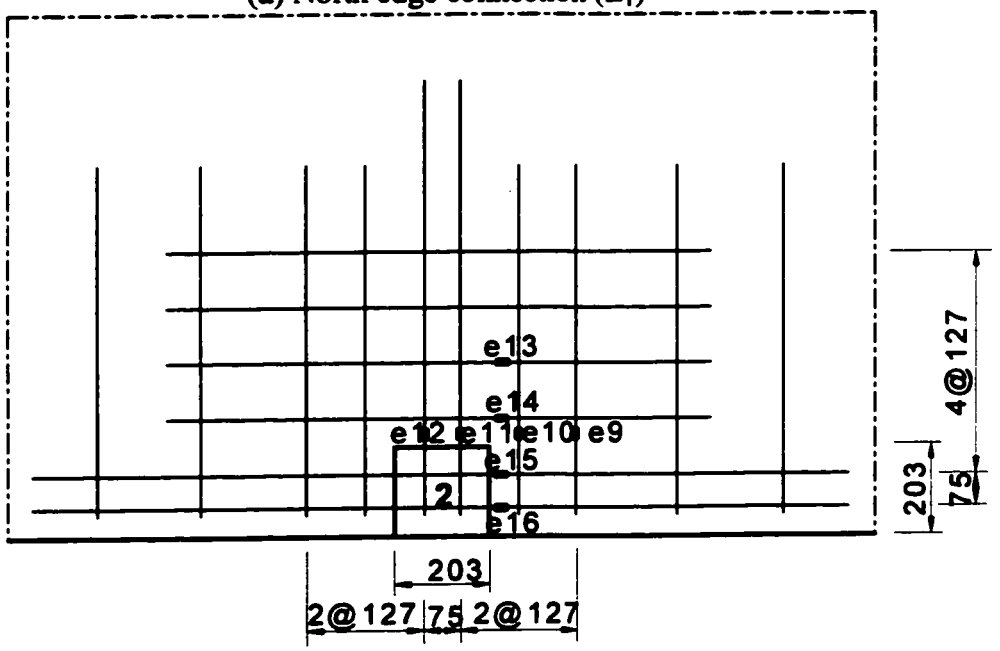

(b) East edge connection (E_2)

Figure 3.13 Strain gauges position on the negative reinforcement of connections E_1 and E_2 of the continuous slab specimen; all the gauges are at 25 mm from the column faces

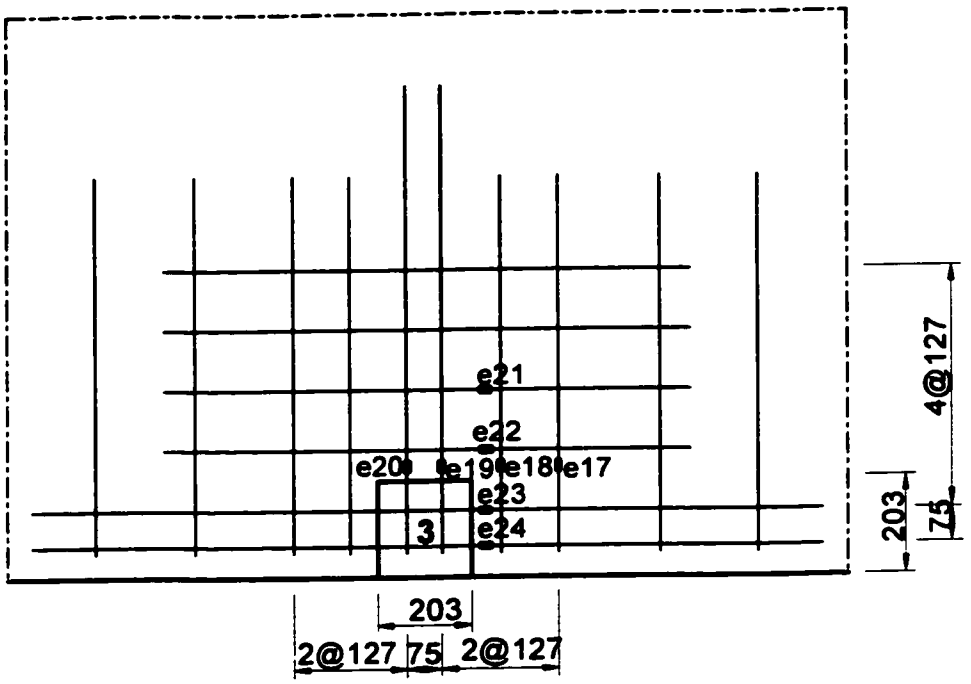

(a) South edge connection (E_3)

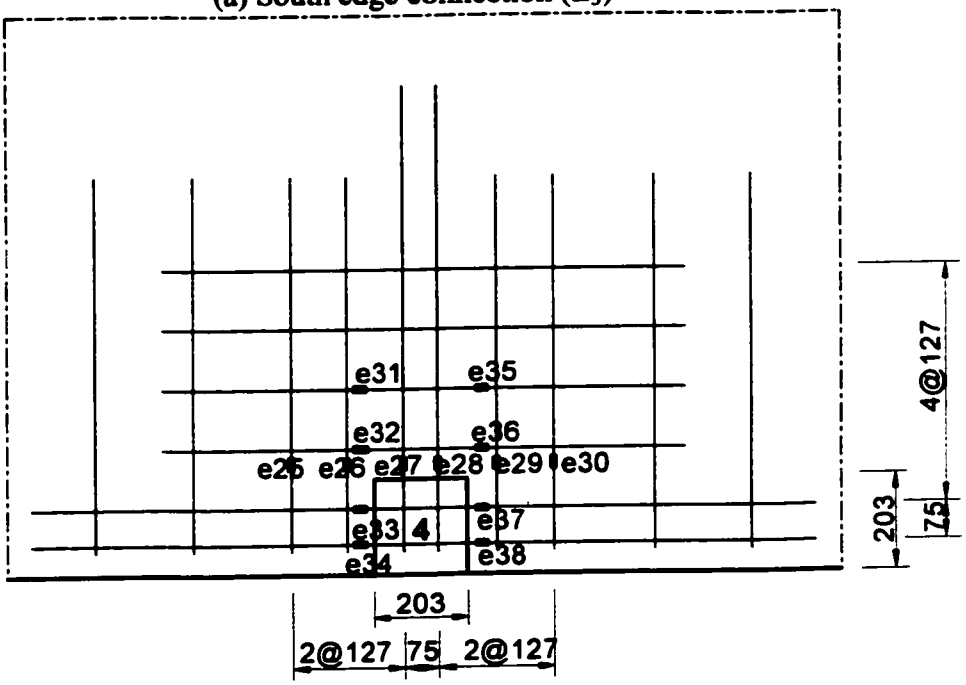

(b) West edge connection (E_4)

Figure 3.14 Strain gauges position on the negative reinforcement of connections E_3 and E_4 of the continuous slab specimen; all the gauges are at 25 mm from the column faces

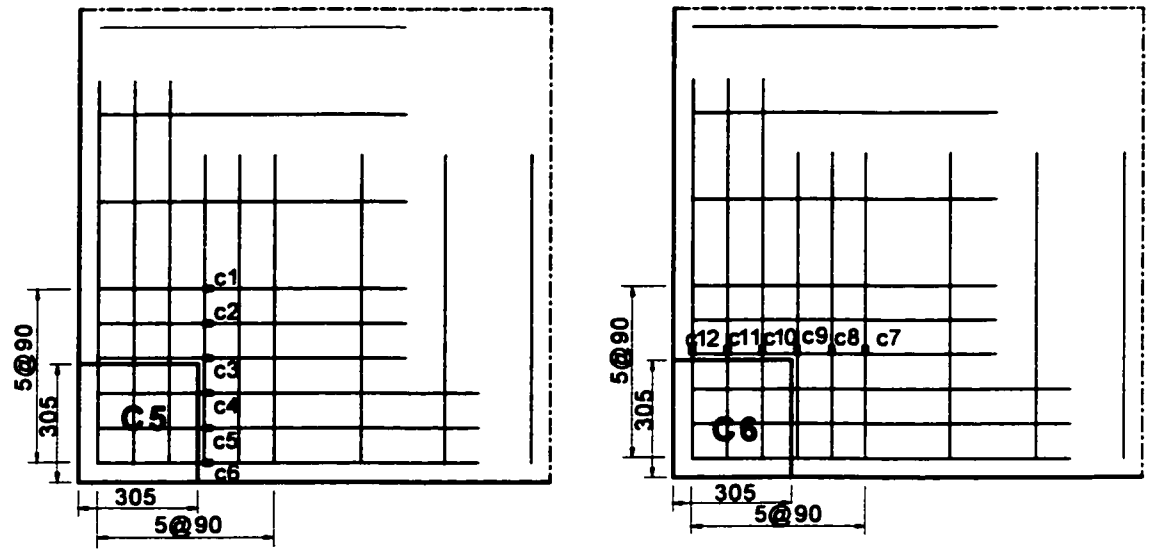

(a) North west corner column slab connection (C_5)

(b) North-East corner column slab connection (C_6)

(c) South-West corner column slab connection (C_7)

(d) South-East corner column slab connection (C_8)

Figure 3.15 Strain gauges position on the negative reinforcement of the corner column slab connection of the continuous slab specimen; all the gauges are at 25 mm from the column faces

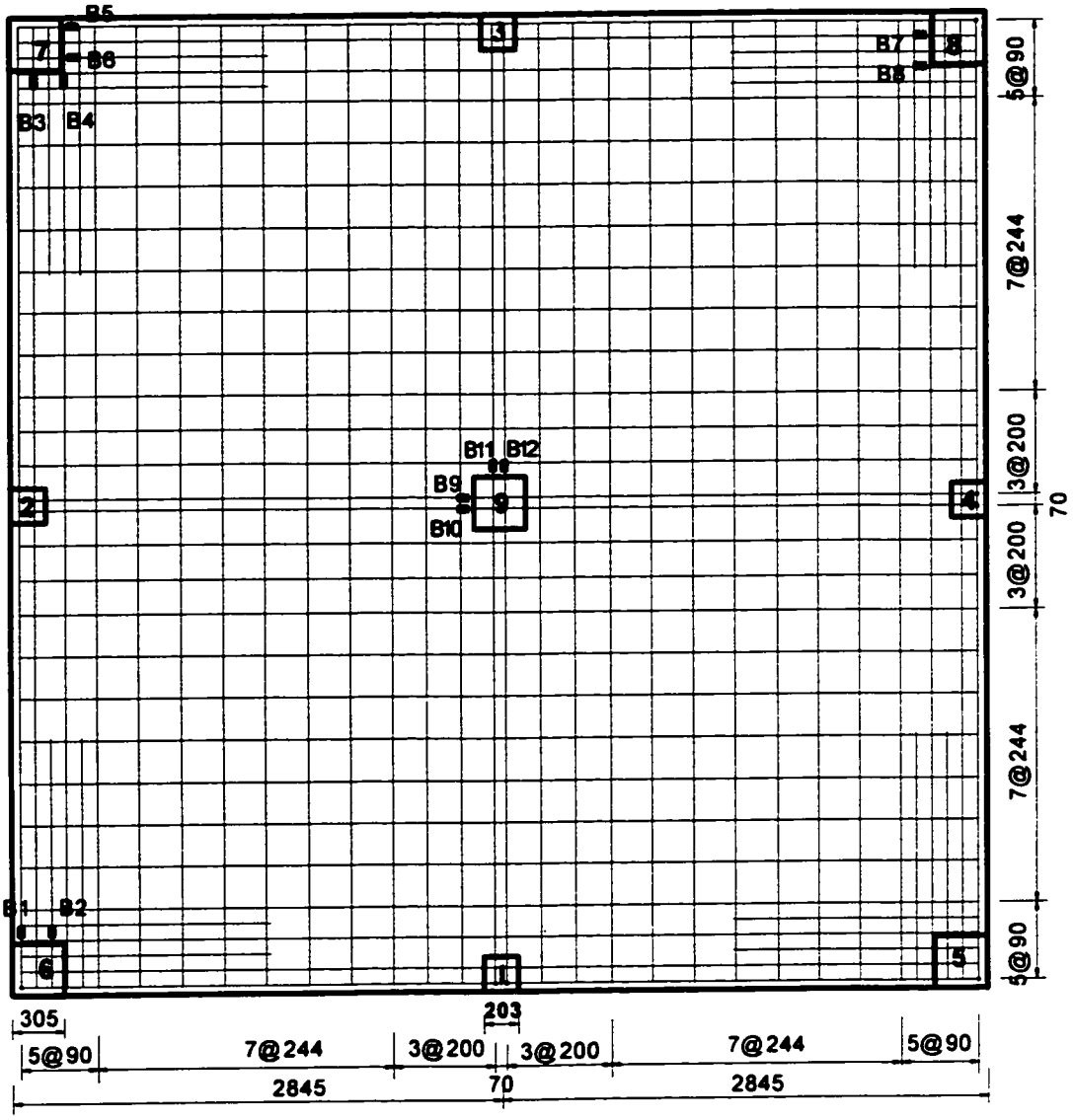

Figure 3.16 Strain gauges position on the bottom reinforcement of the continuous slab specimen; all the gauges are at 25 mm from the column faces

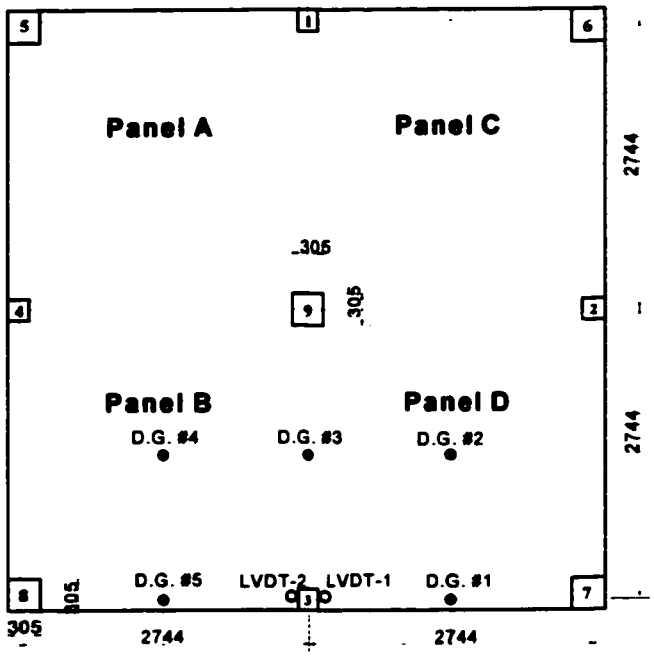

Figure 3.17 Typical position of LVDT's and dial gauges to measure out-of-plane deflection on the test of the edge column slab connections

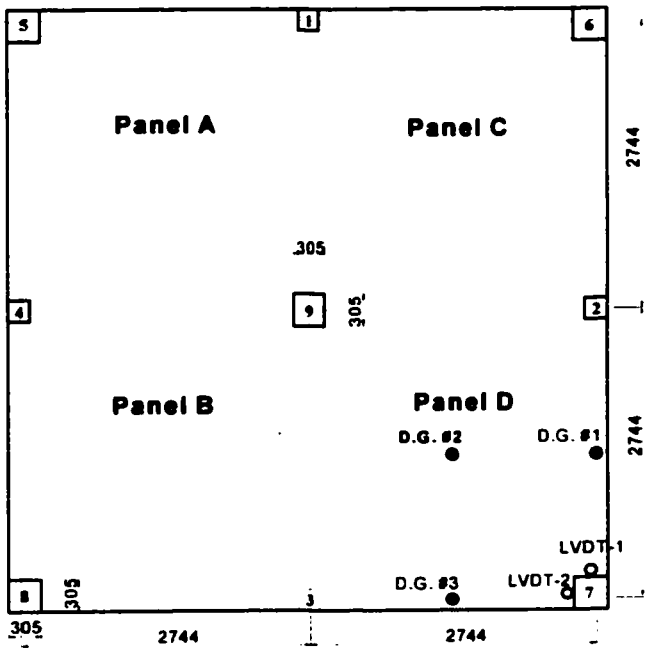

Figure 3.18 Typical position of LVDT's and dial gauges to measure out-of-plane deflection on the test of the corner column slab connections

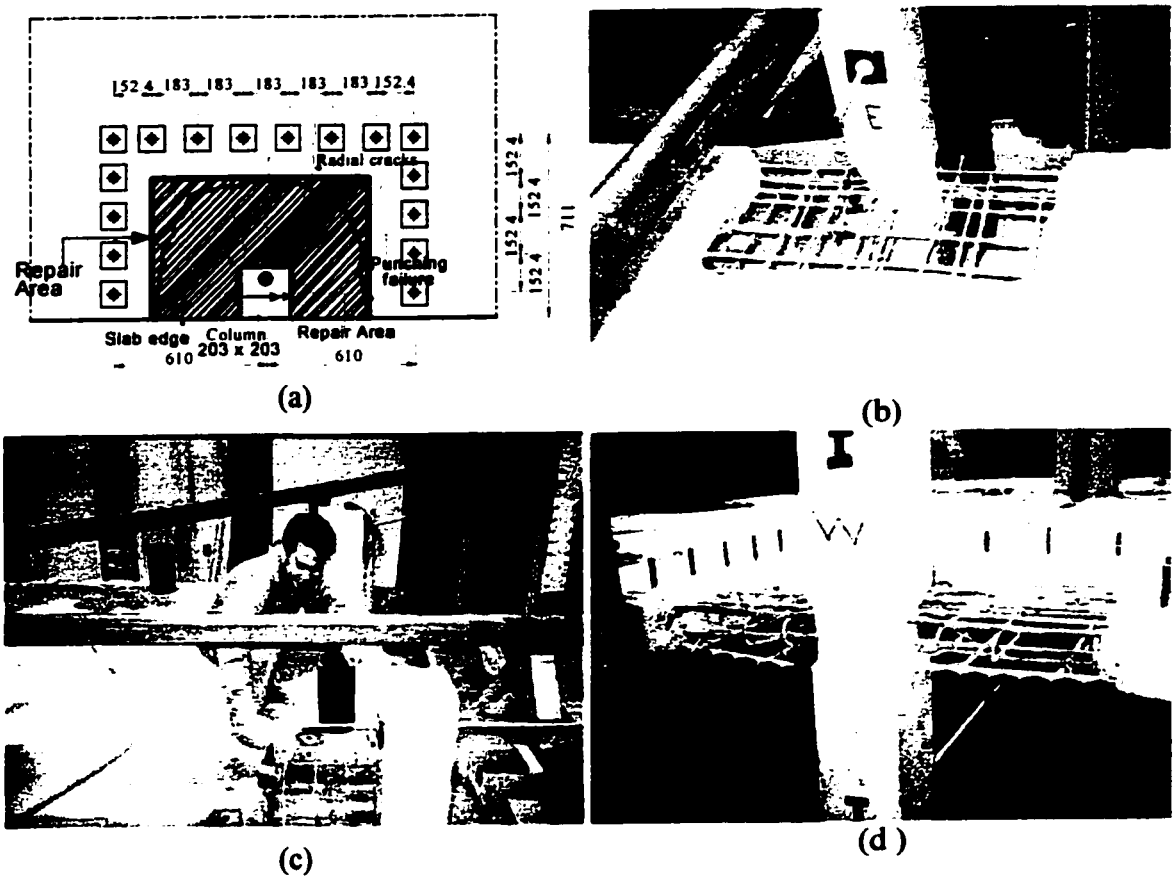

Figure 3.19 Repair edge column slab connections; (a) Damaged concrete to be remove; (b) & (d) Edge reinforcement after removing concrete; (c) Formwork and application of bonding agent before concrete casting

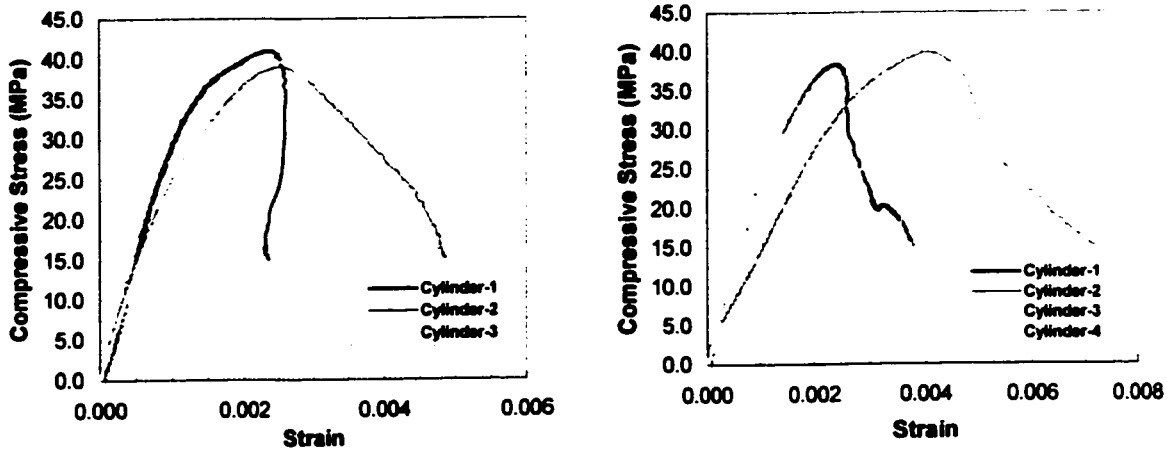

(a) E_{2R} Connection (b) E_{1R} Connection

Figure 3.20 Stress strain relationship of the non-shrinkable concrete cylinder at 28 days for repairing edge connections; (a) E_{2R} Connection; (b) E_{1R} Connection

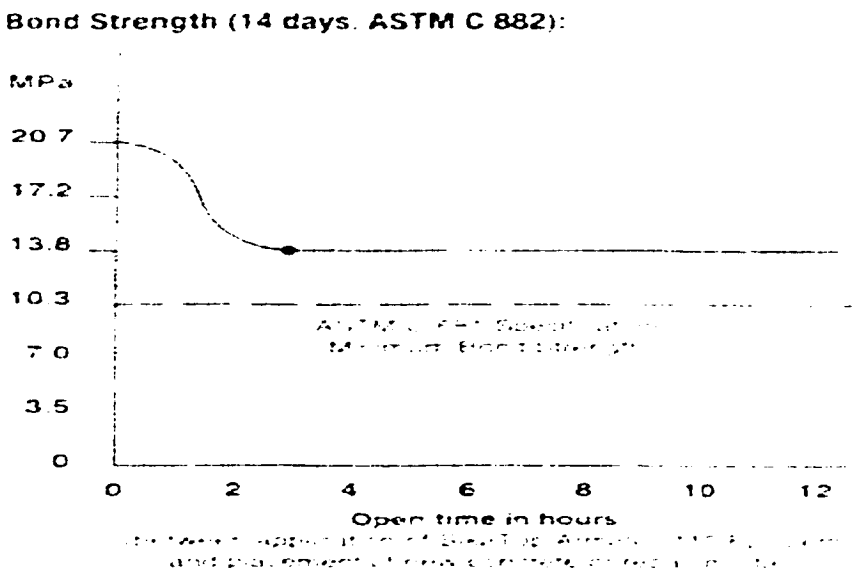

Figure 3.21 Bond strength (14 days) versus open time of SikaTop Armatec 110 EpoCem bonding agent.

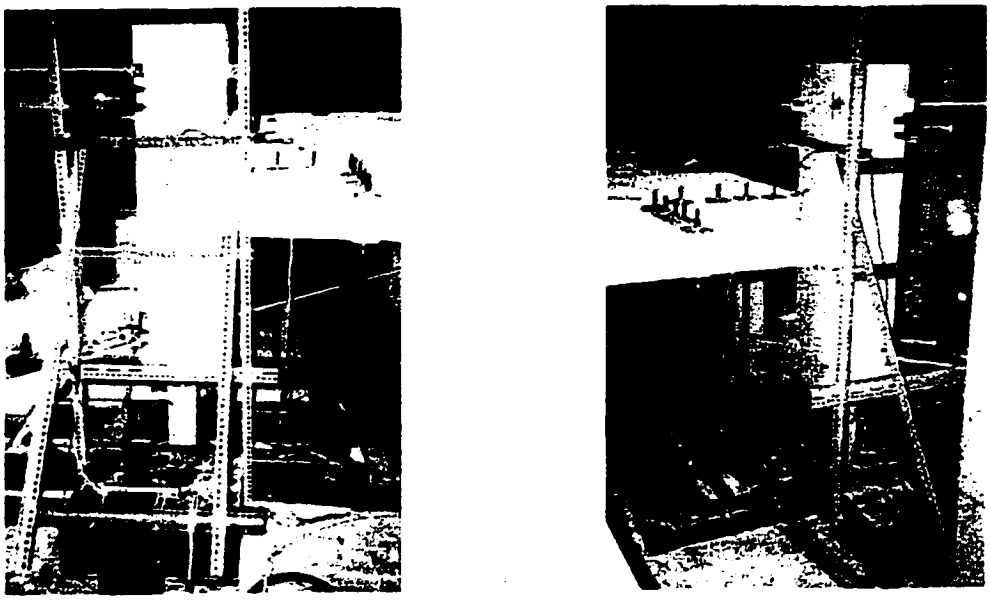

Figure 3.22 Typical test setup of corner column slab connections

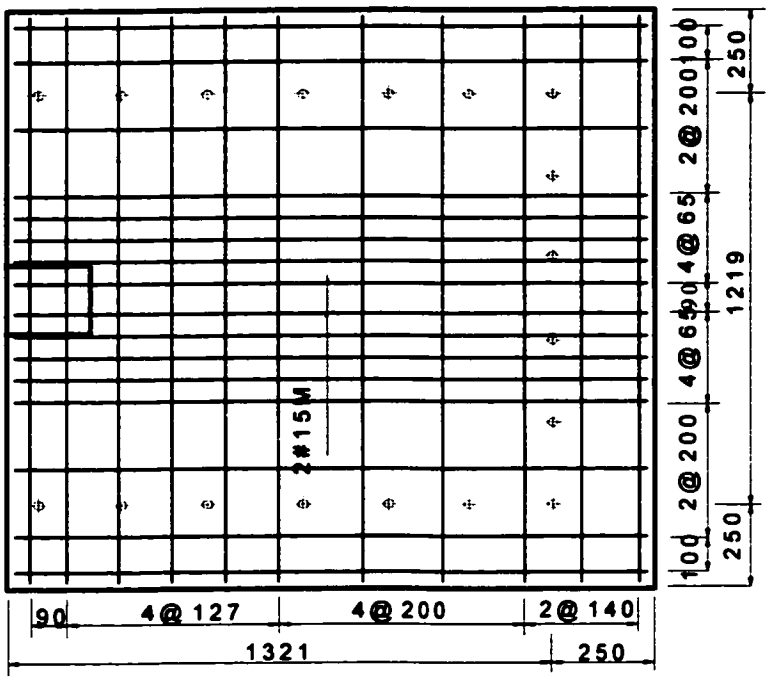

(a) Top Reinforcement

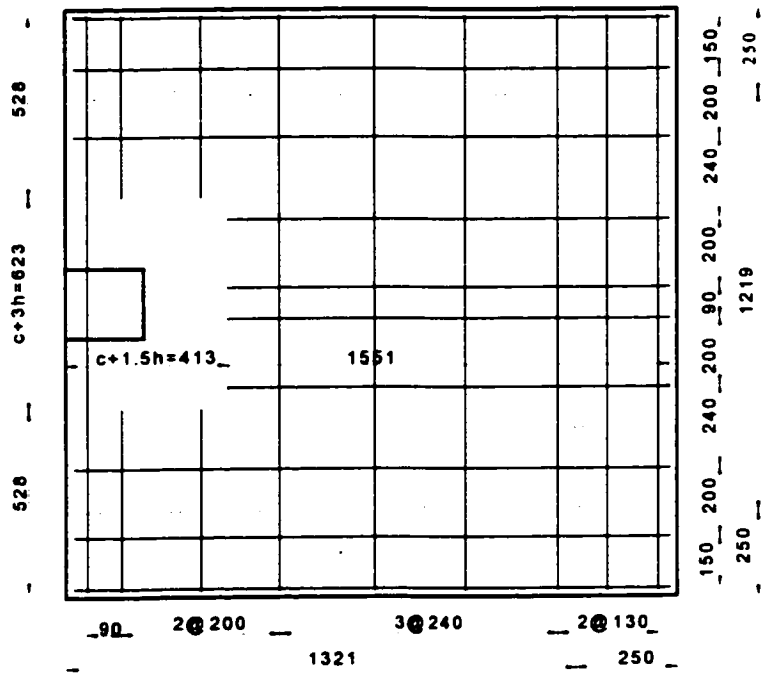

(b) Bottom Reinforcement

Figure 3.23 Reinforcement of the isolated slab specimen of Series I (all bars are #10M, unless indicated in the drawing)

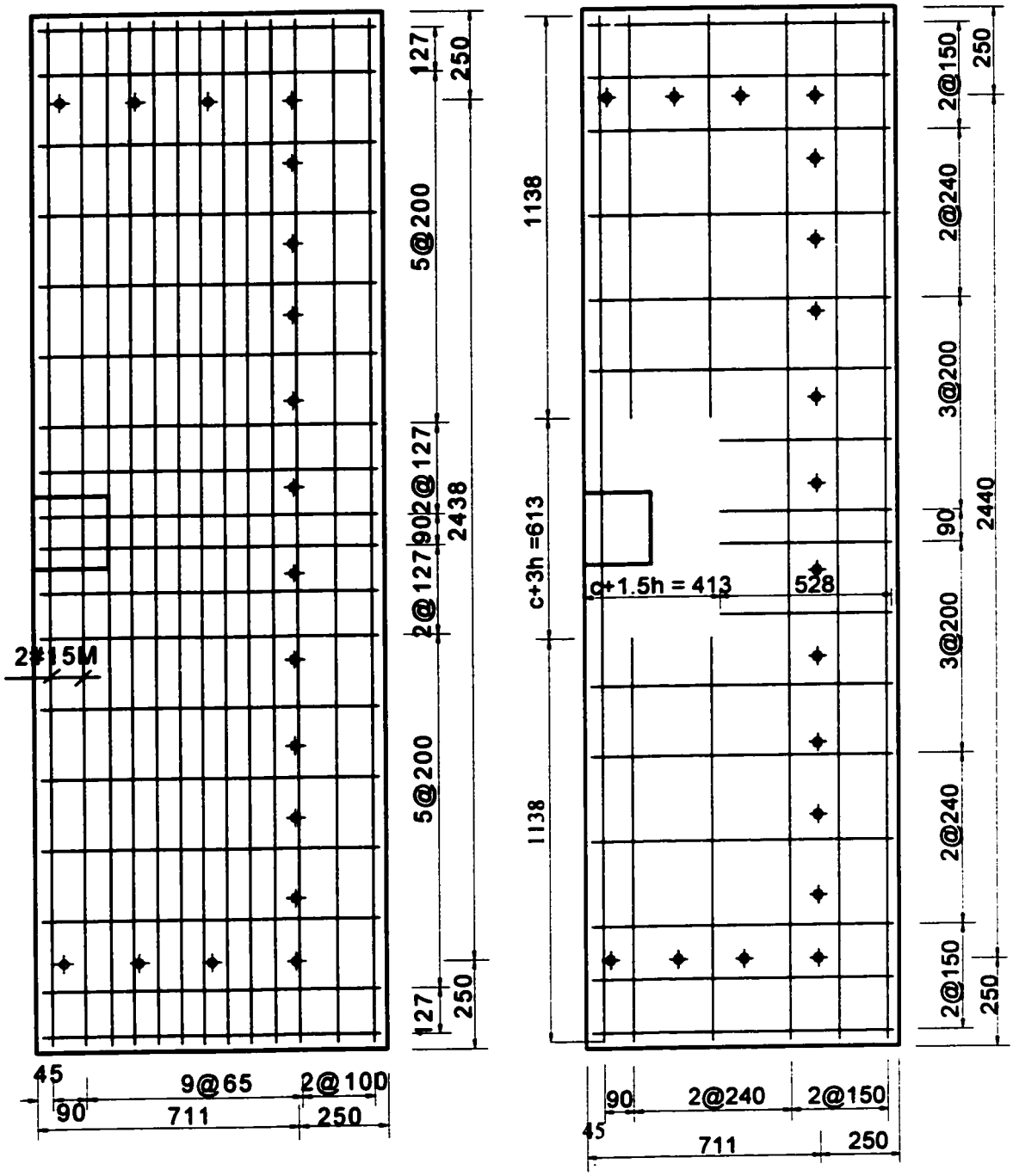

(a) Top reinforcement

(b) Bottom reinforcement

Figure 3.24 Reinforcement of the isolated slab specimen Series II (all bar are #10M, unless indicated in the drawing)

(a) Slab reinforcement

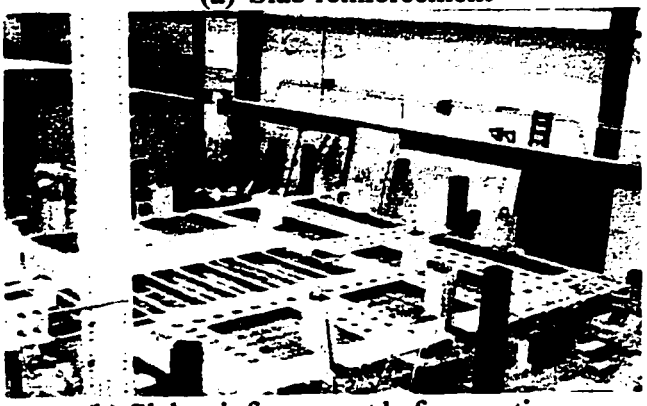

(b) Slab reinforcement before casting

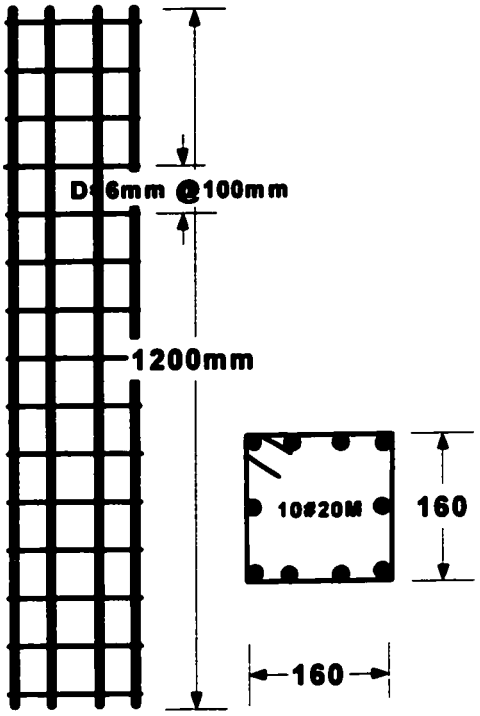

(c) Column reinforcement Series I&II

Figure 3.25 Arrangement of rebars in the isolated slab specimens; (a) slab reinforcement, (b) column reinforcement, and (c) the specimens before casting

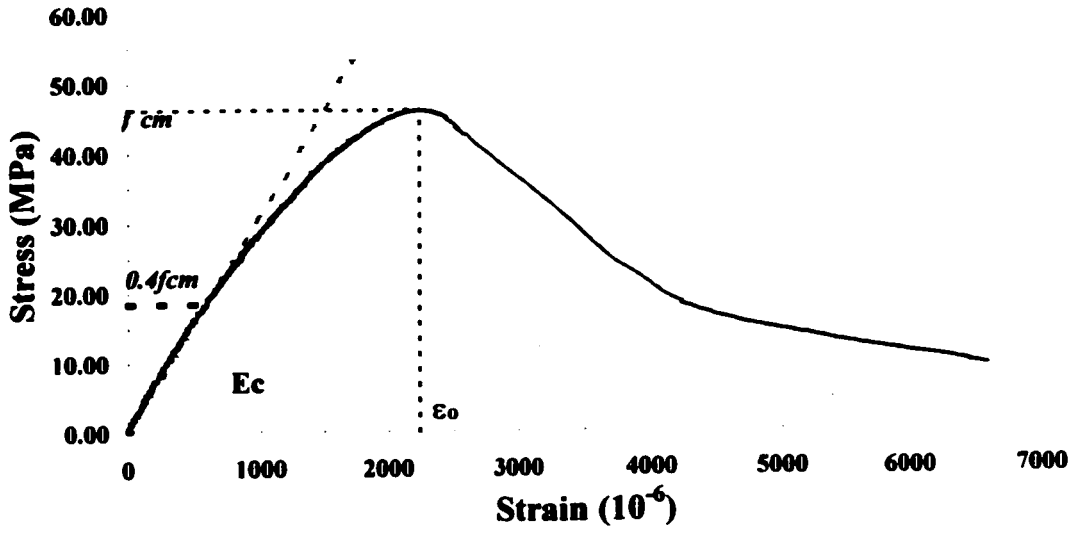

Figure 3.26 Typical stress-strain relationship of concrete cylinder of the isolated slab specimen

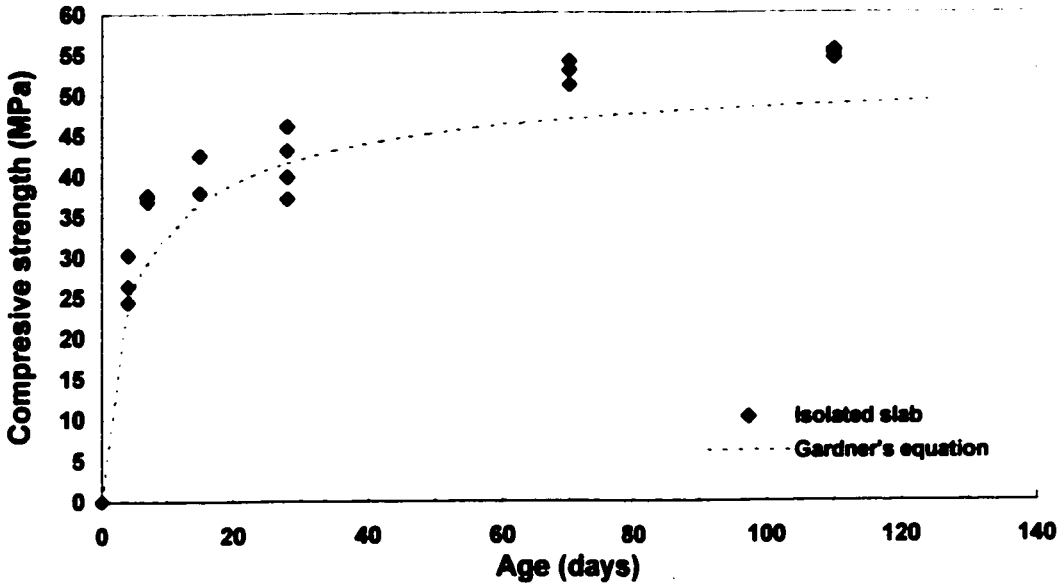

Figure 3.27 Compressive strength development over time of concrete cylinder of the isolated slab specimen

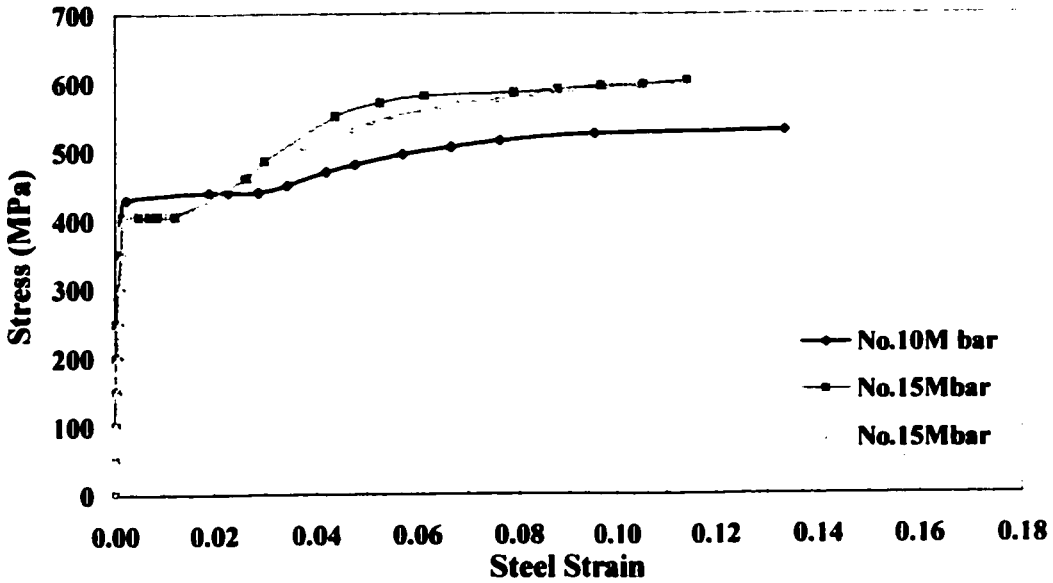

Figure 3.28 Typical stress-strain relationship of bar #10M and #15M used in the isolated slab specimen

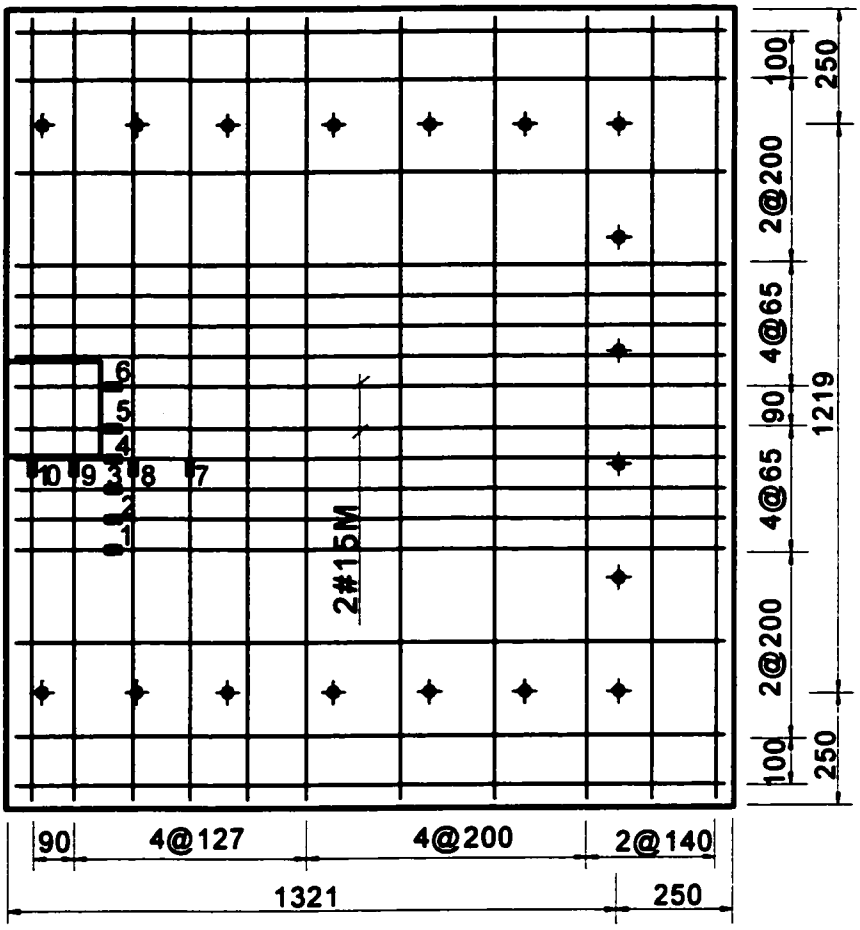

Figure 3.29 Typical position of strain gauges on the negative reinforcement of the isolated slab Series I; all of the strain gauges are at 25 mm from the column faces

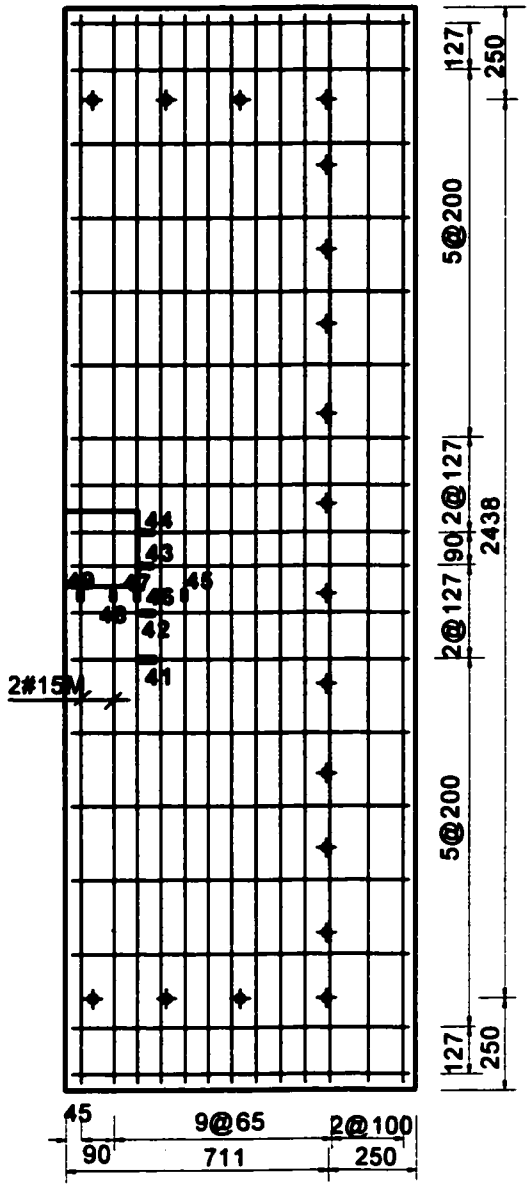

Figure 3.30 Typical position of strain gauges on the negative reinforcement of the isolated slab Series II; all of the strain gauges are at 25 mm from the column faces

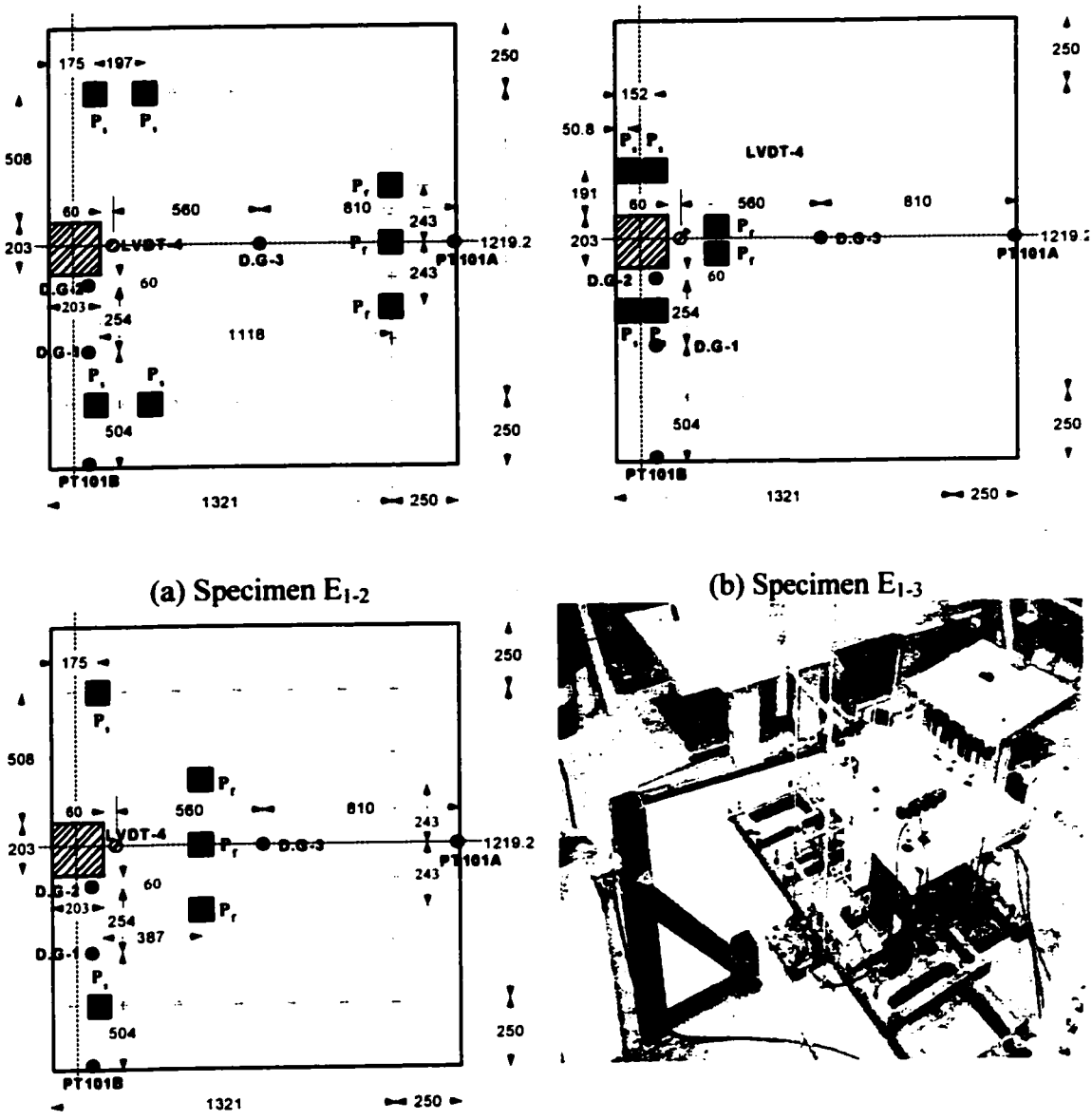

(a) Specimen E_{1-2}

(b) Specimen E_{1-3}

(c) Specimen E_{1-4}

(d) Test set-up specimen E_{1-2}

Figure 3.31 Position of applied vertical loads and gauges for specimen in Series I; (a) specimen E_{1-2}, (b) specimen E_{1-3}, (c) specimen E_{1-4}, and (d) Test of specimen E_{1-2}

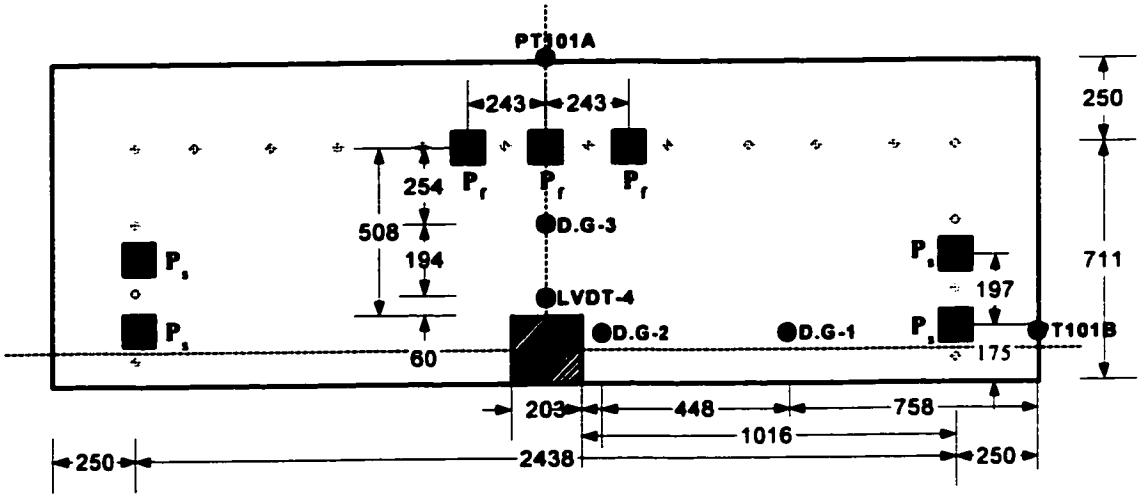

Figure 3.32 Position of applied vertical loads and gauges of isolated edge connection $E_{2\text{-}1}$ of Series II

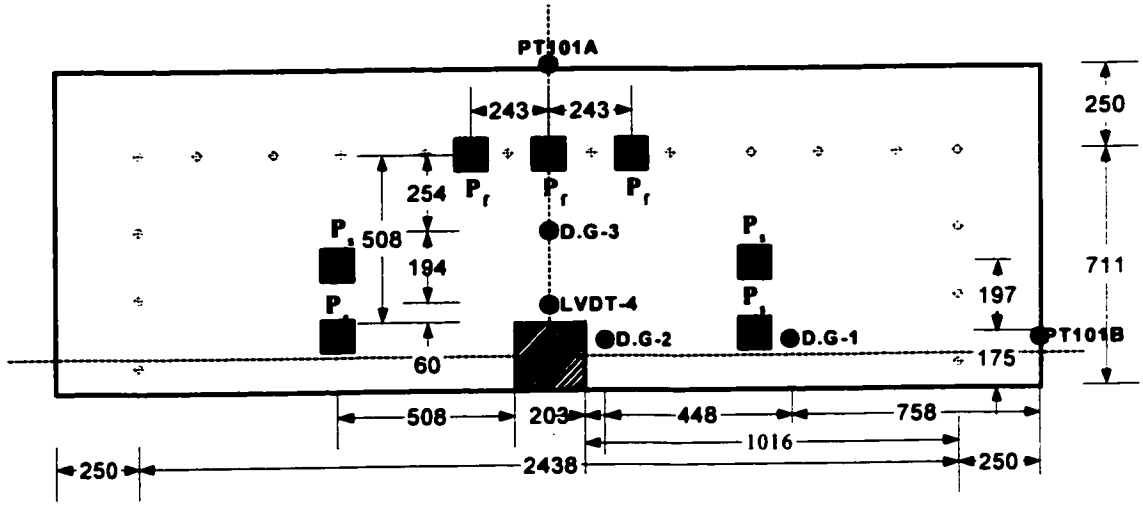

Figure 3.33 Position of applied vertical loads and gauges of isolated edge connection $E_{2\text{-}2}$ of Series II

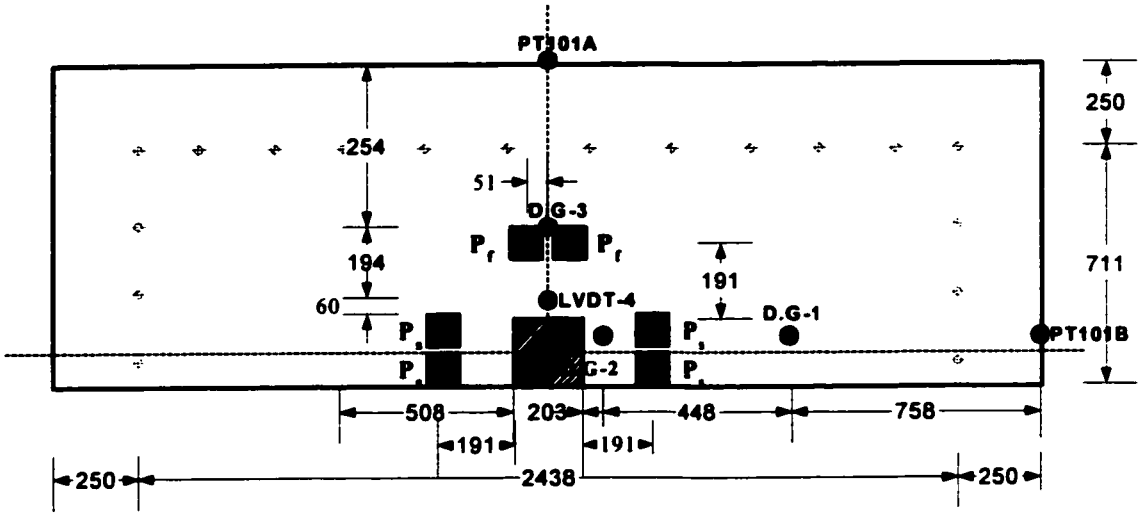

Figure 3.34 Position of applied vertical loads and gauges of isolated edge connection $E_{2\text{-}3}$ of Series II

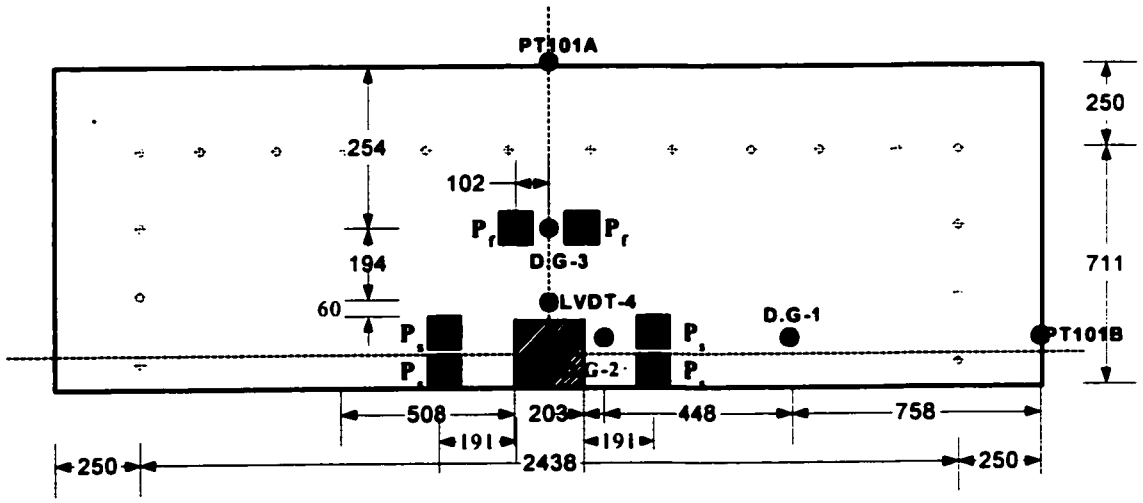

Figure 3.35 Position of applied vertical loads and gauges of isolated edge connection $E_{2\text{-}4}$ of Series II

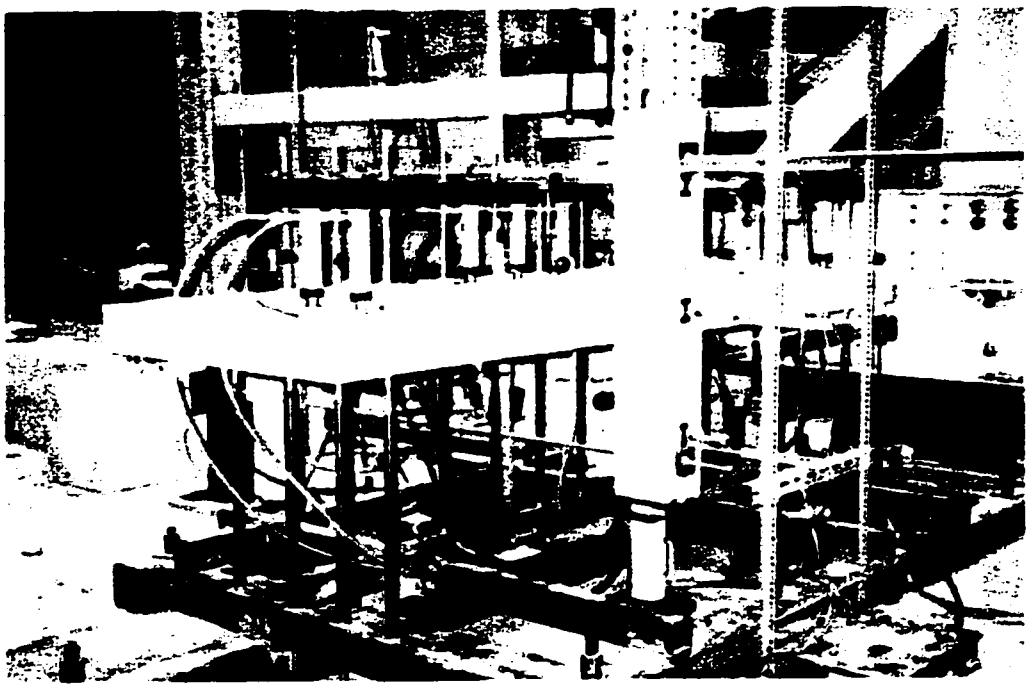

(a) Connection E_{2-1}

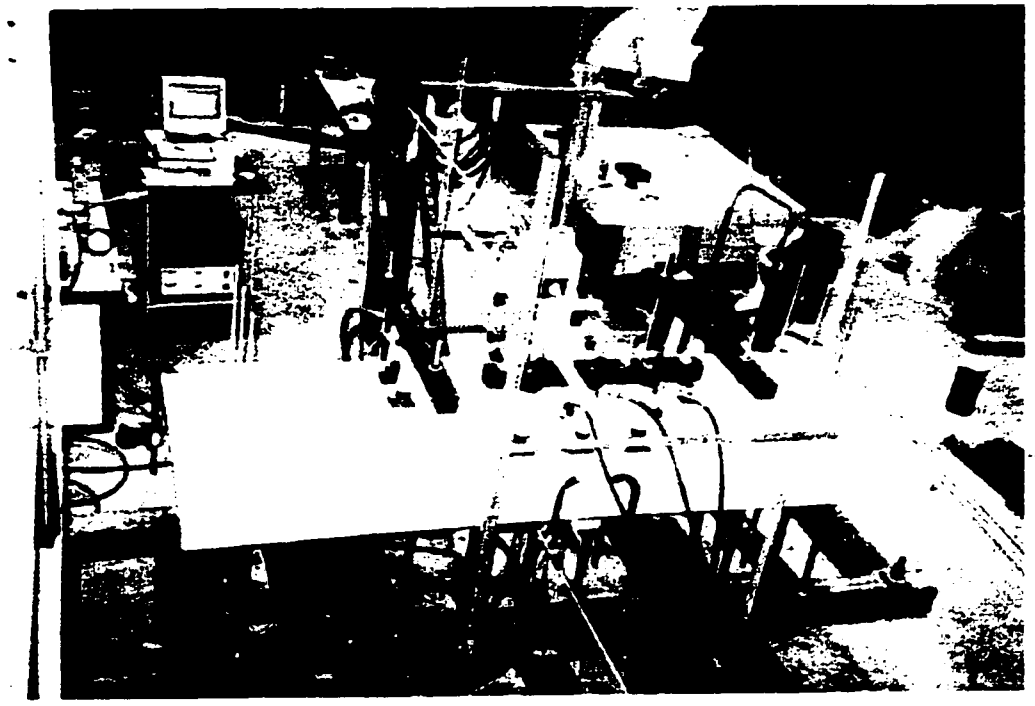

(b) Connection E_{2-2}

Figure 3.36 Test setup of isolated column slab connections in series II

CHAPTER 4
TEST RESULTS

4.1 GENERAL

The main variable considered in this study was the interaction between shear forces and bending moment (*M/V* ratio) on the punching shear strength of edge and corner column slab connections. Additional variables were the reinforcement ratios parallel and perpendicular to the free edge within c_2+3h by $c_1+1.5h$, where c_2 and c_1 are the column dimensions parallel and perpendicular to the slab free edge, respectively. The flexural reinforcement ratios perpendicular and parallel to the slab edge are identified as ρ_x and ρ_y.

This chapter presents the test results of edge connections, repaired edge connections and corner connections in Sections 4.2, 4.3 and 4.4, respectively, under the following categories:

- Failure loads and mechanisms
- Crack patterns
- Failure criterions
- Flexural steel strain
- Out-of-plane slab deflections
- Column Rotations

4.2 TEST RESULTS OF EDGE COLUMN SLAB CONNECTIONS

4.2.1 Failure load and mode of failure

All connections failed in punching shear (*PS*), except one edge column slab connection (E_3) that was subjected to bending moment only which failed in combined flexure and torsion (*FT*). Table 4.1 presents the ultimate load capacity and mode of failure of the edge column slab connections. Connections E_1, E_2 and E_4 of the continuous slab specimen failed in brittle punching shear in which the column stubs punched through the slab. Isolated column slab connections in Series I ($E_{1\text{-}1}$, $E_{1\text{-}2}$, $E_{1\text{-}3}$ and $E_{1\text{-}4}$) and in Series II ($E_{2\text{-}1}$, $E_{2\text{-}2}$, $E_{2\text{-}3}$ and $E_{2\text{-}4}$), where the reinforcement ratio was increased in one direction, failed in more ductile manners compared to the edge connections of the continuous slab.

4.2.2 Crack patterns

This section describes the crack patterns observed during the test of the edge column slab connections. The discussion is divided into three parts; connection subjected to vertical load only, connection subjected to bending moment only and the two connections subjected to combined vertical load and bending moment.

4.2.2.1 Edge connection subjected to vertical load only (E_2)

Circumferential cracks, indicated by (a) in Figure 4.1, were first observed on the slab tension side along the column perimeter at 18% of ultimate load. These cracks propagated through the slab depth toward the bottom slab surface at the free edge as the load was increased. Diagonal radial cracks (b) developed first at the inner corners of the column slab interface at a load of 60 kN followed by radial cracks perpendicular (c) to the column inner face as the load was further increased. Some cracks (d) were also observed in the slab outside the column, perpendicular to the free edge. When the load reached 82 kN, the radial cracks propagated to the other edge connections and interior connection.

Table 4.1 Ultimate load capacity of edge column slab connections and mode of the failures

Slabs	$c_1=c_2$ mm	h mm	ρ_{c2+3h} %	$\rho_{c2+1.5h}$ %	f_y MPa	f_{cm} MPa	V_u kN	M_u kNm	Failure Modes	Type of specimens
E_1	203	140	0.9	0.9	420	43.6	127.4	34.4	PS	Continuous
E_2	203	140	0.9	0.9	420	42.4	220.0	0.0	PS	Continuous
E_3	203	140	0.9	0.9	420	42.7	0.0	29.2	FT	Continuous
E_4	203	140	0.9	0.9	420	43.6	116.7	14.2	PS	Continuous
E_{1-1}*	203	140	1.6	0.9	430	52.8	79.8	3.9	PS	Series I
E_{1-2}	203	140	1.6	0.8	430	52.8	88.2	49.8	PS	Series I
E_{1-3}	203	140	1.6	0.8	430	55.0	307.0	32.2	PS	Series I
E_{1-4}	203	140	1.6	0.8	430	52.8	114.2	41.1	PS	Series I
E_{2-1}	203	140	0.8	1.6	430	52.8	130.5	34.7	PS	Series II
E_{2-2}	203	140	0.8	1.6	430	52.8	178.9	25.3	PS	Series II
E_{2-3}	203	140	0.8	1.6	430	55.0	328.0	9.6	PS	Series II
E_{2-4}	203	140	0.8	1.6	430	55.0	199.4	16.4	PS	Series II

Note: E_{1-1}* is not included on discussion of test results.
V_u and M_u were measured at centroid of column perimeter
Failure modes: *FT* (combined flexure and torsion); *PS* (punching shear)

Figure 4.1 shows the crack patterns of connection E_2 on the first test. From the crack patterns of the slab during the first test, it was concluded that the behavior of the connection did not represent the design load conditions and that the edge columns of conventionally detailed continuous slabs could not be used to obtain the shear-moment interaction curve without support along the lines of contra-flexure.

(a) (b)

Figure 4.1 Crack patterns of connection E_2 on the first test; (a) cracks on the slab tension side, (b) cracks on the slab free edge

On the second test of connection E_2, supports were provided around the connection, and no significant additional cracks were observed except a few circumferential cracks joining the adjacent radial cracks. The crack patterns in this test followed the patterns of the first test. No torsion cracks were developed during the test. Failure of the connection was reached when the column stub punched through the slab. At the moment of punching, crushing of the concrete along the column slab interface in the compression zone was observed. It was evident that punching failure occurs when the compression zone at the bottom slab-column interface lost the compressive force due to crushing of the concrete. Figure 4.2 shows the failure surface of connection E_2 on the second test. The average angle of inclined failure surface to the slab surface was 21°.

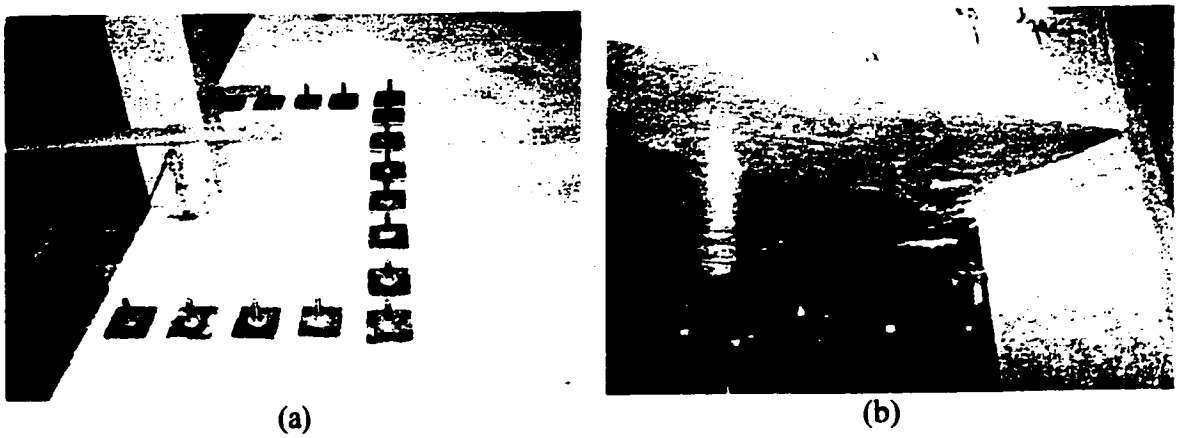

(a) (b)

Figure 4.2 Crack patterns at the failure of second test of connection E_2; (a) cracks on the slab tension side, (b) cracks on the slab free edge

4.2.2.2 Edge connection subjected to bending moment only (E_3)

The first cracks started along the inner column slab interface, followed by torsion cracks originating at the inner column corners and progressing toward the slab free edge. Torsion cracks were observed at 50% of the ultimate capacity of the connection. When the torsion cracks reached the slab edge, they extended through the slab depth in a direction away from the column until reaching the compression face of the slab. Only two radial cracks were observed during the test on the tension side. These cracks started from both inner corners of the column and met with the crack induced by the first test of connection E_2. The crack patterns on the tension side and the free edge of the connection can be seen in Figure 4.3.

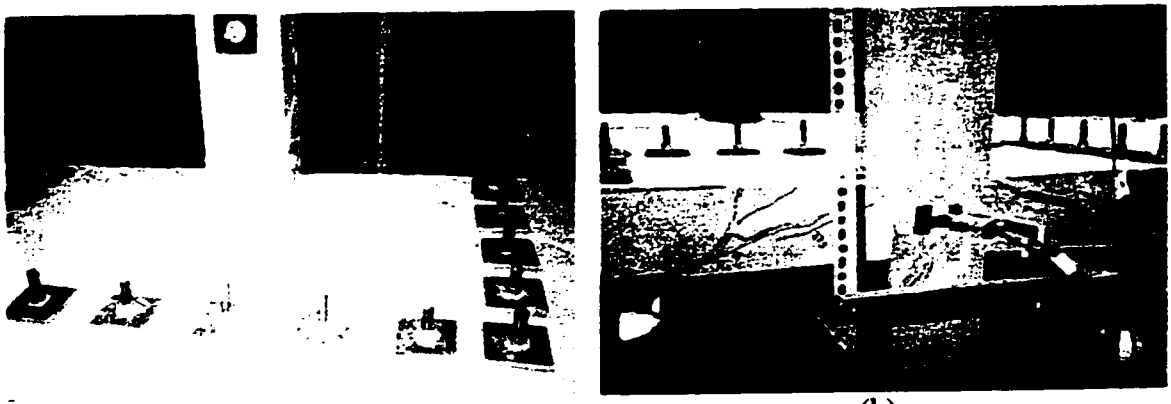

(a) (b)

Figure 4.3 Crack patterns at failure of connection E_3; (a) cracks on the slab tension surface, (b) cracks on the slab free edge

At a load about 70% of ultimate capacity, the torsion and flexural cracks reached completely the compression surface of the slab. Failure of the connection occurred when the concrete along the inner column slab interface and at the tips of the torsion cracks crushed resulting in a large rotation of the column and a decrease of applied load. The failure was very ductile which indicated that the connection failed in combined flexure and torsion.

4.2.2.3 Connections subjected to combined vertical load and bending moment (E_1, E_4)

This type of loading has more practical significant in flat plate structures compared to the connections subjected to vertical load only or bending moment only, since edge column slab connections are always subjected to eccentric loading as mentioned in a previous chapter. In describing the crack patterns of these connections, reference will be made to connections E_2 (shear force only) or E_3 (moment only) as necessary.

The formation of cracks in connection E_1 seemed to be the combined cracks of connections E_2 and E_3. Flexural cracks along the column-slab interface and radial cracks were first observed at loads of 60 kN and 15 kNm for vertical load and moment, respectively. Radial cracks started from both inner column corners and perpendicular to the inner column side progressing diagonally and perpendicular from the column, respectively. Torsion cracks inclined away from the inner corner of the column to the slab free edge progressing to about half of the slab depth were observed at a moment of 17.5 kNm (≈ 54% of ultimate moment). Inclined punching failure surface of the connection did not interact with the torsion cracks so that it could not reach the slab free edge as shown in Figure 4.4.

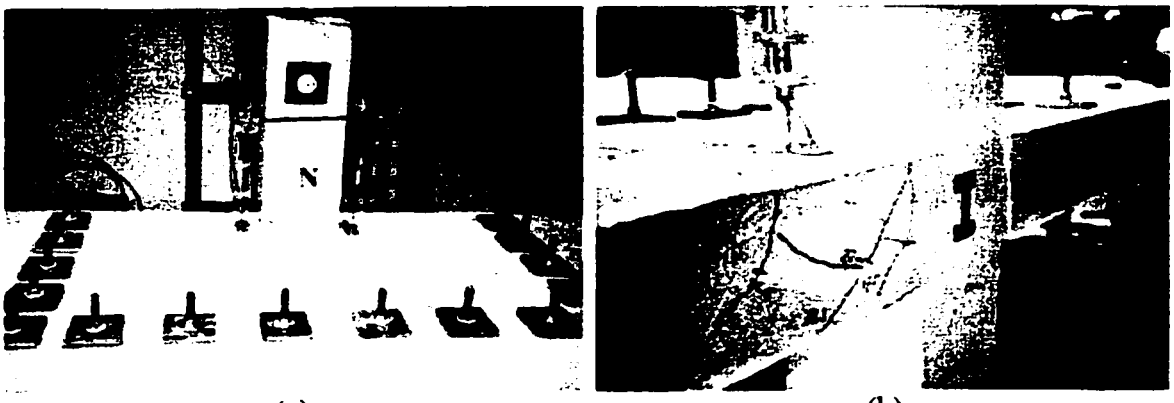

(a) (b)

Figure 4.4 Crack patterns of connection E_1; (a) cracks on the slab tension surface, (b) cracks on the slab free edge

This behavior supports the Regan's approach in developing shear-moment interaction described in Chapter 2. It was again observed, at failure of the connection, that the inner column slab interface crushed in the compression zone. The inclined angle of shear failure surface was about 22.2° to the slab surface.

The crack patterns of connection E_4 were similar to those of connection E_2 even though there was a moment applied on connection E_4. Flexural cracks along the column perimeter progressing through slab depth were observed at 35% of ultimate vertical load and 30% of bending moment, respectively. Radial cracks developed first at the inner column corners at a vertical load of 40 kN, progressing diagonally to the supports. No torsion cracks were observed during the test. This is due to the low M/V ratio applied on the connection. The crack patterns at the connection failure are shown in Figure 4.5. The inclined failure surface formed an angle of 20° with the slab surface.

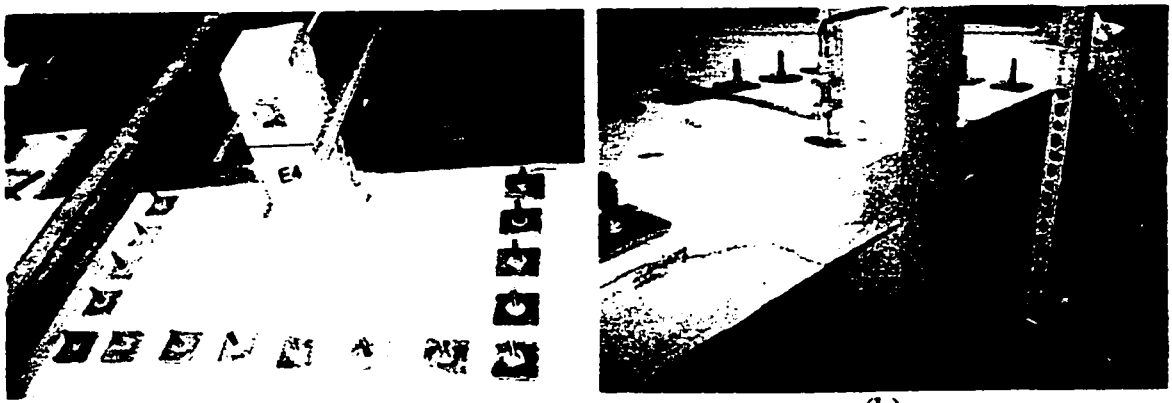

(a) (b)

Figure 4.5 Crack patterns of connection E_4; (a) cracks on the slab tension surface, (b) cracks on the slab free edge

4.2.2.4 Isolated column slab specimens in series I (connections E_{1-1}, E_{1-2}, E_{1-3} and E_{1-4})

Specimen E_{1-1}, which was loaded from the bottom column stub, formed similar crack patterns to those of specimen E_2 described previously. Circumferential cracks around the column on the slab tension side progressing to one third of the slab depth were observed at a vertical load 30% of the ultimate load. Radial cracks were first observed at 47% of the ultimate load. As the load was increased further, radial cracks propagated

away from the column to the slab boundary crossing the supports. At this moment, other transverse cracks perpendicular to the free edge were formed and progressed through the slab depth. No torsion cracks were observed. The surface failure cracks shown in Figure 4.6 inclined at an angle of 25° to the slab surface.

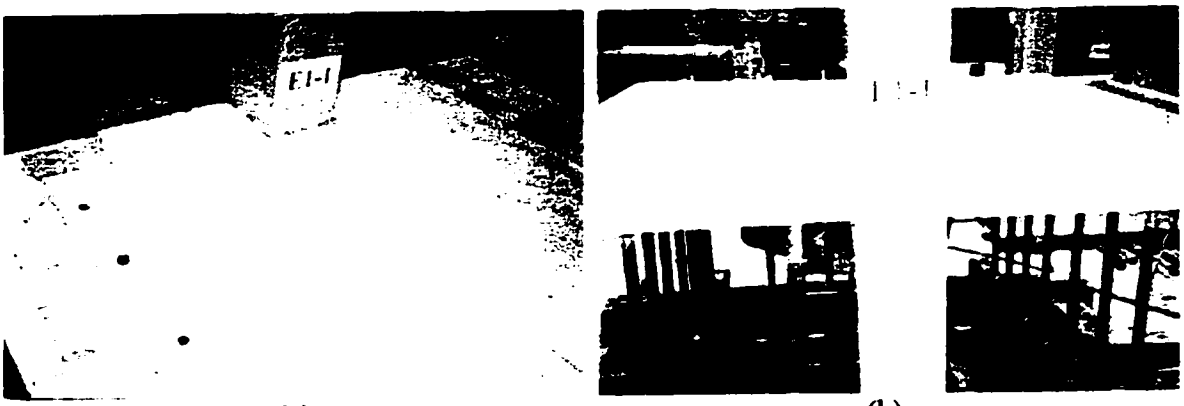

Figure 4.6 Crack pattern at the failure of connection E_{1-1}; (a) cracks at the slab tension side, (b) cracks at the slab free edge

The crack patterns of slab E_{1-2}, E_{1-3} and E_{1-4} were controlled by the position of the applied load on the slab. In all of these specimens, the cracks were initiated by flexure cracks around the column perimeter. These cracks were continued by torsion cracks through the slab depth and propagated away from the column faces. The origin and the angle of inclination of the torsion cracks were affected by the applied bending moment parallel to the slab free edge produced by the applied load.

In specimens E_{1-2} and E_{1-4}, the torsion cracks inclined at angle of 45° from the inner column corner to the slab free edge and propagated through the slab depth away from the column faces. The failure surface of these connections did not interact with the torsion cracks at the slab free edge as shown in Figure 4.7 and Figure 4.8. This confirms that the shear capacity of the connection is reduced by development of torsion on the side column slab interfaces as predicted by Regan (1981).

In specimen E_{1-3}, where the applied load was close to the column, torsion cracks were not significant enough to affect the failure surface of the connection as shown in

Figure 4.9. However, the locations of the vertical load interrupted the radius of the failure surface of the connection.

The inclined failure cracks at the slab free edge were forced to form an angle of 45° with the slab surface by the application of the loads. This may have caused the connection to be stronger than its actual capacity. However, Regan (1981) stated that an inclined angle of the shear failure surface up to 45 degree to the slab surface, does not affect the strength of the connection.

Figure 4.7 Crack patterns at the failure of connection $E_{1\text{-}2}$; (a) cracks on the slab tension surface, (b) cracks on the slab free edge

Figure 4.8 Crack patterns at the failure of connection $E_{1\text{-}4}$; (a) cracks on the slab tension surface, (b) cracks on the slab free edge

(a) (b)

Figure 4.9 Crack patterns at the failure of connection E_{1-3}; (a) cracks on the slab tension surface, (b) cracks on the slab free edge

4.2.2.5 Isolated column slab specimen Series II (E_{2-1}, E_{2-2}, E_{2-3} and E_{2-4})

The crack patterns of the connections in Series II were also controlled by the location of the applied loads on the slab surface. The formation of the first cracks in all connections was similar to those of the connections mentioned previously. However, the load at which the first cracks were observed, varied from one test to the others. The vertical loads at first crack were 55 kN, 40 kN, 62 kN and 75 kN for the connections E_{2-1}, E_{2-2}, E_{2-3} and E_{2-4}, respectively.

Torsion cracks did not appear in all connections. Torsion cracks were observed only in connections E_{2-1} and E_{2-2} of this series. However, pronounced torsion cracks were observed in connection E_{2-1}, in which the inclined shear cracks did not interact with the shear failure at the slab free edge.

Radial cracks formed in a similar way for all connections in Series II. These cracks started either at the inner column corner or the inner side column slab interface at lower loads and propagated toward the slab supports as the loads were increased further. Transverse cracks, perpendicular to the slab free edge, were observed in connection E_{2-1} where the loads on the side column faces were applied at the farthest location in Series II. Transverse cracks were identified as flexural cracks on the span parallel to the slab free edge. The transverse cracks were not observed on the other connections of this series.

All of the connections in Series II failed in punching shear. The crack patterns at failure of the all specimens can be seen in Figure 4.10 to Figure 4.13. The angle of the inclined shear failure surface of these connections varied. For connection $E_{2\text{-}1}$, the inclined shear failure was not visible from the slab free edge. However, this angle can be approximated by taking the radius of the failure surface and was estimated to be 21.5° from the slab surface. In connections $E_{2\text{-}2}$, $E_{2\text{-}3}$ and $E_{2\text{-}4}$, the inclined shear failure angles were 20°, 45° and 22.5°, respectively. At the moment of failure, the concrete at the inner column slab interface lost the compressive force due to concrete crushed in this zone.

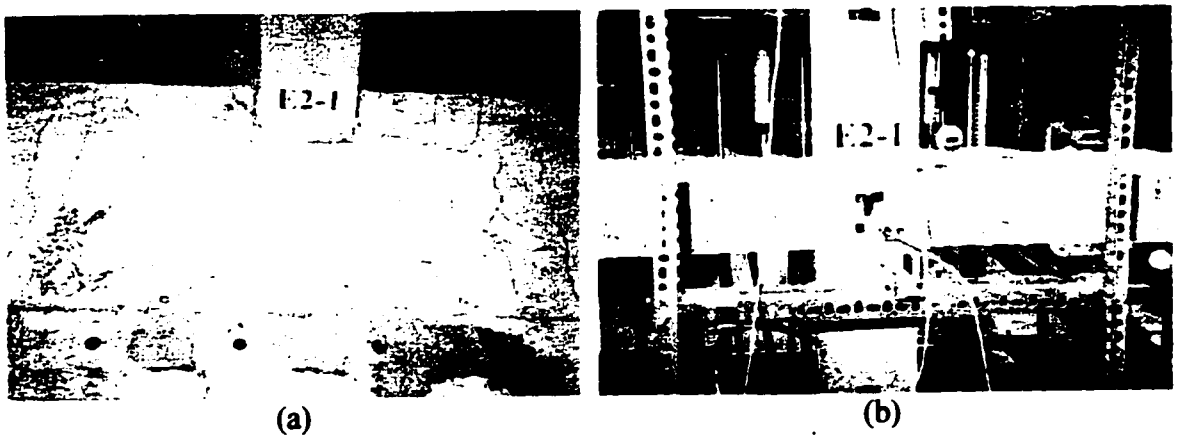

Figure 4.10 Crack patterns at the failure of connection $E_{2\text{-}1}$; (a) cracks on the slab tension surface, (b) cracks on the slab free edge

Figure 4.11 Crack patterns at the failure of connection $E_{2\text{-}2}$; (a) cracks on the slab tension surface, (b) cracks on the slab free edge

(a) (b)

Figure 4.12 Crack patterns at the failure of connection $E_{2\text{-}3}$; (a) cracks on the slab tension surface, (b) cracks on the slab free edge

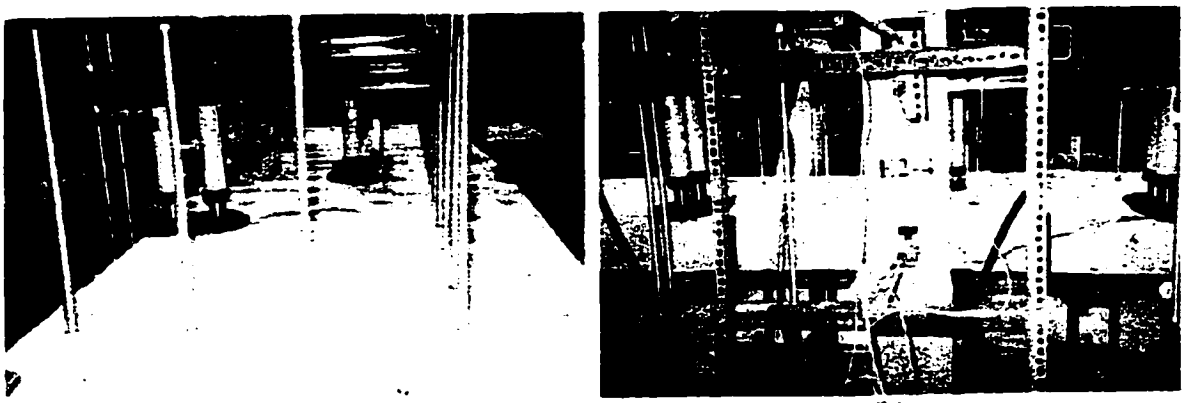

(a) (b)

Figure 4.13 Crack patterns at the failure of connection $E_{2\text{-}4}$; (a) cracks on the slab tension surface, (b) cracks on the slab free edge

4.2.3 Flexural steel strains

Strains were measured on the negative reinforcement within the region c_2+3h by $c_1+1.5h$ at 25 mm from the column faces. Considering the symmetry in geometry, not all of the bars within this area were instrumented. The strains on the bars without gauges within this area are considered to experience the same strain as the instrumented bars located at the same distance from the column faces. Figure 4.14 to Figure 4.17 show the strain recorded during the tests of connections E_1, E_2, E_3 and E_4 of the continuous slab specimen. On the first test of connection E_1, none of the bars perpendicular to the slab free edge yielded but one bar parallel to the slab free edge passing through the column reached its yield capacity. Figure 4.14 shows the strains during loading and unloading of

connection E_1. For connection E3, even though the connection failed in combined flexure and torsion, only the bars perpendicular to the bending moment vector passing through the column yielded.

Figure 4.15 and Figure 4.17 show the strains measured in connections E_2 and E_4, respectively. In connection E_2, the bars passing through the column, perpendicular to the slab free edge, yielded but none of the bars parallel to the slab edge yielded. However, connection E_4 shows the opposite behavior to connection E_2. Bars parallel to the slab free edge yielded but the bars perpendicular to the slab free edge did not yield. This was the effect of the M/V ratio applied to the connections. The M/V ratio applied to connection E_4 was half that on connection E_2. Connection E_4 could not utilize the perpendicular bars to resist bending before it failed in punching shear. The yielding of the parallel bars occurred just before the connection failed. This indicated the failure of the connection initiated on the span parallel to the slab free edge.

The steel strains of the isolated slab specimen in Series I are shown in Figure 4.18 to Figure 4.21. The strains measured during loading and unloading of connections $E_{1\text{-}3}$ and $E_{1\text{-}4}$ are included. Almost all of steel bars perpendicular and parallel to the free edge yielded in the specimen Series I, except specimen $E_{1\text{-}1}$. It should be noted, for specimen $E_{1\text{-}1}$ that none of the bars perpendicular to the slab free edge reached their yield capacity, however, all of the instrumented bars parallel to the slab free edge within the width c_2+3h, reached their yield capacity at punching failure. This indicated that most of the load was resisted by the shorter span of the slab as a result of lack of compatibility of displacement along the slab boundary supports. Consequently, the results of this test are not included.

The steel strains of the isolated slab specimens of Series II are shown in Figure 4.22 to Figure 4.25. All bars perpendicular and parallel to the slab free edge passing through the column yielded. It is interesting to note that the steel strains at the end of the test of connection $E_{2\text{-}3}$ dropped. This indicates the strains after punching failure.

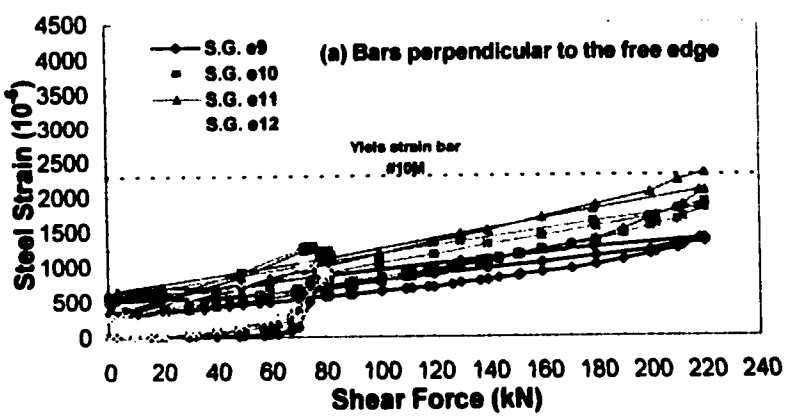

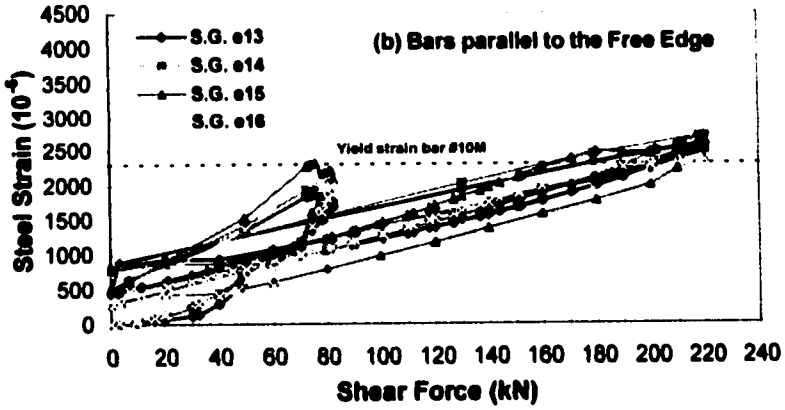

Figure 4.14 Steel strains on the negative reinforcement of connection E_2 of continuous slab specimen; (a) bars perpendicular to the slab free edge, (b) bars parallel to the slab free edge

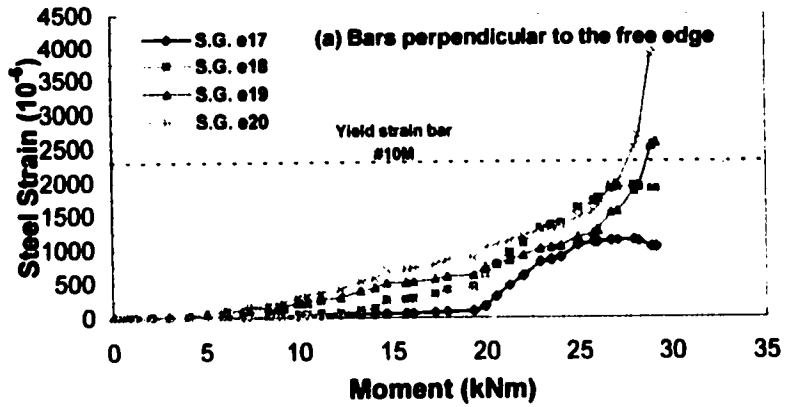

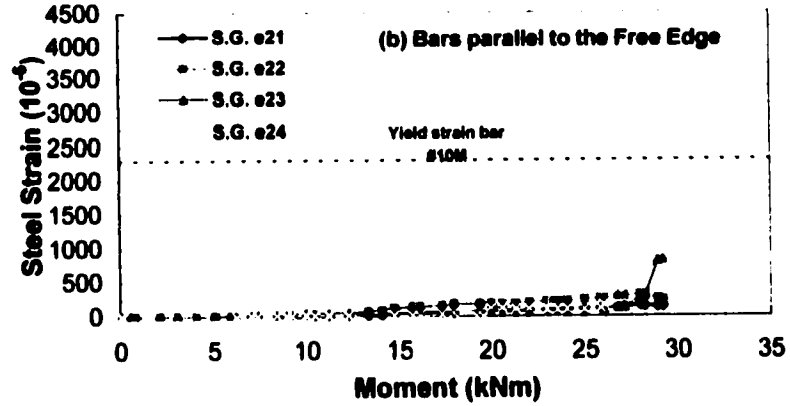

Figure 4.15 Steel strains on the negative reinforcement of connection E_3 of continuous slab specimen; (a) bars perpendicular to the slab free edge, (b) bars parallel to the slab free edge

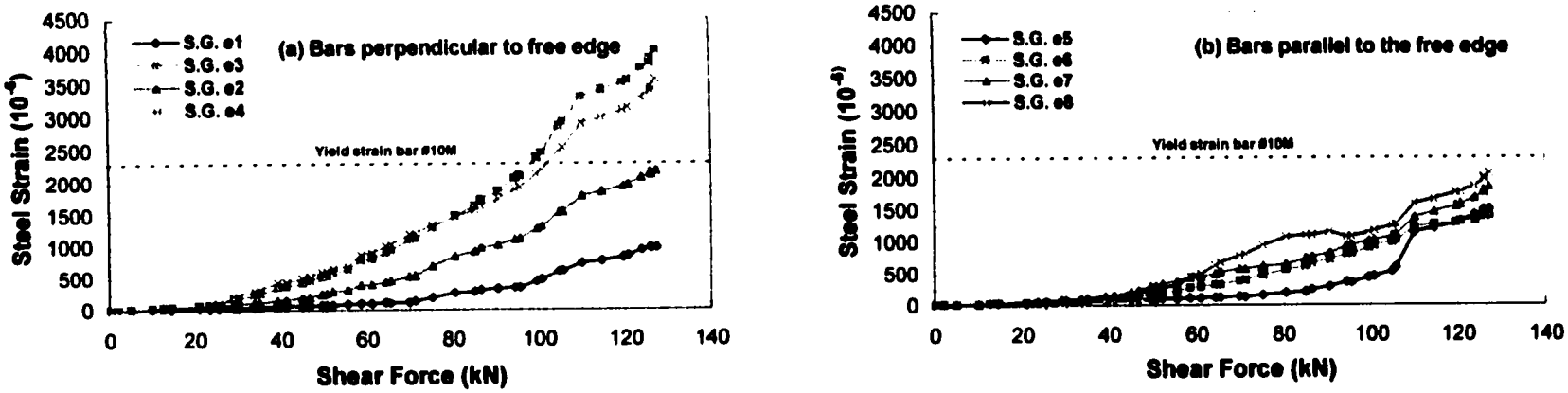

Figure 4.16 Steel strains on the negative reinforcement of connection E_1 of continuous slab specimen; (a) bars perpendicular to the slab free edge, (b) bars parallel to the slab free edge

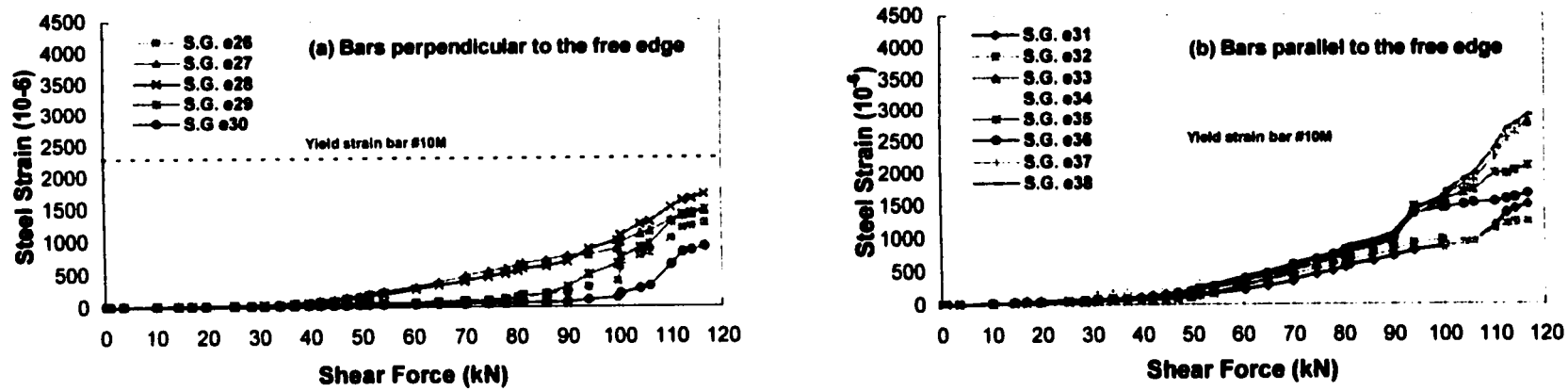

Figure 4.17 Steel strains on the negative reinforcement of connection E_4 of continuous slab specimen; (a) bars perpendicular to the slab free edge, (b) bars parallel to the slab free edge

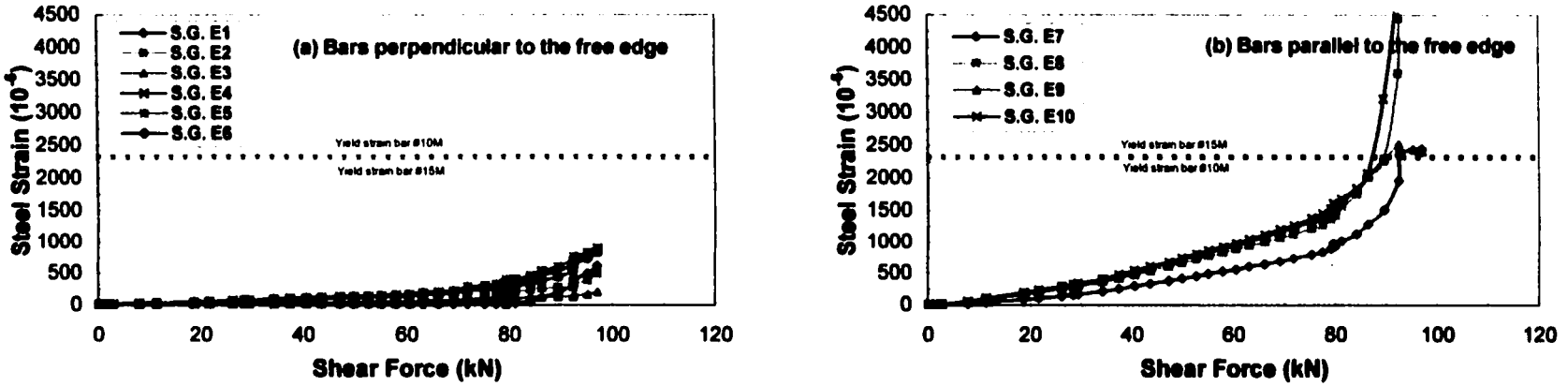

Figure 4.18 Steel strains on the negative reinforcement of isolation slab connection E_{I-1} of the Series I; (a) bars perpendicular to the slab free edge, (b) bars parallel to the slab free edge

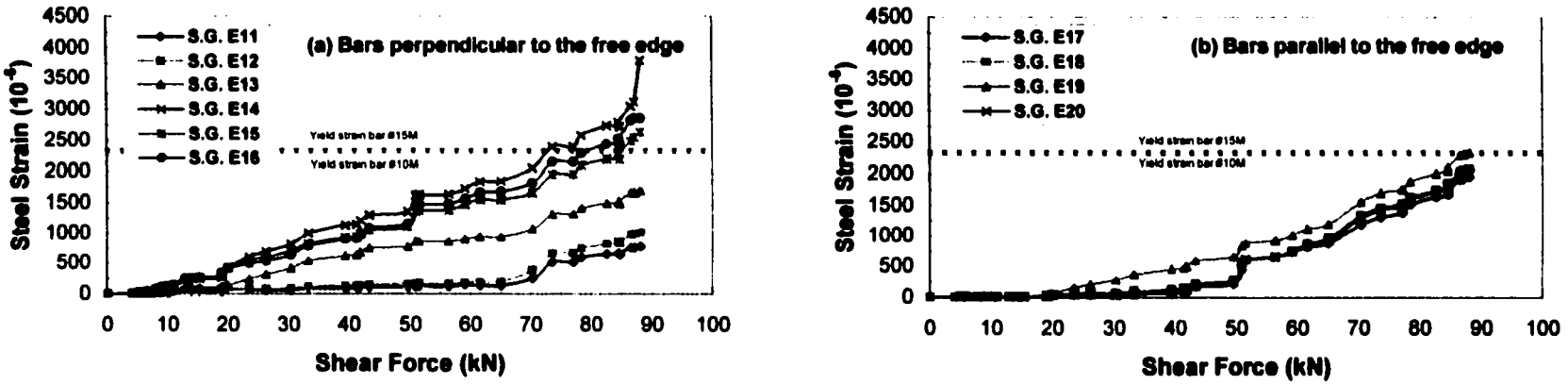

Figure 4.19 Steel strains on the negative reinforcement of isolated slab connection E_{I-2} of the Series I; (a) bars perpendicular to the slab free edge, (b) bars parallel to the slab free edge

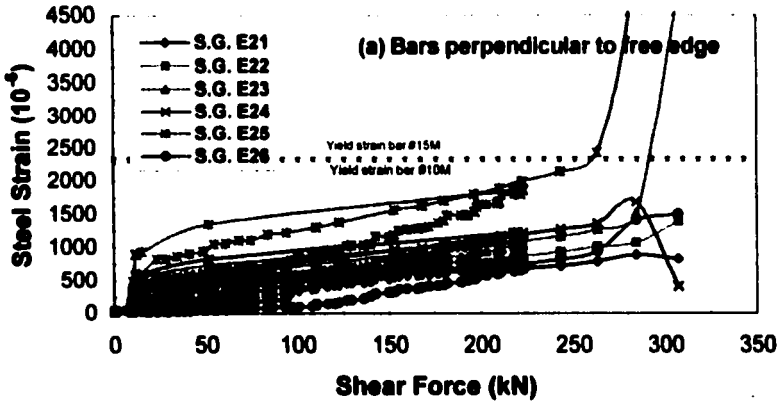

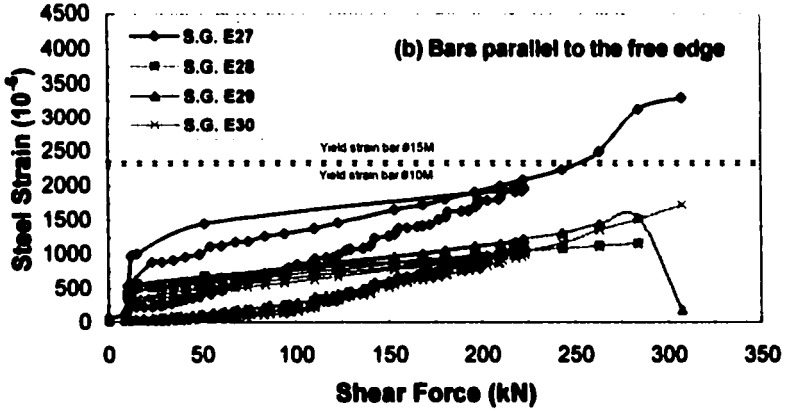

Figure 4.20 Steel strains on the negative reinforcement of isolated slab connection E_{1-3} of the Series I; (a) bars perpendicular to the slab free edge, (b) bars parallel to the slab free edge

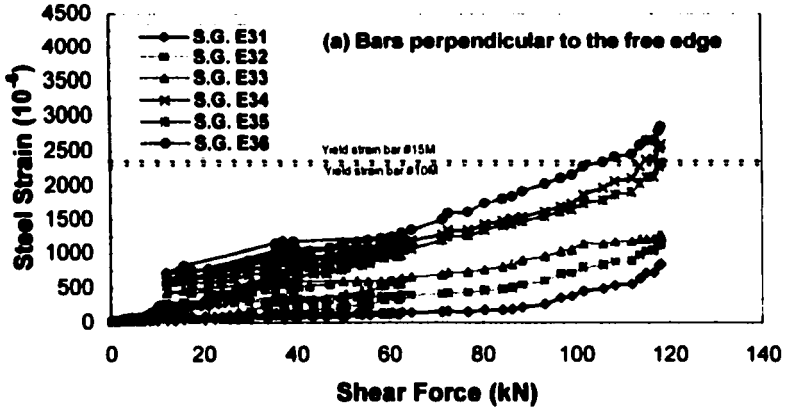

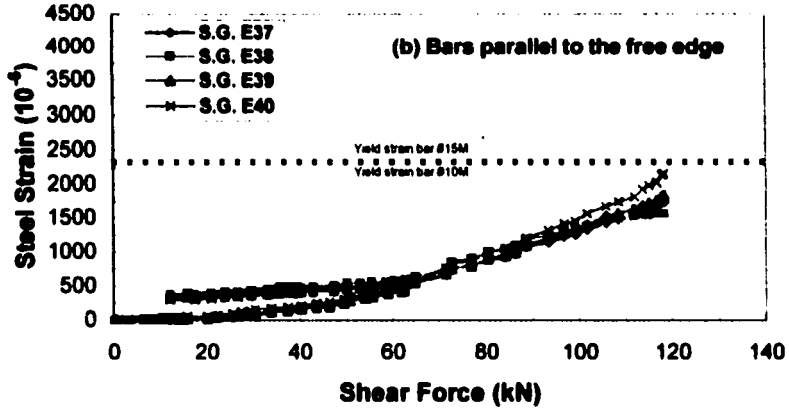

Figure 4.21 Steel strains on the negative reinforcement of isolated slab connection E_{1-4} of the Series I; (a) bars perpendicular to the slab free edge, (b) bars parallel to the slab free edge

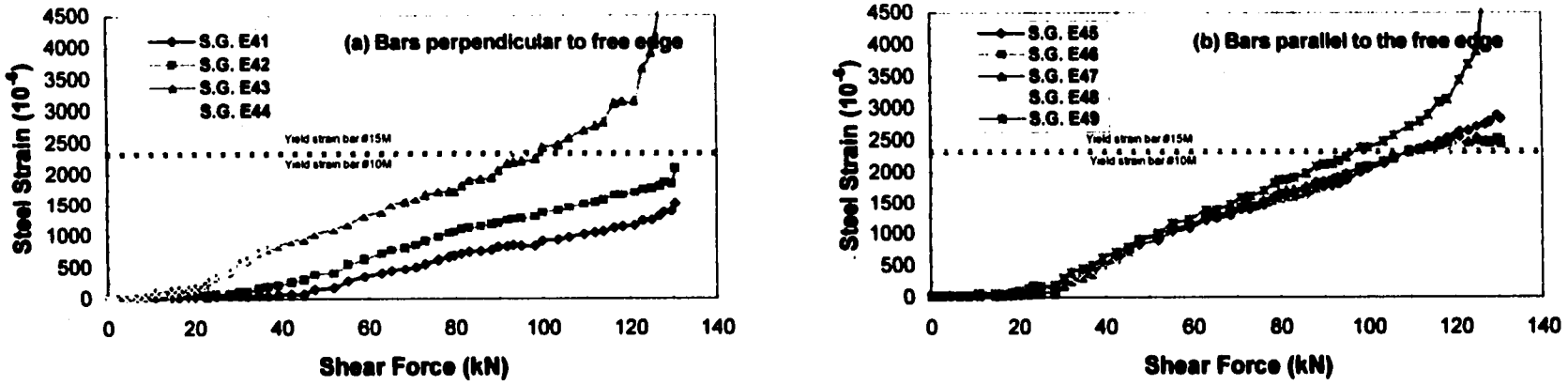

Figure 4.22 Steel strains on the negative reinforcement of isolated slab connection $E_{2\text{-}1}$ of the Series II; (a) bars perpendicular to the slab free edge, (b) bars parallel to the slab free edge

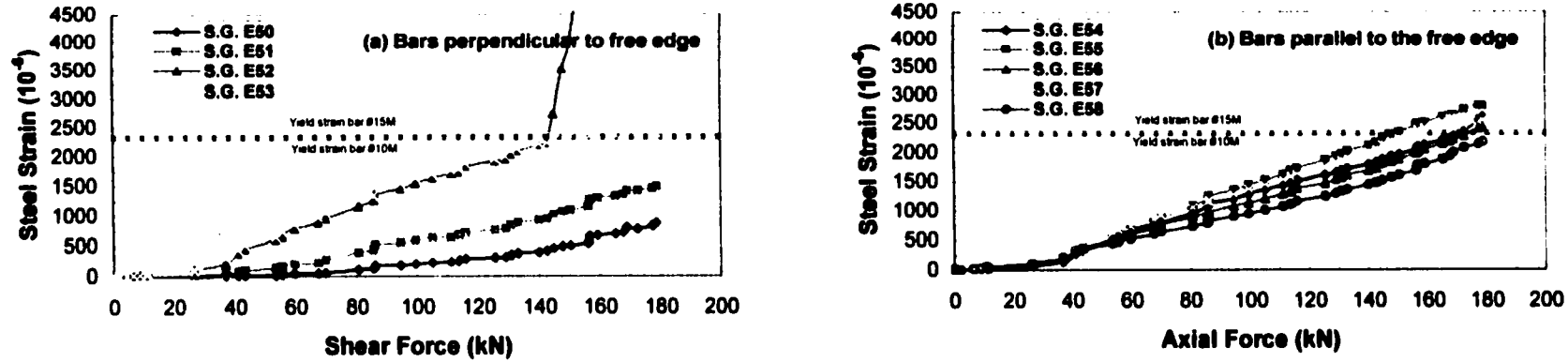

Figure 4.23 Steel strains on the negative reinforcement of isolated slab connection $E_{2\text{-}2}$ of the Series II; (a) bars perpendicular to the slab free edge, (b) bars parallel to the slab free edge

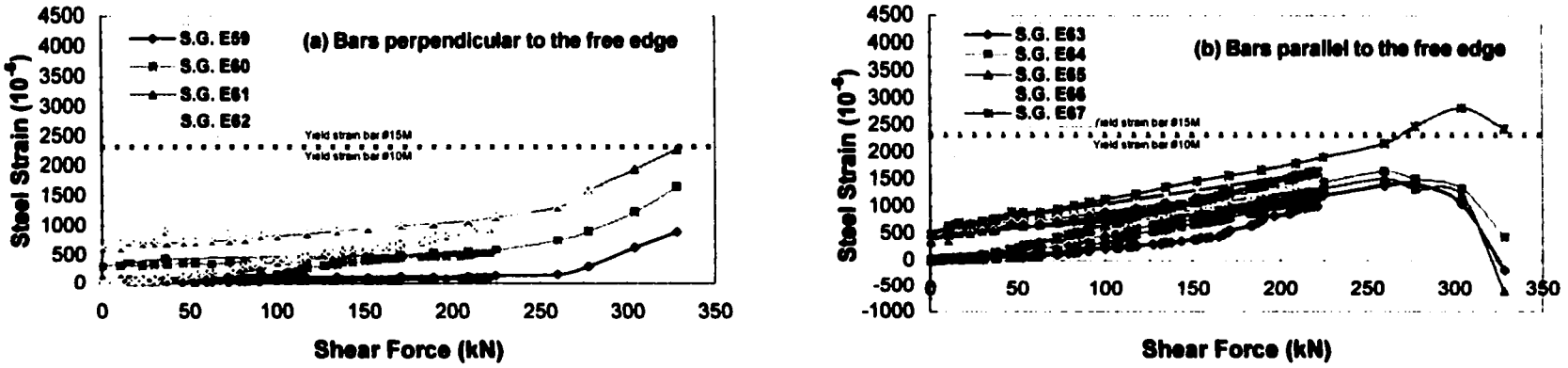

Figure 4.24 Steel strains on the negative reinforcement of isolated slab connection $E_{2\text{-}3}$ of the Series II; (a) bars perpendicular to the slab free edge, (b) bars parallel to the slab free edge

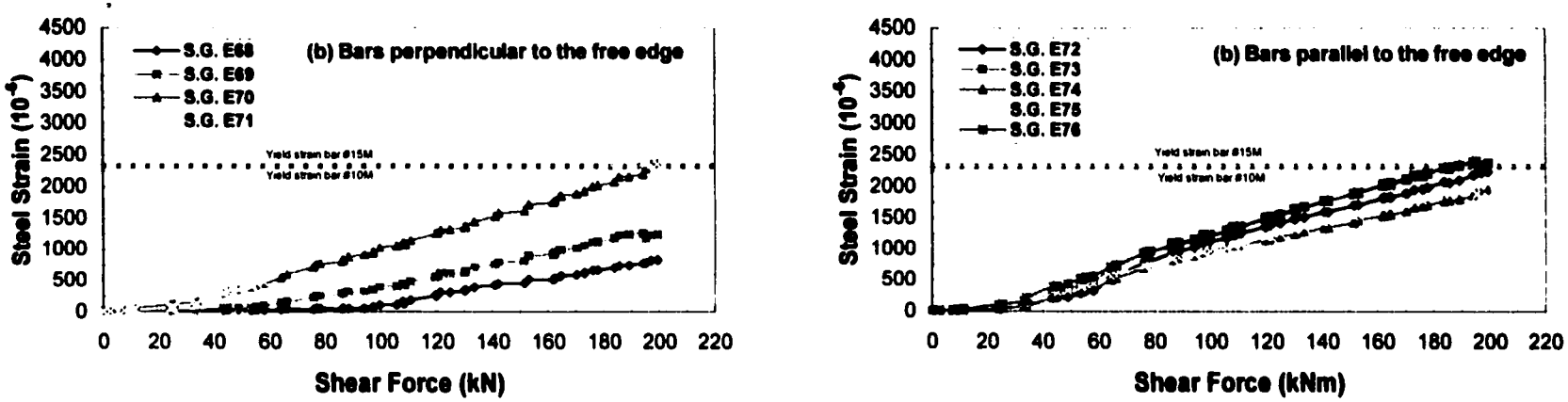

Figure 4.25 Steel strains on the negative reinforcement of isolated slab connection $E_{2\text{-}4}$ of the Series II; (a) bars perpendicular to the slab free edge, (b) bars parallel to the slab free edge

In edge connections of Series II, although there is some scatter in the strain measurements, it can be noted that the bars passed through the column faces either perpendicular or parallel to the slab free edge reached their yield capacity at failure.

4.2.4 Out-of-plane slab deflection

The deflections of the slab 60 mm from the column faces, at mid-span and mid-panel of the continuous slab, corresponding to the tested connection, were recorded during the tests. Typical location of the instrumentation is shown in Figure 3.16. Figure 4.26 to Figure 4.29 show the out-of-plane deflection of the slab during the test of connections E_1, E_2, E_3 and E_4, respectively, of the continuous slab specimen. Positive and negative signs on the deflections represent the top slab surface in tension and compression, respectively. Figure 4.26 and Figure 4.27 show the deflections of the slab during the first and second tests of connection E_2. The deflections around the column appear linear in both tests indicating that the connection had cracked in the first test before the second test was conducted.

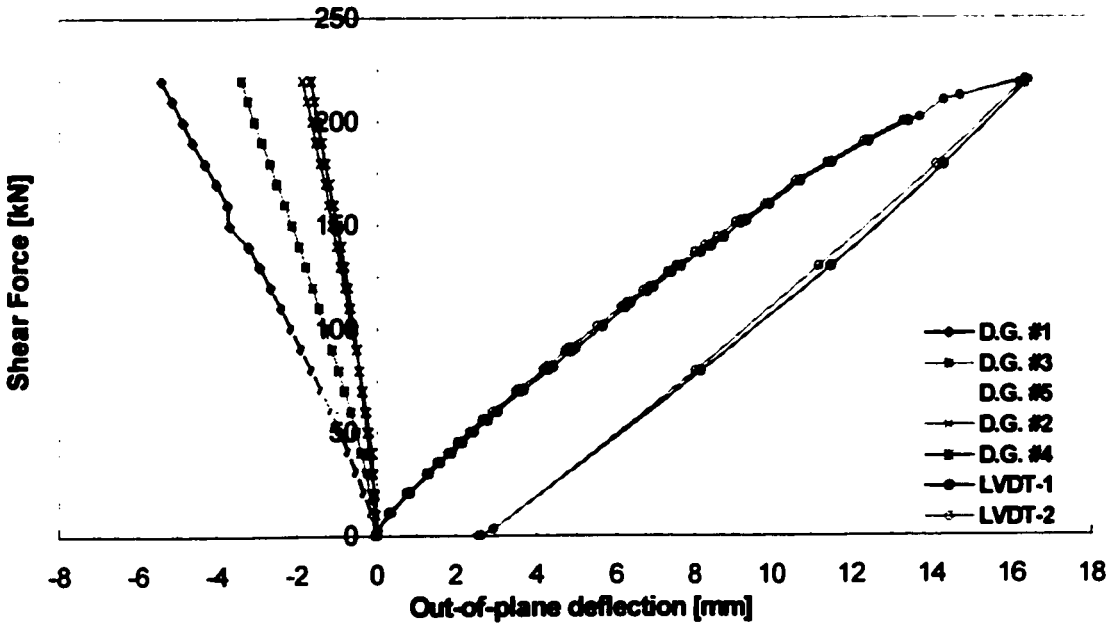

Figure 4.26 Slab deflections on the first test of connection E_2 of the continuous specimen

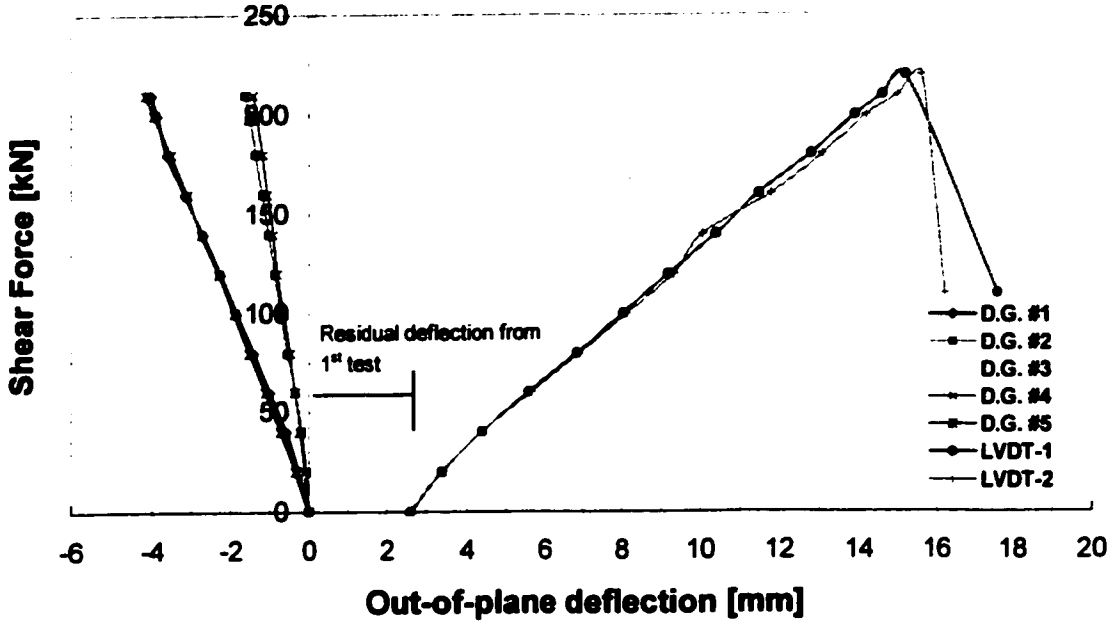

Figure 4.27 Slab deflection on the second test of connection E_2 of the continuous slab specimen

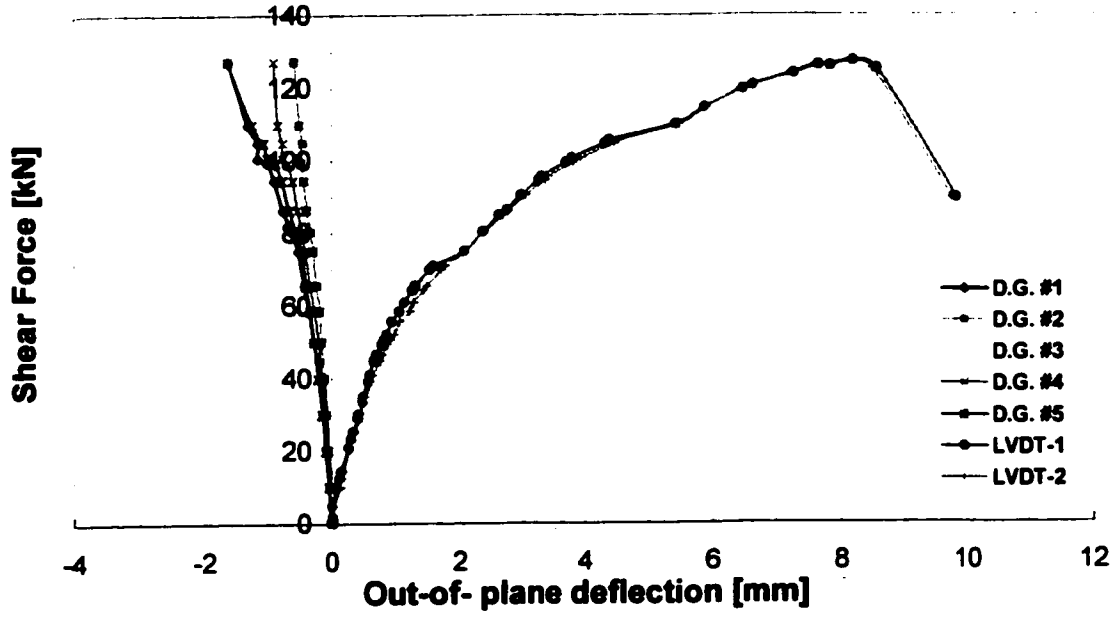

Figure 4.28 Slab deflection on the test of connection E_1 of the continuous slab specimen

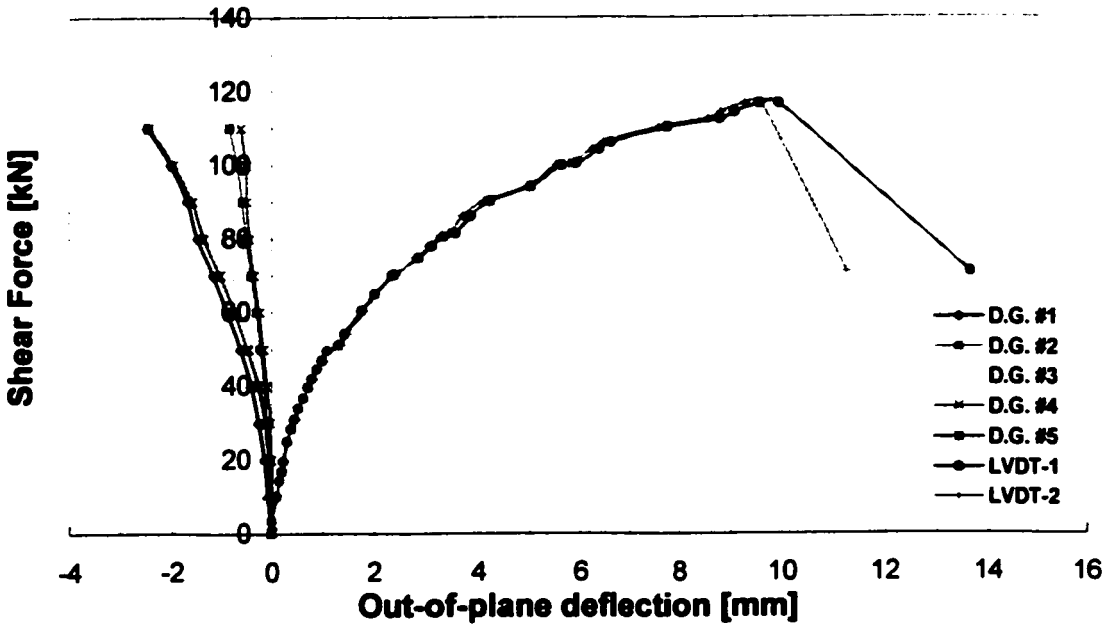

Figure 4.29 Slab deflection on the test of connection E_4 of the continuous slab specimen

In the preliminary test, no supports along the line of contra-flexure were provided. The results of this test are not included. The maximum deflection reached in the first test was 16.4 mm before unloading but on the second test the maximum deflection before failure was 15.6 mm due to existing significant cracks at the connection.

Slab deflections around the columns of connections E_1 and E_4 show similar behaviors as can be seen in Figure 4.28 and Figure 4.29. Both connections were subjected to combined vertical load and moment. The deflections were very small before the cracks occurred, and increased nonlinearly for higher applied load as can be seen in the graphs. The connection stiffness decreased with the occurrence of the cracks. The maximum vertical deflections of connections E_1 and E_4 before failure were 8.2 mm and 9.4 mm, respectively.

The deflections of the slab at the mid-span and mid-panel in all tests were generally a straight line. A small nonlinear behavior happened in the test of connection E_4. The deflections around the column and mid-spans indicated that rotations, as expected, occurred along the assumed simple supports. It was also observed that the

deflections of the span parallel to the slab free edge (i.e. *D.G. #1* and *D.G. #5*) were larger than the deflection of the span perpendicular to the slab free edge (i.e *D.G. #3*). It may be because the slab width participating in connection stiffness is larger in the perpendicular direction to the slab free edge than that in parallel directions so that the slab in perpendicular direction is stiffer than in parallel direction.

4.2.5 Column rotations

Column rotations were determined from the horizontal deflections of the column stubs 343 mm above and below the slab surface and calculated as:

$$\theta_{col} = \frac{\Delta_{top} + \Delta_{bottom}}{Z} \tag{4.1}$$

Where : θ_{col} = the column rotation (radian)

Δ_{top} = horizontal deflection on the top column stub (mm)

Δ_{bottom} = horizontal deflection on the bottom column stub (mm)

Z = lever arm of the two measured deflections (= 826 mm)

Figure 4.30 shows the moment versus column rotation relationship of connections E_1, E_3 and E_4 of the continuous slab specimen. Only connections subjected to applied moment are included. The positive direction of the graph indicates the top and bottom column stubs rotated outward and inward, respectively, and the negative direction indicates the converse.

A rotation of 0.047 radians was achieved in connection E_3 where only bending moment was applied. Connection E_2 achieved a rotation of about 0.018 radians before the connection failed under combined shear force and bending moment. The column of connection E_4 rotated toward the slab due to the low applied M/V ratio and the maximum rotation was –0.003 radians. From these graphs, it can be observed the existence of shear force reduces the column rotation, consequently decreasing the connection ductility.

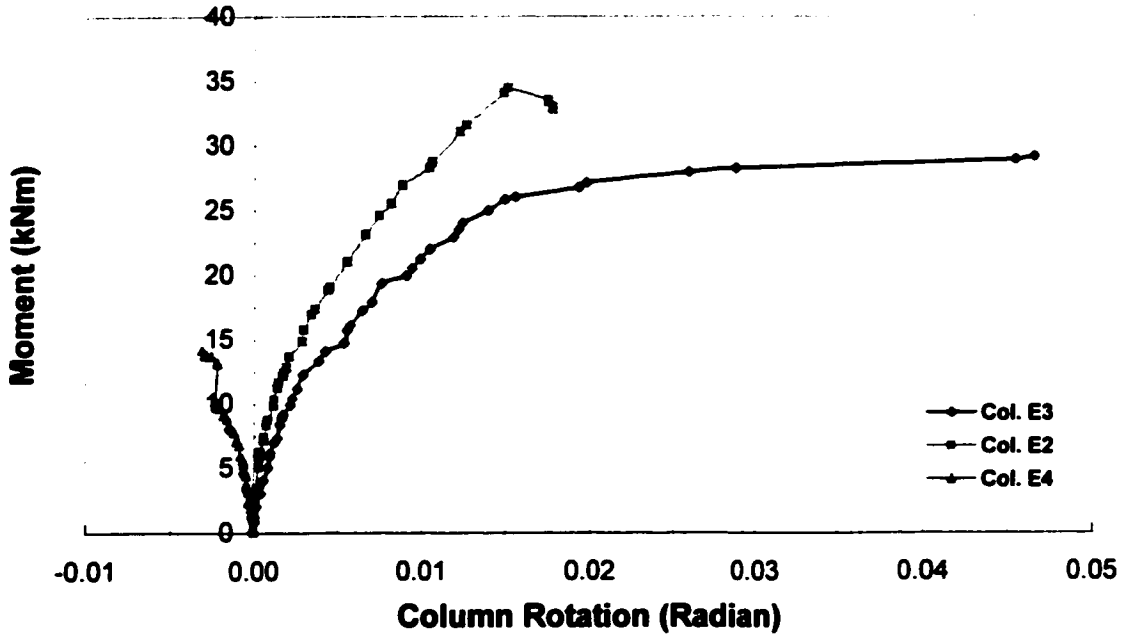

Figure 4.30 Column rotation of connections E_2, E_3 and E_4 of the continuous slab specimen

4.3 REPAIRED EDGE CONNECTIONS

4.3.1 General

The four edge column slab connections of the continuous slab specimen were repaired and retested to failure. Two of these connections were repaired using normal concrete and the other two were repaired using CAH expansive concrete. In this section, the behaviour of the connections is presented relating to the load capacity and failure mechanisms, crack patterns during the test, flexural steel strains, out-of-plane slab deflections and the column rotations.

4.3.2 Ultimate load capacity and failure mechanisms

All connections failed under combined shear force and bending moment. The first test of connection E_{3R} was subjected to shear only but the connection was not tested to failure. The connection was unloaded at 230 kN and retested under combined action of shear force and bending moment. Table 4.2 presents the ultimate load capacity and

failure modes of the repaired connections. All of the connections failed in brittle punching shear.

Table 4.2 Ultimate load capacity of the repaired edge column slab connections

Slabs	$c_1=c_2$ mm	h mm	ρ_{c2+3h} %	$\rho_{c2+1.5h}$ %	f_y MPa	f_{cm} MPa	V_u KN	M_u kNm	Failure Mode	Type of specimens
E_{1R}	203	140	0.9	0.9	420	39.8	90.5	9.8	PS	Continuous
E_{2R}	203	140	0.9	0.9	420	40.0	129.2	20.8	PS	Continuous
E_{3R}^*	203	140	0.9	0.9	420	40.3	230.0	0.0	-	Continuous
E_{3R}	203	140	0.9	0.9	420	40.3	129.1	23.4	PS	Continuous
E_{4R}	203	140	0.9	0.9	420	42.7	120.3	17.1	PS	Continuous

Note: E_{1R}^* was not tested to failure

4.3.3 Crack patterns of the repaired connections

Among four edge column slab connections were repaired, only one (E_{3R}^*) was subjected to vertical load only, the others were tested under combined shear force and bending moment. In general, the crack patterns of all the repaired edge connections were similar to the test of the original edge column connection reported previously. Details of crack development of the edge connections repaired using normal and non-shrinkable concrete are given next.

4.3.3.1 Connections repaired using normal concrete

Connections E_{3R} and E_{4R} were repaired using normal concrete. The crack patterns and the failure crack patterns of these connections are shown in Figure 4.31 to Figure 4.33. On the first test of connection E_{3R}, cracks along the column perimeter were observed first at a vertical load of 60 kN. Radial cracks originating from the inner column corner and inside column slab interface were observed at 70 kN load.

As the loads were increased, the radial cracks progressed away from the column faces to the isolated supports. The connection was unloaded at a vertical load 230 kN

without any failure. No torsion cracks were observed up to this load. The second test of connection E_{3R} was under combined shear force and bending moment. The only additional cracks developed in the second test were torsion cracks; which were observed at a moment of 12 kNm. No cracks were noticed on the slab along the interface of the old concrete and the repaired concrete before failure. The connection failed at 129.1 kN vertical load and 23.4 kNm bending moment. The failure surface was similar to that of connection E_1. The average angle of failure surface was 18.5° to the slab surface.

(a) (b)

Figure 4.31 Crack patterns of connection E_{3R} at the end of the first test; (a)&(b) cracks on the slab tension surface

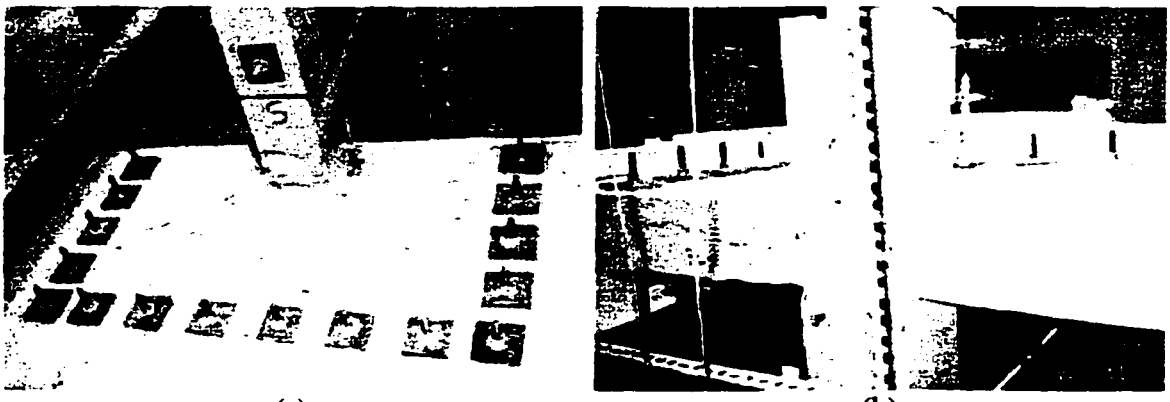

(a) (b)

Figure 4.32 Crack patterns of the second test of connection E_{3R} at the failure ; (a) cracks on the slab tension surface, (b) cracks on the slab free edge

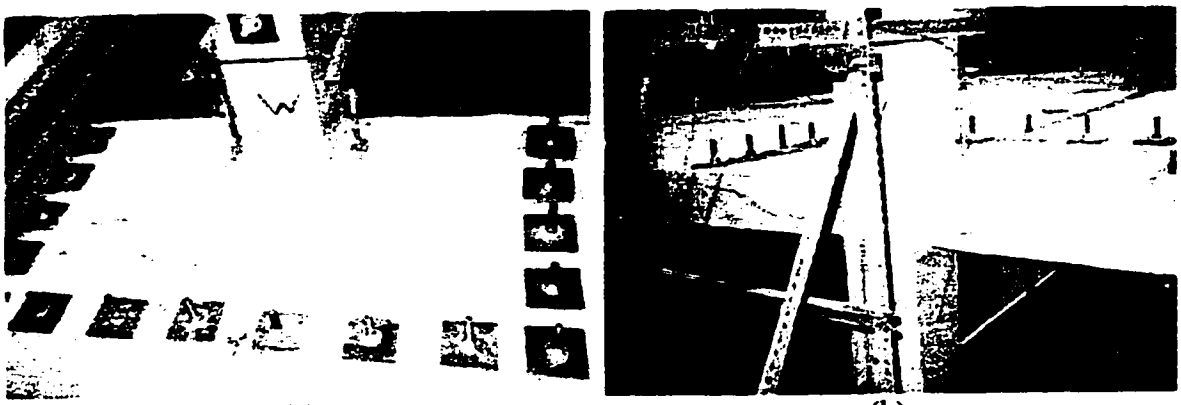

(a) (b)

Figure 4.33 Crack patterns of connection E_{4R} at the failure; (a) cracks on the slab tension surface, (b) cracks on the slab free edge

In the test of connection E_{4R}, radial cracks and circumferential cracks along the column perimeter were developed at 50 kN and 5 kNm for vertical load and bending moment, respectively. Radial cracks started from inner column corners and inner column slab interface progressing diagonally and perpendicular, respectively, toward the supports. Again, no torsion cracks were observed before the connection failed in punching shear at the combined vertical load of 120.3 kN and bending moment of 17.1 kNm. The failure surface was similar to the connection subjected to vertical load only with an average failure angle of 19° to the slab surface.

4.3.3.2 Connections repaired using non-shrinkable CAH concrete

Connections E_{1R} and E_{2R} were repaired using a non-shrinkable CAH (Calcium Aluminate Hydrate) concrete to avoid shrinkage cracks along the repaired joins. Crack patterns of these two connections are slightly different.

The crack patterns of connection E_{1R} after the failure are shown in Figure 4.34. At a vertical load of 40 kN, radial cracks and circumferential cracks along the column perimeter propagating through the slab depth were observed. Few radial cracks were observed before the connection failed in punching shear under combined loads. The failure loads were 90.5 kN and 9.8 kNm for shear force and bending moment, respectively. The average angle of inclined shear failure surface was about 19.5° from the slab surface. No torsion cracks were developed during the test.

(a) (b)

Figure 4.34 Crack patterns of connection E_{1R} at the failure; (a) cracks on the slab tension surface, (b) cracks on the slab free edge

In connection E_{2R}, flexural cracks around the column perimeter, radial cracks and torsion cracks were observed first at a vertical load of 60 kN. Torsion cracks reached the slab edge progressing through the slab depth at 90 kN load. Failure occurred at a vertical load of 129.2 kN and bending moment of 20.8 kNm. The average inclined failure crack angle was 20° to the slab surface. Figure 4.35 shows the crack patterns of connection E_{2R} after the failure.

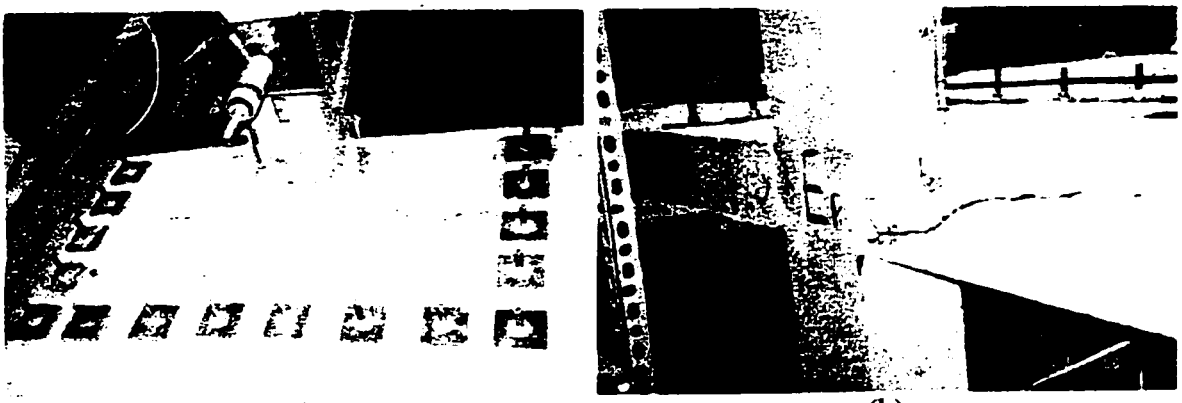

(a) (b)

Figure 4.35 Crack patterns of connection E_{2R} at the failure; (a) cracks on the slab tension surface, (b) cracks on the slab free edge

4.3.4 Flexural steel strains

Figure 4.36 to Figure 4.40 show the steel strains of the repaired connections during the test. The bars perpendicular to the slab free edge passing through the column reached their yield capacity only in the test of connection E_{IR}. However, most of the bars parallel to the slab free edge passing through the column yield. This behavior may be explained according to the column rotations in the next section.

The strains plotted in the graphs do not include the residual strain from any previous tests of the connections. It was observed during removing of the concrete, some rebars were marked and bent by the electrical hammer and the connections were moved back to their original positions before casting the concrete so that any residual strains from the original test may have changed.

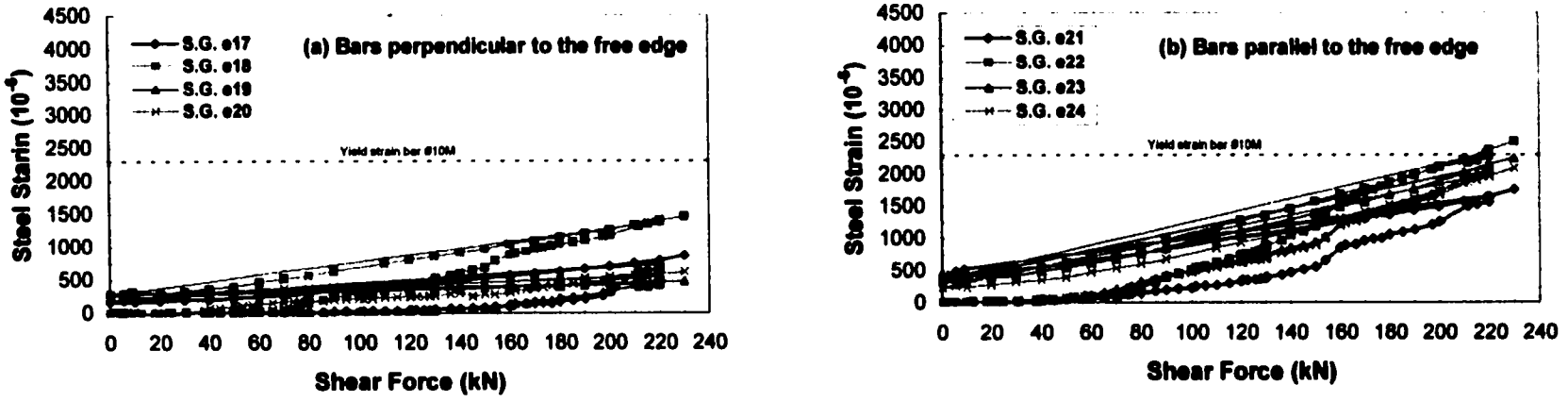

Figure 4.36 Steel strains on the negative reinforcement on the first test of connection E_{3R}^{*} of the continuous slab specimen; (a) bars perpendicular to slab free edge, (b) bar parallel to the slab free edge

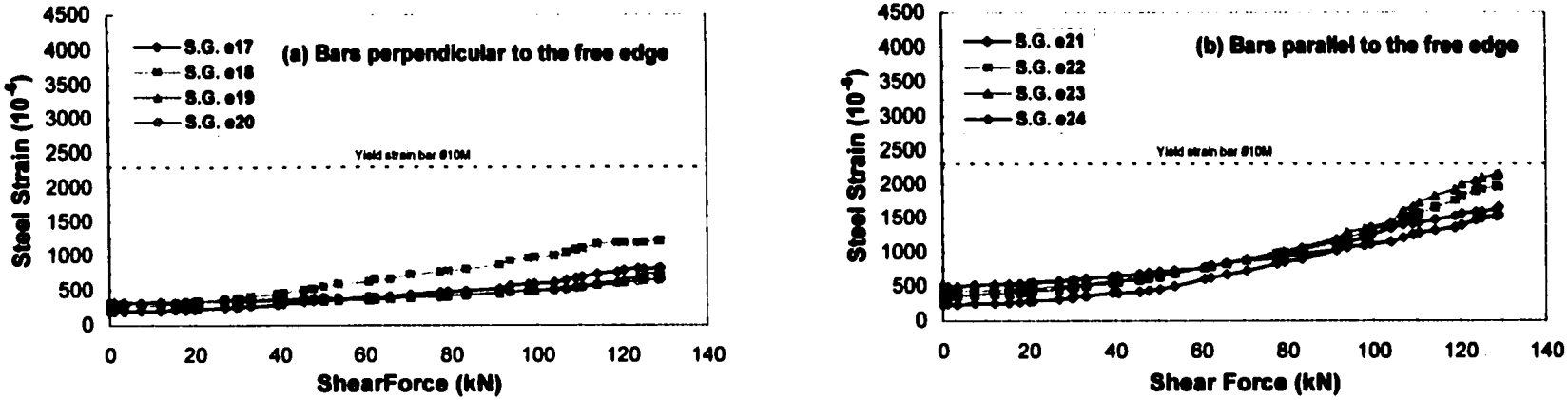

Figure 4.37 Steel strains on negative reinforcement on the second test of connection E_{3R} the continuous slab specimen; (a) bars perpendicular to slab free edge, (b) bar parallel to the slab free edge

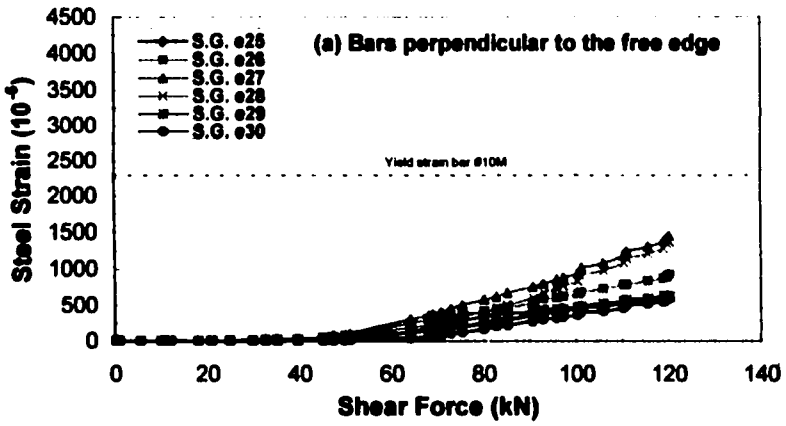

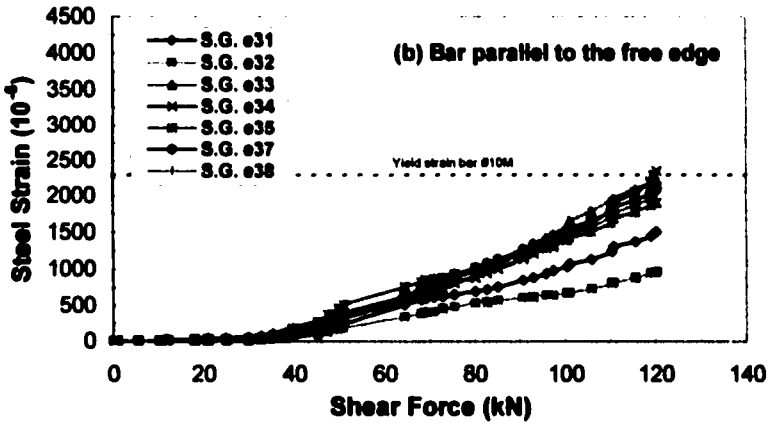

Figure 4.38 Steel strains on negative reinforcement of connection E_{4R} of the continuous slab specimen; (a) bars perpendicular to slab free edge, (b) bar parallel to the slab free edge

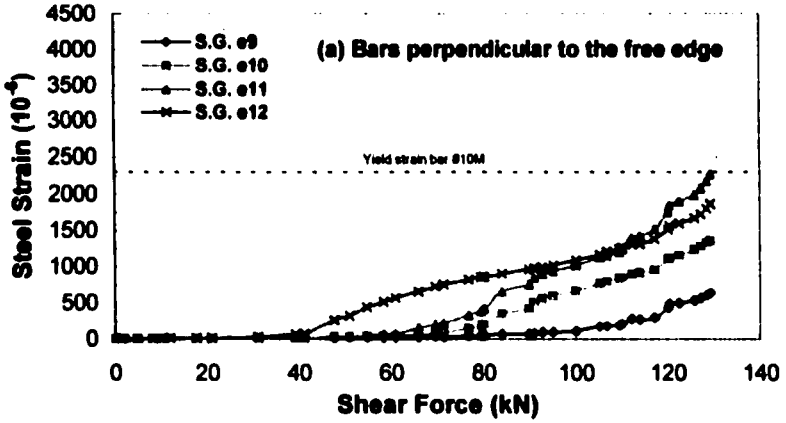

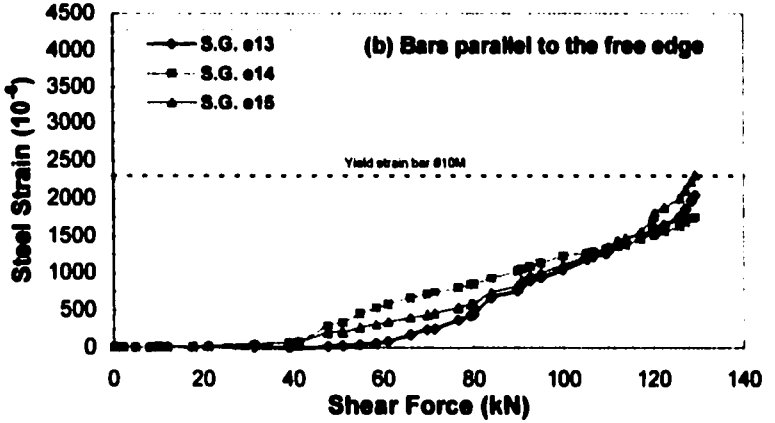

Figure 4.39 Steel strains on negative reinforcement of connection E_{2R} of the continuous slab specimen; (a) bars perpendicular to slab free edge, (b) bar parallel to the slab free edge

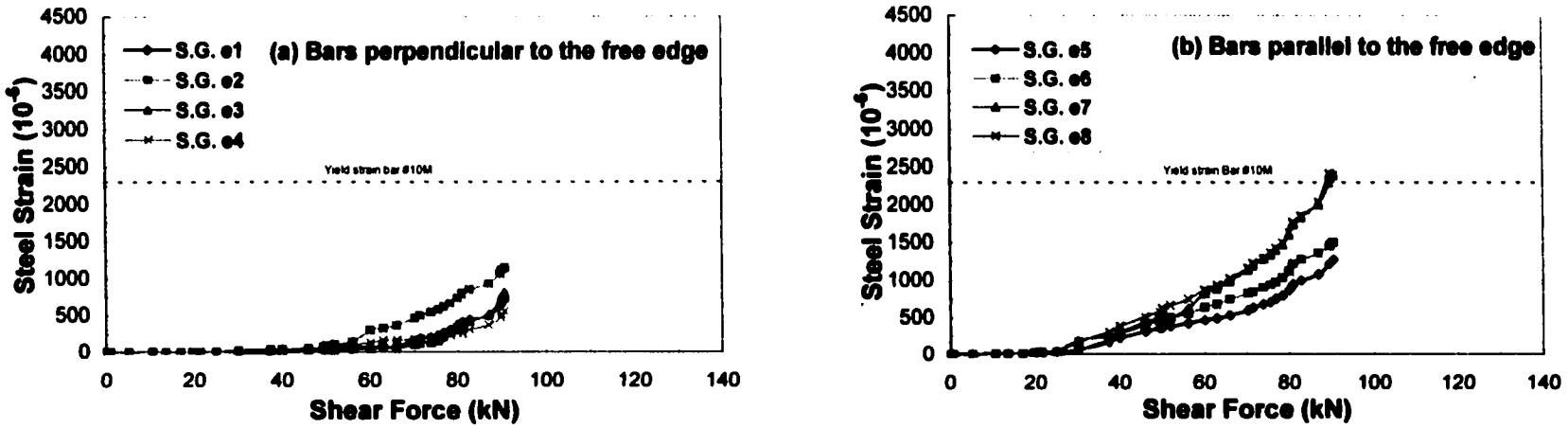

Figure 4.40 Steel strains on negative reinforcement of connection E_{IR} of the continuous slab specimen; (a) bars perpendicular to slab free edge, (b) bar parallel to the slab free edge

4.3.5 Out-of-plane deflection of the slab

The same procedures were used to measure the slab deflections during the test of each repaired connection as the original connections. The out-of-plane deflections of the slab during the test of edge repair connection are shown in Figure 4.41 to Figure 4.45.The maximum deflection around the column connection on the first test of connection E_{3R} was 11.2 mm and on the second test was 8.4 mm including the residual deflection from the first test of 1.9 mm. In both tests, the deflections were linear indicating a constant vertical stiffness of the connection. Figure 4.44 and Figure 4.45 present the deflections of the connections repaired using non-shrinkable concrete. In both graphs, non-linear deflections around the column were obtained starting at low loads. The non-linear deflections were more pronounced on connection E_{1R} where superplasticizer was added in the concrete to provide more free water. These behaviors may be explained based on the nature of the non-shrinkable (expansive) concrete produced by *CAH* materials. In this type of concrete, the more free water is available in the concrete, the more spaces to produce ettringite in the aggregate interfaces are available.

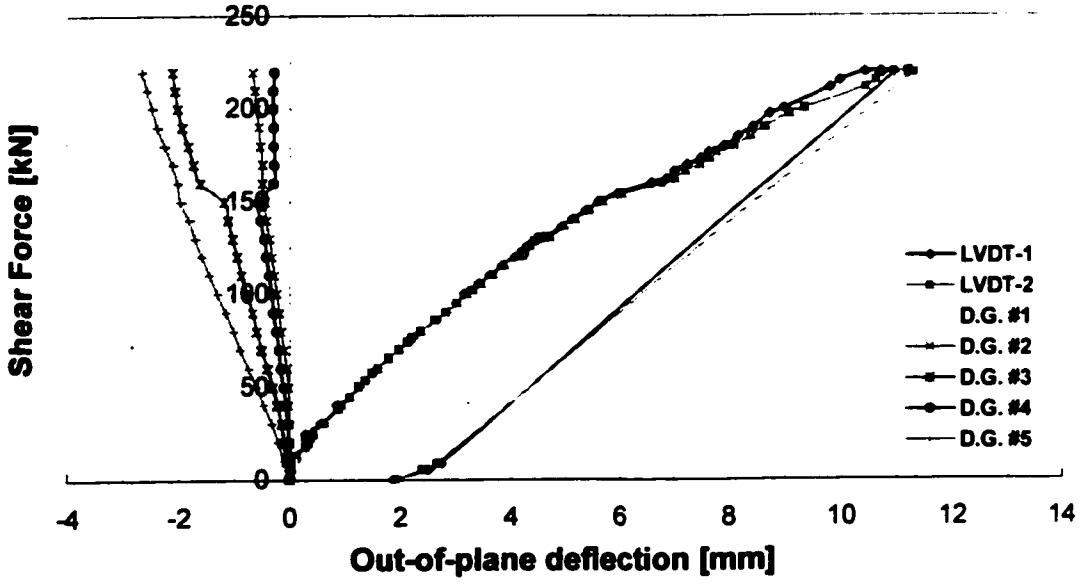

Figure 4.41 Slab deflection on the first test of repaired connection E_{3R} of the continuous slab specimen

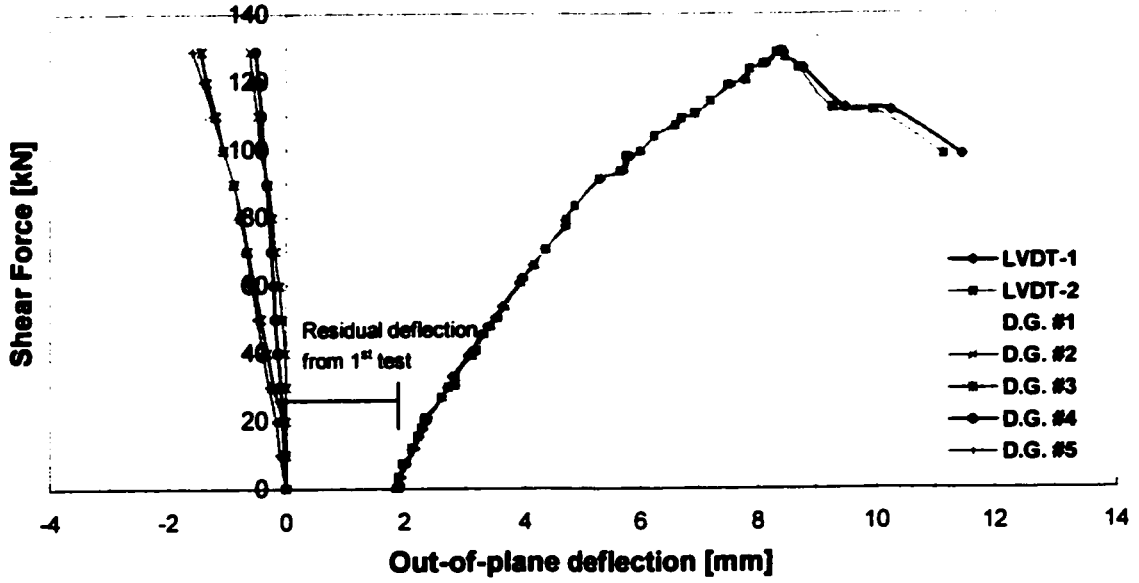

Figure 4.42 Slab deflection on the second test of repaired connection E_{3R} of the continuous slab specimen

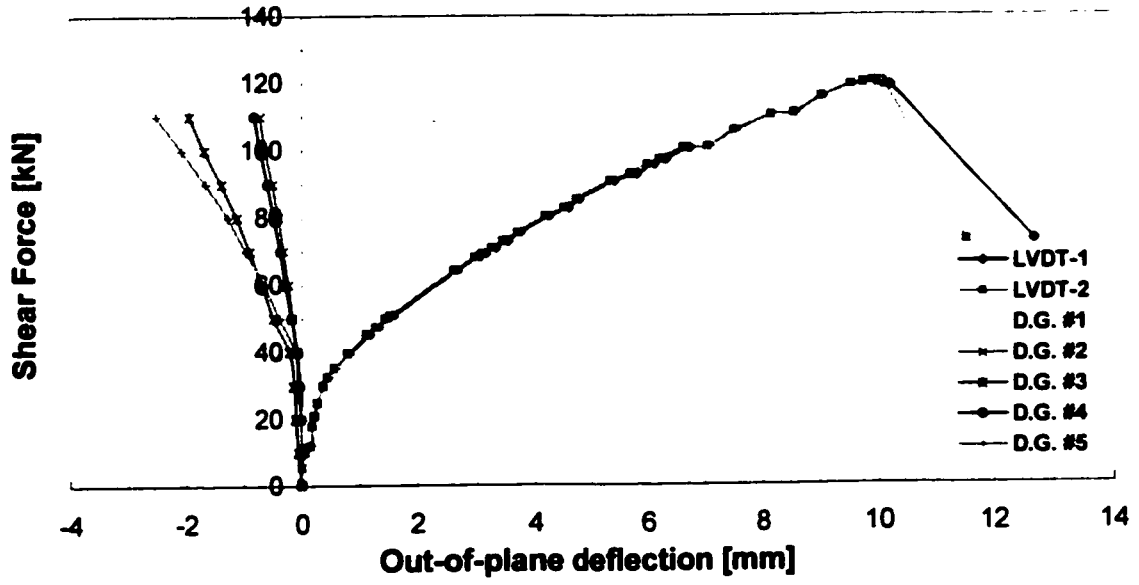

Figure 4.43 Slab deflection on the test of repaired connection E_{4R} of the continuous slab specimen

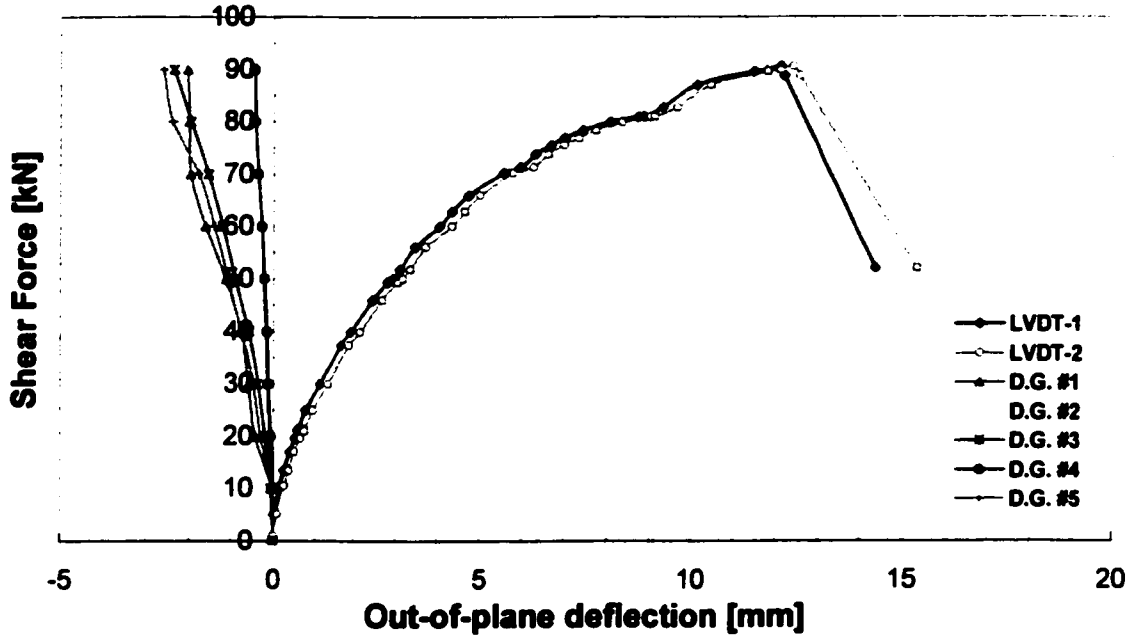

Figure 4.44 Slab deflection on the test of repaired connection E_{1R} of the continuous slab specimen

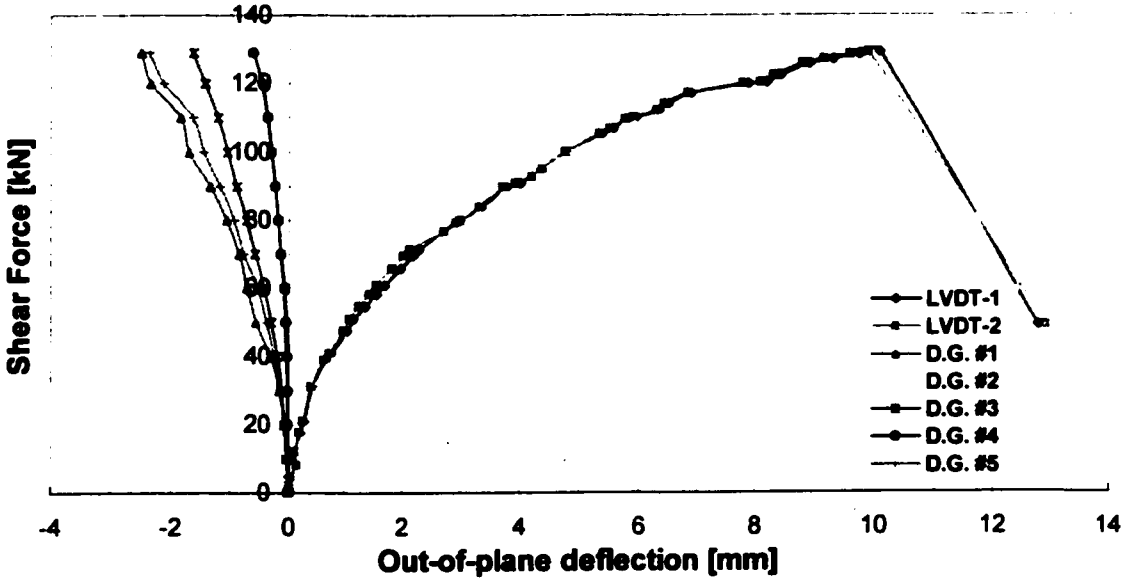

Figure 4.45 Slab deflection on the test of repaired connection E_{2R} of the continuous slab specimen

However, the lack of restraints on the top surface of the slab allowed the concrete to expand freely in that direction, resulting in microcracks in the concrete. These microcracks may have caused the non-linear vertical deflections these connections.

The maximum vertical deflection of the slab in the test of connection E_{4R} was 9.9 mm. After cracks occurred, the deflections increased faster than the loads indicating a reduction in connection stiffness. The deflection of the connection was similar to that of the original connection presented previously.

4.3.6 Column rotations

The column rotations on all tests of the repaired connections are presented in Figure 4.46. The rotations were calculated using equation 4.1. The columns in connections E_{1R} and E_{4R} rotated inward due to low applied moment.

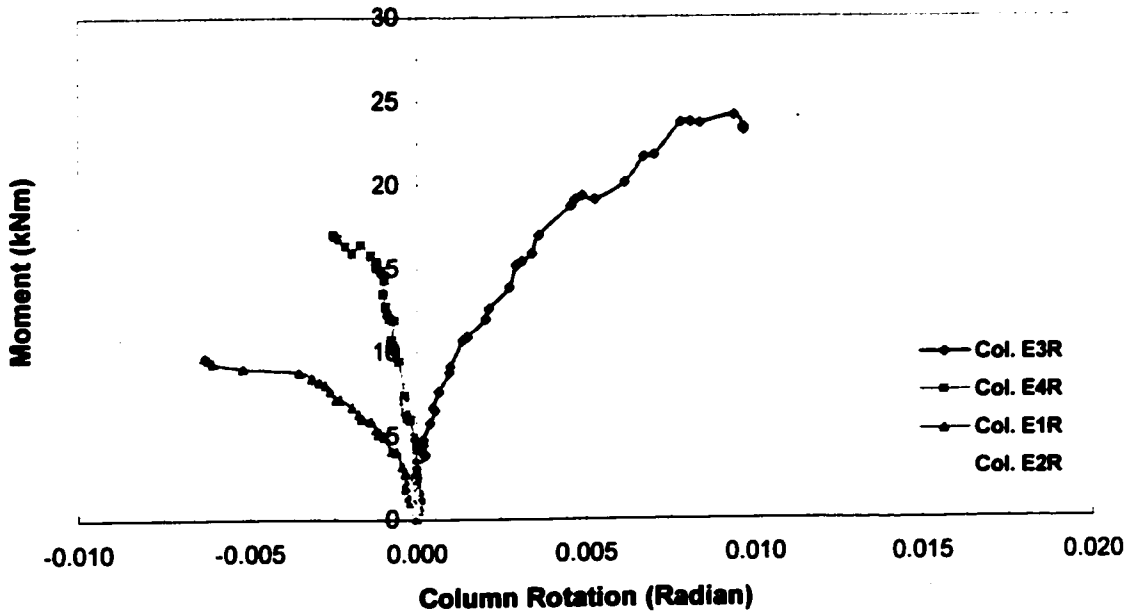

Figure 4.46 Column rotations on the tests of connections E_{1R}, E_{2R}, E_{3R} and E_{4R} of the continuous slab specimen

The maximum column rotations in connections E_{1R}, E_{2R}, E_{3R} and E_{4R} were -0.006, 0.002, 0.094, -0.003 radians, respectively. The largest rotation occurred in connection E_{3R} where the connection had been tested under vertical load only. The existing cracks due to

first test of connection E_{3R}* reduced the stiffness of the connection on the second test (E_{3R}) as indicated by the large rotation of the column stubs.

4.4 CORNER COLUMN SLAB CONNECTIONS

4.4.1 General

Four corner column slab connections of the continuous slab specimen were tested to failure after the tests of the repaired edge connections had been completed. Test results of the corner connections are presented according to the ultimate load capacity, failure mechanisms, crack patterns, flexural steel strains, slab deflections and column rotation in the following section.

4.4.2 Ultimate load capacity and failure mechanisms

Table 4.3 presents the test result of the corner column slab connections of the continuous slab specimen. Connection C_5 was tested twice, with and without biaxial bending moment. In the first test, a large inward rotation occurred causing tension cracks on the lower surface of the slab.

Table 4.3 Ultimate load capacity and failure modes of the corner connections

Slabs	c_1=c_2 mm	h mm	$\rho_{c2+1.5h}$ %	$\rho_{c1+1.5h}$ %	f_y MPa	f_{cm} MPa	V_u kN	M_u kNm	Failure Mode	Type of specimens
C_5^*	305	140	1.11	1.11	420	44.4	59.7	-	-	Continuous
C_5	305	140	1.11	1.11	420	44.4	62.1	27.7	PS	Continuous
C_6	305	140	1.11	1.11	420	44.4	108.6	49.3	PS	Continuous
C_7	305	140	1.11	1.11	420	44.4	93.7	46.6	PS	Continuous
C_8	305	140	1.11	1.11	420	44.4	98.1	38.9	PS	Continuous

Note: V_u and M_u were measured at centroid of column section

4.4.3 Crack patterns

Unlike the test of the edge column slab connections, the vertical load on the corner connections was applied at the centroid of the column section due to the physical limitation of the test system.

4.4.3.1 Corner connection C_5

Figure 4.47 shows crack patterns at the end of the first test of the corner connection C_5. First flexural cracks were observed at the edge slab column interfaces and radial cracks from the inner column corner at a load of 30 kN. As the applied load increased to 50 kN, cracks formed on the bottom slab surface diagonally through the inner corner and joined both slab free edges. These cracks progressed through the slab depth toward the top slab surface. From the crack patterns of the slab, it was concluded the inward column rotation was very large causing the bottom surface of the slab to be tension; therefore, it was necessary to provide a restoring moment to balance the column rotation. The test was terminated at a vertical load of 60 kN.

Figure 4.47 Crack patterns at the end of the first test of connection C_5; (a) cracks on the tension surface of the slab, (b) Cracks on the bottom slab surface

The second test of connection C_5 was done with a restoring moment produced by two equal horizontal forces to eliminate column rotation. Horizontal deflections of the column stubs were monitored. The second test was considered possible because the already cracked lower slab surface would be in compression, when a restoring moment was applied. In this test, additional cracks on the top slab surface were developed at the

inner column corner and propagated away from the column face toward the slab free edges. Figure 4.48 shows the crack patterns at the failure of the second test of connection C_5. The connection failed at a vertical load of 62.1 kN and biaxial bending moment of 27.7 kNm. It should be noted that in the second test, the connection was already damaged; therefore, the load capacity at the failure obtained from this test may not reliably represent the ultimate capacity of connection C_5.

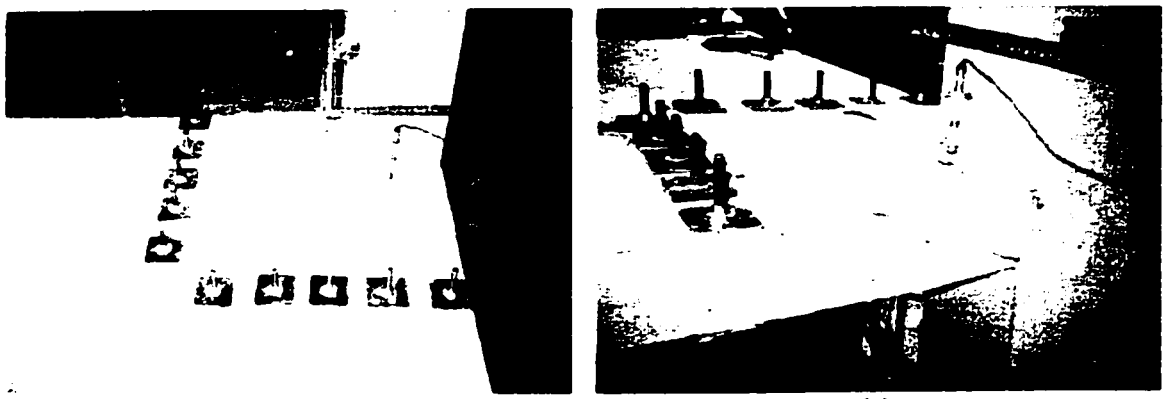

(a) (a)

Figure 4.48 Crack patterns at the failure of connection C_5; (a) cracks on the tension surface of the slab, (b) Cracks on the slab free edge

4.4.3.2 Corner connection C_6

The applied load increments in the second test of connection C_5 were repeated for connection C_6 where the column was maintained vertical. The crack patterns at connection failure are shown in Figure 4.49. As in the edge column slab connections, flexural cracks around the column perimeter were observed first, followed by radial cracks at a vertical load 40 kN. As the load increased, more radial cracks were developed. Torsion cracks were observed only on one side of the column faces just before connection failure and propagated through the slab depth at a vertical load of 105 kN. The connection failed in punching shear due to combined action of a shear force and biaxial bending moment of 108.6 kN and 49.3 kNm, respectively. The average inclined failure crack angle was 25 degrees.

(a) (b)

Figure 4.49 Crack patterns at the failure of connection C_6; (a) cracks on the tension surface of the slab, (b) cracks on the slab free edge

4.4.3.3 Corner connections C_7 and C_8

Connection C_7 was tested with M/V ratio higher than that applied to connection C_6. Therefore, the top column stub was able to rotate outward. Torsion cracks and radial cracks were observed first at a vertical load of 30 kN. The torsion cracks were the major cracks on the connection before it failed under a combined vertical load of 93.7 kN and biaxial bending moment of 46.6 kNm. Figure 4.50 shows the crack patterns and the failure surface of connection C_7. The average angle of the inclined failure cracks was about 27° from the slab surface.

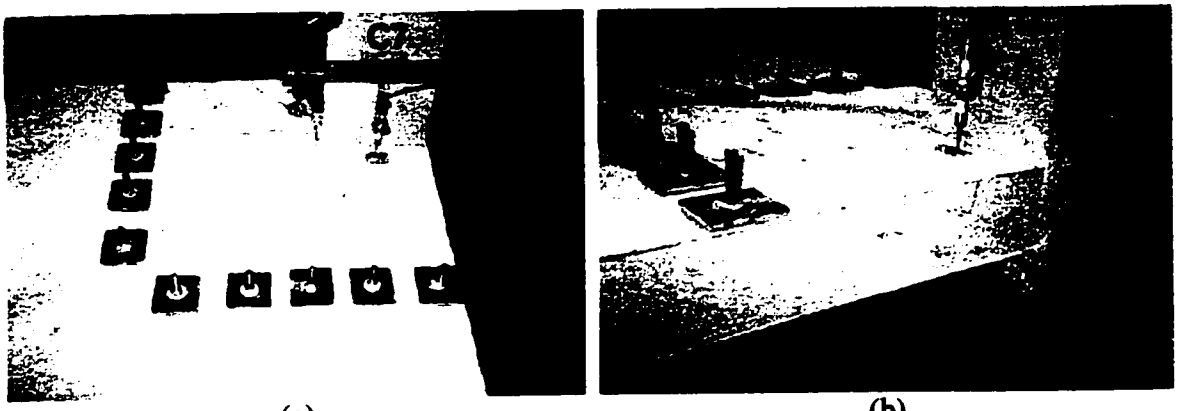

(a) (b)

Figure 4.50 Crack patterns at the failure of connection C_7; (a) cracks on the tension surface of the slab, (b) cracks on the slab free edge

Figure 4.51 shows the crack patterns at the failure of connection C_8. The applied load eccentricity (M/V) was less than that applied to connection C_5, causing inward rotation of the top column stub. Torsion cracks were observed at a load 50 kN. These cracks were not as many as those on connection C_7. Connection C_8 failed under combined action of a vertical load of 98.1 kN and a biaxial bending moment 38.9 kNm. The average angle of inclined failure surface was 25°. Concrete crushing in the lower slab surface initiated from the inner column corner and inclined away from the column faces to the slab free edges.

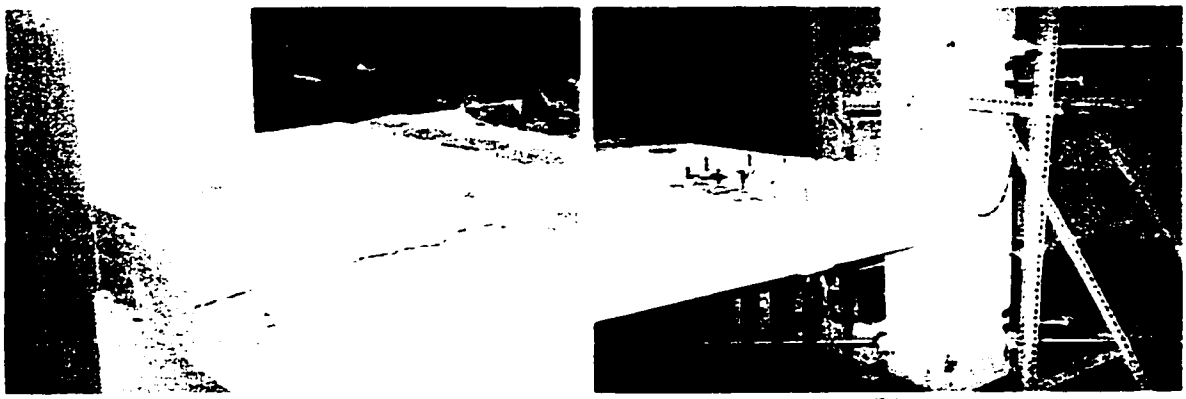

Figure 4.51 Crack patterns at the failure of connection C_8; (a) cracks on the tension surface of the slab, (b) cracks on the slab free edge

4.4.4 Flexural steel strains

Figure 4.52 to Figure 4.55 show the strains of the top and bottom steel during the tests of connections C_5, C_6, C_7 and C_8. During the first test of connection C_5, the steel strains of the bottom bars yielded but the top steel did not. This indicated that the high moment was developed by the eccentricity of the vertical load causing large inward rotations of the top column stub. The bottom slab surface was in tension, which was indicated by the yielding of the bottom rebars, while the top rebars were far below the yield capacity. Applying a restoring moment on the second test changed the behavior of the connection C_5 as indicated by the steel strains during the second test.

Yielding of the rebars occurred within the column faces on the test of connections C_6 and C_7. None of the rebars outside the column faces yielded. First yielding of the

tension rebars in connection C_6 was at a vertical load of 95.6 kN and moment of 42.5 kNm, which was 88% and 86% of the ultimate capacity, respectively. Only two of three rebars passing through each face of the column yielded before failure. The bottom rebars were generally in compression, except the strain slightly changed before connection failure.

In connection C7, all rebars passing through the column faces yielded before failure. First yielding of the rebars occurred at a vertical load of 75.3 kN and a biaxial moment of 37.2 kNm. These loads are about 80% of ultimate vertical load and 80% of ultimate moment that were resisted by connection C_7. The strains of the bottom steel were compressive confirming the bottom slab surface was in compression.

The steel strains in connection C_8 are shown in Figure 4.55, only one of six rebars passing through the column faces yielded at failure of the connection. An applied moment lower than that required to balanced inward column rotation reduced tension forces on top slab reinforcement so that the steel strains were lower in this connection than the other two connections (C_6 and C_7).

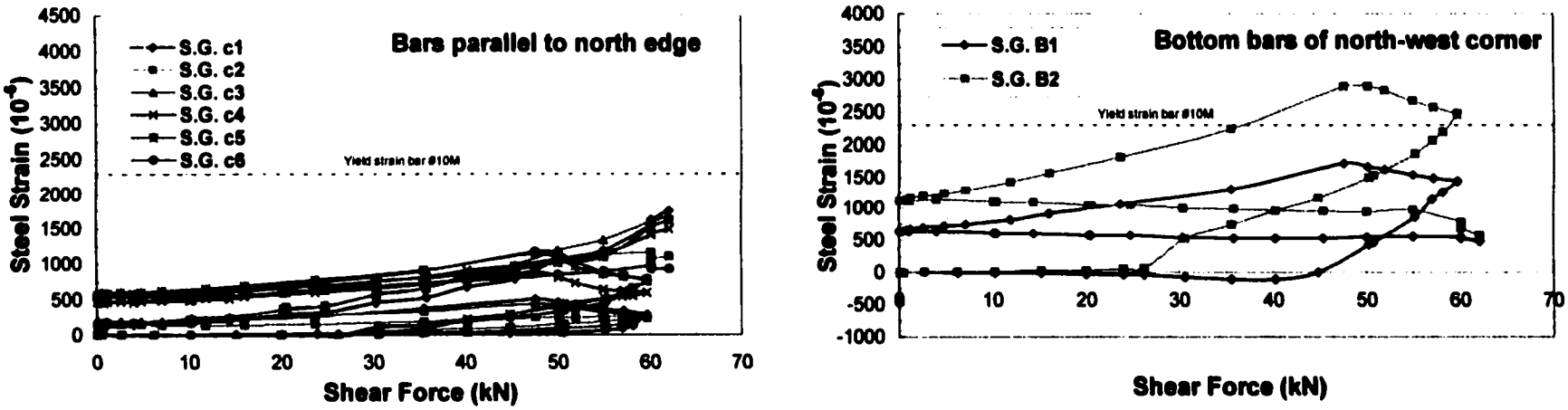

Figure 4.52 Steel strains on the test of connection C_5 of the continuous slab specimen; (a) bars parallel to the north slab edge, (b) bottom bars parallel to the slab free edge

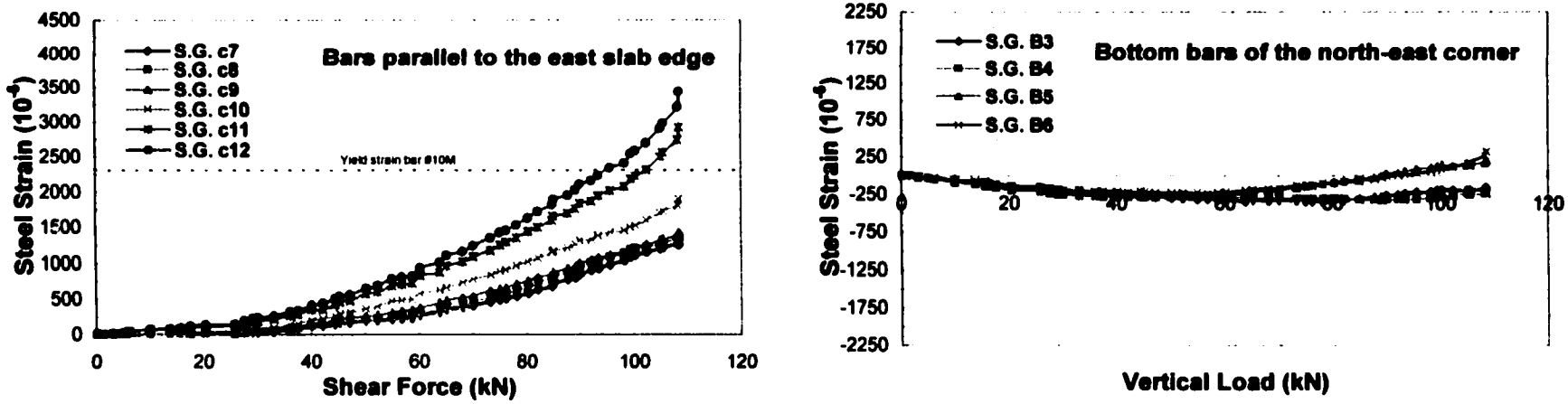

Figure 4.53 Steel strains on the test of connection C_6 of the continuous slab specimen; (a) bars parallel to east slab edge, (b) bottom bars parallel to the slab free edge

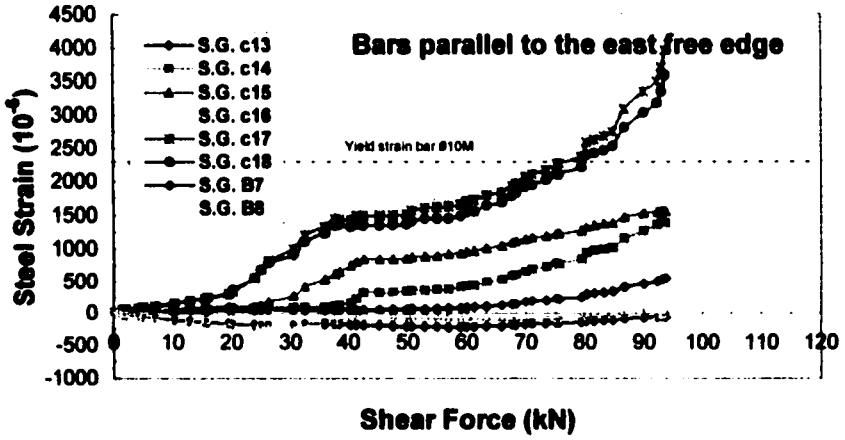

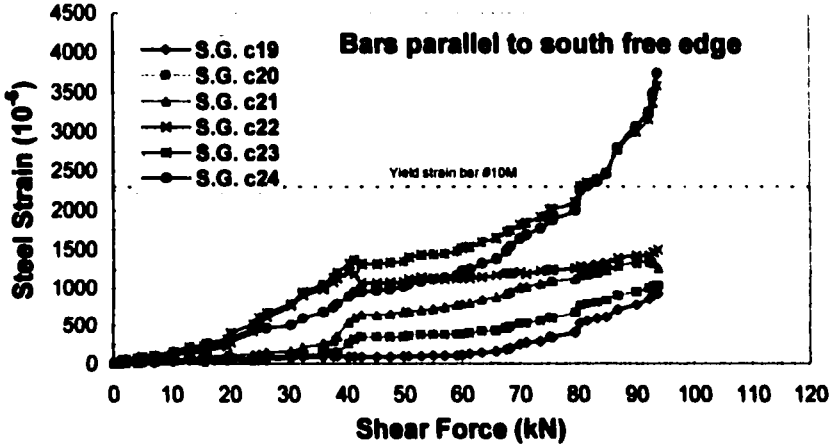

Figure 4.54 Steel strains on the test of connection C_7 of the continuous slab specimen; (a) bars parallel to the east slab edge, (b) bars parallel to the south slab free edge

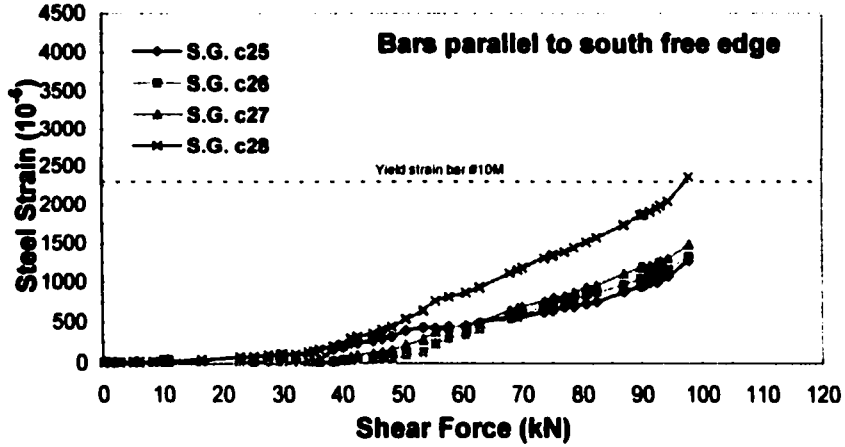

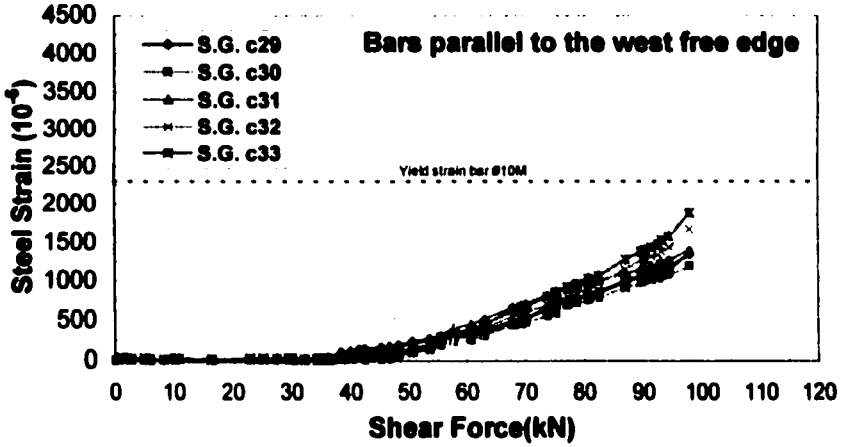

Figure 4.55 Steel strains on the test of connection C_8 of the continuous slab specimen; (a) bars parallel to the south slab edge, (b) bars parallel to the west slab free edge

4.4.5 Out-of-plane slab deflections

Deflections of the slab at 60 mm from the column faces were measured using two LVDT's and deflections of the slab at the middle span and the middle panel were measured using three dial gauges. The locations of the instrumentation are shown in Figure 3.17.

Figure 4.56 to Figure 4.58 show the out-of-plane slab deflection on the tests of corner connections. The test results of connection C_5 are excluded for the reasons described in the previous sections. The slab deflections around the column at cracking load were 1.5 mm, 0.25 mm and 2.1 mm for connections C_6, C_7 and C_8, respectively. The maximum vertical deflections of the slab on this region at the ultimate load capacity were 10.2 mm, 3.17 mm and 6.3 mm for connections C_6, C_7 and C_8, respectively.

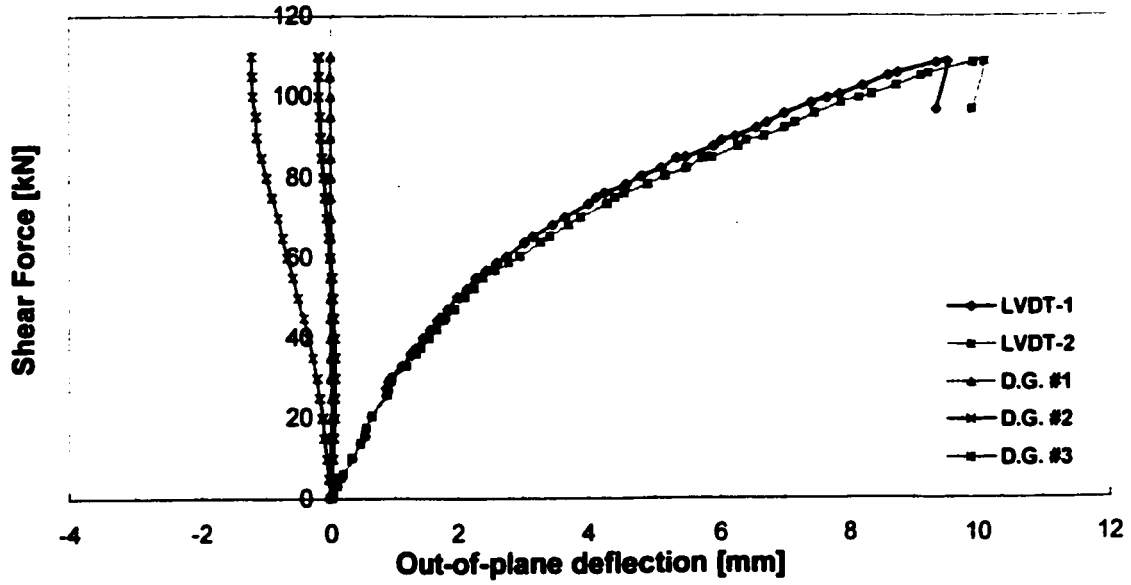

Figure 4.56 Slab out-of-plane deflections on the test of connection C_6 of the continuous slab specimen

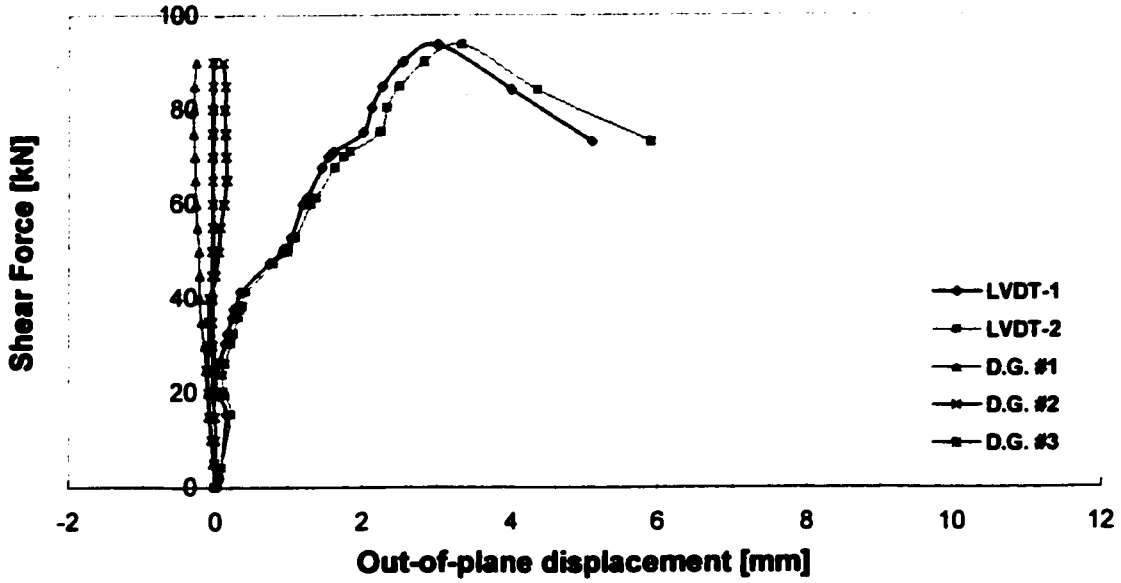

Figure 4.57 Slab out-of-plane deflections on the test of connection C_7 of the continuous slab specimen

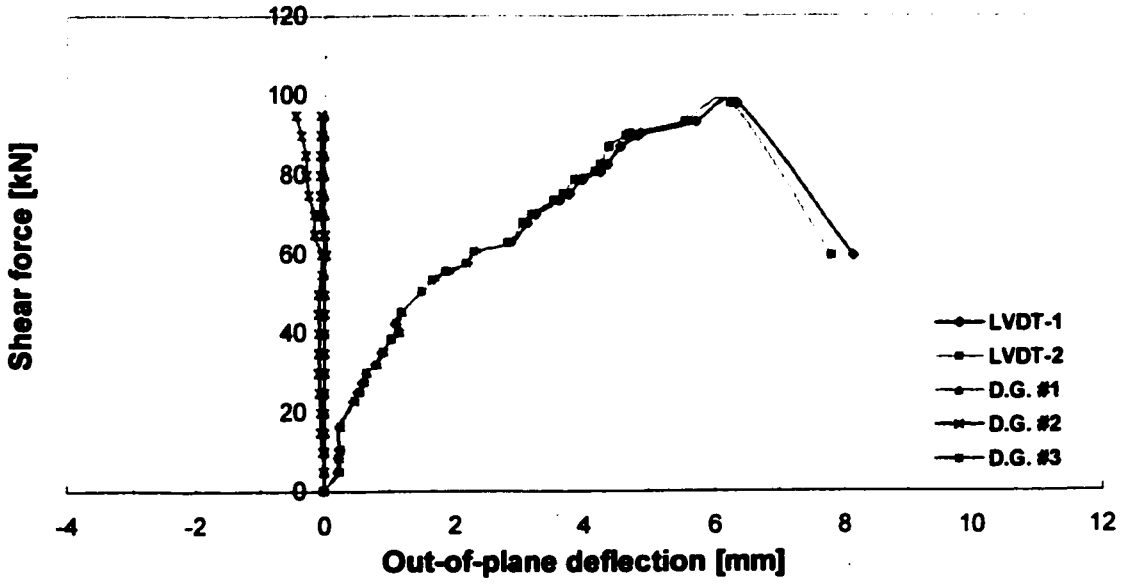

Figure 4.58 Slab out-of-plane deflections on the test of connection C_8 of the continuous slab specimen

4.4.6 Column rotations

Similar to edge connections, diagonal horizontal column deflections were measured at two point on the column stubs 343 mm above and below the slab surfaces. Column rotations were determined using equation 4.1. Figure 4.59 shows the biaxial column rotation during the test of connection C_6, C_7 and C_8.

The *M/V* ratio applied to the connections influenced the direction of the column rotations of the corner connections. If the applied *M/V* ratio is less than that applied on connection C_6, the top column stub rotates inward. If it is larger, the top column stub rotates outward. The column rotations may also be used to explain the behavior of the steel strain in the connections. The steel strains in connection C8 are less than that in connection C7, in which the column rotations were inward and outward, respectively.

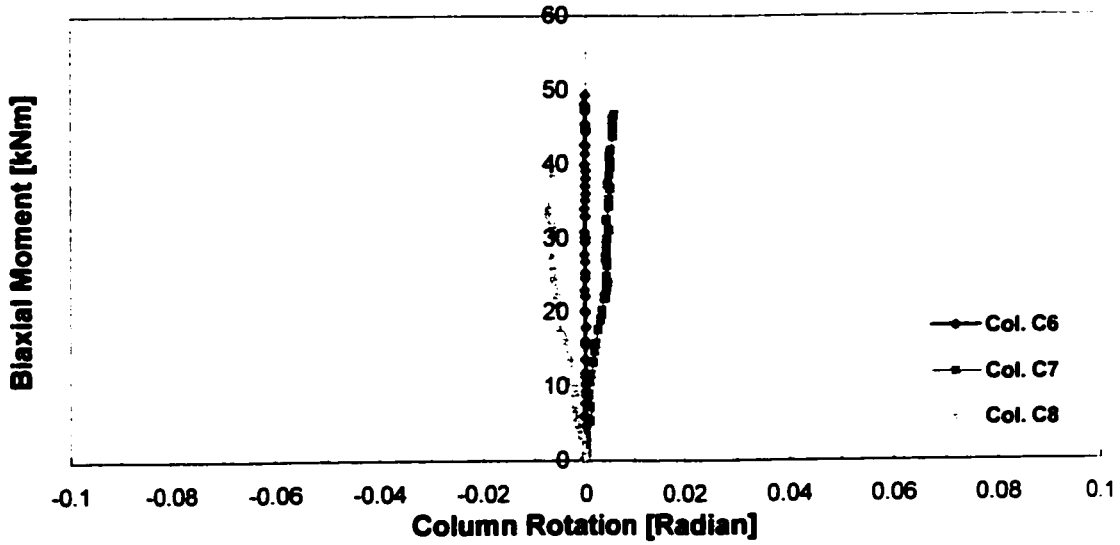

Figure 4.59 Diagonal column rotation on the tests of connections C_6, C_7 and C_8 of the continuous slab specimen

CHAPTER 5
DISCUSSION ON EDGE CONNECTIONS

5.1 GENERAL

Test results presented in Chapter 4 on the edge column slab connections are discussed in this chapter. The discussion is divided into the following categories:

- Interaction between shear and moment
- Load capacity of the tests calculated using the proposed methods and the code predictions
- Effect of the steel ratio (ρ) on the ultimate shear stress
- Shear capacity of repaired edge connections
- Stiffness of repaired edge connections

5.2 INTERACTION BETWEEN SHEAR AND MOMENT

The effect of unbalanced moment on the strength of edge column slab connections has long been recognized. Various approaches proposed to account for this effect have been described in Chapter 2. Code provisions (ACI 318-99, CSA A23.3-94 and CEB-FIP-90) include the effect of unbalanced moment when calculating shear stress along an assumed shear perimeter. The magnitude of the unbalanced moment transferred by the shear stresses varies from one code to the others. The British BS 8110-85 code uses a simple multiplier of 1.25, which is independent to the magnitude of the moment, to account for the effect of unbalanced moment about an axis parallel to the slab free edge; therefore, it is not included in this discussion of interaction between shear and moment

In this section, the code shear-moment interaction is examined using the three series of the test results described previously. Alternative approaches that are fundamentally different to the code approaches are also examined using the same experimental results (i.e. Regan's Approach, Truss Model and Strip Model).

5.2.1 ACI 318-99 and CSA A23.3-94 Codes

The codes assume the shear strength along the shear critical sections is limited by vertical shear stresses. The total shear stress along the critical section is the sum of the shear stress due to the shear force and a fraction of unbalanced moment; which is distributed linearly along the critical shear section. Figure 5.1 and Figure 5.2 show the non-dimensional interaction diagrams between shear and moment predicted by ACI 318-99 and CSA A23.3-94 Codes for the three sets of experimental data, respectively. The ratio V_u/V_o is plotted against the ratio M_{code}/M_o. M_{code} (M_{ACI} or M_{CSA}) is the moment at the centroid of the critical shear section. V_o is the shear force when the moment is zero and M_o is the moment at centroid of the critical shear section when shear force is zero. V_o and M_o are calculated as:

$$V_o = v_{max} b_o d \tag{5.1}$$

$$M_o = \frac{v_{max} J_c}{\gamma_v c_{CD}} \tag{5.2}$$

Where:

$v_{max} = 0.333\sqrt{f_{cm}}$ (MPa) for ACI 318-99

$v_{max} = 0.4\sqrt{f_{cm}}$ (MPa) for CSA A23.3-94

f_{cm} = compressive strength of concrete

b_o = length of shear perimeter

d = effective slab depth

J_c = polar moment of inertia

γ_v = a fraction of unbalanced moment resisted by shear

The code interaction diagrams shown in Figure 5.1 and Figure 5.2 are based on concrete compressive strengths of 42.4 MPa and 52.8 MPa for the continuous slab and isolated slabs, respectively. To compare the experimental data with the codes, the variations in concrete compressive strength are taken into account by multiplying the

ratio V_u/V_o and M_{code}/M_o by factors $\sqrt{42.4/f_{cm}}$ and $\sqrt{52.8/f_{cm}}$ for the continuous and isolated slab specimens, respectively. The interaction diagram consists of two straight lines. Line-1 represents the case when the maximum shear stress governs at the inner face of the shear perimeter (v_{AB}) and Line-2 when the shear stress at slab free edge governs (v_C or v_D). The location of the intersection of Line-1 and Line-2 depends on the magnitude of c_{AB} and c_{CD}.

The ACI 318-99 code is generally conservative for continuous slab connections except for connection E_4 and E_{4R} where the applied load eccentricities are less than the slab effective depth. For isolated slab connections, in general the ACI 318-99 code predicts accurately the degree of shear-moment interactions. However, the code is too conservative for the connections subjected to shear force only.

The CSA A23.3-94 code is based on the same assumptions as the ACI 318-99. Increasing the maximum shear stress by *21%* from the ACI 318-99 results in the CSA A23.3-94 overestimating for most of the experimental data as shown in Figure 5.2. However, CSA A23.3-94 predicts the strength of the connections subjected to moment only (i.e. E_3) better than the ACI 318-99.

The flexural capacity of edge connections provided by the reinforcement perpendicular to the slab free edge within a width of c_2+3h based on the provisions of ACI 318-99 and the CSA A23.3-94 are also presented in the diagrams. Line-3, Line-4 and Line-5 in Figure 5.1 and Figure 5.2 are the flexural capacities of the edge connections of the continuous slabs, isolated slabs in Series I and isolated slabs in Series II, respectively.

If the edge connections do not have sufficient flexural reinforcement, the interaction diagrams follow the Line-1, Line-3 and Line-2 for the continuous slab and Line-1, line-2 for the isolated slab series II. For isolated slabs in Series I, the flexural capacity is very high as indicated by Line-5 due to the large reinforcement perpendicular to the slab free edge placed within the width of c_2+3h.

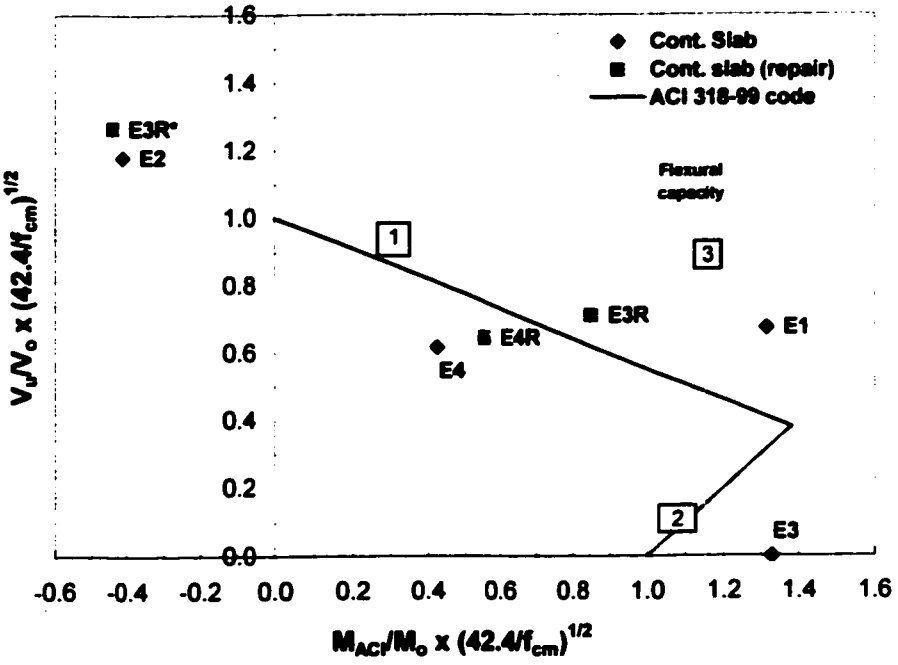

(a) Test of continuous slab

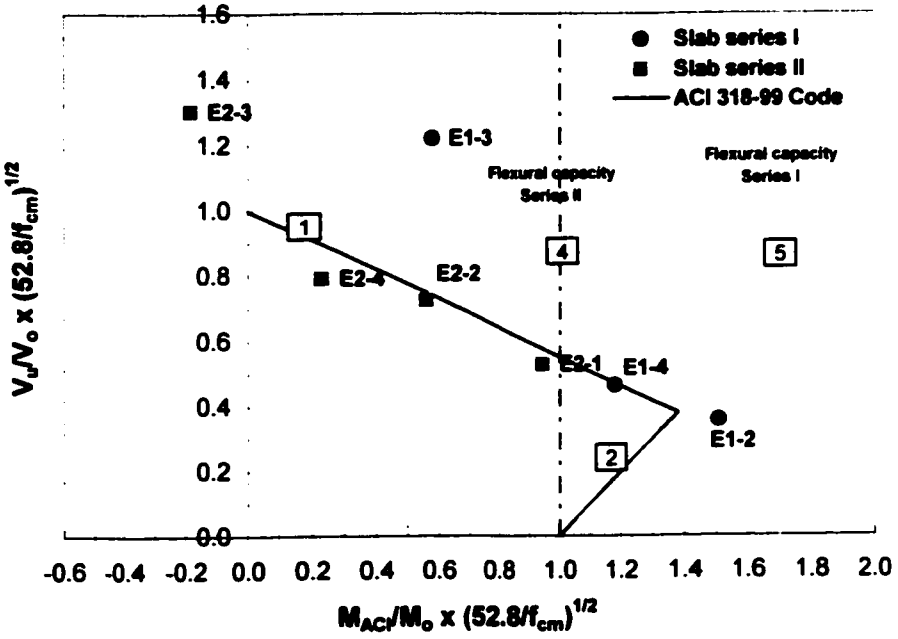

(b) Test of Isolated slabs

Figure 5.1 Interaction between shear force and moment at edge connections according to ACI 318-99; (a) test of continuous slab and repaired slab; (b) test of isolated slab series I and II

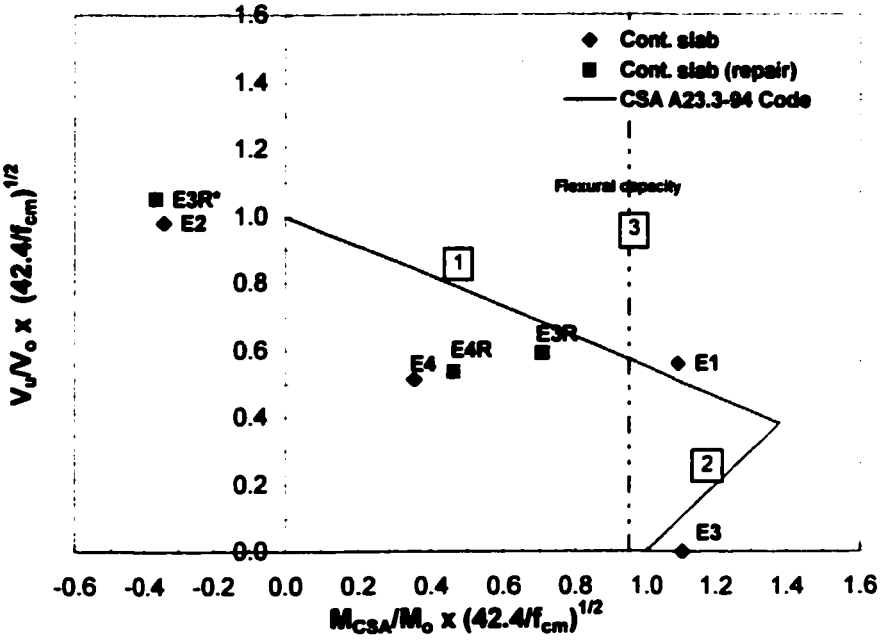

(a) Test of continuous slab

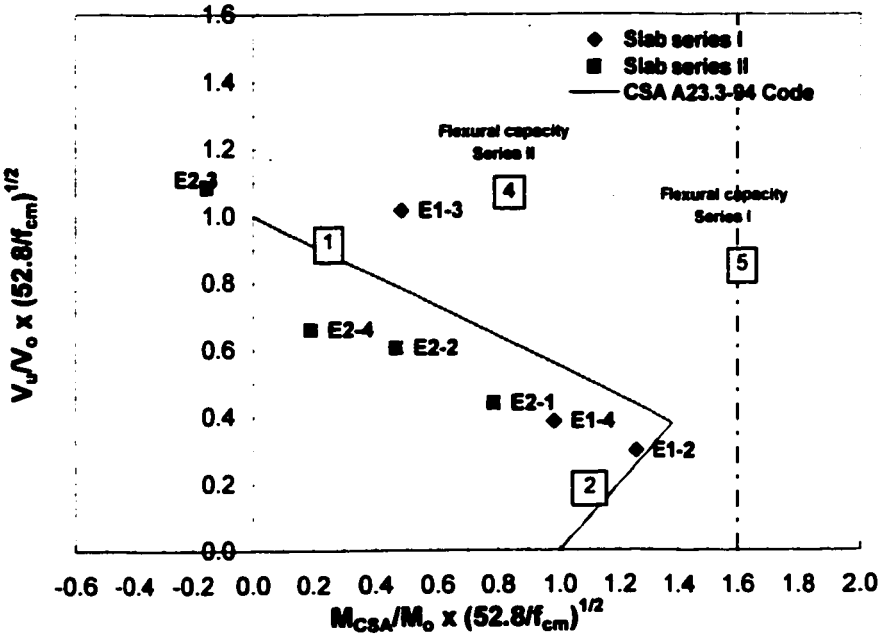

(b) Test of isolated slabs

Figure 5.2 Interaction between shear force and moment at edge connection according to CSA A23.3-94; (a) test of continuous slab and repaired slab; (b) test of isolated slabs series I and II

It is found for both codes that the edge connections did not fail in flexure although the flexural resistance calculated by the codes is exceeded. This is shown by connections E_1 and E_3 of the continuous slab and connections E_{1-2} and E_{1-4} of the isolated slabs.

5.2.2 CEB-FIP MC 1990

CEB-FIP Model Code assumes a uniform plastic shear distribution along a shear perimeter at $2d$ from the column faces. Total shear stress is obtained by the algebraic sum of the shear stresses due to direct shear force and unbalanced moment. To examine the degree of interaction between shear and moment predicted by the code equations, the test results are plotted as a non-dimensional interaction diagram based on the ratio of V_u/V_o against M_{code}/M_o. V_o and M_o are shear force and moment at the centroid of assumed shear perimeter according to equation 2.63 when the moment and shear force are zero, respectively. A linear interaction is obtained. The maximum shear stress used to develop interaction diagram is based on f_{cm} = 42.4 MPa and 52.8 MPa for the continuous slab and isolated slabs, respectively. V_o and M_o are calculated as:

$$V_o = \tau_{sd} u_1 d \tag{5.3}$$

$$M_o = \frac{\tau_{sd} w_1 d}{K} \tag{5.4}$$

Where:

$\tau_{sd} = 0.18\left(1+\sqrt{\frac{200}{d}}\right)(100\rho f_{cm})^{\frac{1}{3}}$ (The partial safety factor is set to unity)

u_1 = length of shear perimeter

w_1 = a properties of the critical section

d = effective slab depth

K = a fraction of M_{code} resisted by shear stress (K = 0.6 for square columns)

f_{cm} = measured cylinder compressive strength of concrete

To account for the effect of variation in concrete strength of experimental data; the ratios V_u/V_o and M_{code}/M_o are multiplied by factors $(42.4/f_{cm})^{1/3}$ and $(52.8/f_{cm})^{1/3}$ for the continuous slab and isolated slabs, respectively. Comparison of the test data and the CEB-FIP MC90 interaction diagram is shown in Figure 5.3. The CEB-FIP MC90 overestimates most of test data except connection E_1 is predicted conservatively. The ultimate capacity of connection E_3, where only moment is applied, is predicted 23% lower than the moment calculated using equation 5.4. It is also interesting to note that taking the shear perimeter at $2d$ from the column faces or loaded area results in its centroid located outside the column section; consequently, almost half of the test moments changed direction.

Flexural capacity of the edge connections is also presented as a vertical straight line in the interaction diagrams. CEB-FIP MC90 does not recommend explicitly the slab effective width to calculate the flexural capacity of the connections. It is assumed that the flexural capacity is provided by the reinforcement perpendicular to the slab free edge within the effective width of c_2+6d. The width is consistent with the recommended width for calculating reinforcement ratio in determining shear resistance of slab column connections.

If edge connections do not have sufficient flexural reinforcement, the interaction diagram follows Line-1 and Line-2 for the continuous slab and isolated slabs in Series II. However, flexural capacity of the isolated slabs in Series I is larger than the flexural capacity calculated from the shear expression (M_o) as indicated by Line-3 in Figure 5.3. Flexural capacity of the CEB-FIP MC90 is conservative for the edge connection failed in flexure (i.e. E_3).

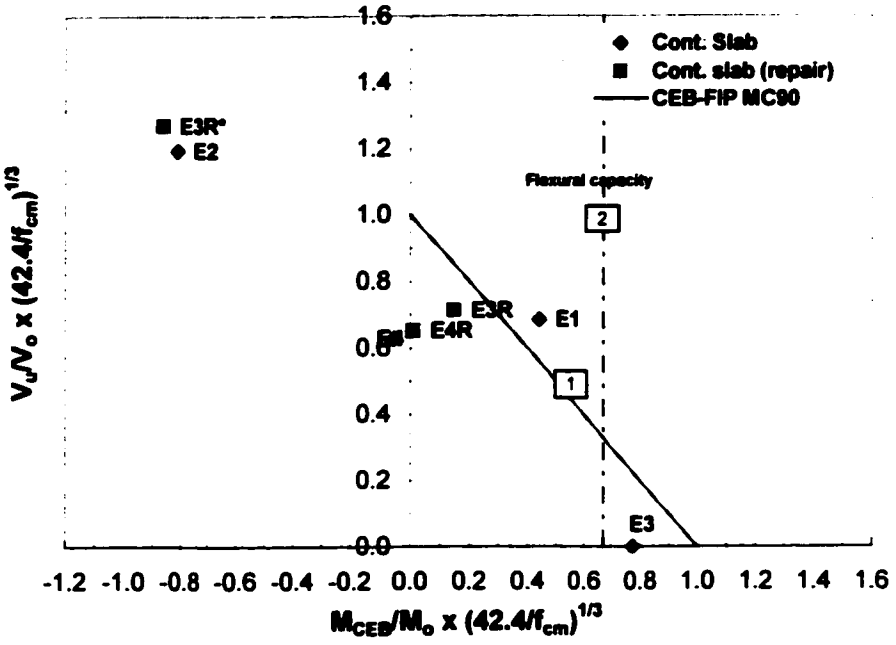

(a) Test of continuous slab

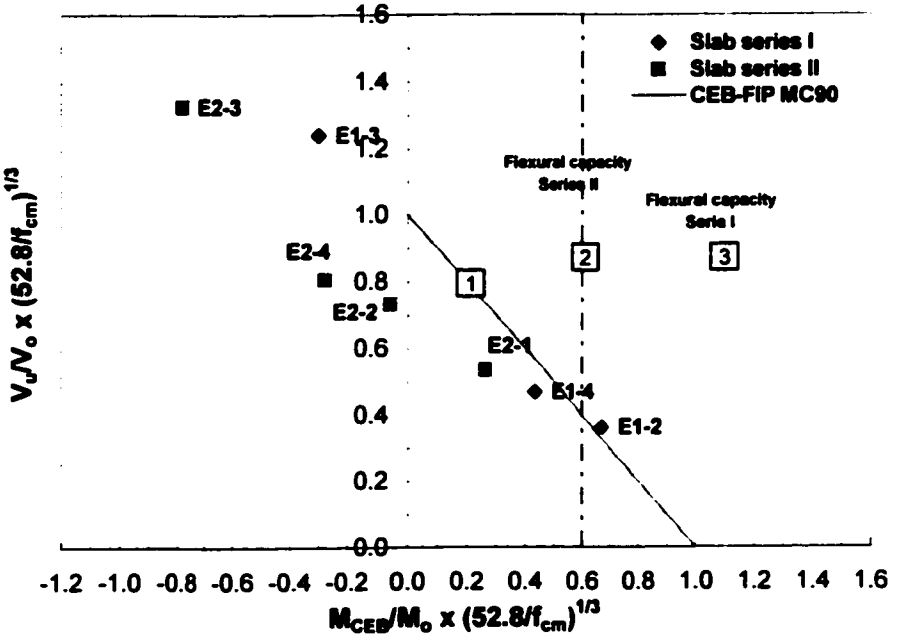

(b) Test of isolated slab

Figure 5.3 Interaction between shear force and moment at edge connection according to CEB-FIP Model Code 1990; (a) test of continuous slab and repaired slab; (b) test of isolated slab series I and II

5.2.3 No interaction between shear force and Moment

Moehle (1988) proposed no interaction between shear force and unbalanced moment on edge column slab connections subjected to shear force and unbalanced moment about an axis parallel to the slab free edge. The effect of unbalanced moment on shear stress along critical shear section at *d/2* from column faces or loaded areas, can be ignored when the ultimate shear force is less than $0.75\phi V_o$ and entire unbalanced moment shall be resisted by flexural resistance provided by the reinforcement within the effective width c_2+2c_1. Assuming the yield line inclines 45^o from inner corner of the column to the slab free edge, the effective width can be taken as c_2+2c_1.

Using the latter effective width, the test results of the present study on edge connections together with Moehle's proposed interaction are plotted in Figure 5.4 based on ratios of V_u/V_o against M_{code}/M_r, V_u is shear force at the column centroid and M_{code} is unbalanced moment at centroid of critical shear section. V_o and M_r are shear force and moment resistance within the effective width given as:

$$V_o = v_c A_c \tag{5.5}$$

$$M_r = \rho f_y d^2 \left(1 - \frac{0.59\rho f_y}{f_{cm}}\right) b_c \tag{5.6}$$

Where:

v_c = maximum shear stress (MPa)

$$= 0.17(1+\frac{2}{\beta_c})\sqrt{f_{cm}} \leq 0.333\sqrt{f_{cm}}$$

$A_c = (c_2+2c_1+2d)d$

ρ = reinforcement ratio within the effective width c_2+2c_1

The measured compressive strength (f_{cm}) is used rather than specified compressive strength (f_{ck}) to calculate V_o and M_r. The reduction factor ϕ is set to unity. The interaction diagrams are shown in Figure 5.4 and Figure 5.5.

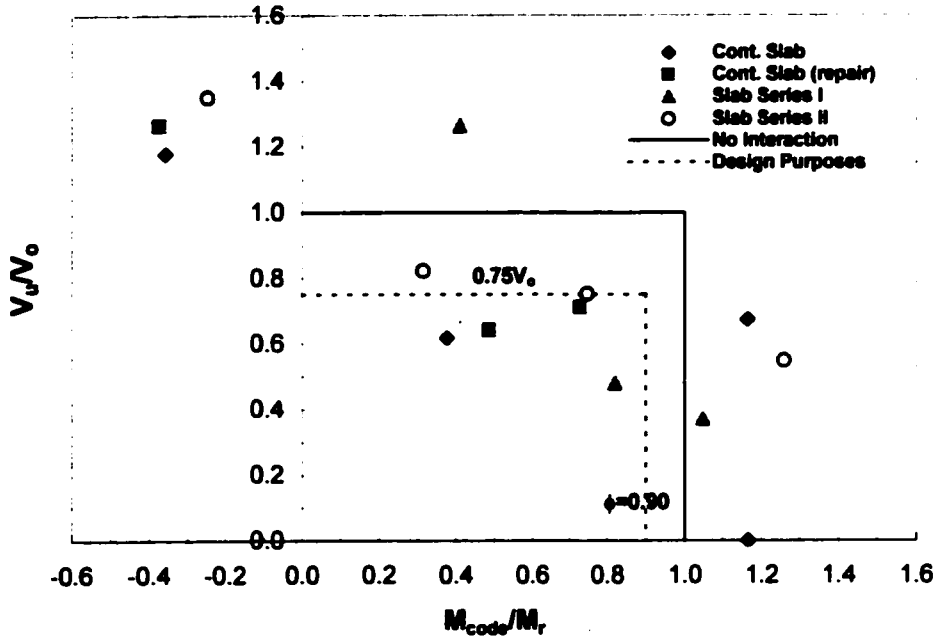

Figure 5.4 Interaction between shear force and moment based on Moehle's approach (1988) considering the moment at centroid of critical shear section

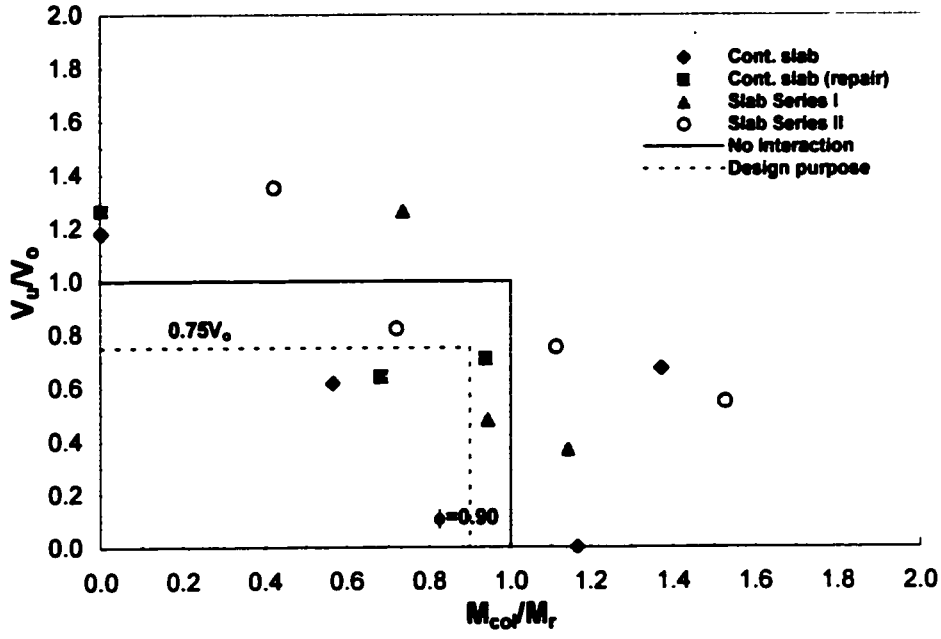

Figure 5.5 Interaction between shear force and moment based on Moehle's approach (1988) considering the moment at column centroid

Figure 5.4 shows that assuming no-interaction between shear force and unbalanced moment considering at centroid of critical shear section overestimates half of the test results. Although the limiting maximum shear force is reduced to 75% of V_o to not include the unbalanced moment for design purposes, the approach is still not safe for all edge connections.

If the shear forces and moments are considered at the centroid of column sections, Moehle's approach for design purposes is better than considering the moments at the centroid of the critical shear section. However, the constant shear strength until flexural capacity is reached still overestimates half of the test results as shown in Figure 5.5. It is also described in Section 5.5 that shear strength decreases with an increase in M/V ratio.

5.2.4 Alternative approaches

Building code approaches have been developed empirically using data banks of test results available in the literature so that their reliability may be limited to those data from which they were developed and calibrated. Alternative approaches to develop shear-moment interaction are based on discrete points, which represent the behavior of the connections transferring the loads. The load capacity of the connections at failure can be obtained using the interaction diagrams. Figure 5.6 to Figure 5.8 show interaction diagrams according to Regan's approach, the Truss Model and the Strip Model for edge connections of the continuous slab, isolated slab Series I and II, respectively. It is difficult to present all tests in a single diagram due to the unique characteristics of the interactions, which are developed from the geometry and material properties of the connections. Therefore, only test results with the same material properties should be presented on the interaction diagram of each series. However, considering small variations on measured compressive strength of –4.9% and +2.8% for continuous slab and +4% for isolated slabs from the concrete strength used in interaction diagrams, all tests are presented in the diagrams for the corresponding series.

Regan's Approach (1981)

Regan's approach to develop the interaction diagram of edge column slab connections subjected to combined shear force and moment about an axis parallel to the slab free edge overestimates some of test results. Six of the thirteen tests of the present study are overestimated. In defining the failure surface area, the angle of the inclined cracks was assumed to be 22.5°. The edge connections of the present study failed with inclined angle ranged from 18.5° to 45°. This assumption is believed to lead to the overestimation of the test results. Regan's statement that development of full torsion on the side faces of the column reduces the shear strength seems to be supported by the experimental results of connections E_1, E_{1-2}, E_{1-4} and E_{2-1} as described in Chapter 4.

The Truss Model (Alexander and Simmonds, 1987)

The Truss Model overestimates most of the tests. It is believed that assuming the reinforcement within c_2+2d yields at connection failure is the reason. It was generally found that only the reinforcement passing through the column yields. It is interesting that the slab clear cover (d') controls punching shear strength of the connections instead of the effective slab depth (d) usually used in building code provisions. Taking $\sqrt{f_c'}$ as the concrete strength contribution may also result in overestimation of the connection capacity. Other researchers (Regan et.al.1981; Gardner, 1992; Sherif, 1995; etc.) concluded that punching shear strength could be best represented by the cube root of the concrete compressive strength. Although the model is claimed to be possible for hand calculation, it is difficult to determine the strut combinations for every load combination.

The Strip Model (1998)

Shear moment interaction diagram based on the Strip Model proposed by Afhami, Alexander and Simmonds (1998) is obtained by connecting four discrete points with straight lines. No torsion reinforcement parallel to the slab free edge was provided so that no shear can be resisted by the spandrel strips when the connections have developed maximum flexural capacity. Non-proportional behavior of the strips considered in the

model agrees with the non-symmetrical failure surface observed during the tests of some connections. The strip model has similarities with Regan's approach as indicated by the slope of the interaction lines shown in Figure 5.6 to Figure 5.8. The Strip Model is the most conservative among the three models considered here. The model describes behavior of loads transferred from the slab to the column.

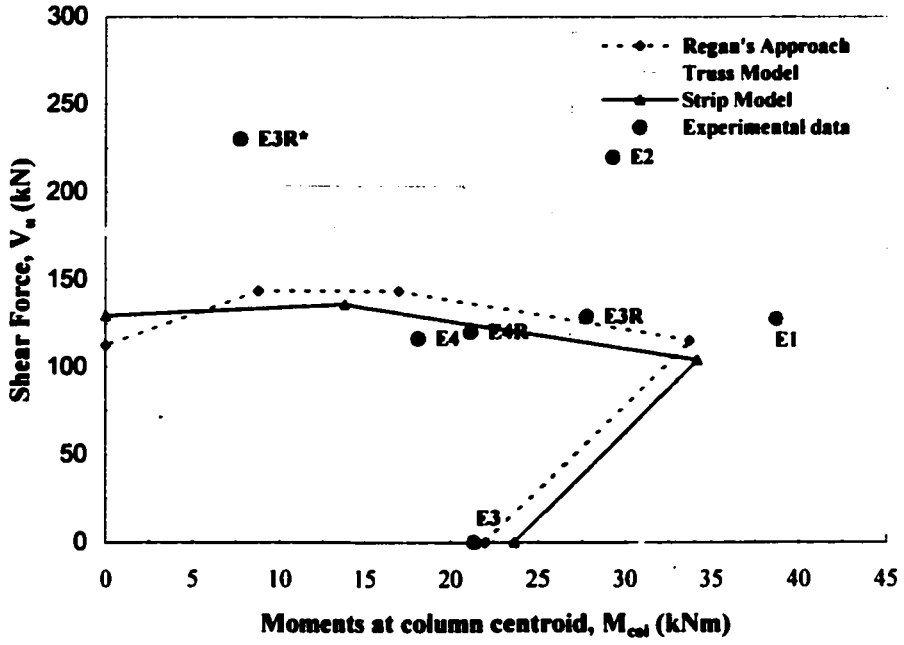

Figure 5.6 Shear-moment interaction of edge column slab connections of the continuous slab for f_{cm} = 42.4 MPa using Regan's approach, the Truss Model and the Strip Model

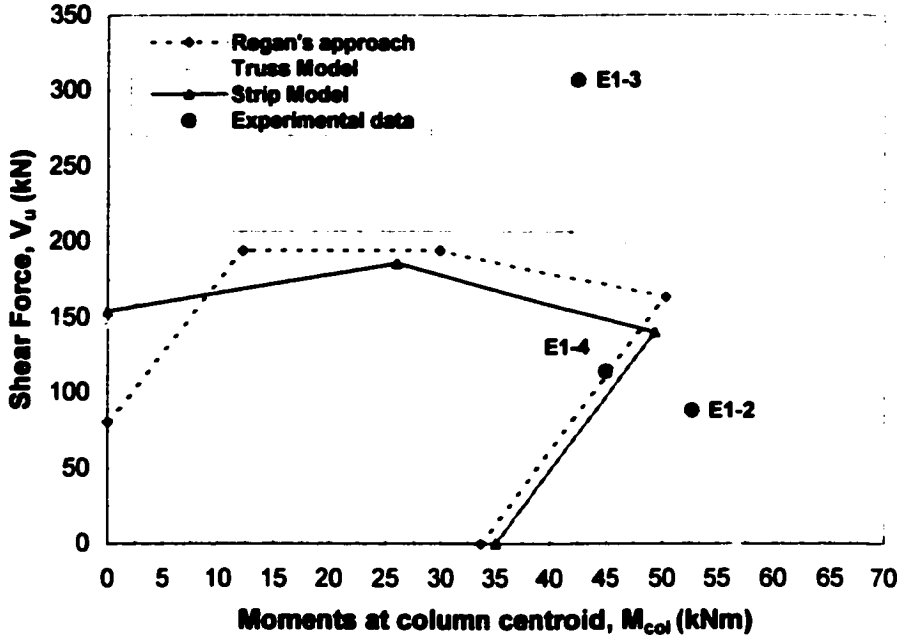

Figure 5.7 Shear-moment interaction of isolated edge column slab connections of series I for f_{cm}=52.8 MPa using Regan's approach, the Truss Model and the Strip Model

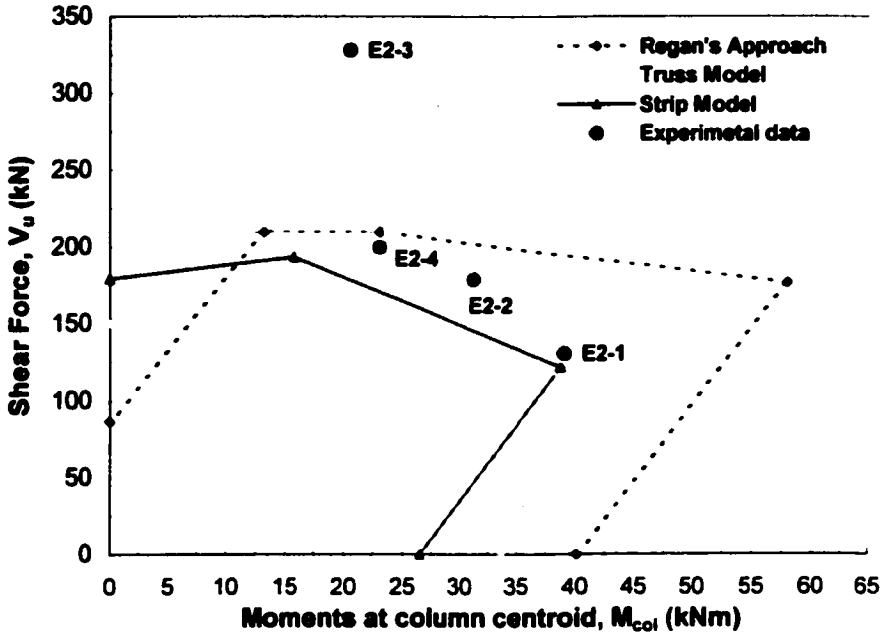

Figure 5.8 Shear-moment interaction of isolated edge column slab connections of series II for f_{cm}=52.8 MPa using Regan's approach, the Truss Model and the Strip Model

5.3 COMPARISON OF LOAD CAPACITY

The capacity of the edge column slab connections of the experimental test was calculated using the selected proposed approaches presented in Chapter 2 and the code provisions (*ACI 318-99*, *CSA A23.3-94*, *BS 8110-85* and *CEB-FIP MC90*). Three of the experimental results namely E_{1R}, E_{2R} and E_{1-1} are excluded in all discussions due to following reasons. Connections E_{1R} and E_{2R} were repaired using *CAH* concrete, which has unique characteristics compared to normal concrete. Connection E_{1-1} failed prematurely due to lack of deflection compatibility along the supports as already mentioned previously.

5.3.1 Using building code provisions

The experimental shear stresses (v_u) calculated using the code parameter and the measured failure shear force (V_u) and moment (M_u), are compared to the code specified shear stress. Table 5.1 shows summary of the statistical results of the capacity of edge connections.

Table 5.1 Summary of statistical results of code predictions on the strength of edge column slab connections

CODES	Comparison	Statistical results		
		Average	Standard Deviation (STD)	Coefficient of Variation (COV)
ACI 318-99	v_u/v_{ACI}	1.20	0.30	0.25
CSAA23.3-94	v_u/v_{CSA}	0.99	0.25	0.25
BS8110-85	v_u/v_{BS}	1.00	0.36	0.36
CEB-FIP 1990 Method-1	v_{u1}/v_{CEB}	0.82	0.25	0.31
CEB-FIP 1990 Method-2	v_{u2}/v_{CEB}	0.97	0.39	0.40

Detailed comparisons between the experimental shear strength and the calculated code strength are shown in Table 5.4 to Table 5.6. In all calculations, the measured compressive strength of the concrete cylinders (f_{cm}) is used rather than the specified compressive strength (f_{ck}).

The American ACI 318-99 Code

The failure shear stress calculated using the ACI 318-99 code assumption ranges from 1.31 MPa ($0.2\sqrt{f_{cm}}$) for connection E_3 to 3.67 MPa ($0.5\sqrt{f_{cm}}$) for connection $E_{2\text{-}3}$ as shown in Table 5.4. The code shear stress resistance of $0.333\sqrt{f_{cm}}$ is over conservative for the connections subjected to shear force only or combined shear force and moment with a low load eccentricity as can be seen in Table 5.4 for slab E_2, E_{3R}*, $E_{1\text{-}3}$ and $E_{2\text{-}3}$. For connections E_2, E_{3R}*, $E_{1\text{-}3}$ and $E_{2\text{-}3}$, the average of the ratio v_u/v_{aci} is 1.57. The failure shear stress of the connection subjected to moment only about the axis parallel to the slab free edge is equal to 1.31 MPa ($0.2\sqrt{f_{cm}}$ or $0.224\sqrt{f_{ck}}$ for $f_{cm} \approx 1.25 f_{ck}$), which is about 34% higher than one way shear strength specified by the code ($0.167\sqrt{f_{ck}}$). For all connections, the average ratio of the failure stress to the code predicted stress, v_u/v_{aci} is 1.20 with standard deviation (STD) and coefficient of variation (COV) equal to 0.30 and 0.25 respectively as shown in Table 5.1. Although the average is quite good, the distribution of calculated shear stress is very scattered.

The Canadian CSA A23.3-94 Code

The failure shear stresses predicted by the CSA A23.3-94 code are presented together with the ACI 318-99 Code in Table 5.4. The calculated failure shear stresses for both codes are based on the same assumptions. The only difference between the codes is the specified limiting maximum shear resistance (v_c). Setting all of the reduction factors equal to unity, leads to the shear stress resistance by the CSA code being 21% higher than those of the ACI code. From Table 5.4, the CSA Code predictions of the failure shear stresses of the connections E_2, E_{3R}*, $E_{1\text{-}3}$ and $E_{2\text{-}3}$ are less conservative than the ACI Code; where the average ratio v_u/v_{csa} of 1.31 is 20% lower than that of the ACI Code. However, for all tests, the average ratio v_u/v_{csa} is 0.99 with STD and COV equal to 0.24 and 0.25, respectively.

The British BS8110-85 Code

The Code recommends a simple multiplier, given by Equation 2.59, to calculate the failure shear stresses when connections are subjected to combined shear force and unbalanced moment about the axis parallel to the slab free edge. In making comparison between the failure shear stress and the shear stress predicted by the code, the concrete shear resistance is calculated using Equation 2.57 ignoring the 40 MPa limit of the cube compressive strength given in the code. Table 5.5 presents the comparison between the failure and the predicted shear stress of the tests.

The shear stress of the tests calculated using the BS 8110-85 provisions ranges from 0.69 MPa ($E_{1\text{-}2}$) to 2.57 MPa ($E_{2\text{-}3}$). The shear stresses of the edge connections subjected to shear force only or combined shear force and moment about the axis parallel to the slab free edge (i.e. E_2, E_{3R}*, $E_{1\text{-}3}$ and $E_{2\text{-}3}$) are underestimated by the code with the average ratio v_u/v_{bs} of these four connections of 1.45. The rest of the connections are overestimated. The British code does not have any provisions to calculate the shear stress on edge connections subjected to moment only (i.e. E_3); therefore, the test result of connection E_3 is excluded in calculating the test statistics. It is found the average v_u/v_{bs} is 1.0 with STD and COV of 0.36 and 0.36, respectively, as shown in Table 5.1. Even though the BS8110-85 code predicts the overall results very well, the distribution of the results has a wide range of scatter as indicated by the value of STD and COV in Table 5.1.

Using a simple multiplier on the shear force to account for the effect of moment transfer in calculating the shear stress of edge connections subjected to combined shear force and moment with high load eccentricity underestimates the results. This method seems to be appropriate only for connections subjected to combined shear force and moments due to gravity loads.

The European CEB-FIP MC90

The CEB-FIP MC90 recommends two different methods to calculate the shear stress of edge column slab connections; using full length of the shear critical section (Method-1) based on equation 2.63 or using a reduced length of shear critical section (Method-2) based on equation 2.65. The shear stress calculated according to Method-1 of the CEB-FIP code results in the failure shear stress ranging from 0.53 MPa (i.e. E_2) to 1.64 MPa (i.e E_{3R}) as shown in Table 5.6. Due to the large critical shear perimeter, $2d$ from the column faces, the direction of the moment as indicated by connections E_2, E_4, $E_{3R}^{\bullet}$, $E_{1\text{-}3}$, $E_{2\text{-}2}$, $E_{2\text{-}3}$ and $E_{2\text{-}4}$ in Table 5.6 resulting in overestimation of the connection capacities. The average ratio v_{u1}/v_{ceb} for all tests is 0.82 with STD and COV equal to 0.25 and 0.31 indicating that Method-1 of CEB-FIP overestimates test results. Even though the average v_{u1}/v_{ceb} is less than the value of Method-2 and the results are less scattered, Method-1 still underestimates the failure shear stress.

Using Method-2 of the CEB code, the failure shear stress of the tests ranges from 0.63 MPa (i.e. $E_{1\text{-}2}$) to 2.36 MPa (i.e. $E_{2\text{-}3}$) as shown in Table 5.6. The average ratio v_{u2}/v_{ceb} for all tests is 0.97 with STD and COV equal to 0.39 and 0.40 respectively, ignoring the test result of connection E_3. Method-2 overestimates the strength of all edge connections subjected to shear force only or combined shear force and moments. It was found that shear strength of the edge connections do not increase by a constant value when unbalanced moment exists on the connections. The shear stress of the edge connections subjected to moment only cannot be predicted by the Method-2 of the CEB Code. Method-2 of CEB provisions is similar to the simple multiplier method of BS 8110-85 code and is inappropriate for application to the present test results.

5.3.2 Using proposed approaches

Some of the proposed approaches described in Chapter 2 are examined using the test results to see how well they predict the strength capacity of edge connections. Regan's approach, the Truss Model and the Strip Model are not intended to use for design purposes; therefore, the comparisons are made between the measured failure

forces and those obtained from the complete shear-moment interactions at the same M/V ratio. For the other approaches (Gardner's, Sherif's and Elgabry's), comparisons are based on shear stress.

Table 5.2 shows a summary of the statistical results presented in Table 5.7 to Table 5.12 at the end of this chapter. Discussion of the alternative approaches may be separated into two groups. The first group is based on modified empirical code approaches i.e. Sherif (1995), Gardner (1996), and Elgabry (1995). The second group is based on analytical approaches i.e. Regan's approach (1981), Truss Model (1987) and Strip Model (1998).

Table 5.2 Summary of statistical results of the proposed approaches on the strength of edge column slab connections

Researchers	Comparison	Statistical results		
		Average	Standard Deviation (STD)	Coefficient of Variation (COV)
Regan (1981)	V_u/V_p	1.14	0.30	0.27
	M_u/M_p	1.16	0.30	0.26
Truss Model (1987)	V_u/V_p	1.04	0.26	0.25
	M_u/M_p	1.03	0.26	0.25
Strip Model (1998)	V_u/V_p	1.25	0.31	0.25
	M_u/M_p	1.26	0.30	0.24
Sherif (1995)	v_u/v_{pred}	0.90	0.30	0.34
Gardner (1996) Method-1	v_{u1}/v_{pred}	1.12	0.21	0.18
Gardner (1996) Method-2	v_{u2}/v_{pred}	1.00	0.40	0.40
Elgabry (1995)	v_u/v_{pred}	1.19	0.29	0.24

Predicted shear forces and moments using Regan's approach, the Truss Model and the Strip Model are obtained by developing a complete interaction diagram for each method. Having a set of failure loads, the predicted loads can be calculated from the diagrams using the same load eccentricity (M/V) as the experimental failure loads.

The statistical comparisons of these approaches to the present test results are shown in Figure 5.2. It can be seen from the average ratio of measured to predicted loads for all three methods are conservative. The Truss Model is the least conservative followed by Regan's approach and Strip Model with the average ratios of V_u/V_p or M_{col}/M_p 1.03, 1.15 and 1.25, respectively. The scatter is similar for all approaches as indicated by coefficients of variation of 0.27, 0.25 and 0.27 for Regan's approach, the Truss Model and the Strip Model, respectively.

It is also found that Regan's approach, the Truss Model and the Strip Model underestimated the strength of specimens subjected to shear force only or combined loads with a very low load eccentricity (i.e. E_2, E_{3R}*, $E_{1\text{-}3}$ and $E_{2\text{-}3}$) as shown in Table 5.7 to Table 5.8. Although the average ratio of measured to predicted loads is conservative, it is not the case for every connection presented here.

The approach by Sherif (1995) underestimates the load capacity of most test results as shown in Table 5.10. The ultimate shear stress, (v_u) was calculated using equations 2.48 and 2.49 of the ACI 318-99 Code expression with reduction in γ_v as given by equation 2.22. The predicted shear stress is calculated using Sherif's proposed equations. It is found that the average ratio v_u/v_{pred} is 0.90 with a standard deviation (STD) and a coefficient of variation (COV) equal to 0.30 and 0.34, respectively. It is also found that the approach is only conservative for the connection subjected to shear force only (E_2), bending moment only (E_3) and the connections subjected to very low load eccentricity. Sherif's approach overestimates for the other connections. This may due to neglecting the effect of applied moments that are less than the flexure capacity provided by the reinforcement within the effective width ($\approx c_2+2c_1 \tan \phi$).

Gardner (1996) recommended two approaches to account for the contribution of unbalanced moment to shear strength of edge column slab connections. An ACI 318-99 code type linear shear stress distribution (Method-1) or a single multiplier as in BS8110-85 (Method-2) may be used. Comparison between measured to predicted shear stress is shown in Table 5.11, where v_{u1} was calculated based on the ACI 318-99

expression with the column perimeter taken as a critical shear section and v_{pred} was calculated using the proposed Equation 2.17. The average v_u/v_{pred} of Method-1 is 1.12 with STD and COV are 0.21 and 0.18, respectively. Gardner's Method-2 predicts exactly the test results as indicated by the average v_u/v_{pred} of 1.0 with STD and COV of 0.40 and 0.40, respectively, as shown in Table 5.2. Although Method-2 gives a better average than Method-1, the distribution of the test data is very scattered as indicated by the value of STD and COV. Method-2 is inappropriate in this case since the method was proposed for slabs subjected to uniform surface load.

Elgabry and Ghali's approach (1995) as given in Table 5.2, does not differ significantly from the ACI 318-99 code prediction given in Table 5.1 on test results. Comparisons between failure and predicted shear stress for all tests of edge connections are shown in Table 5.12. The average ratio v_u/v_{pred} is 1.19 with STD and COV equal to 0.29 and 0.24, respectively. The approach is about 5% better than the ACI 318-99 code prediction.

For the case of square edge column connections subjected to load eccentricity perpendicular to the slab free edge, this result implies that reducing the ratio of l_x/l_y by 0.2 in calculating γ_{vy} and replacing J_x and J_y with I_x and I_y, respectively, does not change the results significantly. The 3% difference of I_x and I_y from J_x and J_y will not be true for thick slabs as in footing slabs (MacGregor and Bartlett, 2000).

5.4 EFFECTIVE WIDTH FOR FLEXURAL RESISTANCE

Test results of connection E_3 together with Stamenkovic's result (*M/E/2*) and Zaghlool's test (*ZV-4*) can be used to find the effective slab width for the flexural resistance provided by reinforcement perpendicular to the slab free edge of edge column slab connections subjected to bending moment only. Table 5.3 shows the comparison between experimental moment and predicted moment.

Table 5.3 Comparison of flexural capacity of edge column slab connections using two effective widths

Slabs	f_{cm} MPa	f_y MPa	Steel ratio (%)		M_{col} kNm	M_r (kNm)		$\frac{M_{col}}{M_{r(c2+3h)}}$	$\frac{M_{col}}{M_{r(c2+2c1)}}$
			ρ_{c2+3h}	ρ_{c2+2c1}		c_2+3h	c_2+2c_1		
E3	42.7	420	0.92	0.94	29.2	25.10	25.01	1.16	1.17
M/E/2	33.1	496	1.00	1.40	8.4	5.04	7.30	1.66	1.15
ZV-4	35.0	437	1.50	1.30	81.4	81.35	60.00	1.32	1.36
							Average :	1.38	1.23

Two different effective widths are considered, namely c_2+3h, currently recommended by ACI 318-99, and c_2+2c_1, draft proposal of ACI 318-2002. The effective width of c_2+2c_1 is a simple form of the effective width proposed by Regan (1981), Moehle (1988) and Sherif (1996) by assuming the torsion yield line forms an angle 45° from the inner column corners to the slab free edge. A more detailed calculation on the effective width may be taken as $c_2+2c_1 \cot \alpha$, where $\cot \alpha$ can be taken as equation 2.5. However, for the three test results presented in Table 5.3, the $\cot \alpha$ is 1.0 so that the simple form of c_2+2c_1 is considered. From the average M_{col}/M_r, flexural resistance provided by the reinforcement within an effective slab width of c_2+2c_1 is better than that of an effective slab width of c_2+3h. The difference is most obvious for the Stamenkovic's thin slab test result (*M/E/2*).

Measured steel strains during the test of connection E_3 show that the bars within a width c_2+2c_1 yielded when the connection failed in flexure (i.e. SG. e17 and SG. e18 in Figure 4.15a).

5.5 EFFECT OF ECCENTRICITY (M_{col}/V_u) ON SHEAR CAPACITY

Normalized failure shear forces are plotted against load eccentricities in Figure 5.9 to study the effect of load eccentricity on shear capacity of edge column slab connections.

The effect of variation in concrete strength (f_{cm}) and reinforcement ratio (ρ_{ave}) is taken into account by dividing the failure shear force by $(\rho_{ave} f_y f_{cm})^{1/3}$. Where ρ_{ave} is the average of reinforcement ratio ρ_{c2+3h} and $\rho_{c1+1.5h}$, f_{cm} is the measured concrete compressive strength and f_y is the yield strength of the reinforcement.

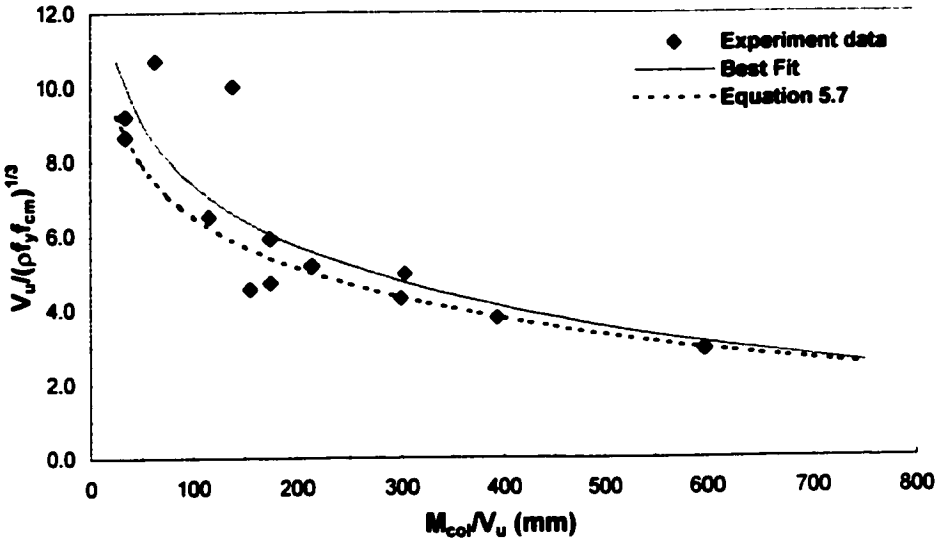

Figure 5.9 Effect of load eccentricity (M_{col}/V_u) on shear capacity of edge column slab connections

The present data shows that shear strength decreases by a logarithmic function with an increase in load eccentricity (e = M_{col}/V_u). Although there is scatter in the data, the relationship between shear force and M/V ratio may be represented by equation 5.7 as shown in Figure 5.9.

$$\frac{V_u}{(\rho f_y f_{cm})^{1/3}} \propto -2.0 Ln\left(1+\frac{M_{col}}{V_u}\right)+15.75 \qquad (5.7)$$

5.6 EFFECT OF STEEL RATIO ON SHEAR STRENGTH

The average of reinforcement ratio (ρ_{ave}) within the area c_2+3h by $c_1+1.5h$ is plotted against $v_{test}/(f_{cm})^{1/2}$ according to ACI 318-99 and CSA A23.3-94 codes in Figure 5.10. The limiting maximum stresses of the ACI and CSA codes are also shown in Figure 5.10. The effect of reinforcement ratio (ρ) on shear strength of the edge column slab connections on the present results is not obvious.

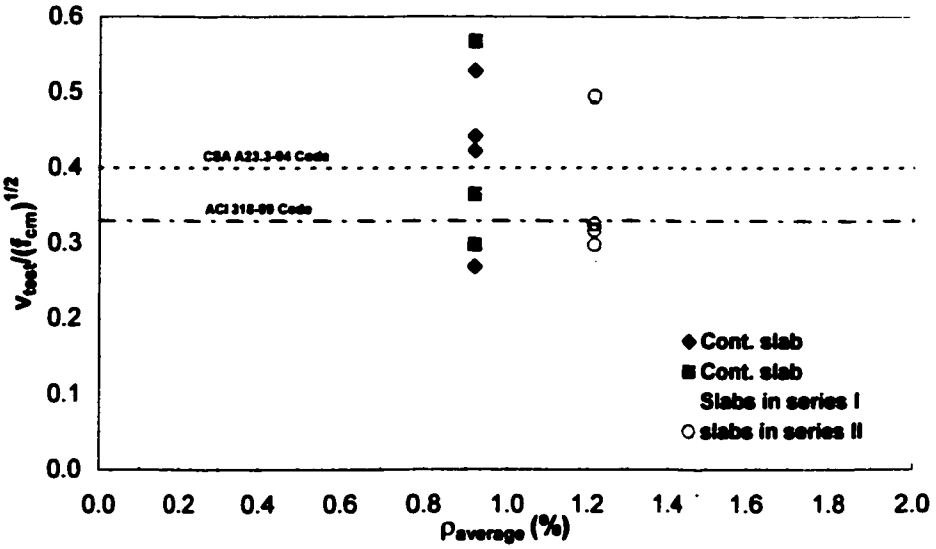

Figure 5.10 Effect of average reinforcement ratio on shear strength according to ACI 318-99 and CSA A23.3-94 codes

5.7 REPAIRED EDGE CONNECTIONS

The behavior of the repaired edge connections was described in Chapter 4. The following discussion covers the effects of repair technique and materials.

5.7.1 Effect of repair technique

Cutting the slab in the vertical position beyond the failure surface give advantages for the strength of the connections compared to just removing the upper parts of the damaged area since large compressive stresses are transferred through the compression zone at the bottom slab column interface.

The electrical hammer jack is a powerful tool to remove the damaged concrete. Less time is needed compared to other techniques (i.e. water pressure) so that less labour costs are required. However, saving on costs in using hammer jacks has to be compensated by the negative effects of creation of micro cracks. Physical observation during the repair process found visible micro cracks on the cut surface and some reinforcement was marked or bent by the hammer jacks.

Direct comparison with other techniques cannot be done since in the present study only a hammer jack was used to remove the damaged concrete. To reduce the negative effects of using a hammer jack, more reshores should be provided to minimize vibration effects on the concrete and also detailed reinforcement drawings should be available during removing the concrete. The size of the hammer jack should be adjusted to slab thickness.

5.7.2 Repair using normal concrete

Connections E_{3R} and E_{4R} were repaired using normal concrete with concrete compression strengths, at the age of testing, of 40.3 MPa and 42.7 MPa, respectively. Load capacity of the repaired connection using normal concrete does not differ significantly from the original connections. The capacity of connection E_{4R} was even higher than the original connection E_4, increasing from 116.7 kN and 14.2 kNm to 120.3 kN and 17.1 kNm for shear force and bending moment, respectively. The results of connection E_{3R} are not comparable to the original connection E_3 since the load and moment applied to the original connection differed from those applied to the repaired connection.

Although normal concrete was used to repair the connections, shrinkage cracks were not visible as good curing was applied to the local repaired area. Therefore, it can be concluded that edge connections repaired using normal concrete can obtain strengths similar to the original connections provided good curing is used.

5.7.3 Repair using CAH expansive concrete

Connections E_{1R} and E_{2R} were repaired using non-shrinkable concrete produced using calcium aluminates hydrate (*CAH*) with compressive strengths at the age of testing $\approx$ 40 MPa for both connections. The existence of superplasticizer in the concrete increases concrete expansion due to more free water available in the concrete. Free water increases the formation of ettringite between aggregate interfaces. It is evident that the load capacity of connection E_{1R} with superplasticizer is lower than that of connection E_{2R} without superplasticizer.

It is believed that confinement is required to increase the capacity of connections repaired using *CAH* concrete. In the present experiment, the top surface of the slab was not restrained; therefore, the repair concrete was free to expand upwards which weakened the interface zone with the aggregates.

The capacity of connection E_{1R} was far below the capacity of the original connection E_1. The results of connection E_{2R} is not comparable to original connection E_2 due to a different applied *M/V* ratio. Comparison between connection E_{2R} and E_1 shows the capacity of connection E_{2R} is still lower than connection E_1.

5.7.4 Stiffness of repaired connections

The stiffnesses of the repaired column connections were less than the original connections. It may due to reinforcement yielding in the original test and micro cracks during repair. The reduction in connection stiffness can be seen from the out-of-plane deflection of the slab around the column. Figure 5.11 and Figure 5.12 show the vertical deflection of the slab on the original test and repaired connection tests. The stiffness does not change significantly in connections repaired using normal concrete (E_{4R}). At low loads before the occurrence of the cracks, the deflection is almost identical. Slight reduction in connection stiffness is apparent after cracks occurred. However, significant change in connection stiffness can be observed for connection E_{1R} as shown in Figure 5.12, where the connection was repaired using CAH expansive concrete. It is

evident that micro cracks occurred in the concrete due lack of restraint to the top surface of the slab during repair.

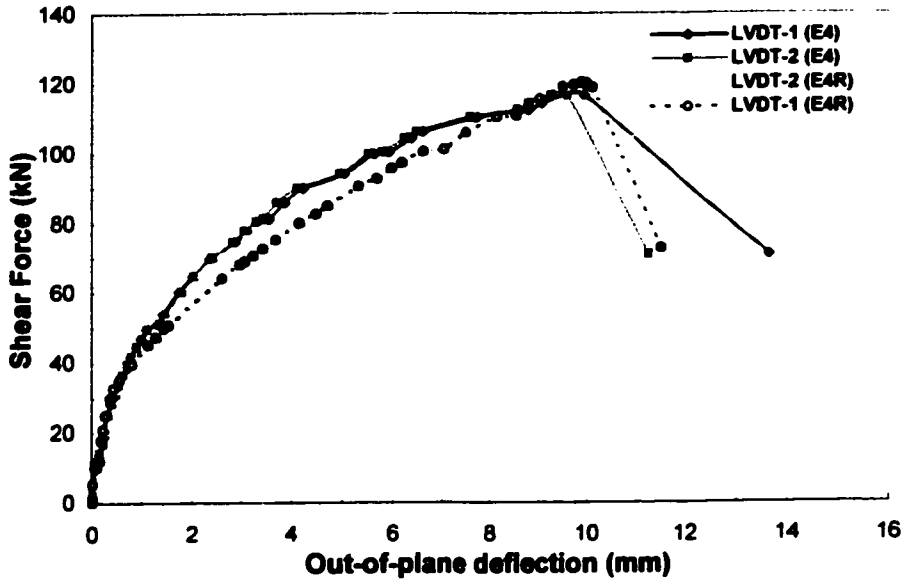

Figure 5.11 Comparison of out-of-plane deflection between original (E_4) and repaired (E_{4R}) test of connection repairing using normal concrete

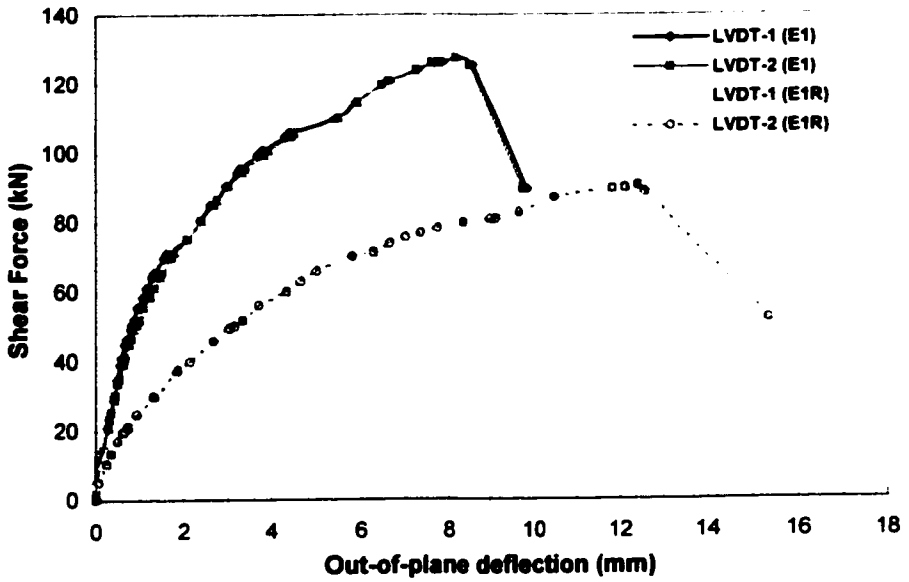

Figure 5.12 Comparison of out-of-plane deflection between original (E_1) and repaired (E_{1R}) test of connection repairing using expansive concrete (CAH)

Table 5.4 Comparison between failure and predicted shear stress according to the American ACI 318-99 and the Canadian CSA A23.3-94 Codes

Slabs	f_{cm}	Test Results				Predicted		Comparison	
	MPa	V_u kN	M_u kNm	M_{ACI} kNm	v_u MPa	v_{aci} MPa	v_{csa} MPa	v_u/v_{aci}	v_u/v_{csa}
E_1	43.6	127.4	34.4	29.2	2.79	2.19	2.64	1.27	1.06
E_2	42.4	220.0	0.0	-9.0	3.45	2.16	2.60	1.60	1.33
E_3	42.7	0.0	29.2	29.2	2.89	2.17	2.61	1.33	1.11
E_4	43.6	116.7	14.2	9.4	1.78	2.19	2.64	0.81	0.67
E_{3R^*}	40.3	230.0	0.0	-9.4	3.60	2.11	2.54	1.71	1.42
E_{3R}	40.3	129.1	23.4	18.1	2.32	2.11	2.54	1.10	0.91
E_{4R}	42.7	120.3	17.1	12.2	1.95	2.17	2.61	0.90	0.75
E_{1-2}	52.8	88.2	49.8	45.7	2.78	2.41	2.91	1.15	0.96
E_{1-3}	55.0	307.0	32.2	17.9	3.65	2.46	2.97	1.49	1.23
E_{1-4}	52.8	114.2	41.1	35.8	2.40	2.41	2.91	1.00	0.82
E_{2-1}	52.8	130.5	34.7	28.6	2.31	2.41	2.91	0.96	0.79
E_{2-2}	52.8	178.9	25.3	17.0	2.36	2.41	2.91	0.98	0.79
E_{2-3}	55.0	328.0	9.3	-5.7	3.67	2.46	2.97	1.49	1.24
E_{2-4}	55.0	199.4	16.4	7.1	2.21	2.46	2.97	0.90	0.74
Average :								1.20	0.99
Standard Deviation :								0.30	0.25
Coefficient of Variation :								0.25	0.25

M_{CSA} is the same as M_{ACI}

M_{CSA} and M_{ACI} are identified as M_s in the code

Table 5.5 Comparison between failure and predicted shear stress according to the British BS 8110-85 Code

Slabs	f_{cm} MPa	Test Results				Predicted	Comparison
		V_u kN	M_u kNm	V_{eff} kN	$v_{u,BS}$ MPa	v_{BS} MPa	v_u/v_{BS}
E_1	43.6	127.4	34.4	159.3	1.22	1.31	0.94
E_2	42.4	220.0	0.0	275.0	1.69	1.30	1.30
E_3	42.7	0.0	29.2	0.0	0.00	1.30	0.00
E_4	43.6	116.7	14.2	145.9	1.12	1.31	0.86
E_{3R^*}	40.3	230.0	0.0	187.5	1.77	1.27	1.39
E_{3R}	40.3	129.1	23.4	161.4	1.24	1.27	0.97
E_{4R}	42.7	120.3	17.1	150.4	1.16	1.30	0.89
E_{1-2}	52.8	88.2	49.8	110.3	0.69	1.62	0.43
E_{1-3}	55.0	307.0	32.2	383.8	2.41	1.64	1.47
E_{1-4}	52.8	114.2	41.1	142.8	0.90	1.62	0.55
E_{2-1}	52.8	130.5	34.7	163.1	1.02	1.55	0.66
E_{2-2}	52.8	178.9	25.3	223.6	1.40	1.55	0.90
E_{2-3}	55.0	328.0	9.3	410.0	2.57	1.57	1.63
E_{2-4}	55.0	199.4	16.4	249.3	1.56	1.57	0.99
						Average :	1.00
						Standard Deviation :	0.36
						Coefficient of Variation :	0.36

Note:

$V_{eff} = 1.25\ V_u$

$v_{u,BS} = V_{eff}/(BS\ perimeter)$ with cube compressive strength, $f_{cu} \approx 1.25\ f_{cm}$

Table 5.6 Comparison between failure and predicted shear stress according to the European CEB-FIP MC90 Method-1 and Method-2

Slabs	f_{cm}	Test Results					Predicted	Comparison	
	MPa	V_u kN	M_u kNm	M_{CEB} kNm	v_{u1} MPa	v_{u2} MPa	v_{ceb} MPa	v_{u1}/v_{ceb}	v_{u2}/v_{ceb}
E_1	43.6	127.4	34.4	16.8	1.58	1.14	1.40	1.13	0.82
E_2	42.4	220.0	0.0	-30.5	0.53	1.97	1.38	0.38	1.42
E_3	42.7	0.0	29.2	29.2	1.07	0.00	1.39	0.77	0.00
E_4	43.6	116.7	14.2	-2.0	0.80	1.04	1.40	0.58	0.75
E_{3R^*}	40.3	230.0	0.0	-9.4	1.38	2.06	1.36	1.02	1.51
E_{3R}	40.3	129.1	23.4	18.1	1.64	1.15	1.36	1.20	0.85
E_{4R}	42.7	120.3	17.1	12.2	1.35	1.08	1.39	0.97	0.78
E_{1-2}	52.8	88.2	49.8	35.9	1.54	0.63	1.49	1.03	0.43
E_{1-3}	55.0	307.0	32.2	-16.3	1.42	2.21	1.51	0.94	1.46
E_{1-4}	52.8	114.2	41.1	23.1	1.34	0.82	1.49	0.90	0.55
E_{2-1}	52.8	130.5	34.7	14.1	1.19	0.94	1.49	0.80	0.63
E_{2-2}	52.8	178.9	25.3	-3.0	1.01	1.29	1.49	0.68	0.86
E_{2-3}	55.0	330.0	7.3	-42.3	0.83	2.36	1.51	0.51	1.57
E_{2-4}	55.0	199.4	16.4	-15.1	0.80	1.43	1.51	0.53	0.95
							Average :	0.82	0.97
							Standard Deviation :	0.25	0.39
							Coefficient of Variation :	0.31	0.40

Note:
v_{u1} = shear stress calculated using CEB-FIP Method-1
v_{u2} = shear stress calculated using CEB-FIP Method-2
M_{CEB} is identified as M_{sd} in the code

Table 5.7 Comparison between failure and predicted shear force and moment according to Regan's approach (1981)

Slabs	f_{cm} MPa	Test Results			Predicted		Comparison	
		V_u kN	M_u kNm	M_{col} kNm	V_p kN	M_p kNm	V_u/V_p	M_{col}/M_p
E_1	43.6	127.4	34.4	38.7	109.1	33.1	1.17	1.17
E_2	42.4	220.0	0.0	7.4	131.1	4.4	1.68	1.68
E_3	42.7	0.0	29.2	29.2	0.0	22.6	1.00	1.29
E_4	43.6	116.7	14.2	18.1	140.2	21.8	0.83	0.83
E_{3R^*}	40.3	230.0	0.0	7.7	163.5	5.5	1.41	1.41
E_{3R}	40.3	129.1	23.4	27.7	126.9	27.3	1.02	1.02
E_{4R}	42.7	120.3	17.1	21.2	135.6	23.8	0.89	0.89
E_{1-2}	52.8	88.2	49.8	52.8	67.9	40.6	1.30	1.30
E_{1-3}	55.0	307.0	32.2	42.5	200.5	27.8	1.53	1.53
E_{1-4}	52.8	114.2	41.1	45.1	115.5	45.4	1.02	0.99
E_{2-1}	52.8	130.5	34.7	39.1	180.4	54.0	0.72	0.72
E_{2-2}	52.8	178.9	25.3	31.3	198.6	34.8	0.90	0.90
E_{2-3}	55.0	328.0	9.6	20.6	210.8	13.3	1.56	1.55
E_{2-4}	55.0	199.4	16.4	23.1	211.5	24.5	0.94	0.94
						Average :	1.15	1.15
						Standard Deviation :	0.30	0.30
						Coefficient of Variation :	0.26	0.26

Table 5.8 Comparison between failure and predicted shear forces and moments according to the Truss Model (1987)

Slabs	f_{cm} MPa	Test Results			Predicted		Comparison	
		V_u kN	M_u kNm	M_{col} kNm	V_p kN	M_p kNm	V_u/V_p	M_{col}/M_p
E_1	43.6	127.4	34.4	38.7	107.0	32.5	1.19	1.19
E_2	42.4	220.0	0.0	7.4	195.8	6.7	1.12	1.10
E_3	42.7	0.0	29.2	29.2	0.0	30.9	1.00	0.94
E_4	43.6	116.7	14.2	18.1	176.8	27.4	0.66	0.66
E_{3R^*}	40.3	230.0	0.0	7.7	193.4	6.6	1.19	1.17
E_{3R}	40.3	129.1	23.4	27.7	141.6	31.0	0.91	0.89
E_{4R}	42.7	120.3	17.1	21.2	163.5	28.8	0.74	0.73
E_{1-2}	52.8	88.2	49.8	52.8	104.8	62.7	0.84	0.84
E_{1-3}	55.0	307.0	32.2	42.5	209.6	28.9	1.47	1.47
E_{1-4}	52.8	114.2	41.1	45.1	151.6	59.6	0.78	0.76
E_{2-1}	52.8	130.5	34.7	39.1	128.1	38.3	1.02	1.02
E_{2-2}	52.8	178.9	25.3	31.3	162.6	28.45	1.10	1.10
E_{2-3}	55.0	328.0	9.6	20.6	212.4	13.4	1.54	1.54
E_{2-4}	55.0	199.4	16.4	23.1	211.2	24.5	0.94	0.94
Average :							1.04	1.03
Standard Deviation :							0.26	0.26
Coefficient of Variation :							0.25	0.25

Table 5.9 Comparison between failure and predicted shear force and moment according to the Strip Model (1998)

Slabs	f_{cm} MPa	Test Results			Predicted		Comparison	
		V_u kN	M_u kNm	M_{col} kNm	V_p kN	M_p kNm	V_u/V_p	M_{col}/M_p
E_1	43.6	127.4	34.4	38.7	107.3	32.6	1.19	1.19
E_2	42.4	220.0	0.0	7.4	131.5	4.4	1.67	1.68
E_3	42.7	0.0	29.2	29.2	0.0	23.6	1.00	1.24
E_4	43.6	116.7	14.2	18.1	127.5	19.8	0.92	0.91
E_{3R^*}	40.3	230.0	0.0	7.7	129.7	4.3	1.77	1.77
E_{3R}	40.3	129.1	23.4	27.7	116.6	25.0	1.11	1.11
E_{4R}	42.7	120.3	17.1	21.2	123.7	21.7	0.97	0.98
E_{1-2}	52.8	88.2	49.8	52.8	70.6	42.3	1.25	1.25
E_{1-3}	55.0	307.0	32.2	42.5	187.4	25.9	1.64	1.64
E_{1-4}	52.8	114.2	41.1	45.1	125.5	47.9	0.94	0.94
E_{2-1}	52.8	130.5	34.7	39.1	125.5	37.6	1.04	1.04
E_{2-2}	52.8	178.9	25.3	31.3	157.0	27.5	1.14	1.14
E_{2-3}	55.0	328.0	9.6	20.6	191.9	12.0	1.71	1.71
E_{2-4}	55.0	199.4	16.4	23.1	179.7	20.8	1.11	1.11
						Average :	1.25	1.26
						Standard Deviation :	0.31	0.30
						Coefficient of Variation :	0.25	0.24

Table 5.10 Comparison between failure and predicted shear stress according to the Sherif's approach (1995)

Slabs	f_{cm}	Test Results						Pred.	Comp.
	MPa	V_u kN	M_u kNm	M_s kNm	M_{flex} kNm	γ_v	v_u MPa	v_{shf} MPa	v_u/v_{shf}
E_1	43.6	127.4	34.4	29.2	15.66	0.46	3.09	2.40	1.29
E_2	42.4	220.0	0.0	-9.0	15.66	0.00	2.56	23.7	1.08
E_3	42.7	0.0	29.2	29.2	15.66	0.46	3.55	2.38	1.49
E_4	43.6	116.7	14.2	9.4	15.66	0.00	1.36	2.40	0.57
E_{3R^*}	40.3	230.0	0.0	-9.4	15.66	0.00	2.67	2.33	1.15
E_{3R}	40.3	129.1	23.4	18.1	15.66	0.14	1.80	2.33	0.79
E_{4R}	42.7	120.3	17.1	12.2	15.66	0.00	1.40	2.38	0.59
E_{1-2}	52.8	88.2	49.8	45.7	30.12	0.34	2.44	2.80	0.87
E_{1-3}	55.0	307.0	32.2	17.9	30.12	0.00	3.01	2.83	1.06
E_{1-4}	52.8	114.2	41.1	35.8	30.12	0.16	1.66	2.80	0.59
E_{2-1}	52.8	130.5	34.7	28.6	23.47	0.18	1.77	2.80	0.63
E_{2-2}	52.8	178.9	25.3	17.0	23.47	0.00	1.76	2.80	0.63
E_{2-3}	55.0	328.0	9.6	-5.7	23.47	0.00	3.22	2.84	1.13
E_{2-4}	55.0	199.4	16.4	7.1	23.47	0.00	1.96	2.84	0.69
								Average :	0.90
								Standard Deviation :	0.30
								Coefficient of Variation :	0.34

Table 5.11 Comparison between failure and predicted shear stress according to the Gardner's approach (1996)

Slabs	f_{cm}	Test Results					Pred.	Comparison	
	MPa	V_u kN	M_u kNm	V_{eff} kN	v_{u1} MPa	v_{u2} MPa	v_{gdr} MPa	v_{u1}/v_{gdr}	v_{u2}/v_{gdr}
E_1	43.6	127.4	34.4	191.1	4.80	2.99	3.57	1.35	0.84
E_2	42.4	220.0	0.0	330.0	3.44	5.16	3.54	0.97	1.69
E_3	42.7	0.0	29.2	0.0	4.76	0.00	3.54	1.34	0.00
E_4	43.6	116.7	14.2	175.1	2.98	2.74	3.57	0.84	0.77
E_{3R^*}	40.3	230.0	0.0	345.0	3.60	5.40	3.48	1.03	1.55
E_{3R}	40.3	129.1	23.4	193.7	3.93	3.03	3.48	1.13	0.87
E_{4R}	42.7	120.3	17.1	180.5	3.28	2.82	3.54	0.92	0.80
E_{1-2}	52.8	88.2	49.8	132.3	5.65	1.81	4.12	1.37	0.44
E_{1-3}	55.0	307.0	32.2	460.5	6.42	6.30	4.17	1.54	1.51
E_{1-4}	52.8	114.2	41.1	171.3	4.39	2.34	4.12	1.07	0.57
E_{2-1}	52.8	130.5	34.7	195.8	4.18	2.68	4.12	1.01	0.65
E_{2-2}	52.8	178.9	25.3	268.4	4.19	3.67	4.12	1.02	0.89
E_{2-3}	55.0	328.0	9.6	492.0	5.02	6.77	4.17	1.20	1.62
E_{2-4}	55.0	199.4	16.4	299.1	3.86	4.09	4.17	0.92	0.98
							Average :	1.12	1.00
							Standard Deviation :	0.21	0.40
							Coefficient of Variation :	0.18	0.40

Note:

v_{u1} = calculated stress according to linear shear stress distribution with critical section taken as the column perimeter

v_{u2} = calculated stress based on a single multiplier on shear stress ($V_{eff}=1.5\ V_u$)

Table 5.12 Comparison between failure and predicted shear stress according to the Elgabry and Ghali's approach (1995)

Slabs	f_{cm} MPa	Test Results				Predicted	Comparison
		V_u kN	M_u kNm	M_s kNm	v_u MPa	v_{elg} MPa	v_u/v_{elg}
E_1	43.6	127.4	34.4	29.2	2.78	2.19	1.27
E_2	42.4	220.0	0.0	-9.0	3.44	2.16	1.59
E_3	42.7	0.0	29.2	29.2	2.86	2.17	1.32
E_4	43.6	116.7	14.2	9.4	1.78	2.19	0.81
E_{3R^*}	40.3	230.0	0.0	-9.4	3.59	2.11	1.70
E_{3R}	40.3	129.1	23.4	18.1	2.31	2.11	1.09
E_{4R}	42.7	120.3	17.1	12.2	1.94	2.17	0.89
E_{1-2}	52.8	88.2	49.8	45.7	2.79	2.41	1.16
E_{1-3}	55.0	307.0	32.2	17.9	3.66	2.46	1.49
E_{1-4}	52.8	114.2	41.1	35.8	2.41	2.41	1.00
E_{2-1}	52.8	130.5	34.7	28.6	2.31	2.41	0.96
E_{2-2}	52.8	178.9	25.3	17.0	2.37	2.41	0.98
E_{2-3}	55.0	328.0	9.3	-5.7	3.67	2.46	1.49
E_{2-4}	55.0	199.4	16.4	7.1	2.21	2.46	0.90
						Average :	1.19
						Standard Deviation :	0.29
						Coefficient of Variation :	0.24

CHAPTER 6

DISCUSSION ON CORNER CONNECTIONS

6.1 GENERAL

Test results presented in Chapter 4 for corner column slab connections are discussed in this chapter. The discussion is divided into the following categories:

- Interaction between shear and moment
- Load capacity of the tests calculated using the proposed methods and the codes predictions
- Effect of the steel ratio (ρ) on the ultimate shear stress

6.2 INTERACTION BETWEEN SHEAR FORCE AND MOMENT

6.2.1 Building code provisions

Shear moment interactions of the building codes (ACI 318-99, CSA A23.3-94 and CEB-FIP MC90) are developed based on the shear stress distributions assumed by the codes for corner column slab connections. V_u/V_o is plotted against M_{code}/M_o for non-dimensional interactions as was done for the edge column slab connections. M_{code} is the applied moment at the centroid of critical shear section of the codes. V_o and M_o are the shear force and moment at the centroid of the assumed critical shear section in the absence of moment and shear force, respectively. The interaction diagrams presented here apply only to corner connections having square column dimensions and subjected to combined shear force and diagonal bending moment.

6.2.1.1 The American ACI 318-99 code

The ACI 318-99 interaction diagram is calculated according to equations 2.50 to 2.52 where shear stress distribution along the critical shear section is assumed to be

linear. For the case of the corner connections in the present study with square column sections and subjected to combined shear force and diagonal bending moment, equations 2.50 to 2.52 can be simplified to the equations 6.1 and 6.2.

$$v_B = \frac{V_u}{A_c} + \frac{\gamma_v M_{ACI} e_B}{J_c} \tag{6.1}$$

$$v_A = v_D = \frac{V_u}{A_c} - \frac{\gamma_v M_{ACI} e_A}{J_c} \tag{6.2}$$

Where e_B and e_A or e_D are distance of point B and A or D from the moment axis through the centroid of critical shear section as shown in Figure 2.23. M_{ACI}, designated as M_s in the code, is the applied moment at the centroid of critical shear section. Other variables were defined in Chapter 2.

For corner connections of the present study, it is found that e_B=-e_A or -e_D; therefore, the magnitude of V_o and M_o at the centroid critical shear section can be calculated as:

$$V_o = v_{max} b_o d \tag{6.3}$$

$$M_o = \frac{v_{max} J_c}{\gamma_v e_A} \tag{6.4}$$

Where, the maximum shear stress is given $v_{max} = 0.333\sqrt{f_c'}$. By applying all of the parameters, it is found that the interaction diagram is linear which is similar to that of interior column connections. Three test results of corner connections are also plotted on the same diagram as shown in Figure 6.1. The ACI 318-99 code underestimates all of test results.

Diagonal flexural capacity of corner connections provided by the average of the reinforcement ratio in two directions within a width of $c+1.5h$ is presented as Line-2 on the interaction diagram. As in the edge connections, if there is not sufficient flexural reinforcement in the connections, the interaction will follow Line-1 and then continued to Line-2.

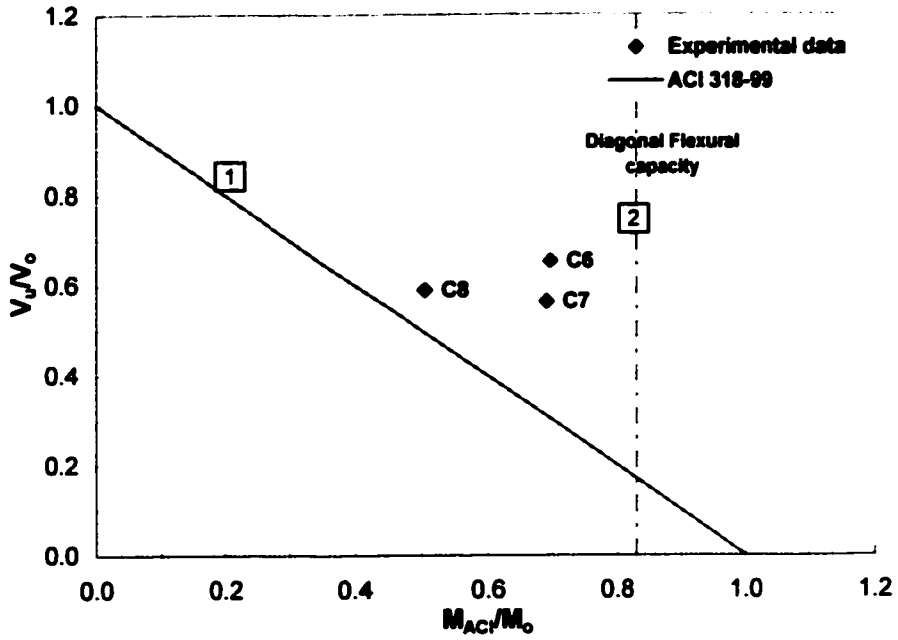

Figure 6.1 Shear moment interaction of corner column connections according to ACI 318-99 Code

6.2.1.2 The Canadian CSA A23.3-94 code

The Canadian CSA A23.3-94 code uses the same assumption as the ACI 318-99 code for the corner connections. Degree of interaction between shear force and moment predicted by the CSA A23.3-94 is better than the ACI 318-99 code as shown in Figure 6.2. The only reason for this is the increase in the specified maximum stress by 21% from $v_{max} = 0.333\sqrt{f_{cm}}$ of the ACI code to $v_{max} = 0.4\sqrt{f_{cm}}$ of the CSA code.

The CSA A23.3-94 also recommends checking the one-way shear capacity of the corner connections. The specified one-way shear strength of the code is presented by Line-2 in Figure 6.2. The one-way shear strength specified by the CSA A23.3 code overestimates the capacity of the corner connections. This is due to shear strength being constant regardless of moment in the calculations.

Diagonal flexural resistance provided by the reinforcement ratio in two directions within a width of $c+1.5h$ is also presented. It shows that all connections failed before reaching the flexural capacity.

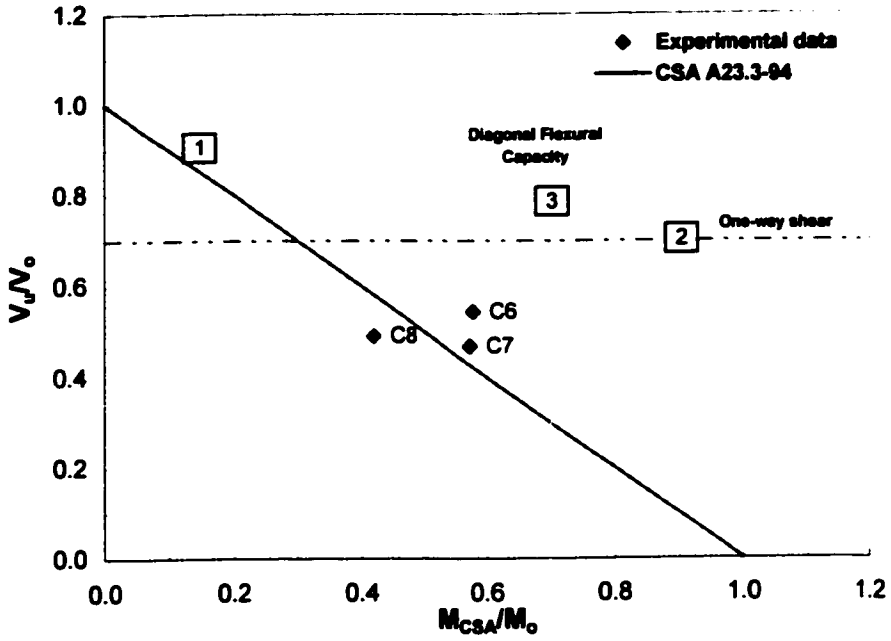

Figure 6.2 Shear moment interaction of corner column connections according to CSA A23.3-94 Code

6.2.1.3 The European CEB-FIP MC90

Interaction diagram of CEB-FIP MC90 is based on equation 2.63 using the full length of the critical shear perimeter. The ratio of V_u/V_o is plotted against the ratio of M_{CEB}/M_o. M_{CEB} is the unbalanced moment at centroid of critical shear section, designated as M_{sd} in the CEB-FIP MC90. V_o and M_o are the shear force and moment at centroid of critical shear section when the absence of moment and shear force, respectively. V_o and M_o can be calculated as:

$$V_o = v_{max} b_o d \tag{6.5}$$

$$M_o = \frac{v_{max} w_1 d}{K} \tag{6.6}$$

A linear interaction is obtained as shown in Figure 6.3. The CEB-FIP MC90 is too conservative for all three tests of corner connections as shown in Figure 6.3. Diagonal flexural capacity of the corner connections is obtained as in the ACI and the CSA codes. The flexural capacity provided by the reinforcement in one direction is calculated within the effective width of *c+3d* as indicated by Line-2 in Figure 6.3. All corner connections failed significantly below the flexural resistance of the CEB-FIP MC90.

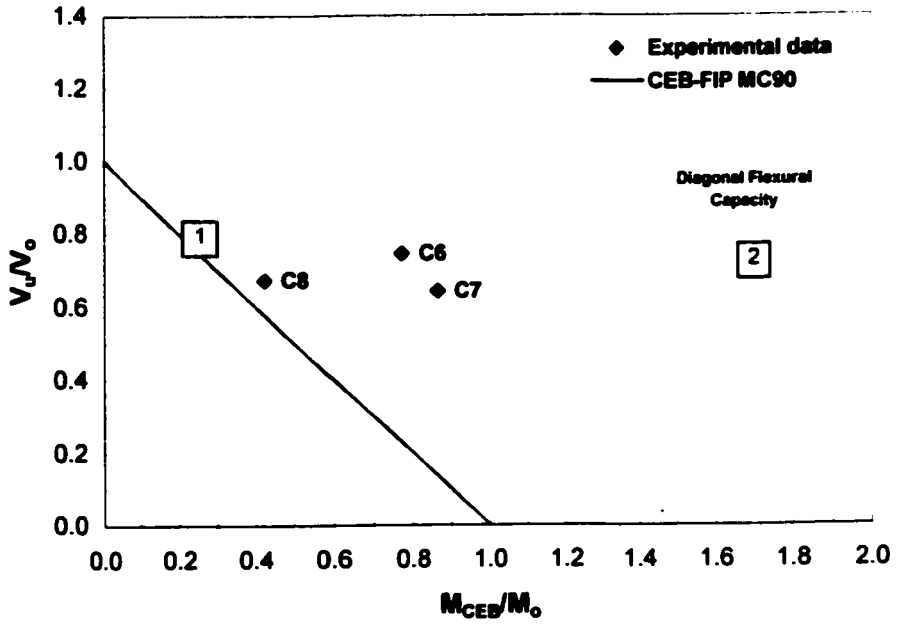

Figure 6.3 Shear moment interaction of corner column connections according to CEB-FIP 1990 Model Code

6.2.2 Alternative approach

Regan's approach is one of the alternative approaches considered in the discussion of the interaction diagrams to predict the capacity of the corner column connections subjected to combined shear force and biaxial bending moment. Regan's approach for corner column connections is similar to that for edge column slab connections. The interaction diagram is based on discrete point interactions connected by straight lines as shown in Figure 6.4.

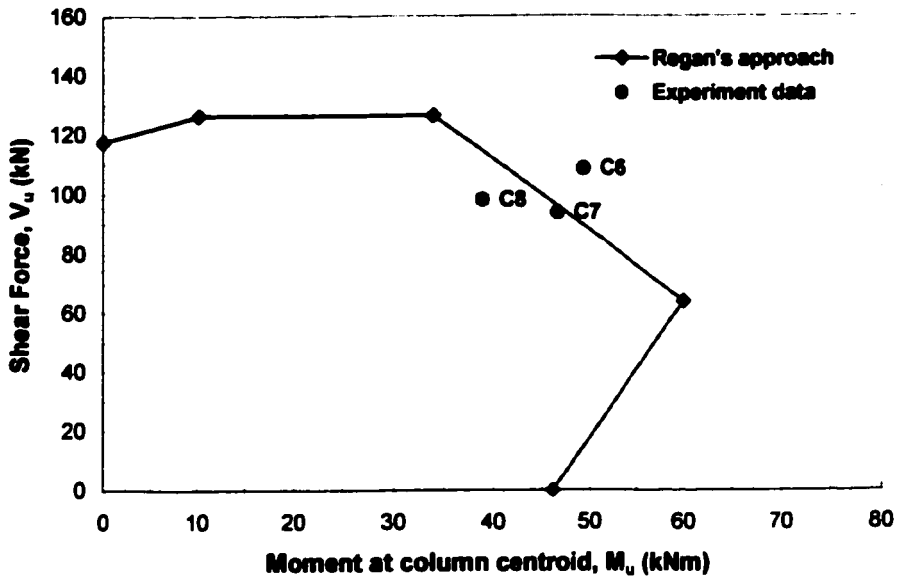

Figure 6.4 Shear-moment interaction of corner column slab connections according to Regan's approach (1981)

The limiting failure surface from which the interaction diagram is developed, is shown in Figure 2.20. It is shown in Figure 6.4 that the interaction between shear and diagonal moment are in good agreement with the three test results.

6.3 COMPARISON OF LOAD CAPACITY

6.3.1 Building code provisions

Shear capacity of corner column slab connections is calculated using the code expressions as was done for the edge column slab connections. The shear stresses are calculated at the assumed critical shear section that varies from one code to the others. To calculate the shear stresses, the measured compressive strength of concrete (f_{cm}) is used rather than the specified strengths (f_{ck}). Connection C_5 is not included in the discussion, as the result of this test may not represent the capacity of the connection. Table 6.1 summarizes the shear strengths of corner connections calculated according to ACI 318-99, CSA A23.3-94, BS8110-85 and CEP-FIP MC90 Codes. The CSA recommendation to check one-way shear strength is also included in Table 6.1.

The ACI 318-99 Codes is conservative for all three connections. Specified shear strength of the code is governed by the maximum shear stress of 2.21 MPa or $0.333\sqrt{f_{cm}}$ $\approx 0.372\sqrt{f_{ck}}$. For all test results, the maximum shear stress occurs at inner corner of the assumed critical shear section as shown in Figure 2.23. The ratios v_{test}/v_{pred} range from 1.10 to 1.35 and the average is 1.23 with coefficient of variation (COV) of 0.10.

Table 6.1 Comparison between failure and predicted shear stress of corner connections according to the code provisions

Method	Slabs	f_{cm} MPa	V_u kN	M_u kNm	Test v_{test} MPa	Predicted v_{pred} MPa	v_{test}/v_{pred}	Avg.	COV
ACI (1999)	C6	44.4	108.6	49.3	2.99	2.21	1.35	1.23	0.10
	C7	44.4	93.7	46.6	2.78	2.21	1.26		
	C8	44.4	98.1	38.9	2.42	2.21	1.10		
CSA (1994) (Two-way shear)	C6	44.4	108.6	49.3	2.99	2.67	1.12	1.02	0.10
	C7	44.4	93.7	46.6	2.78	2.67	1.04		
	C8	44.4	98.1	38.9	2.42	2.67	0.91		
CSA (1994) (One- way shear)	C6	44.4	108.6	49.3	1.07	1.33	0.80	0.74	0.08
	C7	44.4	93.7	46.6	0.92	1.33	0.69		
	C8	44.4	98.1	38.9	0.97	1.33	0.72		
BS (1985)	C6	44.4	108.6	49.3	1.40	1.45	0.96	0.89	0.08
	C7	44.4	93.7	46.6	1.21	1.45	0.83		
	C8	44.4	98.1	38.9	1.26	1.45	0.87		
CEB-FIP (1990) Method-1	C6	44.4	108.6	49.3	2.24	1.48	1.52	1.37	0.18
	C7	44.4	93.7	46.6	2.23	1.48	1.51		
	C8	44.4	98.1	38.9	1.62	1.48	1.10		
CEB-FIP (1990) Method-2	C6	44.4	108.6	49.3	1.63	1.48	1.10	1.02	0.08
	C7	44.4	93.7	46.6	1.41	1.48	0.95		
	C8	44.4	98.1	38.9	1.47	1.48	1.00		

The Canadian CSA A23.3-94 prediction, using the same assumptions for the critical shear perimeter as the ACI 318-99 Code, results in better agreement with the test data than ACI 318-99 code. This is because the governing maximum shear resistance specified by the Canadian CSA A23.3-94 code is *21%* higher than that of the ACI 318-99 Code when all reduction factors are set to unity. The limiting maximum shear stress allowed by the CSA A23.3 is $0.4\sqrt{f_{cm}}$ ($\approx 0.447\sqrt{f_{ck}}$ MPa). The ratios of v_{test}/v_{pred} range from 0.91 to 1.12 MPa and the average is 1.03 with COV of 0.10.

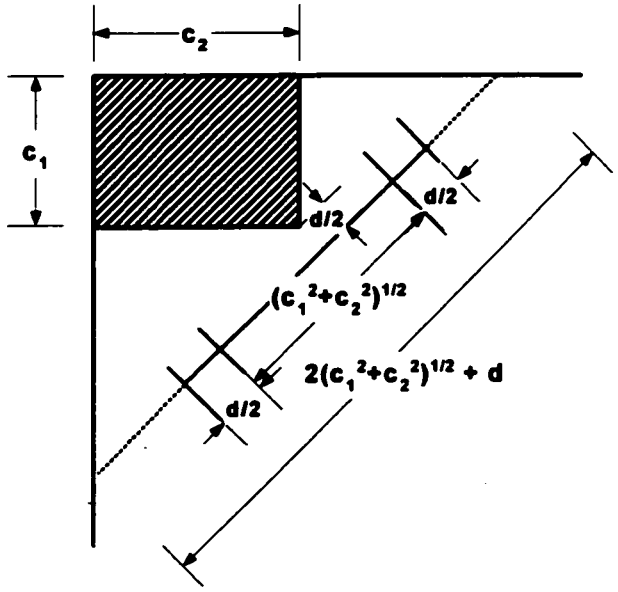

Figure 6.5 Definition of one-way shear perimeters for corner column slab connections

Clause 13.4.6.2 of CSA A23.3-94 stated that the factored shear resistance of corner column slab connections should be determined along a straight line of a critical shear section located at *d/2* from the inner corner column as shown in Figure 6.5. The shear stress considered in this case is one-way shear, which is specified by the code as $v_c = 0.2\lambda\phi_c\sqrt{f_{cm}}$. To compare the failure shear stress with the code predictions, all reduction factors are set to unity as done for two-way shear. It is found that failure stresses calculated based on one-way shear at the corner column slab connections are less than the code values for three test results of the present study as shown in Table 6.1. The average of v_{test}/v_{pred} is 0.74 with coefficient of variation of 0.08. From Figure 6.5, it

appears that the width of the shear perimeter considered for calculating one-way shear is too large. A better definition of the width of the shear perimeter for one-way shear would be $(\sqrt{c_1^2 + c_2^2} + d)$. Using the latter width, the average of v_{test}/v_{pred} is 1.34 with coefficient of variation of 0.08.

The British BS8110-85 Code overestimates all connections (C_6, C_7 and C_8). The shear resistance specified by the code based on cube compressive strength (f_{cu}) is 1.45 MPa. The limit on cube compressive strengths of 40 MPa specified in code expression is ignored. The ratios v_{test}/v_{pred} range from 0.83 to 0.96 and the average is 0.89 with COV of 0.08. Multiplying shear force with a constant of 1.25 to account for the effect of unbalanced moment on the corner connection may not be appropriate since the constant of 1.25 should be applied only to corner connections subjected to uniform gravity load.

The European CEB-FIP MC90 recommends two methods that can be used to calculate the shear strength along an assumed shear perimeter of corner connections from the known shear force (V_u) and Moment (M_u). Method-1 uses a full length of the assumed perimeter at *2d* from the column faces and Method-2 assumes uniform shear distribution due to direct shear force only on the reduced shear perimeter length to account for the effect of unbalanced moment. The lengths of the critical shear perimeter for these two methods are shown in Figure 2.25. The maximum shear resistance allowed by CEB-FIP MC90 is 1.48 MPa. Method-1 of CEB-FIP MC90 is too conservative for all test results. The ratios v_{test}/v_{pred} range from 1.10 to 1.52 and the average is 1.37 with COV of 0.18. This is due to the high shear stress contributed by the unbalanced moment (K=0.6). Method-2 of the CEB-FIP MC90 is in good agreement with the test results even though the unbalanced moment is neglected. In Method-2, the ratios v_{test}/v_{pred} range from 0.95 to 1.10 and the average is 1.02 as shown in Table 6.1.

6.3.2 Alternative approaches

Five alternative approaches available in the literature to predict shear strength of corner connections are considered here. The experimental shear capacity of corner connections is compared with the predicted shear strengths. Table 6.2 shows the

comparison between the experimental and the predicted shear forces using the approaches considered here. Detail discussions on the load capacity of corner connections predicted by Ingvarsson's, Zaghlool's, Regan's, Gardner's and Desayi's approaches, on the test results of the present study are presented next.

Table 6.2 Comparison between failure and predicted shear capacity of corner connections according to the proposed approach in the literature

Method	Slabs	f_{cm} MPa	Test			V_{pred} MPa	V_{test}/V_{pred}	Avg.	COV
			V_u kN	M_u kNm	V_{test} kN				
Ingvarson (1977)	C6	44.4	108.6	49.3	108.6	236.5	0.46	0.43	0.08
	C7	44.4	93.7	46.6	93.7	236.5	0.40		
	C8	44.4	98.1	38.9	98.1	236.5	0.42		
Regan (1981)	C6	44.4	108.6	49.3	108.6	99.5	1.09	1.00	0.09
	C7	44.4	93.7	46.6	93.7	94.7	0.99		
	C8	44.4	98.1	38.9	98.1	106.5	0.92		
Zaghlool (1973)	C6	44.4	108.6	49.3	108.6	92.6	1.17	1.06	0.17
	C7	44.4	93.7	46.6	93.7	81.1	1.16		
	C8	44.4	98.1	38.9	98.1	114.0	0.86		
Gardner Method-1 (1996)	C6	44.4	108.6	49.3	268.4	196.5	1.37	1.25	0.10
	C7	44.4	93.7	46.6	248.8	196.5	1.27		
	C8	44.4	98.1	38.9	218.5	196.5	1.11		
Gardner Method-2 (1996)	C6	44.4	108.6	49.3	217.2	196.5	1.11	1.02	0.08
	C7	44.4	93.7	46.6	187.4	196.5	0.95		
	C8	44.4	98.1	38.9	196.2	196.5	1.00		
Desayi & Shesadri (1997)	C6	44.4	108.6	49.3	108.6	91.0	1.19	1.09	0.08
	C7	44.4	93.7	46.6	93.7	86.6	1.08		
	C8	44.4	98.1	38.9	98.1	97.5	1.01		

6.3.2.1 Ingvarsson's approach (1977)

Ingvarsson's approach based on the work on beam is similar to the one-way shear recommended by the CSA A23.3-94 with the critical section taken at *h/2* instead of *d/2* from the inner corner of the column. The predicted shear strength of corner connections is calculated using equation 2.40. Ingvarsson's approach overestimates all three test results of the present study with the average ratio V_{test}/V_{pred} of 0.43 and coefficient of variation of 0.08. The high-applied moment on the corner connections reduced the shear force capacity, therefore, one-way shear approach as in Ingvarsson's approach and CSA A23.3-94 results in unsafe prediction on the shear strength of corner connections.

Ingvarsson's approach considered large contribution of bottom reinforcement in predicting the shear capacity of the corner connections. However, research by Elstner and Hognestad (1956) showed that the effect of bottom reinforcement on shear strength is negligible.

6.3.2.2 Zaghlool's approach (1973)

Zaghlool's approach (1973) was developed based on an idealized failure surface observed during the test of the connections. Iterations are required to calculate the shear strength of corner column slab connections based on equilibrium and compatibility equations. The approach is conservative for corner connections C_6 and C_7; however, it overestimates the capacity of corner connection C_8. The average ratio V_{test}/V_{pred} for these three connections is 1.06 with coefficient of variation of 0.17.

6.3.2.3 Regan's approach (1981)

Shear capacity of corner connections is obtained from the complete shear-moment interaction diagram developed previously as shown in Figure 6.4. The applied load eccentricity is projected to the line of the interaction diagram to calculate the predicted shear strengths. The average ratio V_{test}/V_{pred} of 1.0 with coefficient of variation of 0.09 shows that Regan's approach predicts well the strength of corner connections, although two connections (C_7 and C_8) are slightly overestimated. Regan's assumption on the angle of inclined failure surface at 22.5° seems to be the cause of overestimation of test results

since experimental results of connections C_6 to C_8 show that the inclined angle of failure surface ranged from 25° to 26.6°.

6.3.2.4 Gardner's approach (1996)

The two methods (Method-1 and Method-2) recommended by Gardner (1996) for calculating shear strength of edge slab column connections are used to predict the shear strength of corner connections. The predicted shear strength is calculated using Equation 2.17.

Gardner's Method-1 is conservative for all three test results with the average ratio of V_{test}/V_{pred} of 1.25 and the COV of 0.1 as can be seen in Table 6.2. However, using a single factor of 2.0 to increase the shear force at corner connections to account for the effect of ignoring unbalanced moment on the connections as recommended by Gardner's Method-2 gives predictions for shear strength of the three corner connections with an average ratio V_{test}/V_{pred} of 1.02 and the COV of 0.08. However, using a single multiplier to account for the effect of unbalanced moments should not be used for the slab loaded other than uniformly distributed loads.

6.3.2.5 Desayi and Sheshadri's approach (1997)

Desayi and Sheshadri's approach (1997) is a modification of the Bond Model by Alexander and Simmonds (1991). Shear stress due to torsion is taken as $0.257\sqrt{f_c'}$ and the effect of load eccentricity is taken into account by expression $(1+k_2e_x)$, where e_x is the applied load eccentricity perpendicular to the moment axis and k_2 is a constant determined from experimental results and equal to unity. The approach is conservative for all corner connections (C_6, C_7 and C_8) as indicated by the average ratio V_{test}/V_{pred} of 1.09 with coefficient of variation of 0.08. It should be noted that shear force obtained using Desayi and Sheshadri's approach is the algebraic sum of ultimate capacity of all strips of a width of 0.875d framing to the column faces. A study by Afhami, Alexander and Simmonds (1998) found that it is possible the loads exceeded the capacity of one strip whilst on the other strips are below the load capacity of those strips.

Observation of the failure surface during the test of corner connections in the present study indicated all strips reached their ultimate capacity. Diagonal moment applied to the connection results in the same component acting on both strips. Therefore, the ultimate capacity of both strips would be reached at the same time. However, it may not the case when the moment acts about an axis parallel to one strip or the column dimension is not square.

6.4 EFFECT OF STEEL RATIO ON SHEAR STRENGTH

Normalized shear strength calculated based on linear stress distribution of the ACI 318-99 and the CSA A23.3-94 are plotted against the average of reinforcement ratio in both directions within an effective width of $c+3h$.

The three corner connection results are plotted in Figure 6.6 together with the ACI and CSA limiting maximum stresses, so that a general conclusion may not be well defined. For all three tests, the ACI 318-99 is conservative, giving a lower bound of the results. However, the CSA A23.3-94 with an increase in the maximum shear stress by 21% of the ACI code shows good agreement with the test results.

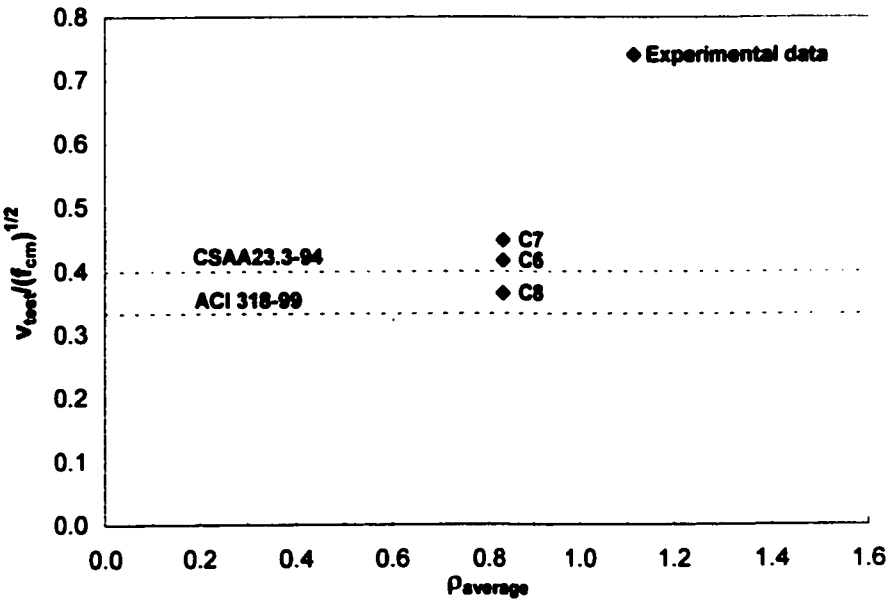

Figure 6.6 Effect of steel ratio on strength of corner column slab connections according to the ACI 318-99 and the CSA A23.3-94

CHAPTER 7
SUMMARY AND CONCLUSIONS

7.1 GENERAL

Flat-plate structures are susceptible to punching shear failure around the column slab connections. Information on punching failure of edge and corner column slab connections is rather limited in the literature. This chapter gives a summary of the present study on the punching shear behavior of edge and corner column slab connections of flat plate structures and the conclusions drawn.

7.2 SUMMARY

The four edge column slab connections of a two bay by two bay flat plate structure and eight isolated edge column slab connections were constructed and tested to failure. After the tests of the four edge connections, the four edge column slab connections of the continuous slab were repaired using two different types of concrete (normal concrete and CAH expansive concrete) and tested to failure. The four corner column slab connections of the continuous slab were tested to failure after tests of the repaired edge connections were completed. Detailed descriptions of the experimental work are given in Chapter 3 of this thesis.

The behaviors of the edge and corner column slab connections and the repaired edge connections are described in Chapter 4. Detailed descriptions of crack development, steel strains, out-of-plane slab deflections and column rotations during the tests of the connections are presented. The failure loads of the edge connections (M_u and V_u), measured at the centroid of column perimeter, and modes of failure are given in Tables 4.1 and 4.2. For corner column slab connections, the failure loads (M_u and V_u), measured at the column centroid, and modes of failure are given in Table 4.3.

Interaction between shear force and unbalanced moment at edge slab connections predicted by the building code provisions of ACI 318-99, CSA A23.3-94, BS8110-85 and CEB-FIP MC90 and the Regan's approach, the Truss Model and the Strip Model, which differ fundamentally from the building codes, were examined using the present experimental data. The shear strengths of edge connections were calculated using the code provisions and six alternative approaches available in the literature (i.e. Regan, the Truss Model, the Strip Model, Sherif, Gardner and Elgabry). The calculated shear strengths were compared to the measured failure strengths. The validity of the building codes and the alternative approaches with the test data were examined using the average, standard deviation (STD) and coefficient of variation (COV) of the ratio of measured to calculated strengths.

For the corner connections, the interactions between shear force and moments developed using the building code provisions of ACI 318-99, CSA A23-94, CEP-FIP MC90 and Regan's approach, were examined. The predicted strengths calculated using the building code provisions and Ingvarsson's, Regan's, Zaghlool's, Gardner's and Desayi's approaches were compared to the failure strength of the connections.

The effects of load eccentricity (M_u/V_u) and reinforcement ratio on the shear strength of edge connections were investigated. The effective slab width of edge slab connections resisting flexure are examined based on two effective slab widths recommended in the literature namely c_2+3h and c_2+2c_1. The strength and stiffness of the repaired edge connections were also investigated.

7.3 CONCLUSIONS

The following conclusions may be drawn after analysis of the test data. The conclusions are divided into two parts, those related to experimental work and those concerning prediction methods.

7.3.1 Conclusions related to experimental work

1. Test set-up is crucial in experimental work since the behavior, and strength, of column slab connections depend on the boundary conditions of the specimens.

2. Punching shear of column slab connections is a shear-flexure phenomenon with, in most cases, yielding of the reinforcement preceding punching failure.

3. Only the rebars passing through the column yielded upon the failure of the connections.

4. Punching shear failure occurred when the concrete in the compression zone failed by concrete crushing.

5. When the side spans of edge column slab connections developed large torsion, indicated by large torsion cracks, the inclined failure shear surface did not interact with the torsion cracks.

6. The angles of the inclined failure plane of the edge column slab connections ranged from 18.5° to 45°. For corner column slab connections, the angles of the inclined failure plane ranged from 24.7° to 26.6° but the ratio of shear force to diagonal moment were similar.

7. Bonding agent Sika Top Armatec 110 Epocem gave an excellent bond between the old concrete and the repaired concrete in the tests of repaired edge column slab connection.

8. Edge connections repaired using normal concrete can have similar strength and stiffness as the original connections. However, edge connections repaired using an expansive CAH concrete exhibited less strength and stiffness compared to the original edge connections

9. The presence of unbalanced moment reduces shear capacity of the connections. The reduction in shear capacity of edge connections due to increase in *M/V* ratios approximates a logarithmic function

7.3.2 Conclusions related to prediction methods

1. Except for gravity only loaded slabs, the use of simple multipliers to accommodate moment for edge and corner connections, as in BS 8110-85, CEB-FIP MC90 Method-2 and Gardner's Method-2, is not appropriate.

2. The ACI 318-99 interaction diagram for edge connections shows good agreement with the test results. The same trend as the ACI 318-99 was also obtained for CSA A23.3-94; however, the Canadian code overestimates most of the experimental data due to the increase in the coefficient of the CSA code.

3. The linear interaction between shear and unbalanced moment of the CEB-FIP MC90 for edge connections, overestimates most of the test data. Assuming a critical shear section *2d* from the column faces results in the centroid of the critical shear section falling outside the column section and the unbalanced moments of some test data, calculated at the centroid of the critical shear section, change their direction.

4. Edge connections subjected to combined shear force and unbalanced moment failed in punching shear, although the flexural resistances calculated using the ACI 318-99 and the CSA A23.3-94 were exceeded. The flexural resistance calculated by CEB-FIP MC90 for specimens in Series *I* is too conservative for all test results.

5. The ACI 318-99 code is the most conservative of the four building codes considered in predicting the shear strength of edge column slab connections. The average v_u/v_{ACI} is 1.20 with *STD* and *COV* of 0.30 and 0.25, respectively.

6. On average CSA A23.3-94 predicts exactly the test results of edge connections although the Canadian code uses the same assumption as the American code. This is due to an increase in 21% of the limiting maximum shear stress.

7. Method-1 of CEB-FIP MC90, using an eccentric shear equation, overestimates the shear strength of edge column slab connections with an average $v_u/v_{c,EB}$ of 0.82 with *STD* and *COV* of 0.25 and 0.31, respectively.

8. The square interaction between shear force and moments for edge connections proposed by Moehle (1988) is inappropriate with many results falling inside the diagram.

9. Interaction diagrams between shear and unbalanced moment developed using Regan's approach, the Truss Model and the Strip Model for edge column slab connections show that the Strip Model is the most conservative for most of the experimental results.

10. All alternative approach predictions (i.e. Regan's, the Truss Model, the Strip Model, Sherif's, Elgabry's, Gardner's and Desayi's) on shear strength of edge connections, except Sherif's approach (1995) are conservative. The average ratio of measured shear strength to calculated shear strength ranges from 0.90 to 1.26, with coefficients of variation (*COV*) from 0.18 to 0.40. Gardner's suggestion to use a linear shear stress distribution, as the ACI 318-99, along a critical shear section taken at the column perimeter has the least scatter with reasonably conservative prediction of the test results.

11. Of the eccentric shear methods for edge connections ACI 318-99, CSA A23.3-94 and CEB-FIP MC90 Method-1 and Gardner's Method-1, taking the shear perimeter at the column perimeter is preferable. Determining the average, of the two directions, flexural steel ratio for the CEB-FIP MC90 Method-1 and Gardner's Method-1 is a complication.

12. The flexural resistance calculated based on the effective slab width of c_2+2c_1 provided better agreement with test data of edge connections than that of c_2+3h, particularly when the slab thickness is thin.

13. Interaction diagrams between shear and diagonal unbalanced moment at corner connections, calculated using the ACI 318-99, the CSA A23.3-94, the CEB-FIP MC90 and the Regan's approach, are in good agreement with the experimental data. The CEB-FIP MC90 is the most conservative.

14. The calculated shear strengths of the corner connections based on ACI 318-99, CSA A23.3-94 and CEB-FIP MC90 shows that the codes are conservative. BS8110-85 overestimates the test results, but it should not be used to the slabs other than uniformly distributed loaded slabs.

15. One-way shear capacity of the corner connections calculated at the shear perimeter specified by the CSA A23.3-94 overestimates all test results. However, using a shorter shear perimeter of $(\sqrt{c_1^2 + c_2^2} + d)$ results in better predictions on one-way shear strength.

16. The calculated shear strengths of the corner connections are in good agreement with Regan's, Zaghlool's, and Desayi's approaches. Ingvarson's approach overestimates all three-test results. Gardner's Method-1 is the most conservative among the alternative approaches for the corner connections.

7.4 RECOMMENDATION FOR FUTURE RESEARCH

Data on the strength of column slab connections obtained from the continuous slab specimen with span ratio (long span to short span ratio) greater than one are very limited in the literature. It will be valuable to investigate this kind of flat plate structure since continuous specimens more closely represent real structures in practical situations.

The unbalanced moment acting at the edge column slab connections may not be only in one direction especially during the earthquake. Therefore, edge connections may

be subjected to biaxial unbalanced moment. Study on the effect of biaxial unbalanced moment, either monotonic or cyclic loading, at edge column slab connections will be valuable to provide more information on behavior of edge column connections. No experimental research has found in the literature by the author on the effect of biaxial unbalanced moments at edge column slab connections.

Corrosion is one of the weaknesses of steel rebars when they are exposed to aggressive environments. Top bars in reinforced concrete flat slabs of a parking garage are susceptible to corrosion so that the steel rebars may be replaced by FRP bars or FRP grids. However, the behavior of FRP reinforced slabs is less well understood than steel reinforced concrete slabs, especially at edge and corner column slab connections. Research on continuous FRP reinforced slab should be considered for the future research.

REFERENCES

ACI Committee 318, 1999, "Building Code Requirements for Reinforced Concrete (ACI 318-99) and Commentary (ACI 318R-99)", *American Concrete Institute*, Detroit.

ACI Committee 318, 1965, "Commentary on Building Code Requirements for Reinforced Concrete (ACI 318-63)", Publication SP 10, *American Concrete Institute*, Detroit.

ACI-ASCE Committee 352, 1988,"Recommendations for Design of Slab-Column Connections in Monolithic Reinforced Concrete Structures", *ACI Structural Journal*, Vol. 85, November-December, pp. 675-696.

ACI-ASCE Committee 426 on Shear and Diagonal Tension, 1974, "The Shear Strength of Reinforced Concrete Members–Slabs", *Journal of Structural Division, Proceedings of ASCE*, Vol. 100, No. ST8, August, pp. 1543-1591.

Adjukiewics, A. and Starosolski, W., 1990, *Reinforced-Concrete Slab-Column Structures*, Developments in Civil Engineering No. 27, Elsevier, 371 pp.

Alexander, S.D.B., 1988, "Shear-Moment Interaction of Slab-column Connections" *Canadian Journal of Civil Engineering*, Vol. 15, pp. 828-833.

Alexander, S.D.B., 1999, "Strip Design for Punching Shear", The Design of Two-Way Slabs, *American Concrete Institute Special Publication, SP-183*, pp.161-179.

Alexander, S.D.B., and Simmonds, S.H., 1986, "Shear-Moment Transfer in Column-Slab Connections", Structural Engineering Report No. 141, Department of Civil Engineering, University of Alberta, Edmonton, Canada, July, 95 pp.

Alexander, S.D.B., and Simmonds, S.H., 1991, "Bond Model for Strength of Slab-Column Joints", Structural Engineering Report No. 174, Department of Civil Engineering, University of Alberta, Edmonton, Canada, June, 179 pp.

Alexander, S.D.B., and Simmonds, S.H., 1992, "Test of Column-Flat Plate Connections", *ACI Structural Journal*, Vol. 89, No. 5, September-October, pp. 492-502.

Alexander, S.D.B., and Simmonds, S.H., 1992, "Bond Model for Concentric Punching Shear", *ACI Structural Journal*, Vol. 89, No. 3, May-June, pp. 325-334.

Afhami, S., Alexander, S.D.B., and Simmonds, S.H., 1998, " Strip Model for Capacity of Slab-Column Connections", Structural Engineering Report No. 223, Department of Civil Engineering, University of Alberta, Edmonton, Canada, August, 231 pp.

Andersson, J.L., 1962, "Genomstansning av plattor understödda av pelare vid frikant", Nordisk Betong, pp. 179-200.

Broms, C.E., 1990, "Punching of Plates-A Question of Concrete Properties in Biaxial Compression and Size Effect", *ACI Structural Journal*, Vol. 87, No. 3, May-June, pp.292-304.

British Standard (BS 8110-85), 1985, "Structural Use of Concrete", *British Standard Institution*, London.

CEB-FIP MC 90 Model Code, 1990, "Model Code for Concrete Structures", *Comitè Euro-International du Bèton et Fèdèration International de la Prècontrainte*, Lausanne, Switzerland.

Corley, W.G., Jirsa, J.O., 1970, "Equivalent Frame Analysis for Slab Design", *ACI Journal, Proceedings*, Vol. 67, No. 11, November, pp. 875-884.

Criswell, M.E., 1974, "Static and Dynamic Response of Reinforced Concrete Slab-Column Connections", *American Concrete Institute Special Publication, SP-42*, Shear in Reinforced Concrete, Vol. 2, pp. 721-746.

Criswell, M.E. and Hawkins, N.W., 1974, "Shear Strength of Slabs: Basic Principle and Their Relation to Current Methods of Analysis", *American Concrete Institute Special Publication, SP-42*, Shear in Reinforced Concrete, Vol. 2, pp. 641-676.

CSA-A23.3-M94, 1994, "Design of Concrete Structures for Buildings", *Canadian Standard Association*, December.

Desayi, P. and Seshadri, H.K., 1997, "Punching Shear Strength of Flat Slab Corner Column Connections. Part 1. Reinforced concrete connections", *Proceeding of the Institution of Civil Engineers; Structures and Buildings*, vol. 122, February.

Desayi, P. and Seshadri, H.K., 1997, "Punching Shear Strength of Flat Slab Corner Column Connections. Part 2. Fibre-Reinforced concrete connections", *Proceeding of the Institution of Civil Engineers; Structures and Buildings*, vol. 122, February.

Di Stasio, J. and Van Buren, M.P., 1960, "Transfer of Bending Moment between Flat Plate Floor and Column", *ACI Journal*, Vol. 32, No. 3, September, pp. 299-341.

Dilger, W.H. and Sherif, A.G., 1995, "Discussion of Proposed Revisions to Building Code Requirements for Reinforced Concrete ACI 318-89 (Revised 1992)", *Concrete International*, Vol. 17, No. 7, July, pp. 70-73.

Dilger, W.H., 2000, "Flat Slab-Column Connections", *Progress in Structural Engineering and Materials*, Vol. 2, issue 3, November, pp. 386-399.

Elgabry, A. and Ghali, A., 1996, "Transfer of Moments between Columns and Slabs: Proposed Code Revisions", *ACI Structural Journal*, Vol. 93, No. 1, January-February, pp. 56-61.

Elstner, R.C. and Hognestad, E., 1956, "Shearing Strength of Reinforced Concrete Slabs", *ACI Journal, Proceedings*, V. 53, No. 1, July, pp. 56-61.

El-Salakawy, E.F., Polak, M.A. and Soliman, M.H., 1998, "Slab-Column Edge Connections Subjected to High Moments", *Canadian Journal Civil Engineering*, Vol. 25, pp. 526-538.

Engineering News Record, 1956, "Flat Slab Breaks From Columns in Building Failure", October 11, pp. 24-25.

Engineering News Record, 1971, "Building Collapse Blamed on Design Construction", July 15, p.19.

Engineering News Record, 1973, " Collapse Kills Five and Destroys Large Portion of 26-Story Building Under Way", March 8, p. 12.

Feld, J., 1964, "Lesson from Failures of Concrete Structures", *American Concrete Institute*, Monograph Series, Monograph No.1, pp. 30-32.

Gagley, J.R., 2001, "Changing from ACI 318-99 to ACI 318-02: What's new?", *Concrete International ACI*, Vol. 23, No. 6, June, pp. 69-182.

Gardner, N.J., 1990, "Relationship of the Punching Shear Capacity of Reinforced Concrete Slabs with Concrete Strength", *ACI Structural Journal*, Vol. 87, No. 1, January-February, pp. 66-71.

Gardner, N.J., 1995, "Discussion on Punching Shear Provisions for Reinforced and Prestressed Concrete Flat Slabs", *Proceedings, CSCE Annual Conference*, Ottawa, June, pp. 247-256.

Gardner, N.J., 1996, "Punching Shear Provisions for Reinforced and Prestressed Concrete Flat Slabs", *CSCE Journal*, Vol. 23, No. 2, April, pp. 502-210.

Gardner, N.J. and Shao, X.Y., 1996, "Punching Shear of Continuous Flat Reinforced Concrete Slabs", *ACI Structural Journal*, Vol. 93, No. 2, March-April, pp. 218-228.

Gardner, N.J. and Kallage, M.R., 1998, "Punching Shear Strength of Continuous Post-Tensioned Concrete Flat Plates", *ACI Material Journal*, Vol. 95, No. 3, May-June, pp.272-283.

Gardner, N.J., Huh, J., and Chung, Lan, 2000, "What Can We Learn from the Sampoong Department Store Collapse", *International Workshop on Punching Shear Capacity on RC Slabs-Proceedings*, Royal Institute of Technology, Stockholm, June, pp. 225-233.

Ghali, A., Elmasri, M.Z. and Dilger, W., 1976, "Punching of Flat Plates Under Static and Dynamic Horizontal Forces", *ACI Journal*, Vol. 73, October, pp.566-572.

Ghali, A. and Megally, S., 1995, "Discussion of Proposed Revisions to Building Code Requirements for Reinforced Concrete ACI 318-89 (Revised 1992)", *Concrete International*, Vol. 17, No. 7, July, pp. 77-82.

Guralnick, S.A. and La Fraugh, W., 1963, "Laboratory Study of a 45-Foot Square Flat Plate Structure", *Journal of the American Concrete Institute*, September, pp. 1107-1185.

Hanson, N.W. and Hanson, J.M., 1968, "Shear and Moment Transfer Between Concrete Slabs and Columns", *Journal, PCA Research and Development Laboratories*, Vol. 10, No. 1, January, pp. 2-16.

Hammill, N. and Ghali, A., 1994, "Punching Shear Resistance of Corner Slab-Column Connections", *ACI Structural Journal*, Vol.91, No. 6, November-December, pp. 697-707.

Hawkins, N.M., 1974, "Shear Strength of Slabs with Moments Transferred to Columns", *American Concrete Institute Special Publication, SP-42*, Shear in Reinforced Concrete, Vol. 2, pp. 817-846.

Hawkins, N.M., Criswell, M.E. and Roll, F., 1974, "Shear Strength of Slabs Without Shear Reinforcement", *American Concrete Institute Special Publication, SP- 42*. Shear in Reinforced Concrete, Vol. 2, pp. 677-720.

Hawkins, N.M. and Mitchell, D., 1979, "Progresssive Collapse of Flat Plate Structures", *ACI Structural Journal, Proceedings*, Vol. 76, No. 7, July, pp. 775-808.

Hawkins, N.M., Bao, A. and Yamazaki, J., 1989, " Moment Transfer form Concrete Slab to Columns", *ACI Structural Journal*, Vol. 86, No. 6, Nov.-Dec., pp. 705-716.

Ingvarsson, Hans, 1977, *Betongplattors Hållfasthet och Armeringsutformning vid Hörnpelare*, Institutionen för Byggnadsstatik Kungl. Tekniska Högskolan. Stockholm, 143pp.

Jirsa, J.O., Sozen, M.A. and Siess, C.P., 1963, "The Effects of Pattern Loading on Reinforced Concrete Floor Slabs", *Structural Research Series No. 269*, Departement of Civil Engineering, University of Illinois, July, 145 pp.

Kinnunen, S. and Nylander, H., 1960, "Punching of Concrete Slabs without Shear Reinforcement", *Transactions No. 158*, Royal Institute of Technology, Stockholm, 112 pp.

Long, A.E., and Masterson, D.M., 1974, "Improved experimental Procedure for Determining the Punching Strength of Reinforced Concrete Flat Slab Structures", *ACI Special Publication, SP-42*, Shear in Reinforced Concrete, Vol. 2, pp. 921-935.

MacGregor, J.G., 1997, *Reinforced Concrete: Mechanics and Design*, 3rd Edition, Prentice Hall Inc., New Jersey, 939pp.

MacGregor, J.G., and Bartlett, F.M., 2000, *Reinforced Concrete: Mechanics and Design*, 1st Canadian Edition, Prentice Hall Canada Inc., Ontario, Canada, 1042 pp.

Mast, P.E., 1968, "Influence Line for Shear Around Columns in Flat Plates", *Final Report 8th Congress, International association for Bridge and Structural Engineering*, New York, September 9-14, pp. 983-993.

Mast, P.E., 1970, "Stresses in Flat Plates near Columns", *ACI Journal*, Vol. 67, No. 10, October, pp. 761-768.

Mast, P.E., 1970, "Plate Stresses at Columns near the Free Edge", An ACI Digest Paper, *ACI Journal*, November, pp. 898-902.

Megally, S. and Ghali, A., 2000, "Punching of Concrete Slabs due to Column Moment Transfer", *Journal of Structural Engineering, ASCE*, Vol. 126, No. 2, February, pp. 180-189.

Mitchell, D. and Cook, W.D., 1984, "Preventing Progressive Collapse of Slab Structures", *Journal of Structural Engineering, ASCE*, Vol. 110, No. 7, July, pp. 1513-1532.

Moe, J., 1961, "Shearing Strength of Reinforced Concrete Slabs and Footing Under Concentrated Loads", Development Department, Bulletin D 47, *Portland Cement Association*, April, 130 pp.

Moehle, J.P., Kreger, M.E. and Leon, R., 1988, "Background to Recommendations for Design of Reinforced Concrete Slab-Column Connections", *ACI Structural Journal*, Vol. 85, November-December, pp. 636-644.

Moehle, J.P., 1988, "Strength of Slab-Column Edge Connections", *ACI Structural Journal*, Vol. 85, January-February, pp. 89-98.

Park, R. and Islam, S., 1976, "Strength of Slab-Column Connections with Shear and Unbalance Flexure", *Journal of the Structural Division, Proceedings of ASCE*, Vol. 102, No. ST9, September, pp. 1879-1901.

Park, R. and Gamble, L.G., 2000, *Reinforced Concrete Slabs*, 2nd Edition, John Wiley & Sons Inc.,New York, USA, 716 pp.

Pöllet, L., 1983, *Untersuchungen von Flachdecken auf Durchstanzen im Bereich von Eck-und Randstützen*, Dr. Ing. Dissertation, Technische Hochschedule Aachen, December.

Regan, P.E., 1981, "Behaviour of Reinforced Concrete Flat Slabs", CIRIA Report 89, *Construction Industry Research and Information Association*, London, 89 pp.

Regan, P.E. and Braestrup, M.W., 1985, "Punching Shear in Reinforced Concrete: A State of Art Report", *Comitſ Euro-International du Bſton, Bulletin d'information No. 168*, Lausanne, January, 232 pp.

Ross, S.S., 1984, *Construction Disasters: Design Failure, Causes and Prevention. An Engineering News-Record Book*, McGraw Hill Inc., New York, USA, 417 pp.

Shehata, I.A.E.M. and Regan, P.E., 1989, "Punching in R.C. Slabs", *ASCE Journal of Structural Engineering*, Vol. 115, No. 7, July, pp. 1726-1740.

Shehata, I.A.E.M., "Simplified Model for Estimating the Punching Resistance of Reinforced Concrete Slabs", *Material and Structures*, Vol. 23. No. 137, pp. 364-370.

Sherif, A.G. and Dilger, W.H., 1996, " Critical Review of the CSA A23.3-94 Punching Shear Strength Provision for Interior Columns", *Canadian Journal for Civil Engineering*, Vol. 23, pp. 998-1011.

Sherif, A.G., 1996, *Behaviour of Reinforced Concrete Flat Slabs*, Ph.D. Thesis, Department of Civil Engineering, University of Calgary, Alberta, June.

Simmonds, S.H., 1999, "Concept and Background of Elastic Frame Analogies for Two-way Slab Systems", *American Concrete Institute Special Publication, SP-183*, The Design of Two-Way Slabs, pp. 1-16.

Simmonds, S.H. and Alexander, S.D.B., 1987, "Truss Model for Edge Column-Slab Connections", *ACI Structural Journal*, Vol. 84, July-August, pp. 296-303.

Sozen, M.A. and Siess, P.C,1963, "Investigation of Multiple-Panel Reinforced Concrete Floor Slabs" (Design Methods-Their Evaluation and Comparison), *Journal of the American Concrete Institute*, August, pp. 999-1029.

Stamenkovic, A. and Chapman, J.C., 1972, "Local strength of Flat Slabs at Column heads", Report 39, *Construction Industry Research and Information Association*, London, pp. 205-232.

Tankut, T., 1969, *The behaviour of Reinforced Concrete Flat Plate Structures Subjected to Various Combinations of Vertical and Horizontal Loads*, Dissertation, University of London, November.

Vanderbilt, M.D., 1972, "Shear Strength of Continuous Plates", *Journal of the Structural Division, ASCE*, Vol. 98, No. ST4, August, pp. 961-973.

Vecchio, F.J. and Bucci, F., 1999, "Analysis of Repaired Reinforced Concrete Structures", *Journal of Structural Engineering, ASCE*, Vol. 125, No. 6, June, pp. 644-652.

Yamazaki, J., 1975, *Shear and Moment Transfer Between Reinforced Concrete Flat Plates and Columns*, Ph.D. Thesis, University of Washington, Seattle.

Zaghlool, E.R.F., de Paiva, H.A.R. and Glockner, P.G., 1970, "Test of Reinforced Concrete Flat Plate Floors", *Journal of the Structural Division, Proceeding of ASCE*, Vol. 96, No. ST3, March, pp. 487-507.

Zaghlool, E.R.F. and de Paiva, H.A.R., 1973, "Strength Analysis of Corner Column-Slab Connections", *Journal of the Structural Division, Proceeding of ASCE*, Vol. 99, No. ST1, January, pp. 53-70.

Zaghlool, E.R.F. and de Paiva, H.A.R., 1973, "Test of Flat-Plate Corner Column-Slab Connections", *Journal of the Structural Division, Proceeding of ASCE*, Vol. 99, No. ST3, March, pp. 551-572.

APPENDIX A

ACI 318-99 and CSA A23.3-94 Code
Critical shear section properties

APPENDIX A

A.1 Properties of critical shear section of ACI 318-99 and CSA A23.3-94

Interior connections:

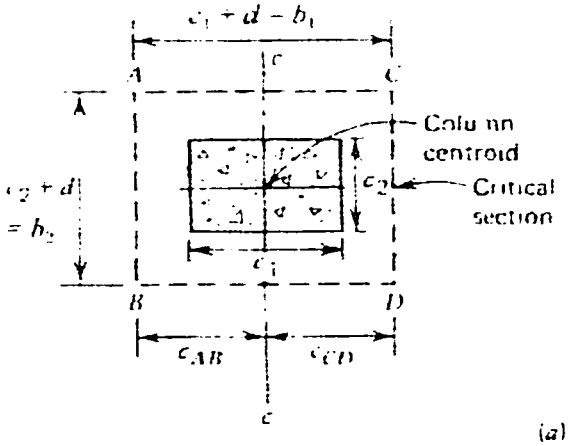

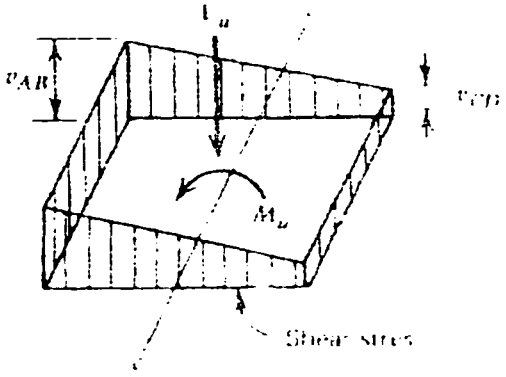

(a)

$$A_c = 2(c_1 + c_2 + 2d)d$$

$$J_c = \frac{2d(c_1+d)^3}{12} + \frac{2(c_1+d)d^3}{12} + 2d(c_2+d)\left(\frac{c_1+d}{2}\right)^2$$

$$c_{AB} = c_{CD} = \frac{1}{2}(c_1 + d)$$

Edge connections:

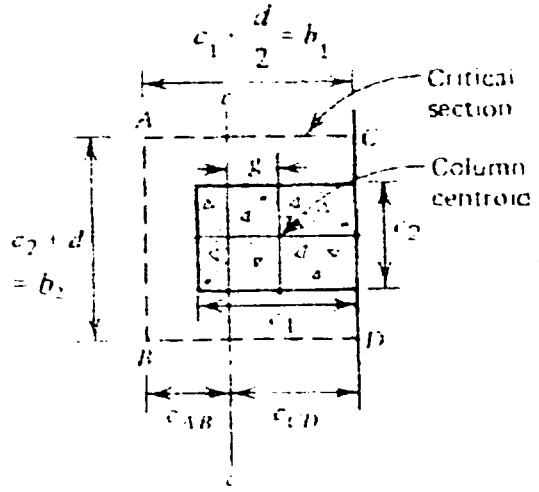

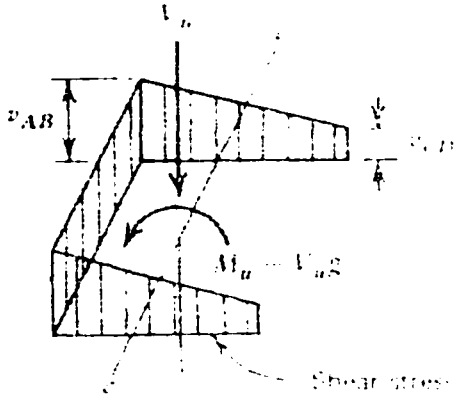

(b)

$$A_c = (c_1 + c_2 + 2d)d$$

$$J_c = \frac{2d(c_1 + (d/2))^3}{12} + \frac{2(c_1 + (d/2))d^3}{12} + (c_2 + d)dc_{AB}^2 + 2(c_1 + (d/2))d\left(\frac{c_1 + (d/2)}{2} - c_{AB}\right)^2$$

$$c_{AB} = \frac{(c_1 + (d/2))^2 d}{A_c}$$

$$c_{CD} = c_1 + \frac{d}{2} - c_{AB}$$

Corner connections:

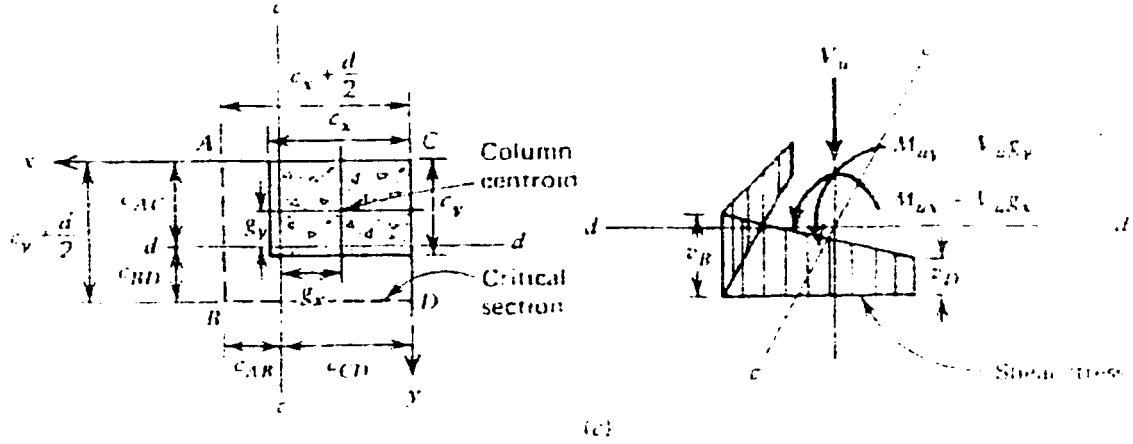

(c)

$$A_c = (c_x + c_y + d)d$$

$$c_{AB} = \frac{(c_x + d/2)^2 d}{2A_c}$$

$$c_{BD} = \frac{(c_y + d/2)^2 d}{2A_c}$$

$$c_{BD} = \frac{(c_y + d/2)^2 d}{2A_c}$$

$$c_{CD} = c_x + \frac{d}{2} - c_{AB}$$

$$c_{AC} = c_y + \frac{d}{2} - c_{BD}$$

$$J_{cx} = \frac{d\left(c_x + \frac{d}{2}\right)^3}{12} + \frac{\left(c_x + \frac{d}{2}\right)d^3}{12} + \left(c_y + \frac{d}{2}\right)dc_{AB}^2 + \left(c_x + \frac{d}{2}\right)d\left(\frac{c_x + \frac{d}{d}}{2} - c_{AB}\right)^2$$

$$J_{cy} = \frac{d\left(c_y + \frac{d}{2}\right)^3}{12} + \frac{\left(c_y + \frac{d}{2}\right)d^3}{12} + \left(c_x + \frac{d}{2}\right)dc_{BD}^2 + \left(c_y + \frac{d}{2}\right)d\left(\frac{c_y + \frac{d}{d}}{2} - c_{BD}\right)^2$$